THE PHARMACOKINETICS OF ENTEROHEPATIC CIRCULATION

A DISSERTATION

SUBMITTED TO THE FACULTY OF

UNIVERSITY OF MINNESOTA

BY

MALEK FATEHI OKOUR

IN PARTIAL FULFILLMENT OF THE REQUIREMENTS

FOR THE DEGREE OF

DOCTOR OF PHILOSOPHY

RICHARD C. BRUNDAGE, Pharm.D, Ph.D., Advisor

DECEMBER 2015

Acknowledgements

"*All the praises and thanks be to Allah, Who has guided us to this, and never could we have found guidance, were it not that Allah had guided us*" **Quran 7:43**

First of all, I would like to thank my family. Throughout the years abroad, my family provided me support and encouragement. This made me realize that my family is the most important part of my life.

I am really thankful to all the patients who participated in the research project and provided data for my dissertation work. Also, I would like to thank all the people who helped, advised and encouraged me during my progress throughout my PhD journey.

A special thanks to my advisor Dr. *Richard Brundage*. Thanks for believing in me and accepting me as one of your students. I would like to thank him for his patience during classes, meetings and discussions. I thank him for answering my questions and directing me to become a better scientist. Working with *Dr. Brundage* did not only make me better on the professional level, but also on a personal one. I am glad that I got to be his student; it will be always my honor. Thank you is the least I can say to *Dr. Brundage* to show my appreciation for everything he has done for me.

I am grateful to Dr. *Pamala Jacobson*, the chair of my dissertation committee, for her enormous support, guidance and encouragement during my PhD. Starting with providing the dataset of mycophenolic acid that ended up being the corner stone of my dissertation projects. Dr. Jacobson was always available when needed and her advice was always on point.

I would also like to thank my committee member, Dr. *Mark Kirstein* for helping me understand the clinical aspects of my projects, in addition to his valuable input on the pharmacometric aspects.

I am grateful to Dr. *Pavan Vaddady* for his time and effort during my internship at Merck. Dr. *Vaddady* delivered a great mentorship that enabled me improve my understanding of the industrial way of drug developments. Also I would like to thank him for being part of my committee.

Thanks to Dr. *Angela Birnbaum* for being a great valuable professor, for her advice, directions, and encouragements. In addition, her efforts as the director of graduate studies are really appreciated.

I highly appreciate Dr. *Lisa Coles* for reviewing my dissertation, as her inputs were very useful. I also learnt a lot from her during our discussions in the pharmacometric classes.

I would also like to thank Dr. *Robert Straka* and the entire faculty in the Experimental and Clinical Pharmacology (ECP) department for their great help and support. Thanks to *Dede*, *Erin*, and *Mary* for their help and administrative support.

Carol Ann, Thanks for being like a second mother to me and all the other students. I am truly thankful from the bottom of my heart for her care.

I am thankful to the ECP department for the ECP fellowship. Also, I am grateful to the Clinical and Translational Science Institute at the University of Minnesota for the CTSI grant and travel award.

I would like to thank *Gaurav Chugh* for introducing me to the field of pharmacometrics.

Thanks to previous alumni: *Akshanth Polepally, Rajneet Oberoi, Aaron Gillman, Harrison Tam, Heather Vezina, and Suresh Agarwal*.

Big thanks to all the graduate students at the ECP department: *Mariam Ahmed, Kinjal Sanghavi, Samuel Callisto, Ali Alhadab , David Hottman, David Margraf, Youssef Roman, Natalie Schmitz, Irene Vuu, Chay Ngee Lim, Shuang Liang, Sai Praneeth Bathena* and *Krista Johnson.*

Thanks to my friends Dr. *Mahmoud Al-Kofahi*, Dr.*Mo'ath Radaideh*, Dr. *Karam Batieha, Dafer Abdulhaq, Tarek R. Khamies*, Dr. *Hamza Kharashgeh*, Dr. *Hosam Zebda, Tyler Newman, Brandon Bud* and *Hamza Adeinat* for being good friends during the journey of my PhD.

Dedication

For my parents *Dr.Fathi Ikour and Fatemah Al-Kofahi*

For my beloved sister and brothers

Abstract

The *EnteroHepatic Circulation* (EHC) is defined as a process that is composed of a circuit of several steps including: liver metabolism, bile secretion, gut metabolism, and reabsorption from the gut back to the systemic circulation. The presence of EHC results in longer apparent drug half-lives and the appearance of multiple secondary peaks. Several empirical modeling strategies are present in the literature; however, they are generally deficient in their applicability to empirical modeling and/or physiological representation of the EHC process. The objective of the current analysis is to further develop our understanding of the application of modeling and simulation to drugs undergoing EHC.

We propose a gallbladder-based model that provides a more physiological representation of the EHC process. The model was used in a sensitivity analysis to evaluate the effect of the extent of EHC on the pharmacokinetic profile and non-compartmental analysis (NCA) calculations. Stochastic Simulation and Estimation (SSE) analysis was conducted to compare parameter estimates from several literature EHC models following a single dose of a drug undergoing EHC. The proposed model was applied in a population pharmacokinetic analysis of unbound mycophenolic acid (MPA), total MPA, mycophenolic acid glucuronide (MPAG) and acyl-MPAG. Finally, a quantitative evaluation of the MPA exposure-response relationship was performed by building a logistic model that described the relationships between total MPA, unbound MPA and acyl-MPAG exposure variables and the probability of acute rejection and leukopenia.

Table of Contents

List of Tables

List of Figures

CHAPTER 1

1. INTRODUCTION TO THE ENTEROHEPATIC CIRCULATION PROCESS

1.1 Enterohepatic Circulation Process

1.1.1 Definition of Enterohepatic Circulation Process

The *EnteroHepatic Circulation* (EHC) is defined as a process that is composed of a circuit of several steps including: liver metabolism, bile secretion, gut metabolism, and reabsorption from the gut back to the systemic circulation (1, 2). As an additional step, fecal elimination of a fraction of the bile-secreted compounds could occur, where this fraction varies from compound to compound.

After transferring from the systemic circulation to the liver, a drug undergoing EHC is usually metabolized into resultant metabolites, where some of these metabolites are then excreted into the bile. In other cases, the drug itself may get secreted to the bile without undergoing metabolism. Regardless, compounds are transferred out of the liver through the biliary system, from which they are either stored in the gallbladder or drained directly to the duodenum[1]. Upon sight, smell, or ingestion of food, the majority of the contents in the gallbladder are released to the duodenum. In the intestine, the metabolites are converted back by the gut flora to the original drug, which is later reabsorbed to the portal circulation. All (or a fraction) of the drug present in the gut goes back to the liver where the EHC circuit repeats. The remaining fraction of the drug present in the gut would undergo fecal elimination.

Several drugs exhibit EHC. A recent review article identified 45 drugs that undergo EHC (3). Examples of these drugs include warfarin, morphine, erythromycin, doxycycline, ceftriaxone, and mycophenolic acid (3). Beside drugs, the EHC process

[1] The duodenum is the initial segment of the small intestinal tract promptly after the stomach, proceeding to the jejunum.

occurs for endogenous compounds. Bile acids are the major endogenous compounds to undergo the EHC process. Other endogenous compounds that can also go through the EHC process include: hormones, like estrogen (4), and thyroxine (T4) and triiodothyronine (T3) (5) ; vitamins like vitamin D (6), and folate(7) ; and growth factors, like insulin-like growth factors (IGFs) (8).

1.1.2 Enterohepatic Circulation versus Biliary Excretion

A misconception about the difference between biliary excretion and EHC processes exists in the literature. As defined previously, the EHC process includes biliary excretion of the drug (or metabolites) to the gut, followed by a *reversible* transfer of a fraction of the drug from the gut to the site of measurement (systemic circulation). In the literature, biliary excretion, as a process by itself, is usually defined as an *irreversible* fecal loss of the drug (or metabolites) from the site of measurement via the biliary route. Therefore, it can be seen that the EHC and biliary excretion processes share similar physiological backgrounds. This could be the cause of the existing misconception regarding the distinction between biliary excretion and EHC processes. However, it is important to differentiate these two processes especially in the context of pharmacokinetic modeling. This is a result of different mass balance effects from these two processes. Biliary excretion involves an irreversible loss of mass and therefore it is justifiable to consider it as an elimination process. In the EHC process, a fraction of drug may undergo fecal elimination; however, the rest of the drug is reabsorbed from the intestine. Therefore, the EHC process involves a distributive component rather than being fully elimination. When considering bile acids, only 3-5% of enterohepatically circulated bile acids are excreted

into the feces and not reabsorbed (9, 10). For modeling simplicity, with assuming no fecal elimination of the drug, the EHC process becomes fully distributive. In that case, it would be more rational it to consider EHC as a distribution rather than a fraction of elimination (11).

1.2 Anatomy of EHC

It is necessary to comprehend the anatomical aspects of the EHC process. This ensures a firm understanding of the kinetics and possible interactions of drugs when EHC occurs. The process of EHC involves several organ and ducts including the liver, portal vein, hepatic artery, hepatic vein, biliary system and gallbladder.

1.2.1 Liver

The liver is the largest internal organ in the body weighing around 1.2 to 1.6 kg. It is located in the right upper quadrant of the abdominal cavity and occupies the entire right subcostal space. The superior surface of the liver is anchored and molded to the diaphragm convexly; whereas the visceral surface is concave and covered in peritoneum (12).

Topologically, the liver is divided into two major lobes, the left and the right lobes (Figure 1-1). Smaller accessory lobes named the quadrate and the caudate lobes are also present and can be seen from the visceral (posterior) surface of the liver (13-15) .

Physiologically, the anatomy of the liver is classifiable into several self-sufficient segments in terms of blood supply. The Couinaud classification is a common physiological classification; dividing the liver into left and right livers (Figure 1-2) (16,

17). The right liver is composed of the anterior and posterior sections, while the left liver is made of medial and lateral sections. Each section is further segregated into two segments, where a segment is distinguished by its own portal triad[2] (18).

1.2.2 Portal Vein

The portal vein is a blood vessel that drains blood from the gut and spleen to the liver (Figure 1-3). It is formed by the junction of the superior mesenteric and splenic veins (19). At the hilum of the liver, the portal vein splits into the left and right portal veins. These two veins ramify further supplying all parts of the liver. The blood carried in these veins is rich in nutrients and compounds that have been absorbed from the gut. Upon reaching the liver, these nutrients and compounds either are metabolized in the liver (with a possible subsequent bile secretion) or continue to systemic circulation.

Regardless of the fact that blood conducted by the portal vein is minimally oxygenated, it still provides the liver with 50-70% of its oxygen demand. This is a result of the high flow rate of the portal vein where 75% of the blood supplied to the liver comes via the portal vein. The hepatic artery satisfies the remaining 25% of liver blood supply.

1.2.3 Hepatic Arteries

The common hepatic arteries originate from the celiac trunk of the aorta, and branch further into the proper hepatic, the gastroduodenal, and the right gastric arteries. The proper hepatic artery bifurcates, at the liver hilum, into the right hepatic and left hepatic arteries (12, 20). Branches of these two hepatic arteries diverge across the liver in

[2] Portal triad (aka portal pedicle) consists of a hepatic artery, portal vein and bile duct. Portal triad refers both to the largest branches of these vessels and to the smaller branches of these vessels.

tandem with the branches of the portal veins reaching the liver sinusoids. Liver sinusoids are hepatic blood vessels that connect the hepatic artery, and portal vein, with the hepatic vein; Figure 1-4**.**

1.2.4 Hepatic Veins

Deoxygenated blood from the sinusoids transfers out of the liver via three hepatic veins: the right hepatic vein, the middle hepatic vein and the left hepatic vein. The right hepatic vein carries blood out of most of the right liver and drains directly to the vena cava. The middle and left hepatic veins unites intra-hepatically into a common hepatic vein before eventually draining into the inferior vena cava (16, 21).

1.2.5 Biliary System

The biliary system consists of the ducts and organs that are involved in the production, transfer, and storage of bile. These include the gallbladder, and intra-hepatic and extra-hepatic biliary ducts.

The production of bile begins at the bile canaliculus. Merging canaliculi form a meshwork of interlober bile ducts and eventually intrahepatic bile ducts. These bile ducts combine forming the sectoral branches, where each branch is part of a portal triad. The union of sectoral braches results in forming the right and the left hepatic bile ducts (22). At the hilum of the liver, the left hepatic duct joins the right hepatic duct to form the common hepatic duct, Figure 1-5.

The gallbladder joins the common hepatic duct via the cystic duct. Below this joining point, it is called the common bile duct. On average, the length of the common bile duct ranges between 10 and 15 cm, with a diameter of 6mm.

The common bile duct then unites with the pancreatic duct forming the ampulla of vater, which drains into the duodenum at the choledochoduodenal junction, which is around 8 cm from the pylorus in the second part of the duodenum. In 13% of the population, this junction can be located more distally in relation to the duodenum (23).

At the choledochoduodenal junction, the sphincter of Oddi, a muscular complex, regulates bile flow and prevents backflow of duodenal contents through the biliary system (12, 17).

1.2.6 Gallbladder

The gallbladder is a tapered-shape hollow bile reservoir that adheres to the inferior surface of the liver by a connective layer called the cystic plate. The average volume of the gallbladder is 30 to 50 ml with an 8 to 10 cm average length. The width of the gallbladder is variable but it is around 4 cm on its widest part. The gallbladder is anatomically divided into 3 parts; the fundus, the body, and the neck (24). The neck of the gallbladder is connected to the common hepatic duct via the cystic duct, which is around 3 to 4 cm long. The proximal part of the cystic duct contains the valves of Heister which is believed to aid in regulating gallbladder emptying and filling (25). The gallbladder receives its blood supply via the cystic artery. The venous drainage of the gallbladder is carried out via the cystic vein draining to the portal vein.

1.3 Microscopic Anatomy of the Liver

The microarchitecture of the liver has been described using several models; the most common model represents the liver as being composed of lobules (Figure1-6).

The lobule has a polygonal prism shape, where the center is occupied by a terminal hepatic venule called the central vein, which is a branch of the hepatic vein. Four to six terminal portal canals demarcate the peripheries of the lobule. A portal canal includes braches of a hepatic artery, portal vein, bile duct. In addition, nerve fibers and lymphatic vessels also run next to the portal canals. The bulk of the lobule is packed with plates of hepatocytes separated by hepatic sinusoids (26) .

The sinusoids are canals that connect portal venules and hepatic arteries with the hepatic venule (Figure 1-4). These canals have discontinuous endothelium that contributes to enhanced permeability. The mixed blood from the terminal branches of the hepatic artery and the hepatic portal vein merge together and flow in the sinusoid toward the central vein of each lobule. Surrounding the sinusoids are cords of the major liver cells, the hepatocytes. The basolateral surface of hepatocytes faces the sinusoid while the canalicular surface faces the bile canaliculus (the first channel in the biliary system). Bile produced by hepatocytes travels from there, through the bile canaliculi, to the bile ducts of the portal triad (12, 27).

1.4 Physiology of the Drug EHC Process

The EHC process can occur for drugs or metabolites. (28). In general, this process is composed of a set of sequential steps including: drug transport and metabolism in the liver, bile secretion, gut metabolism and reabsorption.

In addition to the steps mentioned above, extravascularly administered drugs include an initial step of absorption from the site of administration. Taking the example

case of orally administered drugs, an initial gut absorption step occurs. A more thorough depiction of the EHC steps considering an orally administered drug is described below.

1.4.1 Gut Absorption

Orally administered drugs undergo an absorption process from the gut to the systemic circulation. The magnitude of the absorption depends on several factors that can be categorized into: physiological such as gastric emptying and lumen PH; physiochemical like pKa and drug solubility; and environmental including the presence of food and the gut composition of microflora (1).

Absorption starts with the drug crossing the gut wall, at where the drug may undergo metabolism and transport by the present enzymes and transporters, respectively (29). Both phase 1 and 2 metabolizing enzymes found in the gut wall can result in metabolites that might influence the EHC process. Gut wall transporters like P-glycoprotein, present on the apical surface of the intestinal epithelium, may expel the drug back to the gut lumen and therefore reduce the drug absorption (30).

1.4.2 Drug Transport and Metabolism in the Liver

After crossing the gut wall, the drug reaches the portal vein whose branches anastomose with the branches of hepatic arteries at the hepatic sinusoids. Proceeding through the sinusoids, drug molecules either cross the hepatocyte cell membrane or continue to the hepatic vein (Figure 1-4). This process of crossing the hepatocyte wall is accomplished by passive diffusion or active influx transport. Examples of active transporters at this site include Organic Cation Transport Protein (OCTP), and Organic Anion Transporting Polypeptide (OATP).

Drug molecules that cross the hepatocyte cell wall are exposed to the liver metabolizing enzymes. This may result in a drug biotransformation producing metabolites more polar and greater in molecular weight than the drug.

The formed metabolite molecules (and sometimes the drug itself) transport actively to the bile canaliculi, and to some extent, back to the sinusoids. Active transporters involved in transportation to the bile duct include Multidrug Resistance-associated Protein 2 (MRP2) and P-glycoproteins (31, 32). Examples of transporters involved in moving metabolites from the hepatocytes to the sinusoids include MRP1 and MRP3.

1.4.3 Bile Secretion

The liver synthesizes bile for two main purposes: to help in digesting food in the gut and as a carrier for excretion of endogenous[3] and exogenous compounds. Exogenous compounds include drugs and drug metabolites that are secreted in the bile (33).

On daily basis, hepatocytes secrete approximately 600 mL of bile into the bile canaliculi. Downstream in the bile ductal system, bile undergoes further modifications including secretion and/or reabsorption of compounds. Most of bile contents come directly from hepatocytes; however, it has been estimated that the contribution of the ductal bile cells (cholangiocytes) is around 40% of total bile flow in humans (34).

The bile flow rate through the bile ducts is controlled by the balance between the bile secretory pressure in the liver, the pressure in the cystic duct, and the pressure of the sphincter of Oddi. The liver is capable of producing a maximum secretory pressure of 30

[3] Examples of endogenous compounds include cholesterol and bilirubin.

cm H_2O. The pressure required to open the cystic duct is 8 cm H_2O, while the resting pressure of the sphincter of Oddi ranges between 12 and 15 cm H_2O. As a result, most bile ends up going through the cystic duct to the gallbladder (17).

During fasting, around 75% of bile gets stored in the gallbladder, while the remaining 25% drains directly to the duodenum (35, 36). Bile stored in the gallbladder undergoes further concentration where around 90% of water is absorbed (17). On the sight, smell, or ingestion of food, the gallbladder contracts, while the sphincter of Oddi relaxes causing the release of around 75% of bile stored in the gallbladder to the duodenum (1, 35-40). Once the meal is finished, the gallbladder relaxes and the sphincter of Oddi contracts causing a restart in the cycle of the gallbladder bile storage.

1.4.4 Gut Metabolism and Reabsorption

Metabolites in the gut may undergo back-metabolism by gut microorganisms, and get re-absorbed back to the portal circulation. Most of the metabolic reactions conducted by the gut microorganisms on these metabolites are of the hydrolytic and reductive types. These reactions result in a drug that is less polar with smaller molecular weight, and therefore more able to cross membranes and undergo re-absorption back to the systemic circulation.

Understanding the behavior of gut microorganisms is significant clinically as the co-administration of antibiotics that kill or inhibit the gut microorganisms may result in reducing or obliterating the EHC process (41). β-Glucuronidase is a an enzyme produced by gut microorganisms like *Escherichia coli* and results in the deglucuronidation of

glucuronic acid residues from the metabolites[4] (42). It is important to mention that β-Glucuronidase demonstrates variability across species. For example, it is more active in rats and mice than humans. Such variability may result in inconsistency in the time and extent of observed EHC between different species (42).

1.5 The EHC process and Drug Pharmacokinetics

The EHC process results in major alterations of the pharmacokinetic profile including modification of the drug apparent half-life and the area under plasma concentration curve (AUC) (1). Additionally, the EHC process causes multiple peaks in the concentration-time profile (1, 43).

In a study aiming to evaluate the clinical significance of furosemide acyl glucuronide, a metabolite of furosemide that undergoes EHC, the authors demonstrated that the EHC process causes a longer half-life accompanied by the appearance of secondary peaks (44). In another study conducted by Colburn et al., simulation analysis provided results that support the effect of EHC on the drug half-life; however, it also showed that the EHC process produces a larger volume of distribution (45). In this study, the extent of the EHC process was found to be an important factor, where a larger extent creates greater effect. The magnitude of secondary peaks was shown in another study to be associated with the extent of the hepatic extraction ratio (E); a higher E was shown to cause larger secondary peaks (46).

Several studies were performed in order to evaluate the consequences of the EHC process on the AUC (46-48). However, conclusions based on these studies were

[4] Another enzyme produced by gut microorganisms and metabolize drugs is cysteine conjugate β-lyase.

contradictory. In the studies conducted by Veng Pederson and Miller, AUC was demonstrated to be dependent on the EHC process (47, 48). In another study performed to evaluate the biliary excretion and EHC of glycyrrhizin in rats, the EHC process resulted in larger AUC (49). Other studies showed that the AUC is independent of the EHC process (50). Regardless, the effect of EHC on the AUC calculation had been shown to be dependent on the sampling times in relation to the times of the secondary peaks(46).

Harrison and Gibaldi developed an EHC model to evaluate the effect of cholestasis on the pharmacokinetics of a hypothetical drug undergoing EHC (51). The model included two routes of elimination; renal elimination and fecal elimination. In their analysis, the authors found that the effect of cholestasis on half-life depends on the relative ratio of the two routes of eliminations. When having larger renal elimination than fecal elimination, cholestasis causes shortening of the drug half-life, and vice versa. Using the same model, Chen and Gross showed that an increase in the drug plasma AUC would always occur when there is a reduction in the biliary excretion or an increase in the gut reabsorption rate (52).

The EHC process can be the deciding factor in controlling the final route of metabolite elimination. Huckle et al. performed a study to evaluate the disposition of 3-phenoxybenzoic acid. In the analysis, the authors demonstrated that the biliary secreted glucuronic conjugate of 3-phenoxybenzoic acid are cleaved to the respective benzoic acids in the intestine by gut microflora. Benzoic acids are then reabsorbed and undergo

metabolism to the sulfate ester which is renally excreted (53). Therefore, the occurrence of EHC influences the final elimination route.

1.6 Factors Affecting the EHC Process

Several factors might influence the EHC process of drugs and metabolites. These factors could be generally categorized into physiological such as gastric emptying and lumen pH; physiochemical like molecular weight, pKa and drug solubility; genetics; drug-drug interactions; and lastly, environmental including food, composition of the gut microflora and effect of disease (1)

Drugs undergoing EHC share similar physiochemical characteristics, and as a general rule, a minimum molecular weight of 500 to 600 Da is required as a minimum threshold for biliary excretion in human (1). A molecular weight of less than 600 Da is usually required for renal excretion (1).

Genetic variations in the transporters can result in atypical EHC process. In a study conducted on MRP2-deficient rats, hepatobiliary disposition of paracetamol was demonstrated to be impaired relative to normal rats (54).

Several disease states have been associated with changes to EHC process. For instance, Cholestasis result in reduced hepatic uptake and therefore drug metabolism (55). Another condition, Cirrhosis, results in reduced liver blood flow and function, and therefore inhibiting the hepatic uptake of drugs (56).

Fasting is another factor that results in changes in the EHC. In a study conducted on rats, fasting caused reduced bile synthesis, flow, and recirculation (57). In another

study, the introduction of the breakfast meal to patients resulted in a significant increase in bile flow (58). Another study showed that most of the bile acids in the serum of healthy subjects were found to rise significantly within 30 minutes to 2 hours after eating (59).

1.7 Modeling of EHC

Extensive modeling has been conducted to account for the EHC process observed for some drugs. This has led to a diverse set of approaches implemented in modeling of this process. These approaches can be sorted by their general characteristics into: simple two-compartment models, Tgap-based models, gallbladder-based models, and other modeling strategies**.** In general, these models aid in understanding the consequences of the EHC process, and provide a better modeling framework when EHC exists. This section provides an overview of the modeling approaches used to characterize the EHC process.

1.7.1 Simple Two-Compartment Models

A simple two-compartment model consists of two compartments, where these compartments represent the body and the gut. The transfer rate constants between these two compartments are linear in the sense that their values do not change across time.

Early attempts to model the EHC process use the two-compartment model proposed by Harrison and Gibaldi **(**Figure 1-7) (51). The model consisted of two compartments, body and gut, and included elimination rate constants from both compartment as k_{10} and k_{20}. The rate constant k_{10} represented the sum of renal and non-

biliary elimination of the drug, while the rate constant k_{20} characterized the loss of the drug from the gut via bacterial biotransformation and fecal elimination. The gallbladder emptying and gut absorption processes were described using the rate constants k_{12}, and k_{21}, respectively. The simple two-compartment model assumes that the rate constant k_{12}, representing the gallbladder emptying, is non-changing (constant) (Figure 1-8A). Using the same model, Chen and Gross evaluated the effect of changes in biliary excretion (k_{12}) and reabsorption (k_{21}) processes on the pharmacokinetics of a drug undergoing EHC (52).

Modeling Conclusion

The two-compartment model is simple and easy to implement; however, it crucially disadvantaged as it is not able to capture the secondary peaks observed in the EHC process.

1.7.2 Tgap-Based Compartmental Models

The prominent differentiating characteristic of the Tgap-based models is the use of a single time delay (Tgap) after administering the dose, to represent a single continuous gallbladder emptying; without the addition of compartments in the depiction of the EHC process.

By contrast to the simple two-compartment model, the Tgap model assumes a discontinuous gallbladder emptying and reabsorption process rather than a continuous one. The Tgap term represents the time delay at which the gallbladder emptying and reabsorption process starts. This model presupposes that the rate constant, representing the gallbladder emptying and reabsorption process, follows a single step function (Figure 1-8B). The step function is dependent on time and changes value at Tgap, i.e., it will have

a zero or smaller positive value before Tgap, and a fixed positive value beginning at Tgap and continues unbounded.

A number of studies have been conducted assuming a Tgap-based EHC model. One study done by Steimer et al. assumed a delay in the time between the bile excretion process and the reabsorption process (Figure 1-9) (60). The analyses of this model are similar to the simple two-compartment model; however, the use of Tgap enabled predicting the secondary peaks of the concentration time profile.

Another Tgap model was developed by Colburn et al. and was used to describe the concentrations of phenolphthalein and its glucuronide conjugate obtained from intact and bile duct cannulated rats (Figure 1-10) (61). The model consists of three compartments; compartment 1 represented the blood and quickly equilibrating tissues, compartment 2 represented the slowly equilibrating tissues, and compartment 3 represented the intestine and consisted of 2 sub-compartments (3A, and 3B). The rate constant k_{13} characterized the biliary excretion process, while the rate constant k_{31} characterized the intestinal deconjugation and reabsorption processes. The drug was assumed to undergo fecal elimination only, via the rate constant k_{30}. A Tgap with a value of 3.7 hr was assumed to occur between biliary excretion and intestinal reabsorption processes to account for the time required for the drug transfer in bile and subsequent deconjugation before reabsorption. The model was able to capture secondary peaks in the concentration data adequately, in both intact and bile duct cannulated rats.

Modeling Conclusion

Tgap based models provide the ability to capture a single secondary peak with less modeling complexity. Conversely, this model does not represent the physiology of EHC in humans and animals that have a gallbladder. The simplicity presented in the Tgap models may result in biased estimations of other process originating from the central compartment, such as the elimination process. This is a result of the Tgap model's assumption of bile release from the central compartment rather than a gallbladder compartment. Additionally, Tgap models do not allow for multiple cycles of gallbladder emptying because of the single state shift nature of the step function used to describe the gallbladder-emptying rate constant.

1.7.3 Gallbladder-Based Models

Gallbladder-based models are differentiated from previously mentioned models on the basis that they include an additional compartment, the gallbladder. The addition of this compartment allows for a better portrayal of the EHC process in human and animals containing a gallbladder. This reflects the fractional storage, and subsequent release, of a given drug dose in the gallbladder.

Gallbladder-based models have allowed for a number of iterations categorizable by the function chosen to model the release of the drug from the added gallbladder compartment. These functions are introduced and summarized in the section below.

1.7.3.1 Continuous Release

Within the continuous release model, the gallbladder-emptying rate constant does not change across time. It assumes a fixed rate constant that represents the gallbladder emptying process. In concept, this is similar to the simple two-compartment model in which the rate constant representing the gallbladder emptying process is linear *(*Figure 1-8A).

A four compartment model, developed by Colburn et al, included a gallbladder and liver compartments, in addition to systemic and gut compartments (Figure 1-11) (45). The transfer of drug from the gallbladder to the gut was assumed to be a continuous process. The assumption of a continuous bile flow in this model could limit its applicability, as the gallbladder demonstrates sporadic and discontinuous, rather than, continuous emptying behavior.

Modeling Conclusion

This technique takes on minimal additional complexity among the gallbladder-based models. It does not accurately depict the toggle nature of the gallbladder emptying process, i.e., opening and closing at mealtimes. Therefore, this approach does not reflect the advantages of the additional gallbladder compartment. This results in predictions that are similar to those that exclude the gallbladder.

1.7.3.2 Single Bolus Release

Single bolus release models assume a single release of the drug from the gallbladder compartment, at the time Tgap. These models build on the concept of Tgap-based models, where a single continuous release occurs. However, they differ from Tgap-

based models in the compartment from which this release occurs. In the Tgap-based models, the release starts from the central compartment, while in single bolus release models it starts from the gallbladder compartment.

In a study conducted by Veng Pedersen and Miller in 1980, the authors proposed two gallbladder based models in order to investigative the EHC of doxycycline (Figure 1-12) (62). In these models, two of the compartments represented the blood and the gut. A third compartment was used as a delay compartment, and represented the gallbladder. The difference between these two models is that model 1 assumes a continuous release function, while in model 2 it is a single bolus function. Model 2 assumes that at Tgap the fraction of the drug that had been accumulating in the gallbladder compartment is released to the intestine as single bile burst. The major conclusion of the analysis was the superiority of the single bolus model over the continuous release model in terms of fitting the data.

Another model was developed by the same authors in the same year analyzing cimetidine (47). The structure of the model included 4 compartments: central, peripheral, gut, and gallbladder (Figure 1-13). The model estimated a fraction (F) of the dose that is absorbed from the gut to the systemic circulation, while the remaining fraction (1-F) goes to the gallbladder compartment directly representing the first pass hepatic effect. This model assumed a single bolus release of bile from the gallbladder compartment to the gut at time Tgap. The same modeling strategy was also used by one of the authors to fit ranitidine that also undergoes EHC (48).

Funaki developed the first population pharmacokinetic model that includes a gallbladder compartment(63), where this model assumes a single bolus release (63). The aim of the analysis was to evaluate the usefulness of the model for drugs that undergo EHC. The author selected mycophenolic acid (MPA) as a test drug to use in the model. MPA undergoes EHC, where the EHC process contributes to around 40% (ranges between 10%-60%) of the MPA AUC (64). The model structure is similar to Veng Pedersen and Miller model 2 in Figure 1-12, where the release of bile from the gallbladder was modeled as a single bolus expulsion at Tgap.

Another model was developed by Strandgarden et al. to study the pharmacokinetics of Roquinimex in healthy volunteers (Figure 1-14) (65). The model included a gallbladder compartment, where it empties once at Tgap. The following equation was used to define Tgap:

$$\text{Tgap} = tmax_2 - tmax_1$$

where $tmax_2$ and $tmax_1$ are the times of the secondary peak and the first peak, respectively. Additionally, the authors defined two separate rate constants for absorption and reabsorption processes (k_A, and k_r). The inclusion of the gallbladder in the model improved the fit when compared to a model without a gallbladder.

A model developed by Ide eta al. to conduct a population pharmacokinetic analysis of pravastatin, incorporated a gallbladder compartment to represent the EHC nature of the drug (66). The reabsorption of the drug from the gallbladder was assumed to

occur at Tgap. However, the transfer of drug representing this reabsorption was linked directly to the central compartment, rather than the gut compartment, as seen in Figure 1-15.

Modeling Conclusion

Single bolus release models suffer from some of the drawbacks observed with the Tgap models. Assuming a single bolus release does not account for multiple cycles of gallbladder emptying at mealtimes. Additionally, even though they contain a gallbladder compartment, single bolus release is not representative of the bounded gallbladder emptying with respect to time. Despite this, the single bolus release models have provided adequate modeling results for data that demonstrate a single secondary peak.

1.7.3.3 Switch Function Release

In the switch function release models, the rate constant controlling the gallbladder emptying process is described using a piece-wise function (Figure 1-8C). This function yields a positive-valued rate constant within the time intervals that represent the durations of gallbladder emptying cycles. Outside these intervals, the yielded rate constant is fixed at zero, or a smaller positive value.

Jiao et al developed a model that described the pharmacokinetics of MPA and its metabolite, MPAG, simultaneously (67). The model consisted of gut, MPA central, MPA peripheral, MPAG, and gallbladder compartments (Figure 1-16**)**. The rate constant from the gallbladder to the gut (k_{51}) was assumed to equal zero except at the duration of meal times, where it was estimated at a positive value. Two meal times were assumed, where

the duration of a mealtime was fixed to 0.01 hours. The percentage of MPA that undergoes EHC ($EHC\%$) was calculated according to the following equation:

$$EHC\% = \frac{k_{45}}{k_{45} + k_{40}} * 100$$

Another model established by Sam et al. was created to simultaneously model MPA and it metabolites; MPAG and acyl-MPAG (68). Beside a gut compartment, the model included MPA central, MPA peripheral, gallbladder and another two compartments, one for each metabolite (Figure 1-17). Both of the metabolites were linked to the gallbladder compartment as the author assumed that both of MPAG and acyl-MPAG undergoes EHC. The rate constant from the gallbladder to the gut (k_{GB}) was assumed to equal zero except at the duration of the meal time; it was estimated at a positive value. The mealtime was assumed to start at 8 hours post-dose and for a duration fixed to 1.5 hours. The extent of EHC was calculated based on the $EHC\%$ of MPAG ($EHC\%_{\mathrm{MPAG}}$) as the following:

$$EHC\%_{\mathrm{MPAG}} = \frac{k_{3G}}{k_{3G} + k_{30}} * 100$$

The study performed by de Winter et al. aimed to develop a population pharmacokinetic model of total MPA, unbound MPA, total MPAG, and unbound MPAG (69). The model consisted of gut, MPA central, MPA peripheral, MPAG, protein binding,

and gallbladder compartments (Figure 1-18). The addition of the protein-binding compartment was used to describe the competitive binding of MPA and MPAG on the protein binding sites. The rate constant from the gallbladder to the gut (k_{72}) was assumed to equal zero except at the duration of the meal time where it was fixed to 10 hr-1. The duration of the mealtime was fixed to 1 hour after the mealtime that was estimated 7.9 hours after dose.

Yau et al. built a five-compartment model to conduct a population pharmacokinetic analysis of MPA and MPAG (70). The model structure is similar to Jiao et al. model in Figure 1-16. However, the current model is different when it comes to the assumption about the rate constant of gallbladder emptying. This model assumed that the rate constant from the gallbladder to the gut is a zero order and equals $\frac{A_{bile}}{T_{bile}}$, where A_{bile} is the amount of drug in the gallbladder compartment, and T_{bile} is the duration of gallbladder emptying. This rate constant is assumed to equal zero except during the durations of mealtime. To evaluate the extent of EHC, the authors calculated both of $AUC_{\infty,with\ EHC}$ and $AUC_{\infty,without\ EHC}$, where $AUC_{\infty,with\ EHC}$ was calculated using the trapezoidal rule. On the other hand, $AUC_{\infty,without\ EHC}$ was calculated according to the following equation:

$$AUC_{\infty,\ without\ EHC} = AUC_{EHC\ start} + \frac{C_{EHC\ start}}{\lambda_z}$$

where $AUC_{EHC\ start}$ is the part of $AUC_{\infty,with\ EHC}$ between time zero to the beginning of the EHC process, and $C_{EHC\ start}$ is plasma concentration at the start of the EHC process.

The parameter λ_z is the first order rate constant estimated by least regression of the terminal part of the model based concentrations. Next, the calculation of the extent of EHC was done according to the following equation:

$$EHC\% = \frac{AUC_{\infty,with\ EHC} - AUC_{\infty,\ \ without\ EHC}}{AUC_{\infty,with\ EHC}}\ X\ 100\%$$

The switch model was also used in a study that evaluated the pharmacokinetics of the nonsteroidal anti-inflammatory drug sulindac (Figure 1-19) (71). The model describes the pharmacokinetics of the drug and two of its metabolites; sulindac sulfide and sulindac sulfone (exisulind). A gallbladder compartment was included in the model, where sulindac was assumed to undergo EHC. The reabsorption from the gallbladder was controlled by a rate constant k_{51} . This rate constant is assumed to equal zero except during the durations of mealtime. The authors assumed that the duration of mealtime equals 0.75 hr.

Rosner et al. developed a two-stage population model to describe the pharmacokinetics of irinotecan, and its metabolites; SN-38, SN-38 –glucuronide (SN-38G), and APC (72) (Figure 1-20). The model evaluated the disposition of irinotecan using two compartments, central and peripheral. Irinotecan is metabolized to APC and SN-38, which is further glucuronidated to SN-38G. The authors assumed that SN-38 undergoes EHC, rather than SN-38G as they found that doing so provide better fit to the data. SN-38 was assumed to be secreted into a gallbladder compartment via a first order rate constant. The empting of gallbladder content was described using two rate constants, one as a baseline (k_{BG}), and another one (k_{BG1}) only effective at the durations of gallbladder emptying. The rate constant k_{BG1} is a step function that takes the value zero

except at durations of gallbladder empting cycles. Moreover, the authors consider that the ratio (k_{BG1}/ k_{BG}) provides a measure of EHC extent.

As a variation of the switch function models, the gallbladder emptying was assumed to occur instantaneously; where all or a fraction of the drug stored in the gallbladder, is released at each gallbladder emptying cycle. This is achieved by using a large value for the gallbladder-emptying rate constant in addition to assuming very short gallbladder emptying intervals. Shepard et al. proposed a model which consisted of blood, liver, and gut compartments, in addition to a gallbladder compartment (Figure 1-21) (46). Gallbladder emptying was assumed to occur at several cycles of regular intervals (once every 6 hours). The emptying process resulted in an instantaneous full emptying of the content of the gallbladder. This is followed by another cycle of filling that proceeds until the next gallbladder emptying after 6 hours, and so on. Plusquellec and Houin developed a model that takes into account multiple cycles of gallbladder emptying (73). The model structure is the same as the model created by Veng Pedersen et al for Cimetidine in Figure 1-13 (47). A fraction of the drug (F) was assumed to transfer from the gut to the central compartment, while (1-F) goes to the gallbladder compartment. However, another fraction was implemented in the model. The model assumed that a fraction (F_b) of the drug, stored in the gallbladder compartment, is secreted at each gallbladder emptying, while the remaining fraction (1-F_b) stays in the gallbladder until next emptying.

Modeling Conclusion

Models based around the switch release concept are comparatively easy to implement in practice. To their benefit, they are usable with multiple gallbladder emptying cycles that can vary in timing and duration. However, the discontinuities inherent in piece-wise functions pose problems in numerical integration of the Switch-Release models.

1.7.3.4 Sigmoid Function Release

This approach of gallbladder-based modeling utilizes a sigmoid function to control the gallbladder-emptying rate constant. The path of the sigmoid function is S shaped allowing for a continuous, gradual shift in the rate constant value.

In a study conducted by Jain et al. to evaluate the pharmacokinetics of sorafenib, a population model was built (74). The model consisted of one compartment disposition model attached to a chain of transit compartments in addition to a gallbladder compartment (Figure 1-22). A fraction of the dose (F_{ent}) was assumed to transfer from the central compartment to the gallbladder compartment by the first order rate constants, k_b. The rate of transfer from the gallbladder to the gut compartment was controlled by $f(t) * k_{ehc}$ where $f(t)$ is a sigmoid function as the following:

$$f(t) = \frac{(time - DT)^{40}}{(time - DT)^{40} + (t^{*})^{40}}$$

Here DT is the time of dose administration, and t^* is the gallbladder emptying time. The use of a large hill parameter (here its 40) results in a steeper sigmoidal function and according to the authors, this represents the all or none concept of the gallbladder emptying.

Modeling Conclusion

Similar to the switch approach, sigmoid function release models allow for multiple cycles of gallbladder emptying, with dynamic changes in timing and duration of emptying cycles. However, using the sigmoid function is more complex to implement because of the need for additional parametrization.

1.7.3.5 Sine Function Release

The sine function release models are another predominant gallbladder based model, relying on a sine function to control the gallbladder-emptying rate constant. The cyclic behavior of the sine function allow for its use in modeling the varying gallbladder-emptying rate constant.

Wajima et al. performed a study that implemented the sine function in modeling EHC after single or multiple dosing strategies (Figure 1-23) (75). The model consisted of three compartments, gut, central, and gallbladder. The model assumed a first order rate constant transferring drug from central to gallbladder. However, the transfer rate constant from the gallbladder to the central compartment (K_{b1}) is coupled with a sine function as $K_{b1} * f(t)$, where $f(t)$ is defined according to the following equation:

$$f(t) = \begin{cases} \sin(2\pi * \frac{time - \ acrophase}{period}) & ,when \ f(t) \geq 0 \\ 0 & ,when \ f(t) < 0 \end{cases}$$

The parameter "$acrophase$" represents the time of the appearance the first full sine wave. In other words, it is the time of the beginning of the first gallbladder opening. The parameter "$period$" is the duration of one complete sine wave, and it reflects the periodicity (frequency) of the gallbladder openings. The use of this sine function implies that the beginning of the EHC process occurs "$acrophase$" hour(s) after the first dose and the EHC cycle is repeated once every "$period$" hour(s).

Huntjens et al. evaluated the EHC process in two nonsteroidal anti-inflammatory drugs; diclofenac and rofecoxib, with the use of sine function (76). Diclofenac and rofecoxib are drugs that act by inhibiting the cyclooxygenase (COX), resulting in an inhibition of the formation of the inflammation mediators prostaglandins (PGs) and thromboxanes (77). The aim of this study was to develop a pharmacokinetic model of EHC for both diclofenac and rofecoxib in rats. Additionally, the authors wanted to evaluate the impact of the EHC process on pharmacokinetic exposure and the pharmacodynamic biomarker prostaglandins E2 (PGE2). The pharmacokinetic modeling of diclofenac was conducted simultaneously on diclofenac and its metabolite 4-hydroxydiclofenac (Figure 1-24). The parent drug and metabolite had two disposition compartments (central, and peripheral). An additional gallbladder compartment was linked to both central compartments of diclofenac and 4-hydroxydiclofenac. To represent the periodic bile flow, the transfer rate constant from the EHC compartment to the central

compartments was modeled nonlinearly using the sine function. More compartments were added based on the route of administration, specifically oral and peritoneal. The same model was also used by the authors to fit blood concentrations data collected after rofecoxib dosing. Simulations analysis revealed that EHC causes 95%, and 15% increase in the exposure of diclofenac and rofecoxib, respectively. Additionally, it was predicted that the presence of EHC causes an extended duration of the inhibition effect on PGE2, however, without changing the maximum inhibition.

Modeling Conclusion

The sine release approach enables modeling multiple cycles of gallbladder emptying. With that said, it does not provide flexibility in terms of modeling observed irregularity in these cycles, as each cycle's timing and duration cannot be controlled separately. The use of regular multiple gallbladder emptying is less relevant physiologically since the emptying process is related to the timing of food intake (78). Different from the switch function, the sine function is a continuous function and therefore less prone to modeling related numerical difficulties.

1.7.4 Other Modeling Strategies

While the main methods of modeling the EHC process have been summarized above, other modeling strategies have been developed to account for the EHC process.

A population pharmacokinetic study was conducted to build a model for single or multiple doses of ezetimibe given to healthy subjects(79). Ezetimibe is conjugated with glucuronide in the liver, and then a fraction is secreted via bile into the gut where it undergoes EHC (79). A two compartment disposition model best described the data.

However, and to account for the EHC process, a secondary input was introduced to the gut compartment at a pre-specified mealtime. This secondary input contained a fraction of the absorbed dose, where this fraction was estimated. According to the authors, this fraction represents the fraction of ezetimibe dose that undergoes EHC.

In another pharmacokinetic study of irinotecan and its SN-38, and APC metabolites, a different model was developed (80) (Figure 1-25). Unlike the Rosner et al model of irinotecan, this model assumes that irinotecan is the entity that undergoes EHC. To account for the EHC process, the authors connected a chain of 5 compartments as a loop that starts and then get back to the central compartment of irinotecan. The choice of 5 compartments was based on sensitivity analysis of different number of compartments. This chain of compartments is connected to each other and to the central compartment by rate constants all given the same value.

Another EHC model was created in a population pharmacokinetic study of nevirapine (81). The model consisted of transit absorption, gut, central, peripheral and two additional compartments, named gut1, and gut2 (Figure 1-26). The authors assumed two changing conditions, A and B, where in condition A the first gut compartment (gut1) receives drug from the central compartment, where at the same time drug transfers from the second gut compartment (gut2) to the central. In condition B, the opposite occurs, where gut1 becomes an absorption compartment and gut2 becomes a depot. The modeling of altering conditions was done using NONMEM reserved variable MTIME. The number of switching between conditions A and B was determined empirically. The authors found that this model was able to adequately capture the EHC process.

Kim et al. performed a study with the goal of building a population pharmacokinetic model of fimasartan in rats, dogs, and humans simultaneously (82). The process started by building a model in each of these species, followed by linking them together and estimating all parameters simultaneously. The model in each species is the same and consisted of two or three sequential absorption compartments linked to three disposition compartments; central, shallow peripheral, and deep peripheral (Figure 1-27**)**. From the gut, a fraction of the drug transfers to the central compartment $(1 - Fr_{liver})$, while the rest of the drug (Fr_{liver}), transfers to the liver compartment. In the liver, the drug is either eliminated or transferred to another compartment called the gallbladder compartment. The gallbladder emptying process was modeled using an inducible first order process($K_{bile.gut(t)}$), as the following:

$$K_{bile.gut(t)} = K_{bile.gut.base} * X_{bile\ flow}$$

Where $K_{bile.gut.base}$ represents the baseline bile flow rate parameter, and $X_{bile\ flow}$ is the bile flow rate that is described using a turn over model as the following:

$$\frac{dX_{bile\ flow}}{dt} = K_{out}[(1 +* stim_{bile\ flow}) - X_{bile\ flow}]$$

In this turn over model, the production of bile flow was described using the zero order rate constant k_{in}, while the offset was described using the first order rate constant k_{out}.

The authors assumed a continuous bile flow as a baseline, and the relationship between k_{in} and k_{out} was described as the following:

$$K_{in} = K_{out}(1 + stim_{bile\ flow})$$

Using a square pulse function, the $stim_{bile\ flow}$ was estimated as a positive value when constrained between specific times, and was fixed to zero outsides these times. In order to evaluate the extent of EHC, the authors calculated the fraction of the drug that undergoes EHC as $Fr_{EHC} = (Fr_{liver} * Fr_{liv.bile})$, where $Fr_{liv.bile}$ is:

$$Fr_{liv.bile} = \frac{k_{liv.bile}}{k_{liv.bile} + k_{el}}$$

Modeling Conclusion

The use of uncommon strategies has been implemented in modeling the EHC process. Even though these models do not represent the physiology of EHC, they were successful in providing good fit results.

1.8 Conclusion

This chapter provided an overview of the EHC process. EHC is a composite distributive and eliminative process involving several organs and ducts. Therefore, a detailed description of the anatomy and physiology of these organs and ducts was discussed. Additionally, an examination of the effect of the EHC process on the drug pharmacokinetics was provided. Finally, this chapter included a section that discussed the various modeling strategies used to account for the EHC process. In this section, the

various literature models were categorized based on common features, and evaluated in comparison to each other. In general, the gallbladder-based models provided the best physiological representation when compared to the other modeling strategies. The use of a continuous release gallbladder based model ignores a major component of the physiology of a gallbladder emptying process, i.e., the toggle nature, and does not take advantage of the additional gallbladder compartment. Single bolus release gallbladder models also ignore the toggle nature of gallbladder emptying process. The use of sine, switch, or sigmoid functions allow for modeling multiple mealtimes. The sine function assumes fixed intervals between mealtimes. As opposed to the sine function, the use of switch or sigmoid functions provides more flexibility in terms of modeling the gallbladder emptying process being related to mealtimes. However, the switch function is a discontinuous function and therefore is prone to more numerical difficulties than the sigmoid function, while the sigmoid function is more modeling friendly. The Sigmoid function release models appear to be superior to the rest modeling strategies.

In the following chapters, the construction, assessment, and utility of a more physiological gallbladder-based EHC model will be described. This model will take into account a physiological representation of the bile secretion, gallbladder filling and emptying, duration of gallbladder emptying and irregular mealtimes. In conclusion, this introductory chapter forms the basis for understanding of concepts needed for subsequent chapters.

Figure 1-1: Topological Anatomy of the Liver

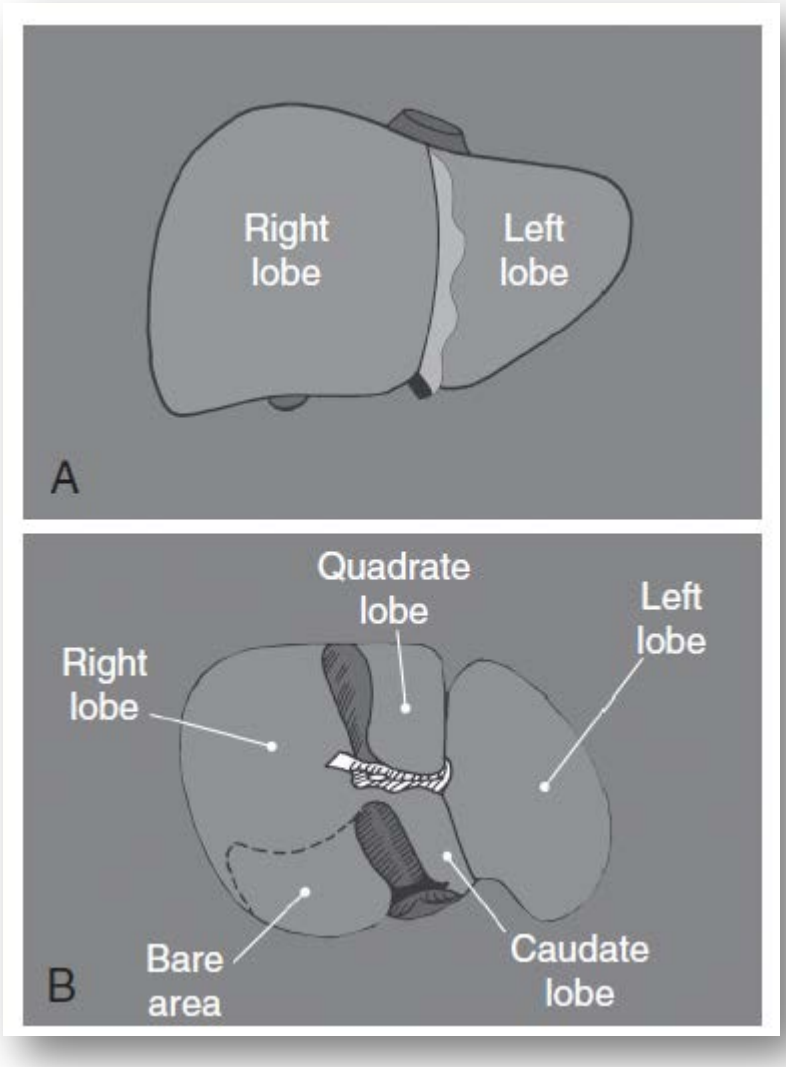

A. Anterior view, B. Posterior view. Reprinted from Transplantation of the Liver (p. 24) by Ronald W. Busuttil, Goran B. Klintmalm, 2014, Philadelphia, PA, Elsevier. Copyright 2015 by the Elsevier. Adapted with permission.

Figure 1-2: Couinaud Liver Physiological Anatomy

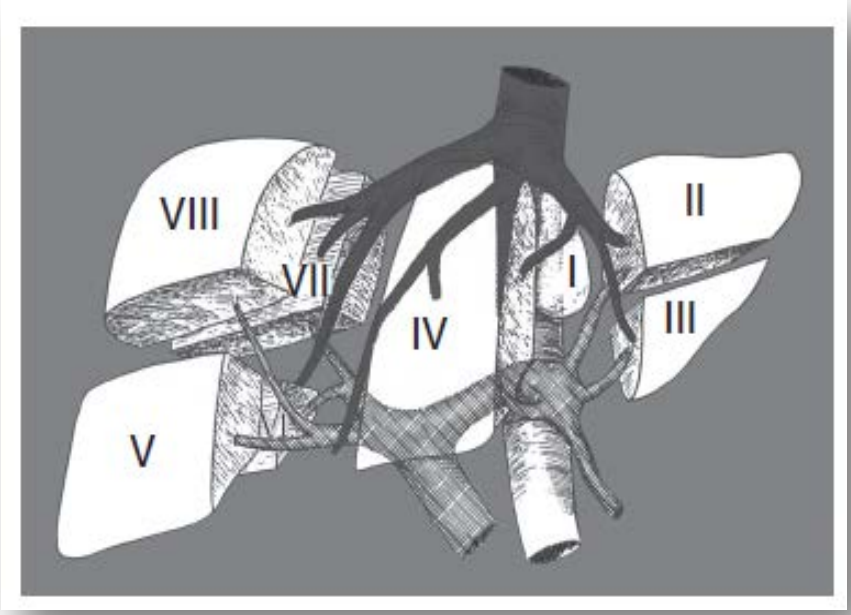

Roman Numerals refer to the different liver segments. Light gray is the portal pedicle, while the dark gray is the hepatic vein. Reprinted from Transplantation of the Liver (p. 25) by Ronald W. Busuttil, Goran B. Klintmalm, 2014, Philadelphia, PA, Elsevier. Copyright 2015 by the Elsevier. Adapted with permission.

Figure 1-3: The Portal Vein and its Tributaries

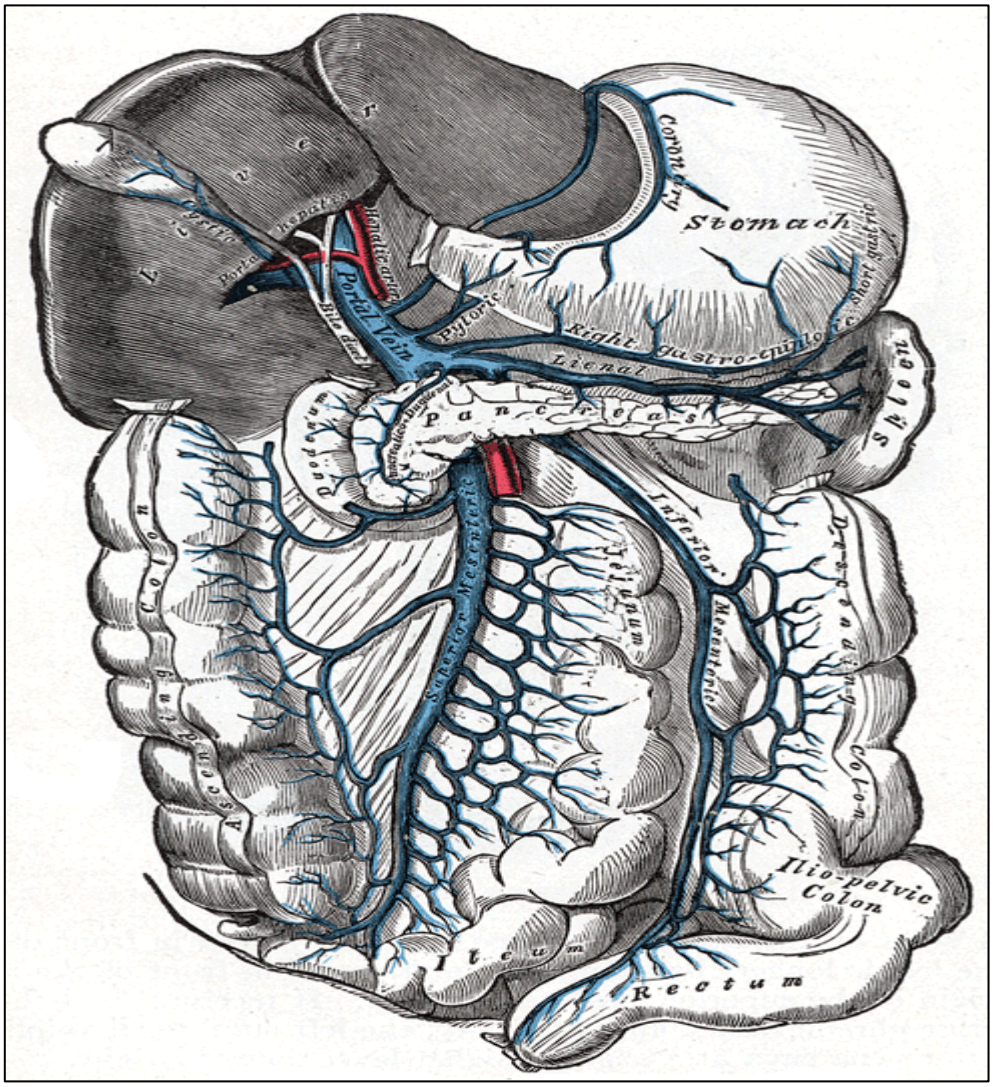

From Gray's Anatomy; the 1918. Copyright has expired, and thus the image is in the public domain.

Figure 1-4: Depiction of the Liver Sinusoid

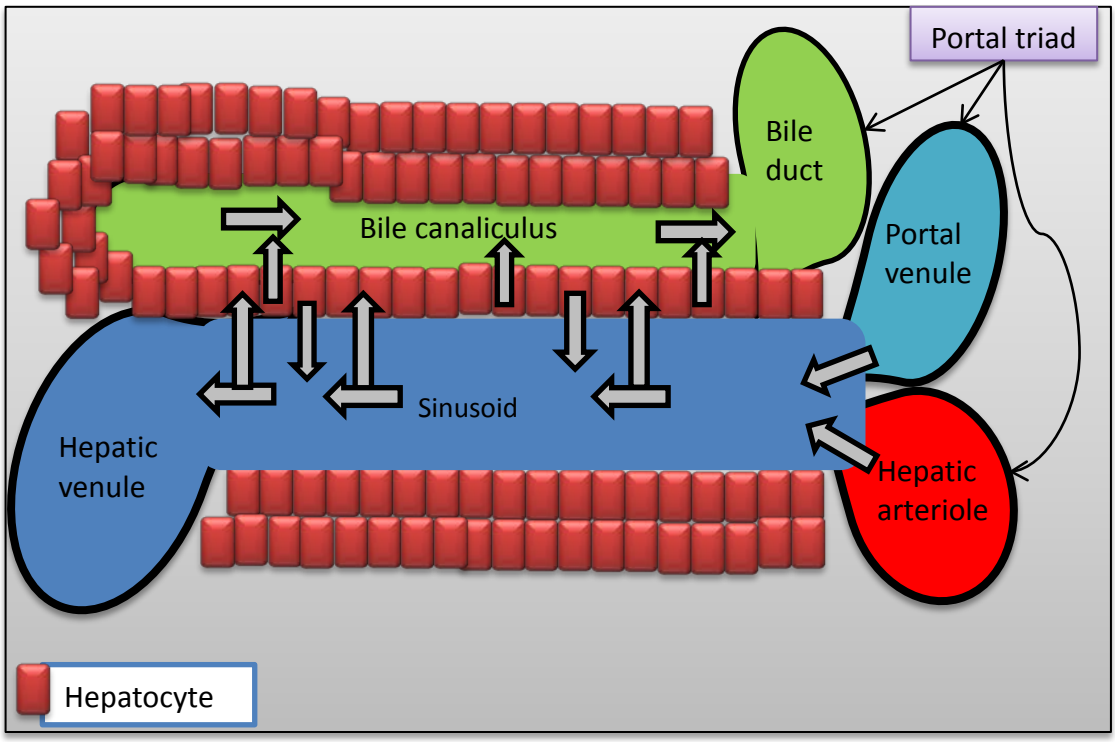

This figure shows a schematic presentation of the liver sinusoid. Arrows represent the possible pathway and flow of drug molecules in the liver sinusoid. Draining from the portal venule and hepatic arteriole, drug molecules pass through the sinusoid. Drug molecules may then transfer to the hepatocytes at which metabolism may occur. Drug and metabolites may go back to the sinusoid and then drain via the hepatic venule, or transport to the bile canaliculus and then to the bile duct.

Figure 1-5: The Liver and the Biliary System

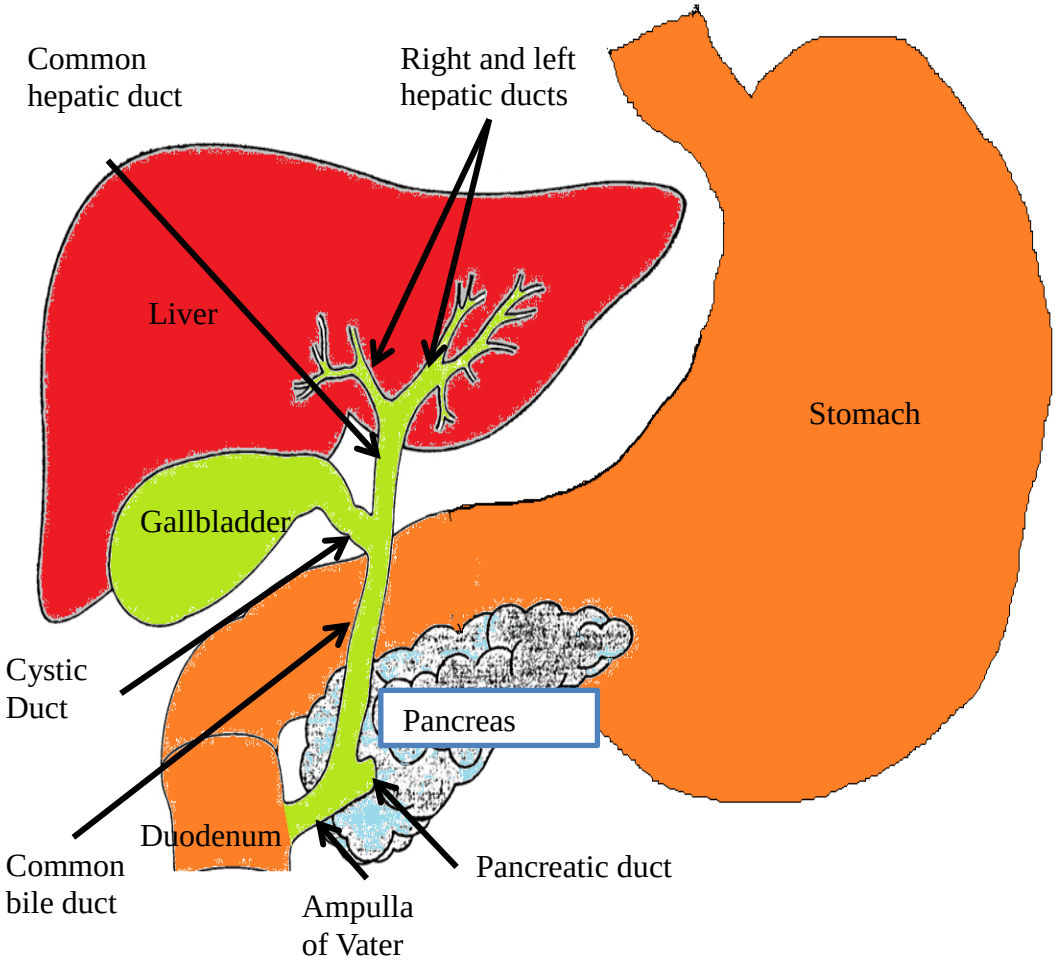

Modified from: https://catalog.niddk.nih.gov/imagelibrary/detail.cfm?id=134

Figure 1-6: Microscopic Anatomy of Liver

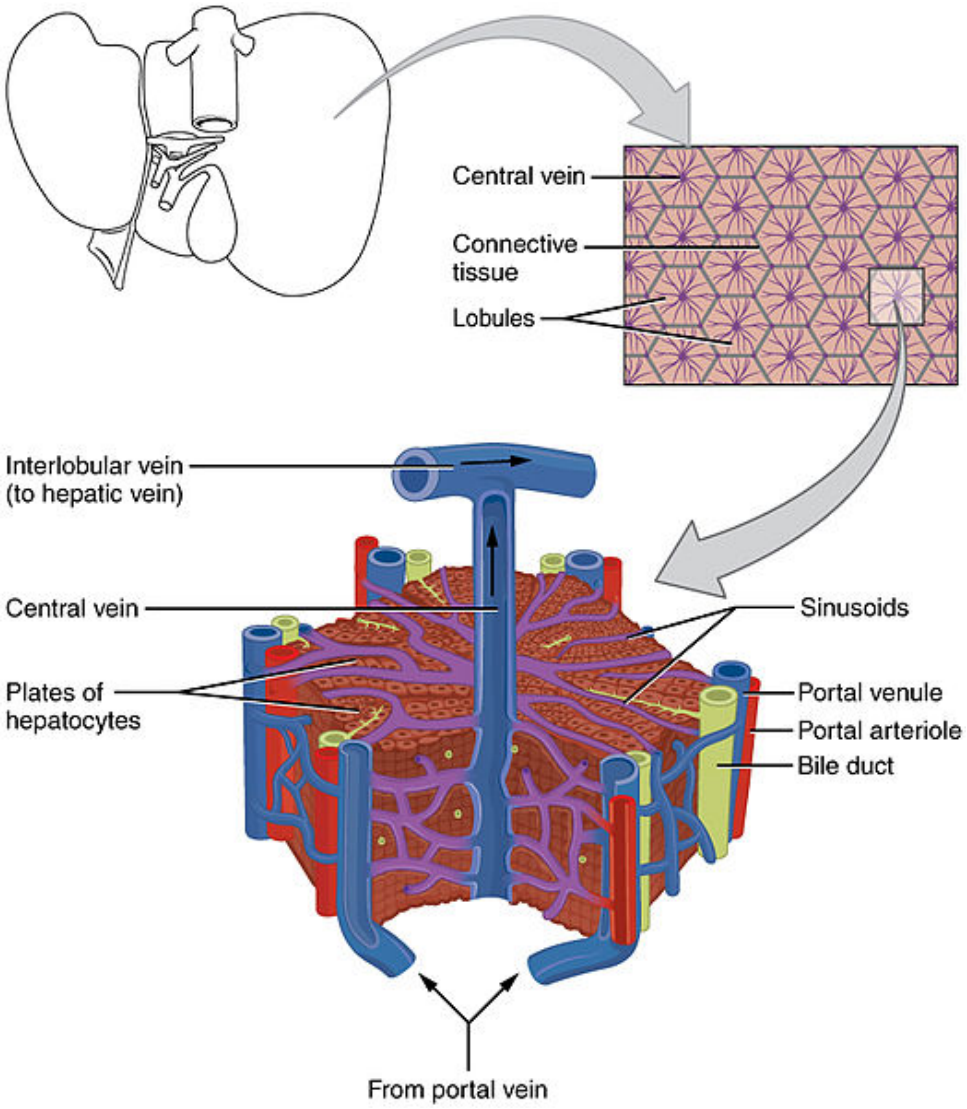

From Wikipedia: Illustration from Anatomy & Physiology, Connexions Website. http://cnx.org/content/col11496/1.6/, Jun 19, 2013.

Figure 1-7: Harrison and Gibaldi Simple Two-Compartment Model

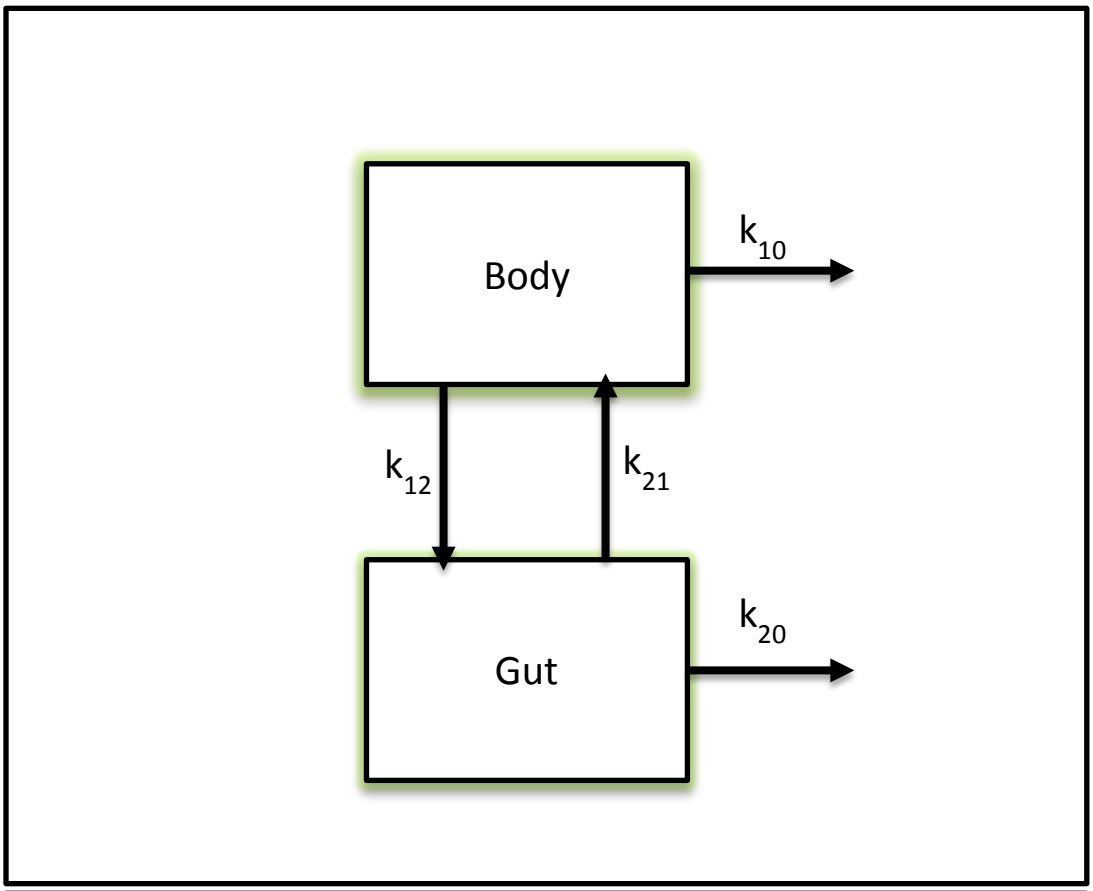

Key:

- **Compartments;** Body: body compartment, Gut: gut compartment
- **Rate constants;** k_{12}: biliary secretion, k_{21}: gut conjugation and subsequent reabsorption, k_{10}: renal elimination, k_{20}: fecal elimination.

Reference: Harrison LI, Gibaldi M. Influence of cholestasis on drug elimination: Pharmacokinetics. Journal of pharmaceutical sciences. 1976;65 (9):1346-8

Figure 1-8: Rate Constant Functions

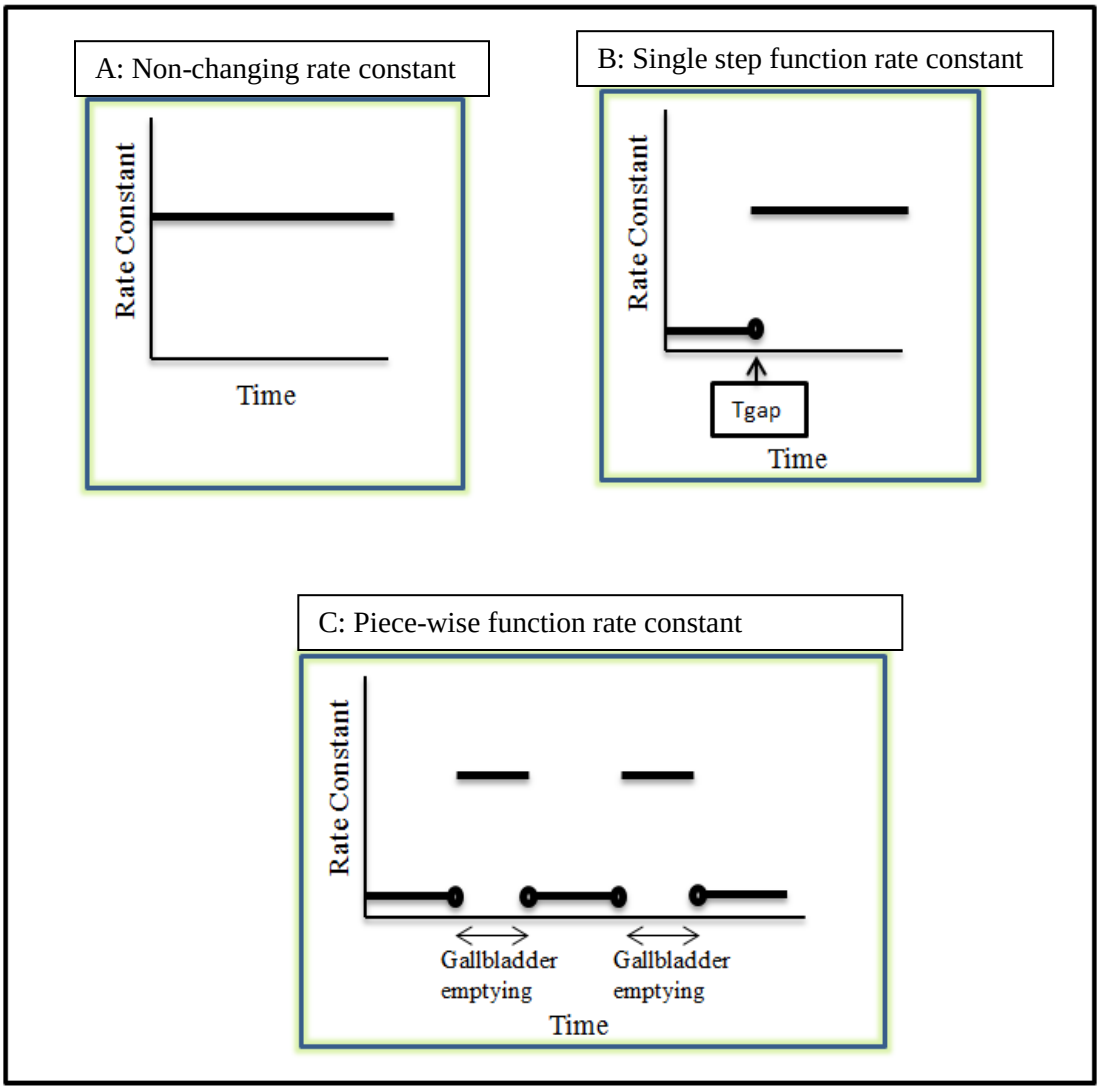

This figure shows several functions that have been used in literature to describe the rate constant representing gallbladder emptying. **A**: applies to simple two-compartment and continuous release models; **B**: applies to Tgap and single bolus release models; while **C**: applies to switch function release models.

Figure 1-9: Steimer et al Tgap-Based Compartmental Model

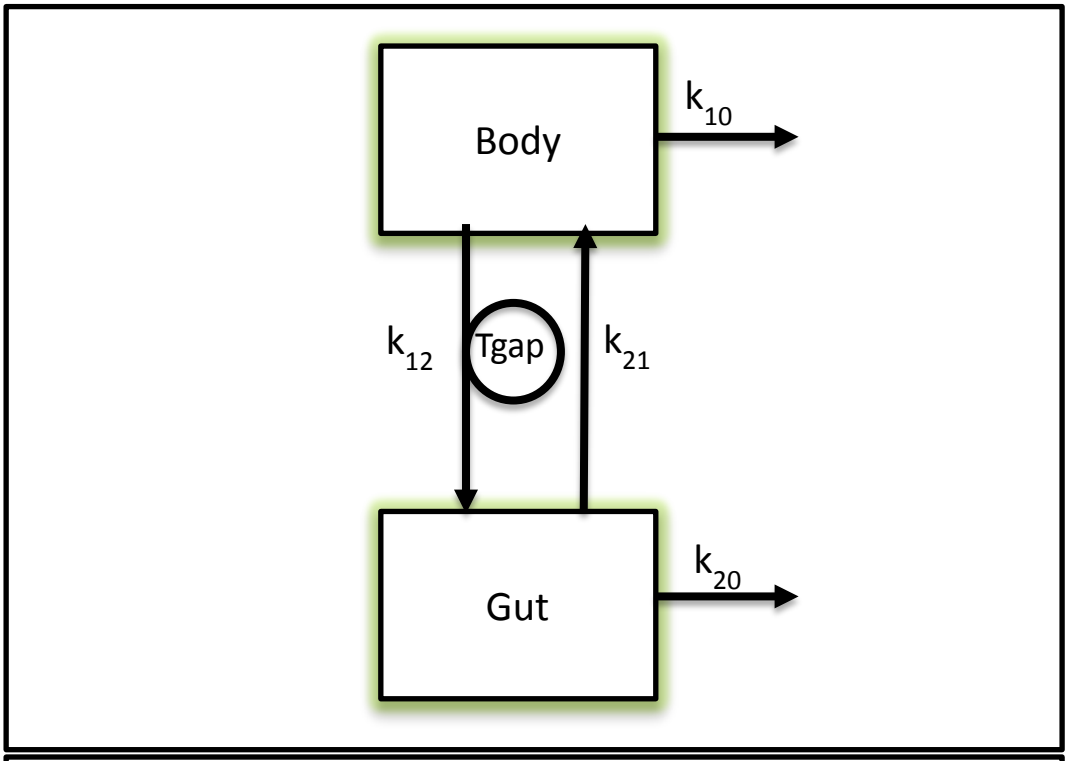

Key:

- **Compartments;** Body: body compartment, Gut: gut compartment
- **Rate constants;** k_{12}: biliary secretion, k_{21}: gut conjugation and subsequent reabsorption, k_{10}: renal elimination, k_{20}: fecal elimination, Tgap: a continuous lag time in drug reabsorption.

Reference: Steimer JL, Plusquellec Y, Guillaume A, Boisvieux JF. A time-lag model for pharmacokinetics of drugs subject to enterohepatic circulation. Journal of pharmaceutical sciences. 1982;71(3):297-302.

Figure 1-10: Colburn et al Tgap-Based Compartmental Model, 1979

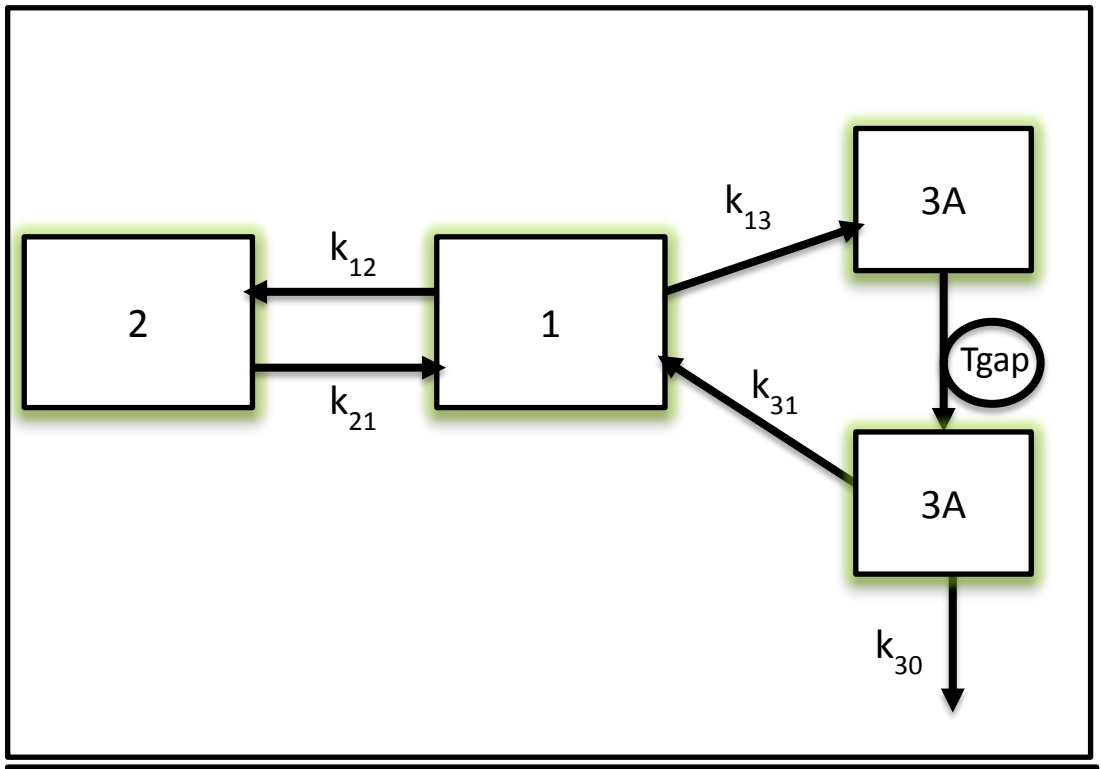

Key:

- **Compartments**: 1: blood and quickly equilibrating tissues, 2: slowly equilibrating tissues, 3A and 3B: intestinal compartments.
- **Rate constants:** k_{12} and k_{21} : intercompartmental transfer rate constants, k_{13}: biliary secretion, k_{31}: gut deconjugation and subsequent reabsorption, k_{30}: fecal elimination

Reference: Colburn WA, Hirom P, Parker RJ, Milburn P. A pharmacokinetic model for enterohepatic recirculation in the rat: phenolphthalein, a model drug. Drug Metabolism and Disposition. 1979;7(2):100-2.

Figure 1-11: Colburn et al Continuous Release Model, 1982

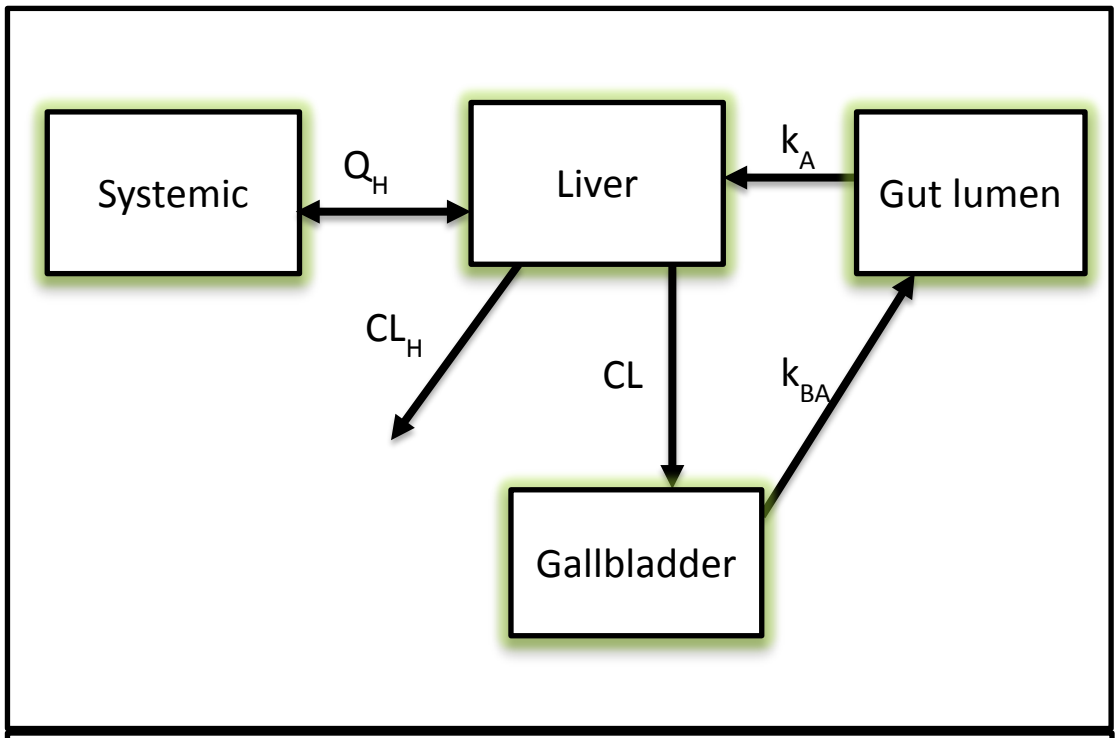

Key:

- **Compartments**: Systemic: represents the body, Liver: liver compartment, Gut lumen: intestinal compartment, Gallbladder: represents the gallbladder.
- **Rate constants and parameters**: Q_H: hepatic blood flow, CL_H : irreversible hepatic organ clearance, CL_{HR} : recirculating hepatic organ clearance, k_A : absorption rate constant, k_{BA} : gallbladder emptying process.

Reference: Colburn WA. Pharmacokinetic and biopharmaceutic parameters during enterohepatic circulation of drugs. Journal of pharmaceutical sciences. 1982;71(1):131-3

Figure 1-12: Veng Pedersen and Miller Single Bolus Release Models of Doxycycline

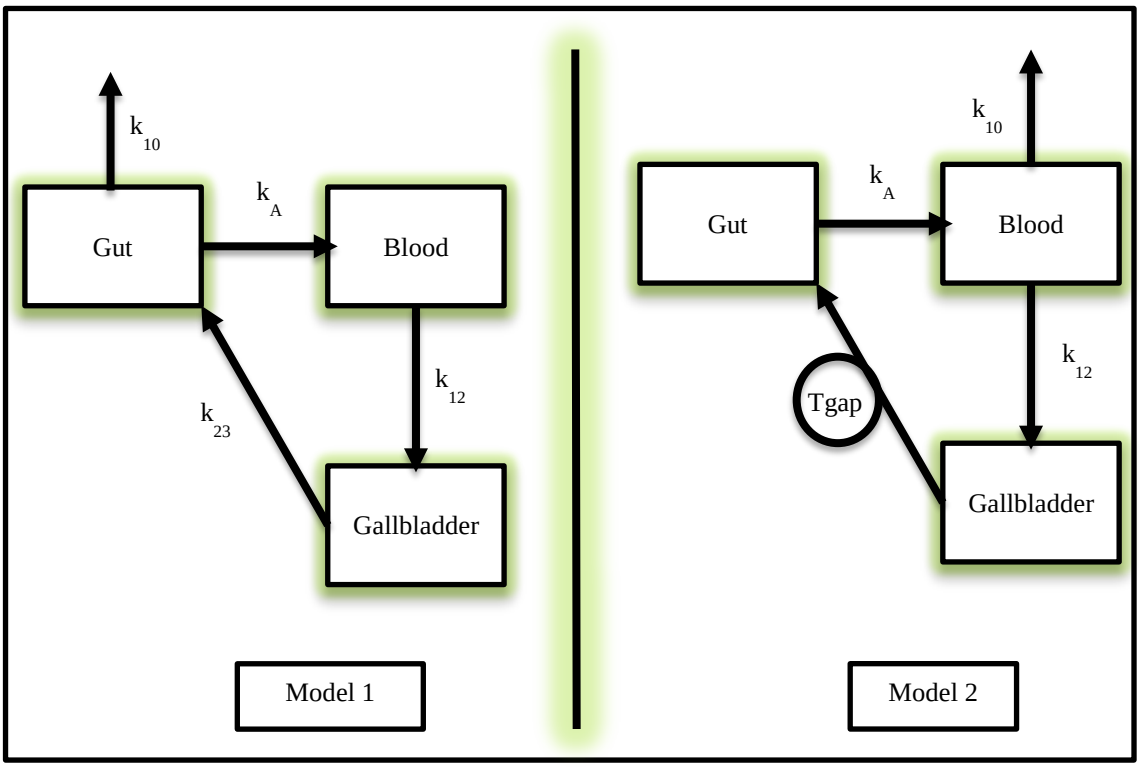

Key:

- **Compartments**: Blood: represents the blood, Gallbladder: intermediate compartment representing the gallbladder, Gut: intestinal compartment
- **Rate constants and parameters:** k_A : absorption rate constant , k_{10} : elimination rate constant , k_{23} : reabsorption rate constant , k_{12}: represents the biliary elimination.

Reference: Pedersen PV, Miller R. Pharmacokinetics of doxycycline reabsorption. Journal of pharmaceutical sciences. 1980;69(2):204-7.

Figure 1-13: Veng Pedersen and Miller Single Bolus Release Model of Cimetidine

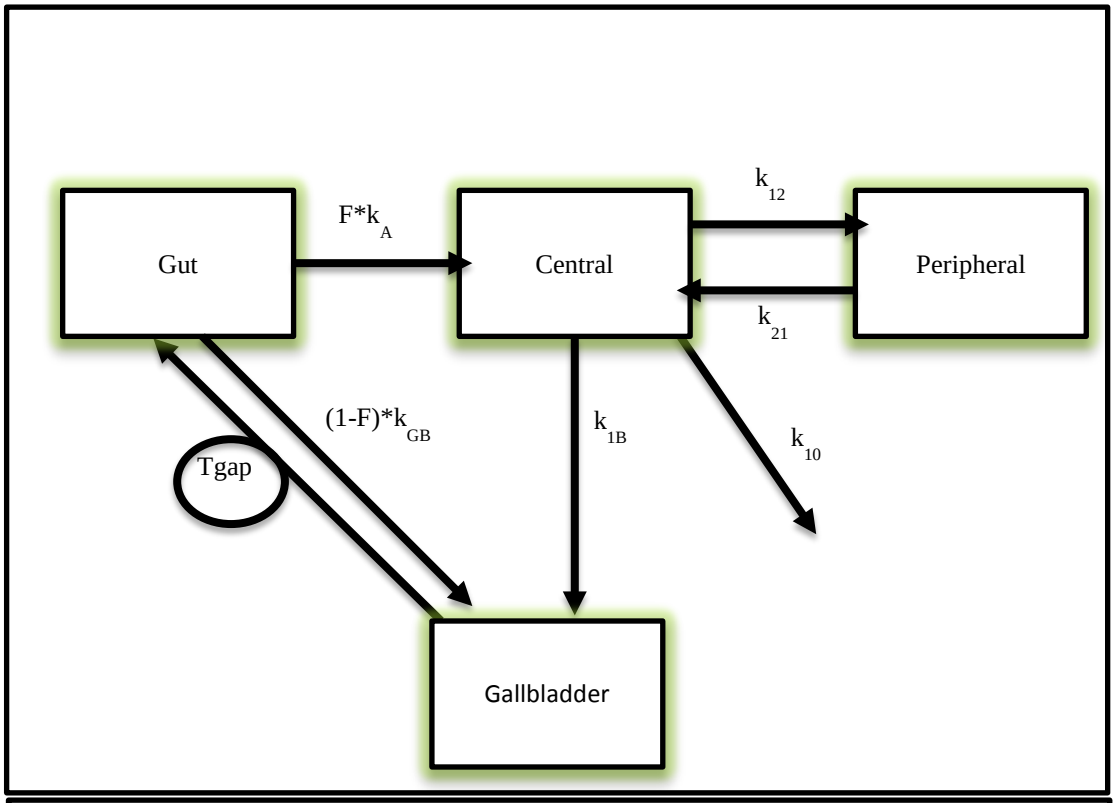

Key:

- **Compartments**: Central: central compartment representing the blood, Peripheral: peripheral compartment, Gut : gut compartment , Gallbladder: the gallbladder compartment
- **Rate constants and parameters:** k_A : absorption rate constant , k_{10} : elimination rate constant , k_{1B} : biliary secretion rate constant , k_{12} and k_{21} : intercompartmental transfer rate constants, k_{GB} : transfer rate constant representing the first pass effect via the portal circulation.

Reference: Pedersen PV, Miller R. Pharmacokinetics and bioavailability of cimetidine in humans. Journal of pharmaceutical sciences. 1980;69(4):394-8

Figure 1-14: Strandgården et al Single Bolus Release Model

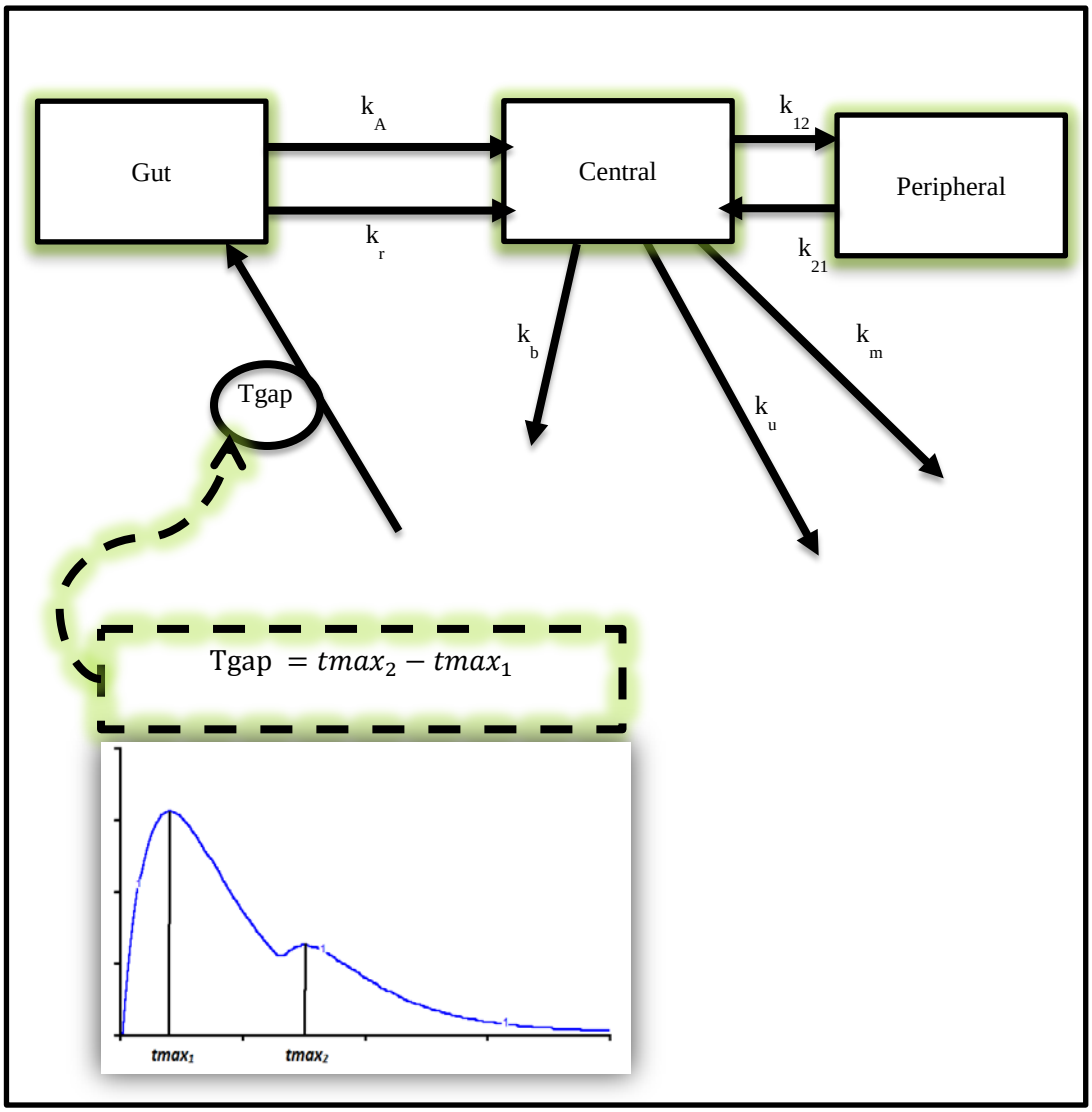

Key:

- **Compartments**: Central: central compartment representing the blood, 2: peripheral compartment , B : gallbladder compartment , A: gut compartment
- **Rate constants and parameters:** k_A : absorption rate constant , k_r : reabsorption rate constant , k_{20} : fecal elimination, k_{12} and k_{21} : intercompartmental transfer rate constants, k_b : biliary secretion of drug, k_u : urinary excretion of drug, k_m : urinary and fecal excretion rate constant of metabolites.

Reference: Strandgården K, Höglund P, Grönquist L, Svensson L, Olov Gunnarsson P. Absorption and disposition including enterohepatic circulation of (14C) roquinimex after oral administration to healthy volunteers. Biopharmaceutics & drug disposition. 2000;21(2):53-67.

Figure 1-15: Ide et al Single Bolus Release Model

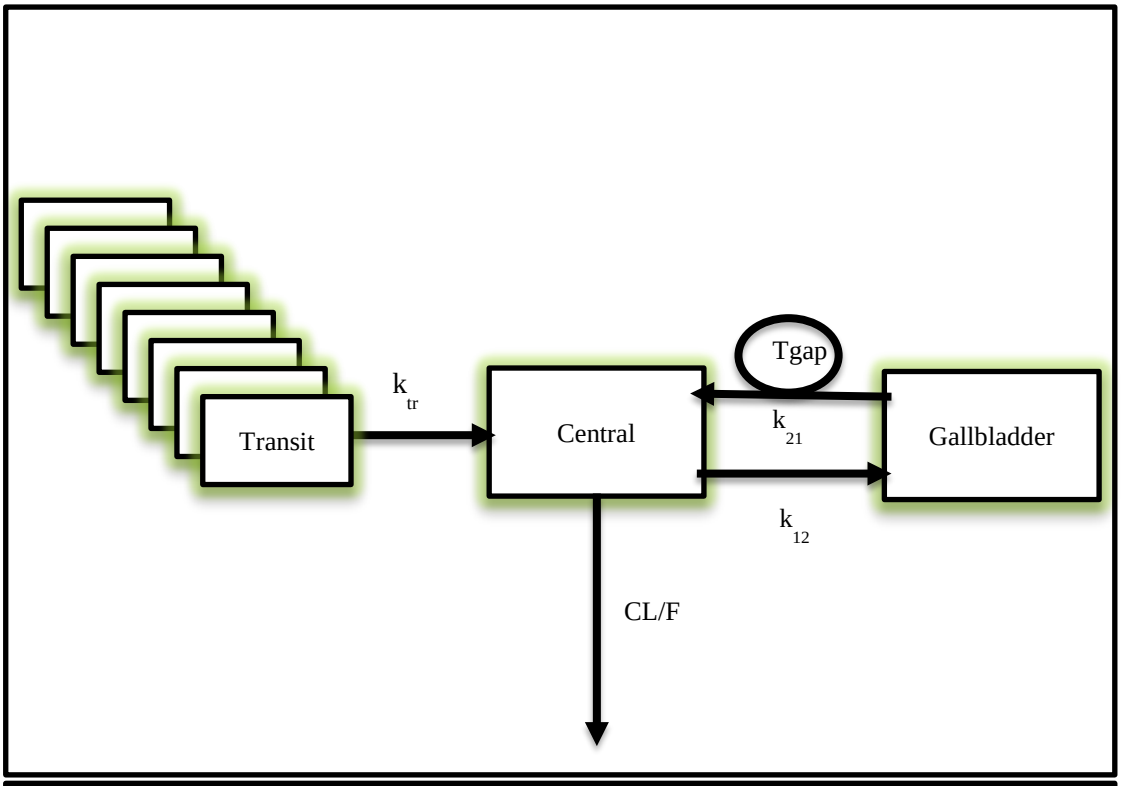

Key:

- **Compartments**: Central: central compartment representing the blood, Gallbladder : gallbladder compartment, transit: transit absorption compartments
- **Rate constants and parameters:** k_{tr} : transit absorption model rate constant rate constant , k_r : re-absorption rate constant , k_{21} : biliary secretion rate constant, k_{21} : gallbladder emptying rate constant, CL/F: apparent clearance

Reference: Ide T, Sasaki T, Maeda K, Higuchi S, Sugiyama Y, Ieiri I. Quantitative population pharmacokinetic analysis of pravastatin using an enterohepatic circulation model combined with pharmacogenomic information on SLCO1B1 and ABCC2 polymorphisms. The Journal of Clinical Pharmacology. 2009;49(11):1309-17.

Figure 1-16: Jiao et al Switch Function Release Model

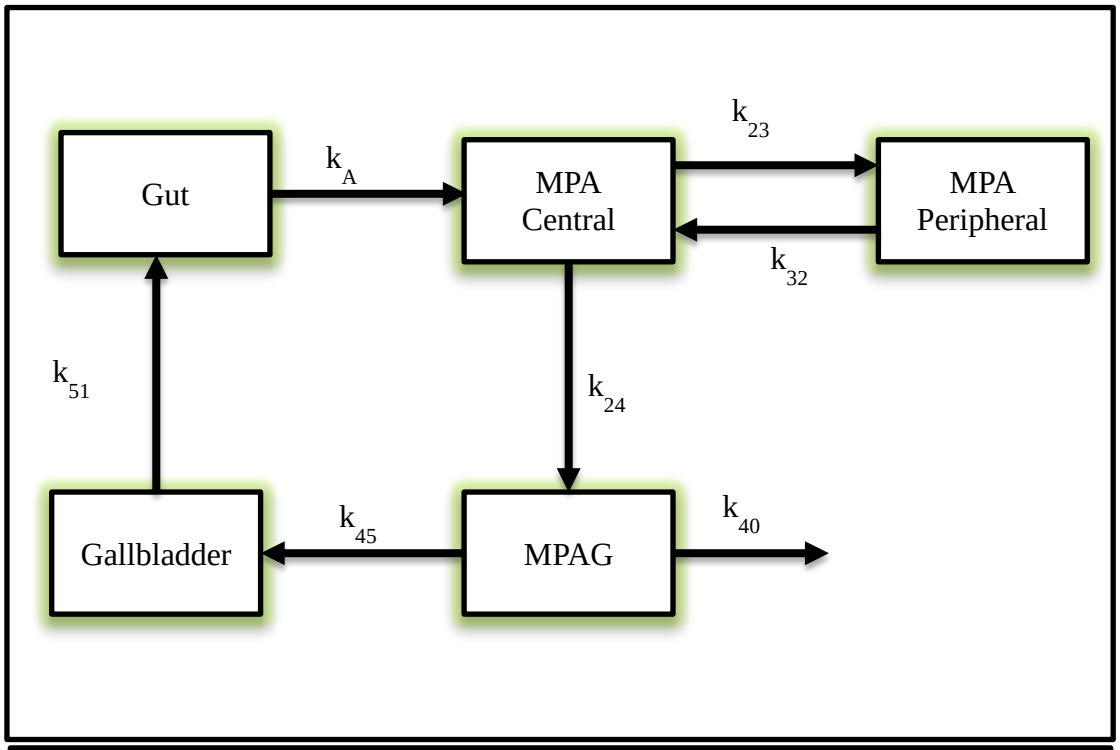

Key:

- **Compartments**: Gut: gut compartment, MPA central: central compartment for MPA, MPA peripheral: peripheral compartment for MPA, Gallbladder: represents the gallbladder, MPAG: MPAG metabolite compartment
- **Rate constants and parameters:** k_A : absorption rate constant, k_{23} and k_{32}: intercompartmental rate constants, k_{24}: MPA metabolism to MPAG rate constant, k_{40}: MPAG renal elimination rate constant, k_{45}: MPAG enterohepatic circulation rate constant and represents the biliary secretion process, k_{51}: gallbladder emptying rate constant.

Reference: Jiao Z, Ding Jj, Shen J, Liang Hq, Zhong Lj, Wang Y, et al. Population pharmacokinetic modelling for enterohepatic circulation of mycophenolic acid in healthy Chinese and the influence of polymorphisms in UGT1A9. British journal of clinical pharmacology. 2008;65(6):893-907

Figure 1-17: Sam et al Switch Function Release Model

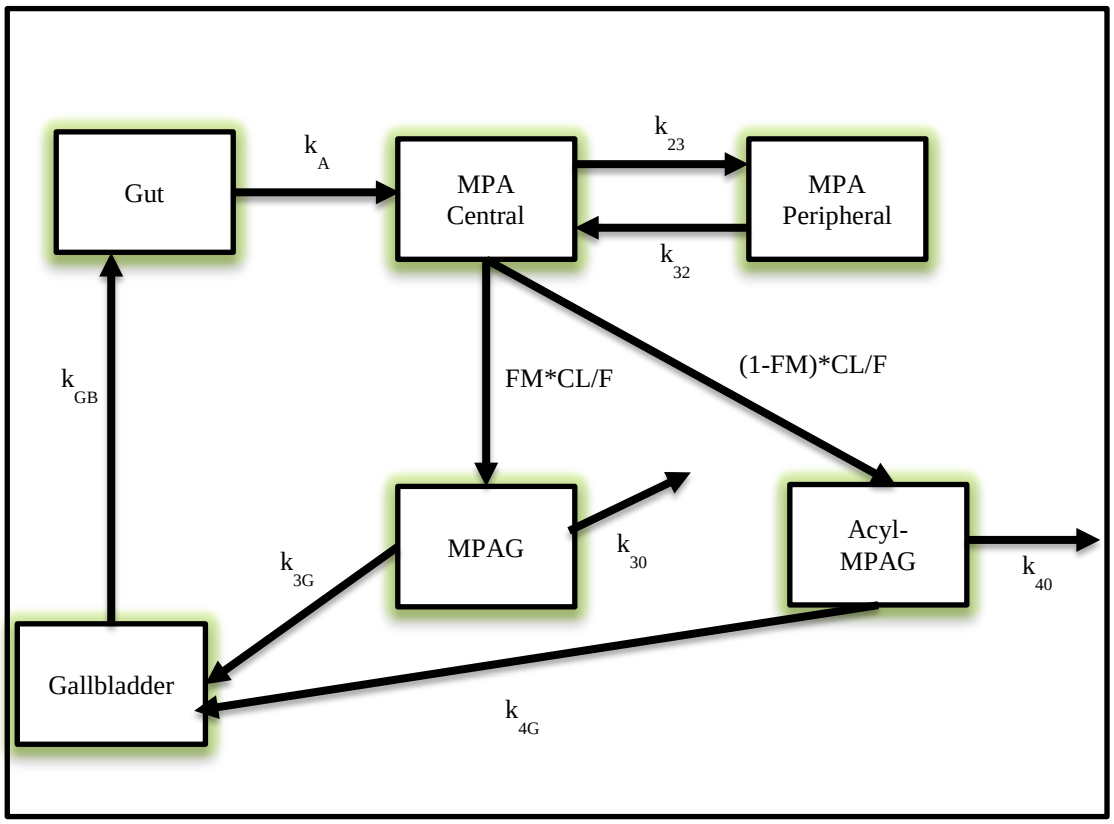

Key:

- **Compartments**: Gut: gut compartment, MPA central: central compartment for MPA, MPA peripheral: peripheral compartment for MPA, Gallbladder: represents the gallbladder, MPAG: MPAG metabolite compartment, acyl-MPAG: acyl-MPAG metabolite compartment
- **Rate constants and parameters:** k_A : absorption rate constant, k_{23} and k_{32}: intercompartmental rate constants, CL: MPA clearance, F: bioavailability, FM: fraction of MPA metabolized to MPAG, K_{20}: MPAG elimination rate constant, k_{40}: acyl-MPAG elimination rate constant, k_{3G} and k_{3G}: MPAG and acyl-MPAG biliary secretion rate constants, respectively, k_{GB}: gallbladder emptying rate constant

Reference: Sam WJ, Akhlaghi F, Rosenbaum SE. Population pharmacokinetics of mycophenolic acid and its 2 glucuronidated metabolites in kidney transplant recipients. The Journal of Clinical Pharmacology. 2009;49(2):185-95

Figure 1-18: de Winter et al Switch Function Release Model

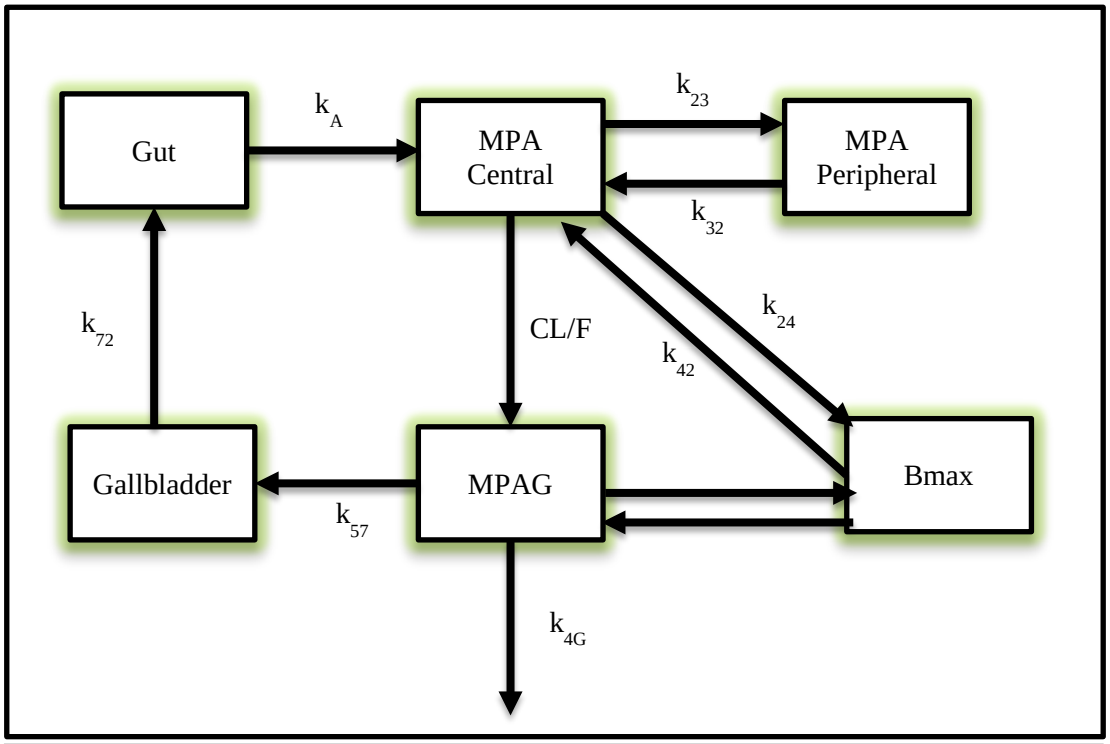

Key:

- **Compartments**: Gut: gut compartment, MPA central: central compartment for MPA, MPA peripheral: peripheral compartment for MPA, Gallbladder: represents the gallbladder, MPAG: MPAG metabolite compartment, Bmax: represents protein binding
- **Rate constants and parameters:** k_A : absorption rate constant, k_{23} and k_{32}: intercompartmental rate constants, CL: MPA clearance, F: bioavailability, K_{4G}: MPAG elimination rate constant, k_{57}: MPAG biliary secretion rate constants, k_{72}: gallbladder emptying rate constant, k_{24} and k_{42}: MPA protein binding and unbinding rate constants respectively, k_{56} and k_{65}: MPAG protein binding and unbinding rate constants.

Reference: de Winter BC, van Gelder T, Sombogaard F, Shaw LM, van Hest RM, Mathot RA. Pharmacokinetic role of protein binding of mycophenolic acid and its glucuronide metabolite in renal transplant recipients. Journal of pharmacokinetics and pharmacodynamics. 2009;36(6):541-64.

Figure 1-19: Berg et al Switch Function Release Model

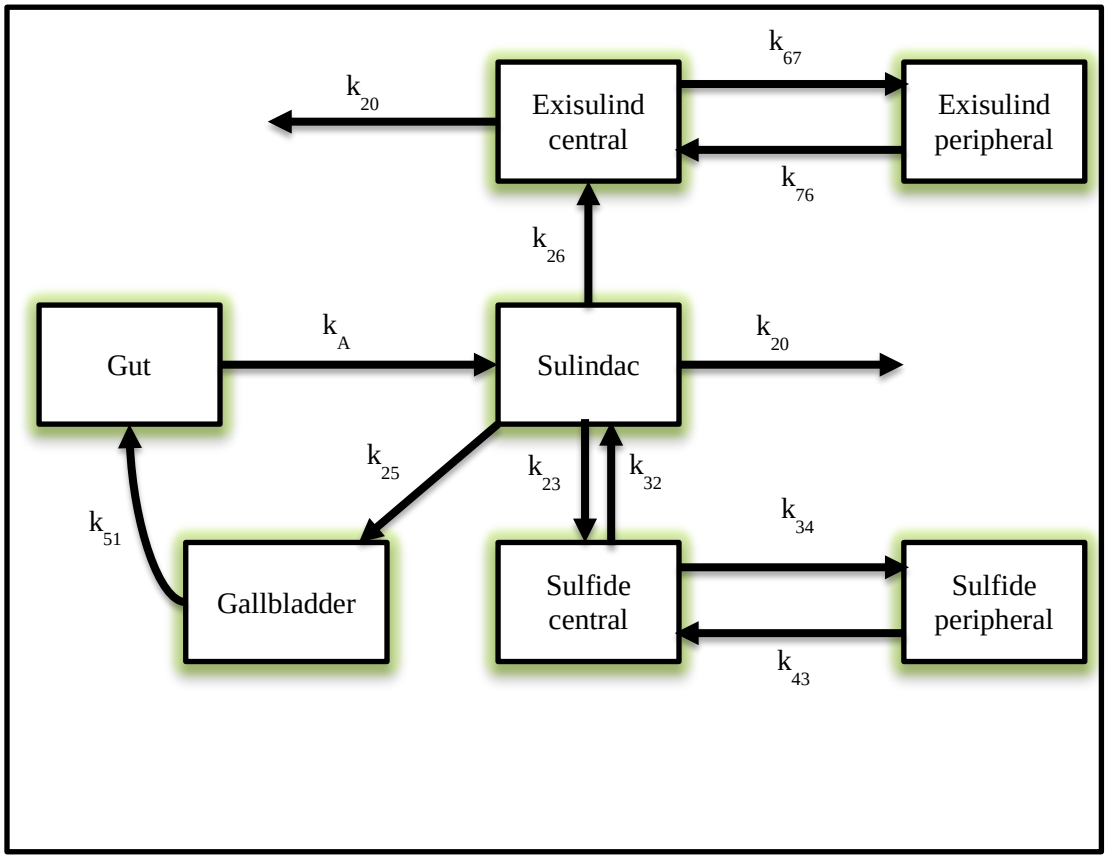

Key:

- **Compartments**: Sulindac : Sulindac compartment, Sulfide central: sulindac sulfide central compartment, Sulfide peripheral: sulindac sulfide peripheral compartment, Exisulind central : sulindac sulfone (exisulind) central compartment, Exisulind peripheral: sulindac sulfone (exisulind) peripheral compartment, gut: gut compartment, Gallbladder: gallbladder compartment
- **Rate constants and parameters:** k_{23} : formation rate constant of Sulfide, k_{32} : the reversible formation of Sulindac from Sulfide, k_{26} : formation rate constant of Exisulind, k_{20} : Sulindac elimination rate constant, k_{20} : Exisulind elimination rate constant, k_{25} :biliary excretion rate constant of Sulindac, k_{51} : bile secretion rate constant from the gallbladder to the gut, k_A :absorption rate constant , k_{34} and k_{43} :intercompartmental transfer rate constants of Sulfide, k_{67} and k_{76} : intercompartmental transfer rate constants of Exisulind.

Source: Berg AK, Mandrekar SJ, Ziegler KLA, Carlson EC, Szabo E, Ames MM, et al. Population pharmacokinetic model for cancer chemoprevention with sulindac in healthy subjects. The Journal of Clinical Pharmacology. 2013;53(4):403-12.

Figure 1-20: Rosner et al Switch Function Release Model

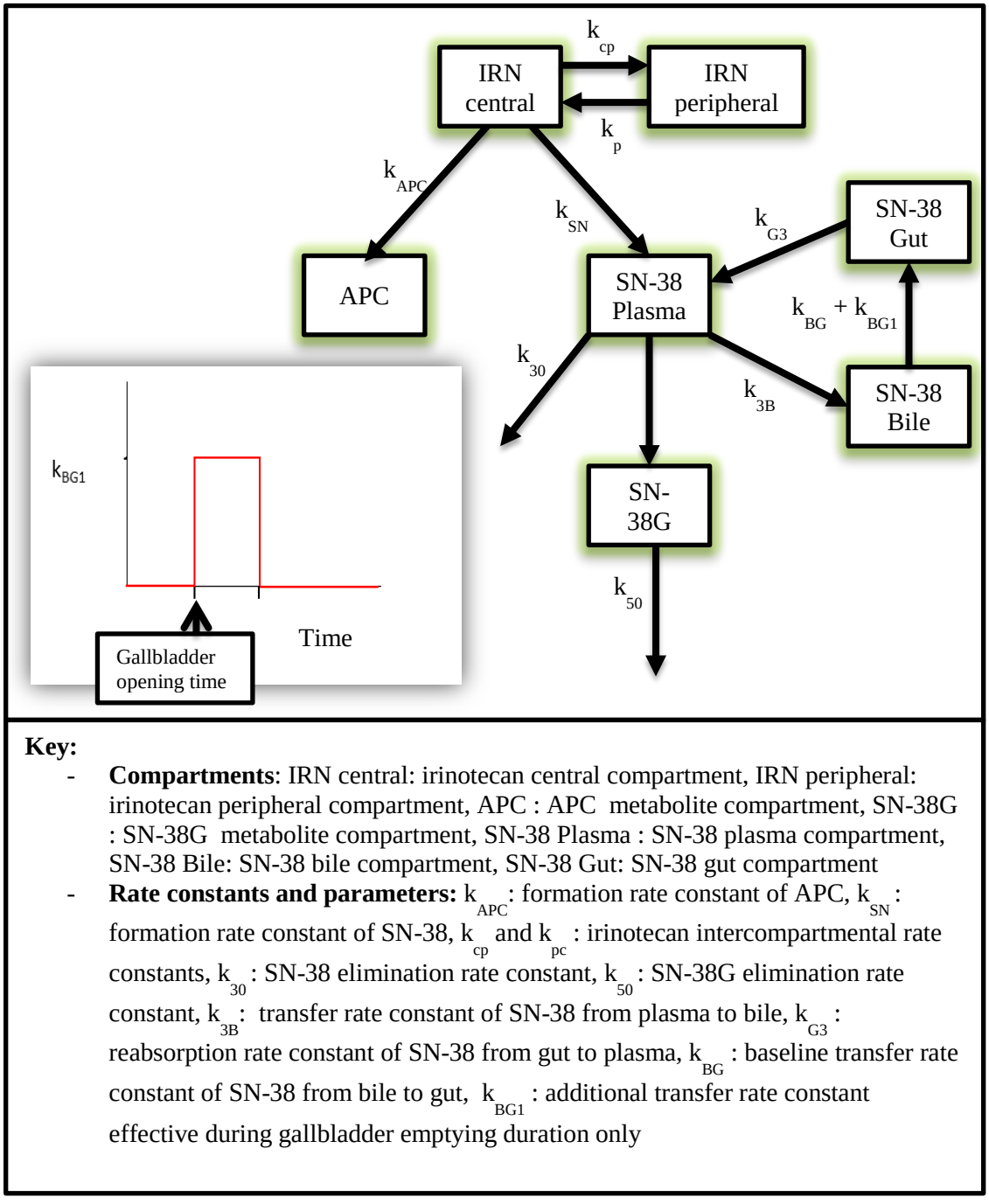

Key:

- **Compartments**: IRN central: irinotecan central compartment, IRN peripheral: irinotecan peripheral compartment, APC : APC metabolite compartment, SN-38G : SN-38G metabolite compartment, SN-38 Plasma : SN-38 plasma compartment, SN-38 Bile: SN-38 bile compartment, SN-38 Gut: SN-38 gut compartment
- **Rate constants and parameters:** k_{APC}: formation rate constant of APC, k_{SN} : formation rate constant of SN-38, k_{cp} and k_{pc} : irinotecan intercompartmental rate constants, k_{30} : SN-38 elimination rate constant, k_{50} : SN-38G elimination rate constant, k_{3B} : transfer rate constant of SN-38 from plasma to bile, k_{G3} : reabsorption rate constant of SN-38 from gut to plasma, k_{BG} : baseline transfer rate constant of SN-38 from bile to gut, k_{BG1} : additional transfer rate constant effective during gallbladder emptying duration only

Reference: Rosner GL, Panetta J, Innocenti F, Ratain M. Pharmacogenetic pathway analysis of irinotecan. Clinical Pharmacology & Therapeutics. 2008;84(3):393-402.

Figure 1-21: Shepard et al Switch Function Release Model

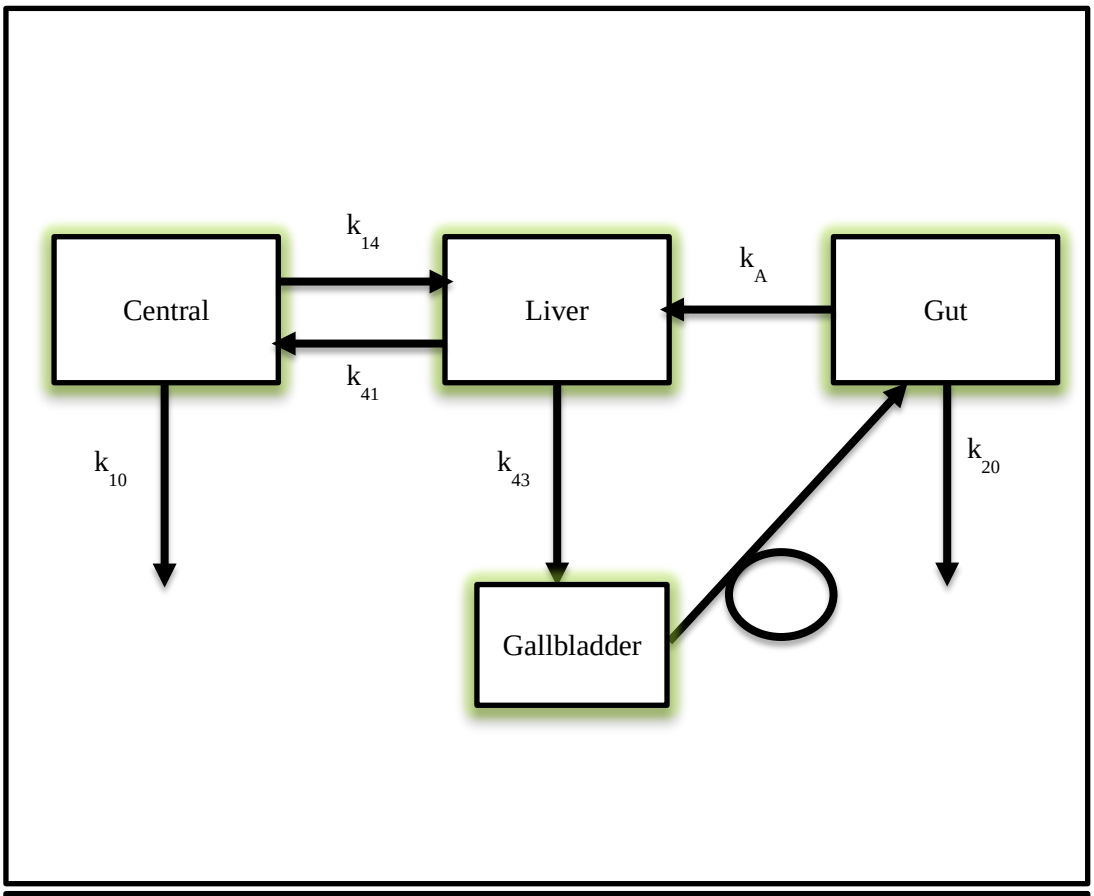

Key:

- **Compartments**: Central: central compartment representing the blood, Gut: the gut , Gallbladder : the gallbladder compartment , Liver: the liver compartment
- **Rate constants and parameters:** k_A : absorption rate constant , k_{10}: nonbiliary elimination rate constant , k_{20} : fecal elimination, k_{14} and k_{14} : represent the drug transfer from and to the liver from the systemic circulation, k_{43} : biliary secretion rate constant

Reference: Shepard TA, Reuning RH, Aarons LJ. Estimation of area under the curve for drugs subject to enterohepatic cycling. Journal of pharmacokinetics and biopharmaceutics. 1985;13(6):589-608.

Figure 1-22: Jain et al Sigmoid Function Release Model

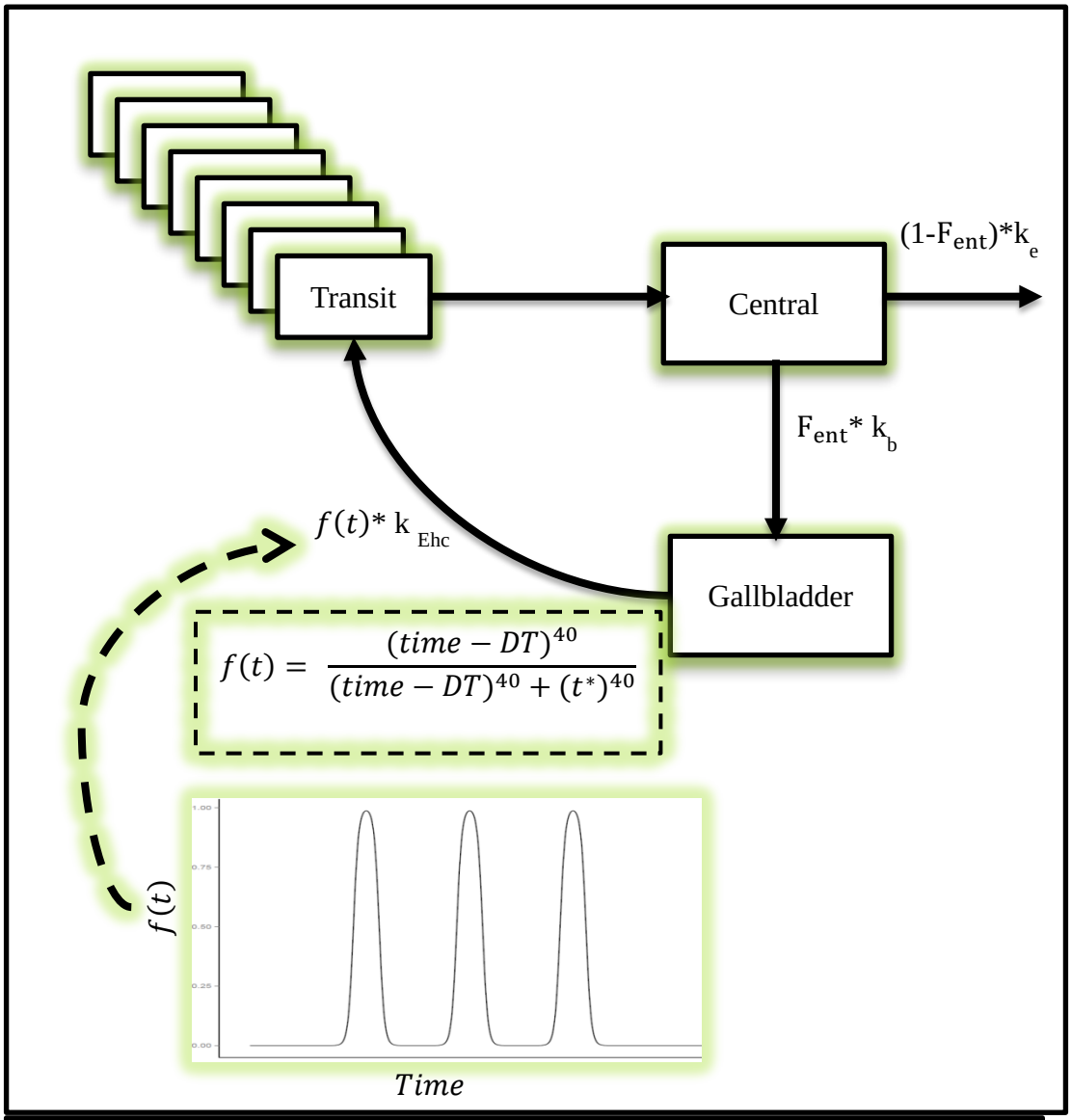

Key:

- **Compartments**: Central: central compartmen, Gallbladder : gallbladder compartment, transit: transit absorption compartments
- **Rate constants and parameters:** k_A : absorption rate constant rate constant , k_r : re-absorption rate constant , k_{21} : biliary secretion rate constant, k_{21} : gallbladder emptying rate constant, CL/F: apparent clearance, F_{ent}: fraction of the dose transfers from the central compartment to the gallbladder compartment.

Reference: Jain L, Woo S, Gardner ER, Dahut WL, Kohn EC, Kummar S, et al. Population pharmacokinetic analysis of sorafenib in patients with solid tumours. British journal of clinical pharmacology. 2011;72(2):294-305.

Figure 1-23: Wajima et al Sine Function Release Model

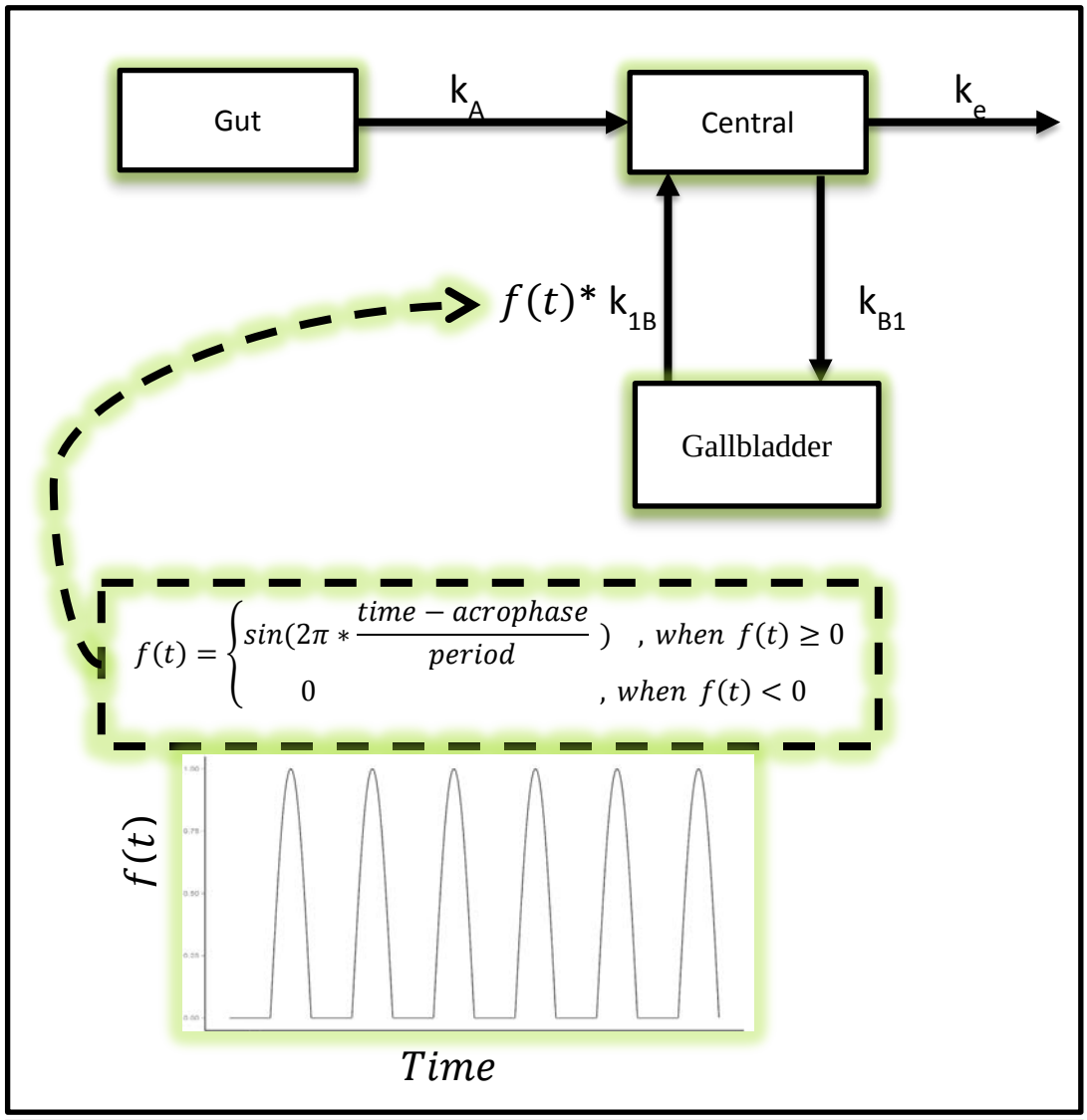

Key:

- **Compartments**: Central : central compartment representing the blood, Gallbladder : gallbladder compartment, Gut: gut compartment
- **Rate constants and parameters:** k_A : absorption rate constant rate constant , k_{B1}: re-absorption rate constant , k_{1B} : biliary secretion rate constant, k_e elimination rate constant.

Reference: Wajima T, Yano Y, Oguma T. A pharmacokinetic model for analysis of drug disposition profiles undergoing enterohepatic circulation. Journal of pharmacy and pharmacology. 2002;54(7):929-34.

Figure 1-24: Huntjens et al Sine Function Release Model

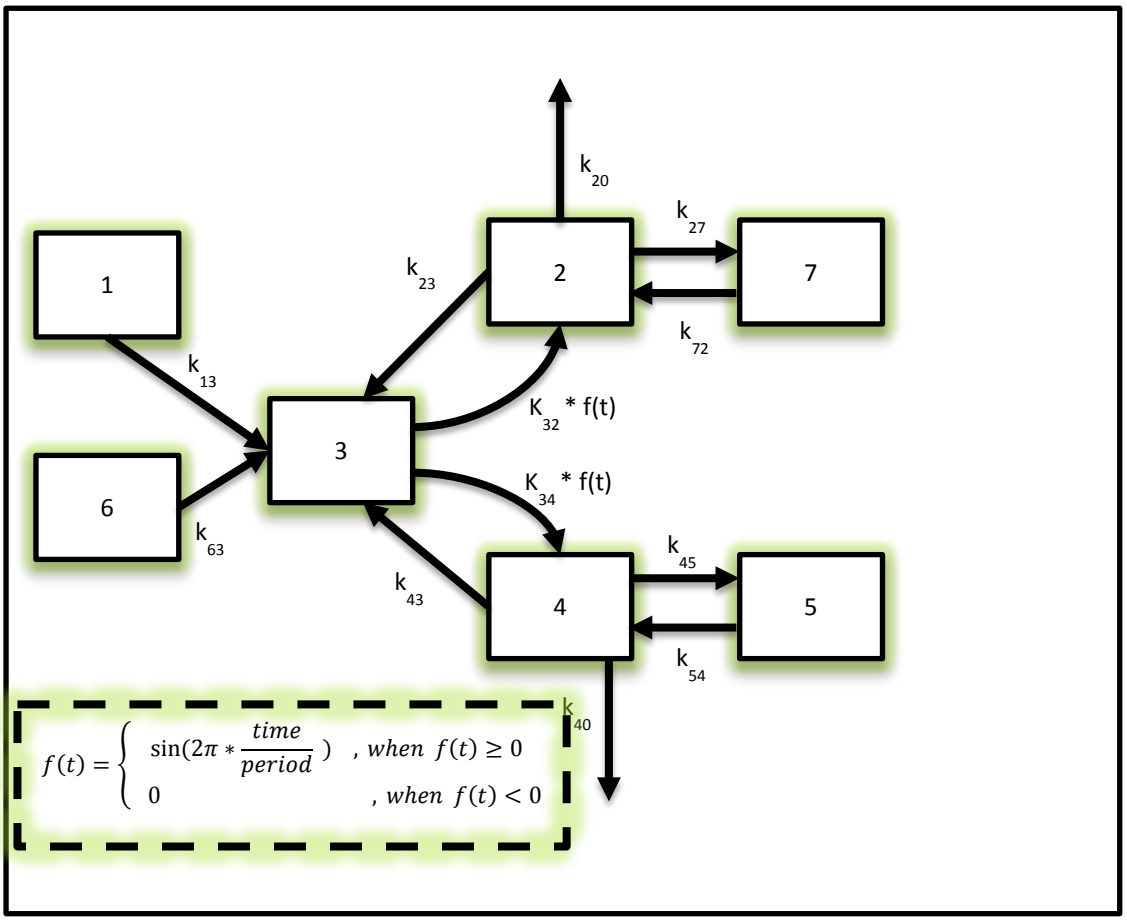

Key:

- **Compartments**: 1: representing gut for oral dosing, 2: diclofenac central compartment,3: EHC compartment, 4: 4-hydroxydiclofenac central compartment, 5 and 7: peripheral compartments for diclofenac and 4-hydroxydiclofenac, respectively, 6: representing administration for intraperitoneal dosing
- **Rate constants and parameters:** k_{13} : oral absorption rate constant , k_{63} : intraperitoneal absorption rate constant , k_{23} : diclofenac biliary excretion , k_{43} : 4-hydroxydiclofenac biliary excretion , k_{27} and k_{72} : diclofenac intercompartmental rate constants, k_{45} and k_{54} : 4-hydroxydiclofenac intercompartmental rate constants, K_{32} and K_{34} : transfer rate constant from EHC compartment to central compartment for diclofenac and 4-hydroxydiclofenac, respectively.

Reference: Huntjens D, Strougo A, Chain A, Metcalf A, Summerfield S, Spalding D, et al. Population pharmacokinetic modelling of the enterohepatic recirculation of diclofenac and rofecoxib in rats. British journal of pharmacology. 2008;153(5):1072-84.

Figure 1-25: Younis et al Model

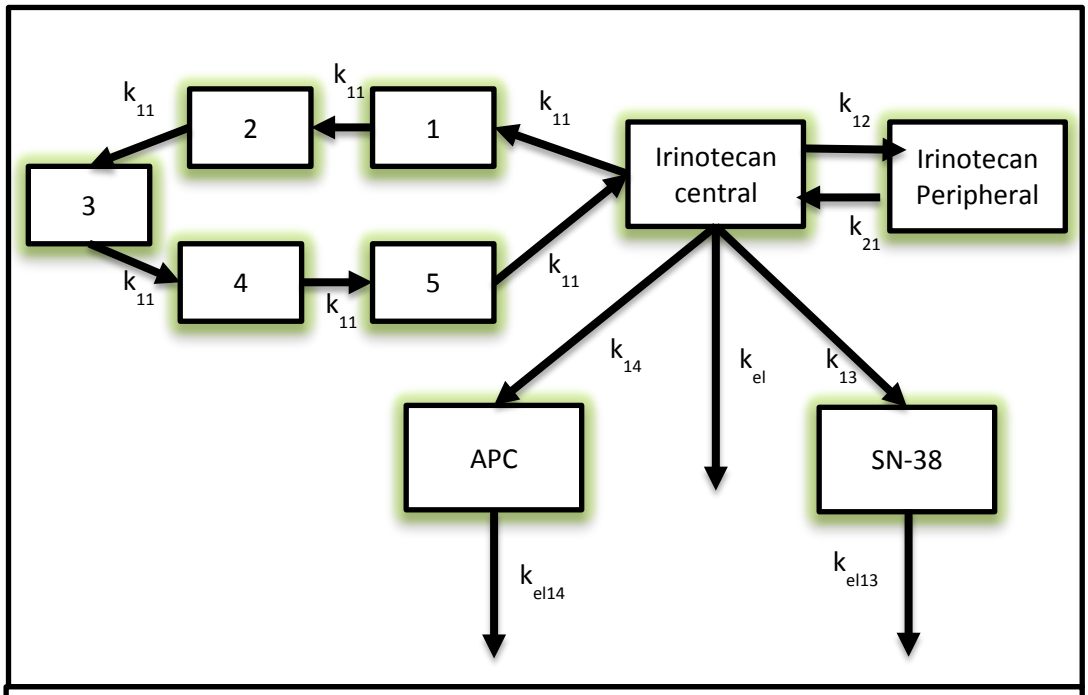

Key:

- **Compartments**: Irinotecan central: irinotecan central compartment, Irinotecan peripheral: irinotecan peripheral compartment, APC : APC metabolite compartment, SN-38 : SN-38 metabolite compartment, 1-5: chain of 5 compartments that take off then get back to the central compartment of irinotecan to represent the EHC process
- **Rate constants and parameters:** k_{14} : formation rate constant of APC, k_{13} : formation rate constant of SN-38, k_{12} and k_{21} : irinotecan intercompartmental rate constants, k_{el} : irinotecan elimination rate constant, k_{el14} : APC elimination rate constant, k_{el13} : SN-38 elimination rate constant, k_{11} : transfer rate constant between the recirculation chain compartments, in addition to connecting the chain to the Irinotecan central compartment.

Reference: Younis IR, Malone S, Friedman HS, Schaaf LJ, Petros WP. Enterohepatic recirculation model of irinotecan (CPT-11) and metabolite pharmacokinetics in patients with glioma. Cancer chemotherapy and pharmacology. 2009;63(3):517-24.

Figure 1-26: Ibarra et al Model

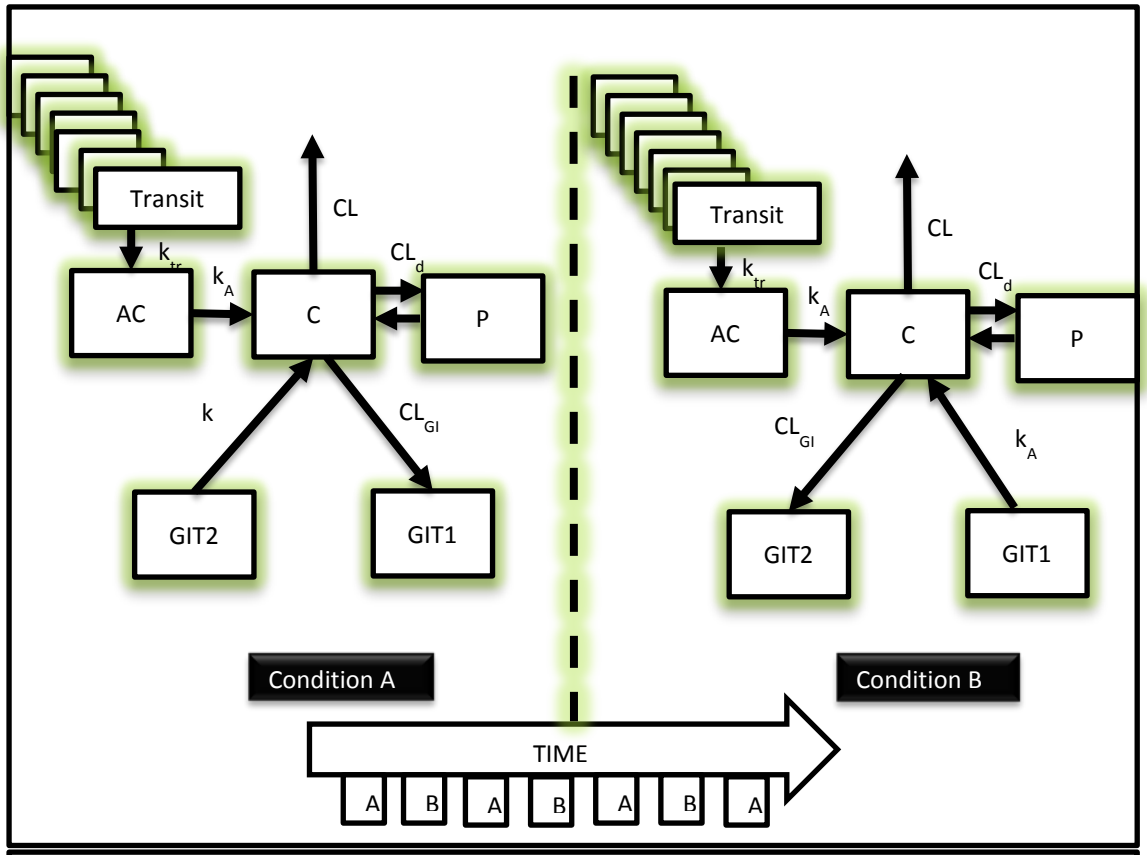

Key:

- **Compartments**: C: nevirapine central compartment, GIT1 and GIT2: gut compartments, transit: transit absorption compartments, AC: absorption compartment, P: peripheral compartment
- **Rate constants and parameters:** k_A : absorption rate constant, CL : elimination clearance, CL_{GIT} : Clearance from plasma to gut, CL_d : intercompartmental clearance.

Reference: Ibarra M, Vázquez M, Fagiolino P. Population pharmacokinetic model to analyze nevirapine multiple-peaks profile after a single oral dose. Journal of pharmacokinetics and pharmacodynamics. 2014;41(4):363-73.

Figure 1-27: Kim et al Model

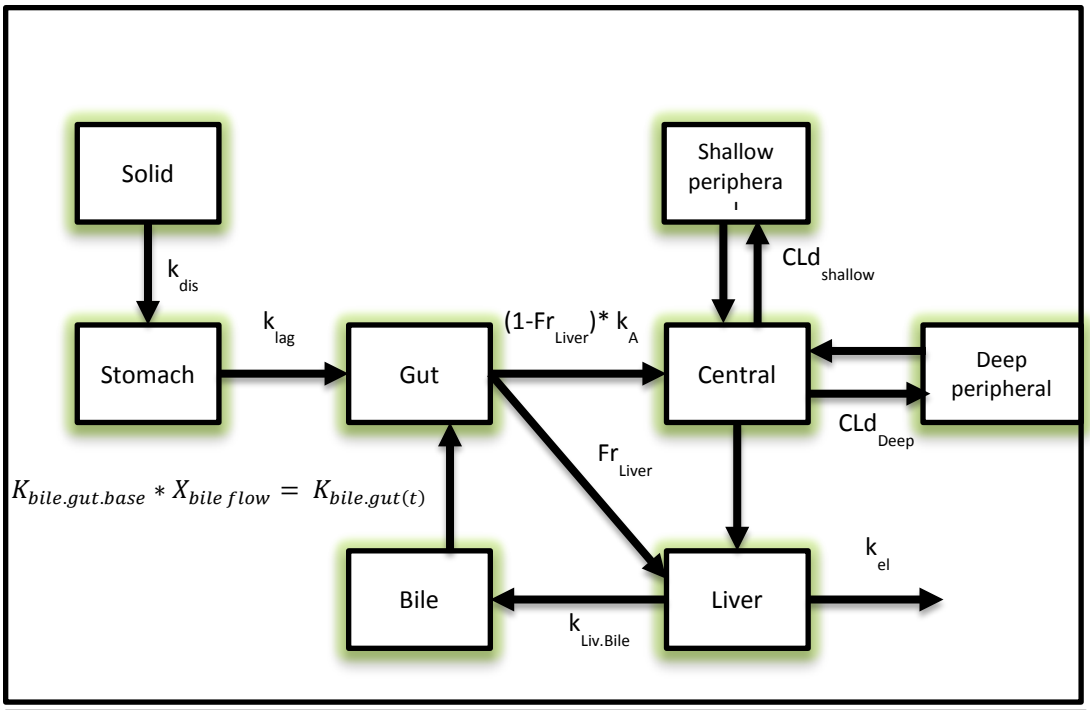

Key:

- **Compartments**: solid: tablet and capsule formulations compartment, Stomach: Stomach compartment, gut : gut compartment, central : fimasartan central compartment, Shallow peripheral: fimasartan shallow peripheral compartment, Deep peripheral: fimasartan deep peripheral compartment, Liver: the liver compartment
- **Rate constants and parameters:** k_{dis} : dissolution rate constant of for the tablet and capsule formulations, k_{lag} : transfer rate constant from the stomach to the gut, k_A : absorption rate constant, $CLd_{shallow}$ and CLd_{Deep} :intercompartmental clearances for shallow and deep peripheral compartments, k_{el} : elimination rate constant, : transfer rate constant from liver to gallbladder, $K_{bile.gut(t)}$: transfer rate constant from gallbladder to the gut, $K_{bile.gut.base}$:Baseline bile flow rate parameter, $X_{bile\ flow}$: bile flow rate.

Source: Kim TH, Shin S, Landersdorfer CB, Chi YH, Paik SH, Myung J, et al. Population Pharmacokinetic Modeling of the Enterohepatic Recirculation of Fimasartan in Rats, Dogs, and Humans. The AAPS Journal. 2015:1-14

CHAPTER 2

2 A PHARMACOKINETIC MODEL FOR DRUGS UNDERGOING ENTEROHEPATIC CIRCULATION: A SENSITIVITY ANALYSIS

2.1 Introduction

Understanding the consequences that follow the presence of EHC is a challenging topic. When a drug undergoes EHC, the typical linear pharmacokinetic analysis procedure becomes inappropriate in terms of describing the observations associated with the EHC. This is a result of the pulsatile behavior of the gallbladder emptying process, which causes dynamic changes in the timing and duration of emptying cycles. In addition to the appearance of secondary peaks, this pulsatile behavior causes time-dependent variation in the pharmacokinetics of the drug undergoing EHC.

In general, the EHC process causes elongation of the apparent half-life of the drug and larger area AUC (1). These results, and others, came from a number of models proposed in the 1970s and 1980s to evaluate the effect of EHC process on the pharmacokinetic profile (45, 46, 51, 52, 60).

2.1.1 Modeling of EHC

The Harrison and Gibaldi simple two-compartment model, which consists of body and gut compartments, demonstrated that when the biliary excretion is inhibited, the half-life is either increased or decreased depending on the relative ratio of non-biliary and fecal elimination routes (51, 52) . This simple two-compartment model assumes that the rate constant representing the gallbladder emptying is linear. Therefore, this model was not successful in predicting the multiple peaks seen in EHC.

Steimer et al. altered the simple two compartment model by including a Tgap in the model (60). The Tgap is defined as a single continuous time delay representing a single

gallbladder opening that then remains open. By contrast to the simple two-compartment model, the Tgap model assumes a discontinuous gallbladder emptying and reabsorption process rather than a continuous one. Therefore, the Tgap model presupposes that the rate constant representing the gallbladder emptying and reabsorption process follows a step function. The use of a lag time (Tgap) in the modeling process enabled the capture of the secondary peak observed (60, 83). However, the concept of Tgap does not represent the physiology of the EHC in humans where multiple times a day the gallbladder stores a fraction of the drug and releases most of it upon the sight, smell, or ingestion of food (1, 36-38).

Models that include the gallbladder as a separate compartment where the release of the gallbladder contents is modeled using various functions have been implemented to represent the pulsatile behavior of gallbladder emptying (45, 46, 74, 75, 82). These gallbladder-based models are preferable as they allow the prediction of several EHC features: secondary peaks and multiple cycles of gallbladder emptying.

2.1.2 EHC and AUC Calculations

Several literature studies were performed in order to evaluate the consequences of EHC on the drug AUC calculations. The results from these studies were inconclusive; some studies demonstrated an effect of EHC on the AUC while others concluded the opposite. The studies of Veng Pedersen and Miller showed that the AUC is dependent on the extent of EHC; therefore, the AUC should not be used to calculate clearance unless corrected by subtracting the portion of AUC caused by EHC(47, 48). Other studies

showed that the AUC is a suitable variable that can be used to predict clearance regardless of the presence of EHC (50). It is important to mention that the accuracy of calculating the AUC had been shown to be dependent on the selected sampling times in relation to the times of the secondary peaks (46).

2.1.3 Study Objectives

Literature modeling strategies of the EHC varies; however, gallbladder-based models provide the best current physiological representation of the process. Regardless, the addition of a gallbladder into the model does not fully depict the physiology of EHC. A more physiological gallbladder-based EHC model is needed. This model should take into account a physiological representation of the bile secretion, gallbladder filling and emptying, duration of gallbladder emptying and irregular mealtimes. With all these considered, the objectives of the current analysis are to propose a gallbladder-based EHC model; to use the model in performing sensitivity analyses to evaluate the effect of the extent of EHC on the pharmacokinetic profile and the non-compartmental analysis (NCA) calculations.

2.2 Methods

The analysis conducted in this study is divided into several steps. First, a gallbladder-based model that describes the EHC process was developed and used to perform determinant simulations assuming various extents of EHC. Next, these simulations were compared to evaluate the effect of the EHC on the pharmacokinetic

profiles of orally and intravenously administered drugs. The influence of the EHC process on the NCA calculations was determined assuming two sampling schemes that differs by the selected sampling times in relation to meal times. From these two sampling schemes, simulated concentrations were generated. An NCA analysis was conducted for each sampling scheme and extent of EHC combination that was simulated.

2.2.1 The Gallbladder-Based EHC Model

The proposed EHC model is composed of three compartments: gut, central, and gallbladder (**Figure 2-1**). In this model, the absorption process is described using the first order rate constant (k_A). The elimination from the central compartment is defined using the rate constant k_{20} which is calculated as the ratio of clearance (CL) divided by volume of distribution (V), i.e., $k_{20} = \frac{CL}{V}$. The rate constant k_{23} is used to describe the EHC distribution process out of the central compartment. The extent of EHC (EHC%) represents the percentage of the mass in the central compartment that gets distributed via the EHC process, and calculated according to the following equation:

$$EHC\% = \frac{k_{23}}{k_{23} + k_{20}} * 100$$

It is assumed that 75% of the drug distributed by the EHC goes to the gallbladder, while the remaining 25% drains directly to the gut compartment (35, 36). The drug in the gallbladder gets stored there until mealtimes (mt) at which a release, using the rate constant (k_{GG}), results in eliminating 75% of the drug from the gallbladder within an

assumed duration of 30 minutes (35, 39, 40).

2.2.2 Simulation Method

The proposed model was used to perform simulations where a single dose of 1000 mg is introduced into either the gut compartment or the central compartment to reflect the oral and intravenous routes of administration, respectively. Simulations were conducted using the Stella software (84) where several EHC% (0%, 20%, 40%, 60%, and 80%) were considered. The model parameters used in these simulations are presented in **table 2-1A**. Based on these values, the terminal half-life of the drug when there is no EHC occurring, i.e., EHC% = 0, equals 5 hours according to following equation:

$$t_{1/2} = \frac{0.693 * V}{CL}$$

To capture the various EHC extents, different values of the rate constant k_{23} were used; refer to **table 2-1B**. Regardless of the assumed EHC%, the mealtimes (mt) at which the gallbladder emptying starts were fixed at 1, 4, and 10 hours after the dose. These values were selected in order to reflect the times of breakfast, lunch, and dinner meals, respectively. It was assumed that the cycles of gallbladder emptying starts exactly at the same time of meals. For each one of the meals, the duration of gallbladder emptying was assumed to be 30 minutes (39). The transfer rate constant (k_{GG}) from the gallbladder to the gut assumed the value zero except within the duration of meals it is fixed to a 2.77 hr^{-1}. At the end of the meal duration, i.e., 30 minutes, k_{GG} returns to zero

until next meal, refer to the equation below:

$$k_{GG} = \begin{cases} 2.77\,, & mt \leq time\ after\ dose \leq (mt + 30\ mins) \\ 0\,, & else \end{cases}$$

where mt is the mealtime.

The value 2.77 hr^{-1} was selected based on a simulation analysis revealing that such value results in eliminating 75% of the drug from the gallbladder within 30 minutes.

2.2.3 Pharmacokinetic Evaluation

Evaluation of the pharmacokinetic profiles after intravenous and oral dosing was conducted in terms of several observations, variables and parameters. The magnitude of secondary peaks was noted and compared across the various EHC%. Additionally, the primary peak (C_{max}) and time to C_{max} (T_{max}) of the oral profiles were noted. Furthermore, an analysis of the instantaneous half-life, which is related to the instantaneous first derivative of the log concentrations ($logCp$) with respect to time, was calculated as the following:

$$\text{instantaneous half} - \text{life} = \frac{-0.693}{\frac{\partial}{\partial t} logCp}$$

Another analysis was conducted to determine the apparent half-life, which is defined as the average time required to eliminate half of the drug. This analysis was done by conducting a univariate linear regression on the $logCp$ versus time for the various EHC%. In these regressions, the apparent half-life was determined for each scenario as a

function of the estimated slope of the regression line according to the following:

$$\text{apparent half} - \text{life} = \frac{-0.693}{slope}$$

where $slope$ is estimated according to the following function:

$$logCp = intercept + slope * time + \varepsilon$$

where ε represents the random error term.

Additional visual comparison was performed in terms of drug amount eliminated from of the system versus time. The simulated complete AUC is 200 hr*mg/L. An analysis of the time required to reach 95% of the complete AUC ($AUC_{95\%}$) was determined based on the cumulative integration of the concentrations across time.

2.2.4 Non-Compartmental Analysis (NCA)

To evaluate the effect of EHC% on NCA calculations, 14 plasma concentrations were simulated assuming the oral route using two different sampling schemes: a conventional and a meal-directed sampling scheme, see Figure 2-2. The conventional sampling scheme emphasizes frequent samples at early times and more spread out samples at later times, without regard to mealtimes. For this scheme, samples were collected at times: 0, 0.5, 1, 1.5, 2, 3, 4, 6, 8, 12, 24, 36, 48, and 72 hours. The alternative meal-directed scheme is similar to the conventional scheme in early times; however, sampling times after 12 hours were chosen to be 1 or 2 hour after food intake. Therefore, the concentration samples in the meal-directed scheme were taken at times: 0, 0.5, 1, 1.5, 2, 3, 4, 6, 8, 12, 26, 36, 50, and 74 hours. It can be noticed that the sample times in both

of these schemes are exactly the same, except for the 11th, 13th, and 14th time points. In contrast to the conventional scheme, these three time points are advanced by two hours in the meal-directed scheme; i.e. 24, 48, and 72 hours in conventional scheme become 26, 50, and 74 hours in the meal-directed scheme. This advancement of time was done in order to sample at points occurring after mealtimes, therefore covering secondary peaks.

Simulated samples were analyzed using the NCA module in WinNonlin version 6.4 (Pharsight Corporation, CA, USA). The terminal half-life ($t_{1/2}$) was determined from the terminal elimination rate constant (λ_Z) that was estimated by linear regression of the terminal descending phase of the $logCp$. The linear trapezoidal rule was used in calculating the area under the time concentration curve from time 0 to the last sampled concentration (AUC_{0-last}). Extrapolation from the last simulated concentration (C_{last}) to infinity was performed to calculate ($AUC_{0-\infty}$) according to the following equation:

$$AUC_{0-\infty} = AUC_{0-last} + \frac{C_{last}}{\lambda_Z}$$

The percentage of $AUC_{0-\infty}$ that is due to extrapolation from time of last simulated concentration C_{last} (T_{last}) to infinity ($AUC\%Extrap$) is calculated as:

$$AUC\%Extrap = \frac{AUC_{0-\infty} - AUC_{0-last}}{AUC_{0-\infty}} * 100$$

Oral clearance ($\frac{CL}{F}$) and apparent volume of distribution $\left(\frac{V}{\mathrm{F}}\right)$ were calculated according

to the following equations:

$$\frac{CL}{\mathrm{F}} = \frac{Dose}{AUC_{0-\infty}}$$

$$\frac{V}{\mathrm{F}} = \frac{Dose}{\lambda_Z * \quad AUC_{0-\infty}}$$

The estimated values of the parameters and variables obtained from the NCA were compared to the parameters and variables used in simulating the datasets by computing relative bias. Relative bias provides a measure of the magnitude of deviation and was calculated according to the following equation:

$$Relative\ Bias\% = 100 * \frac{\hat{\theta}_i - \theta_i}{\theta_i}$$

where θ_i as the true ith parameter or variable used in the simulations, and $\hat{\theta}_i$ is the NCA estimated ith parameter or variable that corresponds to θ_i.

2.3 Results

Figures 2-3 and 2-4 are the linear and log-linear concentration time profiles when simulating various EHC% after oral and IV dosing. These plots show multiple secondary peaks that are observed at the specified mealtimes. The secondary peak at first mealtime (1 hr after the dose) is less prominent than other secondary peaks; however, it becomes more noticeable with higher extent of EHC%. In the case of oral dosing, another observation is manifested; the higher the extent of EHC% gets, the lower the primary peak (C_{max}), and the earlier the time to C_{max} (T_{max}) (Table 2-2).

Visual analysis also demonstrated that the increased extent of EHC% causes flattening in the exposure profiles, accompanied by a reduced maximum exposure. The increased extent of EHC% causes the drug to stay longer in the system and to take more time to get eliminated when compared to lower EHC% or no EHC at all. This can also be demonstrated when observing the drug amount eliminated versus time plots (Figure 2-5). With higher extent of EHC%, more time is required to eliminate 95% of the drug from the system.

The influence of EHC process on the half-life can be seen in Figures 2-6, 2-7. In Figure 2-6, the Y-axis represents the instantaneous half-life displayed between -15 and 15 hours, as the instantaneous half-life may transiently increase to much longer values. The instantaneous half-life of a drug without EHC (EHC%=0) reaches the value 5 hours in the terminal phase and does not change after that. When the drug undergoes an EHC, the system is nonlinear and the instantaneous terminal half-life is no longer constant. The terminal half-life changes with time and no single value can be obtained to represent the amount of time it takes to decrease the concentration by one-half. The presence of EHC results in deviation of the changing half-lives from the simulation value 5 hours with higher %EHC resulting in higher deviations from the non-EHC terminal half-life. The linear regression line running through the logarithm of the plasma concentration data demonstrates the effect of EHC on the apparent half-life, Figure 2-7. It can be seen that higher EHC% resulted in longer apparent half-life.

The cumulative AUC versus time of the various EHC% can be seen in Figure 2-8. With increased EHC%, more time is required to reach the theoretical 200 hr*mg/L value.

Examined quantitatively, the times needed to reach 95% of the AUC ($AUC_{95\%}$) for the various EHC% can be seen in Table 2-3.

The sampling times of the conventional and the meal-based schemes are seen in Figures 2-9. These plots shows that at the later sampling times, the conventional sampling scheme generally capture minima, while the meal-based sampling scheme capture maxima. The results of the NCA after oral dosing can be seen in Table 2-4 stratified by the two sampling schemes and across the different EHC%: $t_{1/2}$, $AUC_{0-\infty}$, $\frac{CL}{F}$, and $\frac{V}{F}$. The corresponding relative bias of these estimates can be found in Table 2-5. When there is no EHC, i.e., EHC=0%, similar NCA estimates are obtained regardless of the sampling scheme. However, the presence of EHC caused biased NCA estimates where this bias changed depending on the sampling scheme and the EHC%. Considering the same EHC%, the two sampling schemes resulted in different NCA estimates. Additionally, higher EHC% was associated with higher degrees of bias in both sampling schemes.

2.4 Discussion

A gallbladder-based EHC model was developed taking into account the physiological aspects of the hepatobiliary system. The model provides more physiological representation of the bile secretion, gallbladder filling and emptying, duration of gallbladder emptying and irregular mealtimes. Because modeling the EHC process has been challenging, the current model may help in better model, evaluate and understand the effect of EHC on drugs pharmacokinetics. The proposed model consists

of gut, central, and gallbladder compartments where the EHC is assumed to be a distribution process that emanates out of the central compartment. A literature review of EHC modeling revealed the presence of conflicting notions that EHC should be modeled as an elimination rather than a distribution process. As discussed in the first chapter, elimination involves an irreversible removal of drug from the site of measurement, while with distribution the drug is reversibly transferred from the site of measurement. EHC involves distribution and fecal elimination processes; therefore, it would be more rationale to consider both of these processes in the model. For the sake of simplicity, the fecal elimination process was assumed negligible and therefore not represented in the current model. In terms of modeling, this means that the rate constant controlling the transfer of drug for the EHC process was considered as a distribution rate constant rather than a fraction of the elimination rate constant.

During fasting, around 75% of produced bile gets stored in the gallbladder while the remaining 25% drains directly to the duodenum (35, 36). On the sight, smell or ingestion of food, the gallbladder contracts while the sphincter of Oddi relaxes (1). This causes around 75% of bile stored in the gallbladder to be released to the duodenum (36-39). The current model mimics and assumes that the EHC process is divided into two routes. The major route denoting 75% of the EHC of the drug was assumed to be transferred from the central compartment to the gallbladder where it gets stored until mealtimes. At mealtimes, the rate constant K_{GG} (2.77 hr^{-1}) transfers 75% of the drug stored in the gallbladder to the gut within 30 minutes duration (39). The other route that

represents the remaining 25% of the EHC of the drug is assumed to continuously drain to the gut with no dependency on mealtimes.

The presented model does not include a representation of the first-pass hepatic effect. The inclusion of this process would be required to evaluate the effect of EHC on AUC calculations, concentration time profile and the bioavailability fraction. Another limitation of the model is assuming that 100% of the drug secreted to the gut would be reabsorbed back to the system during each EHC cycle, i.e., no fecal elimination. This assumption was based on the observation that only 3-5% of enterohepatically circulated bile acids is excreted into the feces and not reabsorbed (9, 10). Therefore, the fecal elimination process was considered negligible. Such an assumption may be invalid for drugs not extensively reabsorbed. Nevertheless, a modification of the current model can be made for such drugs by including an additional exit rate constant.

An evaluation of the effect of varying degrees of EHC% on the shape of the concentration versus time profiles was performed on orally and intravenously administrated single doses of drug. Regardless of the assumed EHC%, the model was successful in capturing the multiple secondary peak phenomenon. This observation provides validity of the model as secondary peaks are prominent feature of EHC. The magnitude of these secondary peaks was found to correlate with the EHC% where higher secondary peaks result from higher EHC%. This is expected as more drug mass is being enterohepatically distributed with higher EHC.

The C_{max} and T_{max} of oral concentration time profiles were shown to be affected by the EHC% as well where increased EHC% results in a lower C_{max} and earlier T_{max}.

The lower C_{max} is due to the EHC process causing the distribution of the drug out of the central compartment and therefore lowering the mass remaining in the central compartment at the time of C_{max}. The earlier Tmax with higher EHC% is caused by the earlier equilibrium between the system rate in and rate out processes.

Evaluating the time required to eliminate the drug from the system revealed its dependence on the EHC%. As the univariate regression analysis showed, the presence of EHC results in elongating the apparent half-life of the drug where higher EHC% is associated with longer apparent half-life. Interestingly, faster drop in the concentrations and therefore the instantaneous half-life can be observed at the times between gallbladder emptying cycles, as seen in Figures 2-4 and 2-6. The non-stationary gallbladder-emptying rate constant keeps the concentration profile from looking like a conventional two compartment. From the central compartment point of view, the unidirectional EHC distributional output into the gallbladder act as an elimination process at the times between gallbladder emptying. Therefore, the behavior of the profile at these times mimics an increased elimination process and therefore shorter half-life.

The instantaneous half-life analysis demonstrated a challenging aspect associated with drugs undergoing EHC. Without EHC, the elimination phase is represented by a non-changing instantaneous half-life. However, the presence of EHC results in nonlinearity in the instantaneous half-life; therefore, no single value is available to represent a terminal half-life. Additionally, the EHC process causes a general deviation of the instantaneous half-life, where greater EHC% is associated with larger deviation. These results present a problem associated with the traditional definition of half-life when

the drug undergoes EHC. The half-life is usually defined using linear systems as a single value that represents the time required to reduce the drug by half (85). Such a definition is not valid in a non-linear system like EHC and therefore it may be not useful in such situations. All that said, it is important to keep in mind that EHC causes a longer time to reduce the aggregate drug in the system by half where higher EHC% is associated with longer time.

The time required to cover the $AUC_{95\%}$ is dependent upon EHC%. Regardless of the route of administration, higher EHC% is associated with longer time. When there is no EHC, the drug needs around 20 hours to reach the $AUC_{95\%}$, for oral and IV dosing. This duration, for both oral and IV, rise to around 30, 40, 60, and 125 hours for the 20%, 40%, 60%, and 80% EHC%, respectively. Such results demonstrate that when a drug undergoes EHC, a planned sampling strategy should reflect sampling times that extend beyond what might be suggested by early preclinical pharmacokinetic studies. This extension in sampling times correlates with EHC%, where higher EHC% requires longer times to eliminate drug in single dose studies and longer time to reach steady state in multiple doses studies.

In general, the presence of EHC causes biased parameter estimates with NCA, where bias varies depending on the sampling scheme, and escalates with increasing EHC%. It is remarkably obvious that the sampling schemes masks the presence of most secondary peaks, especially at later times of higher EHC%. The NCA conducted to evaluate the two sampling schemes, conventional and meal-based, demonstrated interesting results. In the conventional sampling scheme, greater EHC% was associated

with an increased positive relative bias in the estimated $t_{1/2}$, oral clearance as well as volume of distribution; and an increased negative bias in the calculated $AUC_{0-\infty}$. On the other hand, the meal-based sampling scheme demonstrated that larger EHC% causes higher positive relative bias in estimated $t_{1/2}$, $AUC_{0-\infty}$ and volume of distribution; and higher negative bias in oral clearance. These results demonstrate the influence of sampling times on the estimation of parameters of a drug undergoing EHC. The choice of sampling times results in positive or negative bias in the estimates of the NCA parameters.

2.5 Conclusion

In this study, a more physiologic gallbladder-based model was built and used to evaluate the effect of the EHC process on the shape of the concentration time profile and parameter estimates in a noncompartmental analysis. A sensitivity analysis was performed while considering various degrees of EHC%. The presence of EHC results in nonlinearity in the system and causes changes in the pharmacokinetic profile. For drugs that undergo EHC, sampling times need to be extended over a longer duration of time than what is traditionally done with other drugs. The comparison of two sampling schemes from a drug undergoing various degrees of EHC% demonstrated a major influence of the selected sampling times on the NCA estimations. Bias in the NCA calculations was dependent on the sampling times. In conclusion, caution should be taken when designing studies for drugs undergoing EHC. Timing of meals may be an important factor to consider when designing pharmacokinetic studies and defining sampling times

for drugs that undergo EHC. Future studies that attempt to identify best sampling strategies in the presence of EHC are needed.

Table 2-1: Parameters Used in the Simulation

A: The values of all[a] the parameters used in the simulation

Parameter	**Value (unit)**
Clearance (CL)	5 (L/hr)
Volume of distribution (V)	36 (L)
Absorption rate constant (k_A)	0.75 (hr^{-1})
Gallbladder to gut rate constant (k_{GG})	2.77 (hr^{-1})
Mealtimes (post-dose)	1, 4, 10 (hr)
Duration of gallbladder emptying	30 (min)

B: The k_{23} parameter values used in the simulation for the various EHC percentages used

EHC Percent[b] (%)	**k_{23} (hr^{-1})**
0%	0
20%	0.035
40%	0.093
60%	0.208
80%	0.556

[a] Except the parameter k_{23} for which different values are used at different EHC percents, refer to table1B

[b]EHC Percent is the fraction of the dose that undergoes enterohepatic circulation and defined according to the equation present in the text

Table 2-2: Observed Maximum Concentrations (Cmax) and the Time to Maximum Concentrations (Tmax) for the Various EHC% after Oral Adminstration.

EHC Percent (%)	**C_{max} (mg/L)**	**Tmax (hr)**
0	18.9	2.70
20	18.03	2.50
40	16.96	2.30
60	15.16	2.10
80	11.63	1.80

Table 2-3: Time Required to Reach 95% of the AUC (AUC95%) for the Various EHC%, After Intravenous and Oral Dosing

EHC Percent (%)	Oral (hr)	Intravenous (hr)
0	23	21.6
20	32	30.4
40	41.6	39.4
60	62.5	60.6
80	126.7	125.2

Table 2-4: Results of the Non-Compartmental Analysis (NCA) After Oral Dosing at Varying EHC%

A: Conventional Sampling Scheme:

EHC Percent (%)	$\boldsymbol{\lambda_Z}$ **(1/hr)**	$\boldsymbol{t_{1/2}}$ **(hr)**	**Tmax (hr)**	**Cmax (mg/L)**	$\boldsymbol{AUC_{0-last}}$ **(hr*mg/L)**	$\boldsymbol{AUC_{0-\infty}}$ **(hr*mg/L)**	$\boldsymbol{AUC\%\ Extrap}$ **(%)**	**V/F (L)**	**CL/F (L/hr)**
0	0.14	5.02	3	18.83	210.45	210.46	0.01	34.38	4.75
20	0.10	6.62	3	17.88	206.12	206.25	0.06	46.29	4.85
40	0.09	7.60	2	16.85	198.59	198.95	0.18	55.12	5.03
60	0.08	8.17	2	15.16	184.73	185.24	0.28	63.62	5.40
80	0.09	7.70	2	11.39	153.08	153.31	0.15	72.42	6.52

B: Meal-Based Sampling Scheme:

EHC Percent (%)	$\boldsymbol{\lambda_Z}$ **(1/hr)**	$\boldsymbol{t_{1/2}}$ **(hr)**	**Tmax (hr)**	**Cmax (mg/L)**	$\boldsymbol{AUC_{0-last}}$ **(hr*mg/L)**	$\boldsymbol{AUC_{0-\infty}}$ **(hr*mg/L)**	$\boldsymbol{AUC\%\ Extrap}$ **(%)**	**V/F (L)**	**CL/F (L/hr)**
0	0.14	5.01	3	18.83	213.18	213.19	0.00	33.94	4.69
20	0.10	7.12	3	17.88	216.96	217.15	0.09	47.28	4.61
40	0.07	9.93	2	16.85	223.77	224.97	0.53	63.65	4.44
60	0.05	14.91	2	15.16	237.25	244.17	2.83	88.09	4.10
80	0.03	27.22	2	11.39	258.55	306.42	15.62	128.2	3.26

Table 2-5: Relative Bias (RBias%) in the NCA Estimated Parameters

A: Conventional Sampling Scheme:

EHC%	**RBias $t_{1/2}$**	**RBias $AUC_{0-\infty}$**	**RBias V/F**	**RBias CL/F**
0%	0.40	5.23	-4.50	-5.00
20%	32.40	3.13	28.58	-3.00
40%	52.00	-0.53	53.11	0.60
60%	63.40	-7.38	76.72	8.00
80%	54.00	-23.35	101.17	30.40

B: Meal-Based Sampling Scheme:

EHC%	**RBias $t_{1/2}$**	**RBias $AUC_{0-\infty}$**	**RBias V/F**	**RBias CL/F**
0%	0.20	6.60	-5.72	-6.20
20%	42.40	8.58	31.33	-7.80
40%	98.60	12.49	76.81	-11.20
60%	198.20	22.09	144.69	-18.00
80%	444.40	53.21	256.03	-34.80

Figure 2-1: Depiction of the Simulation Model Used

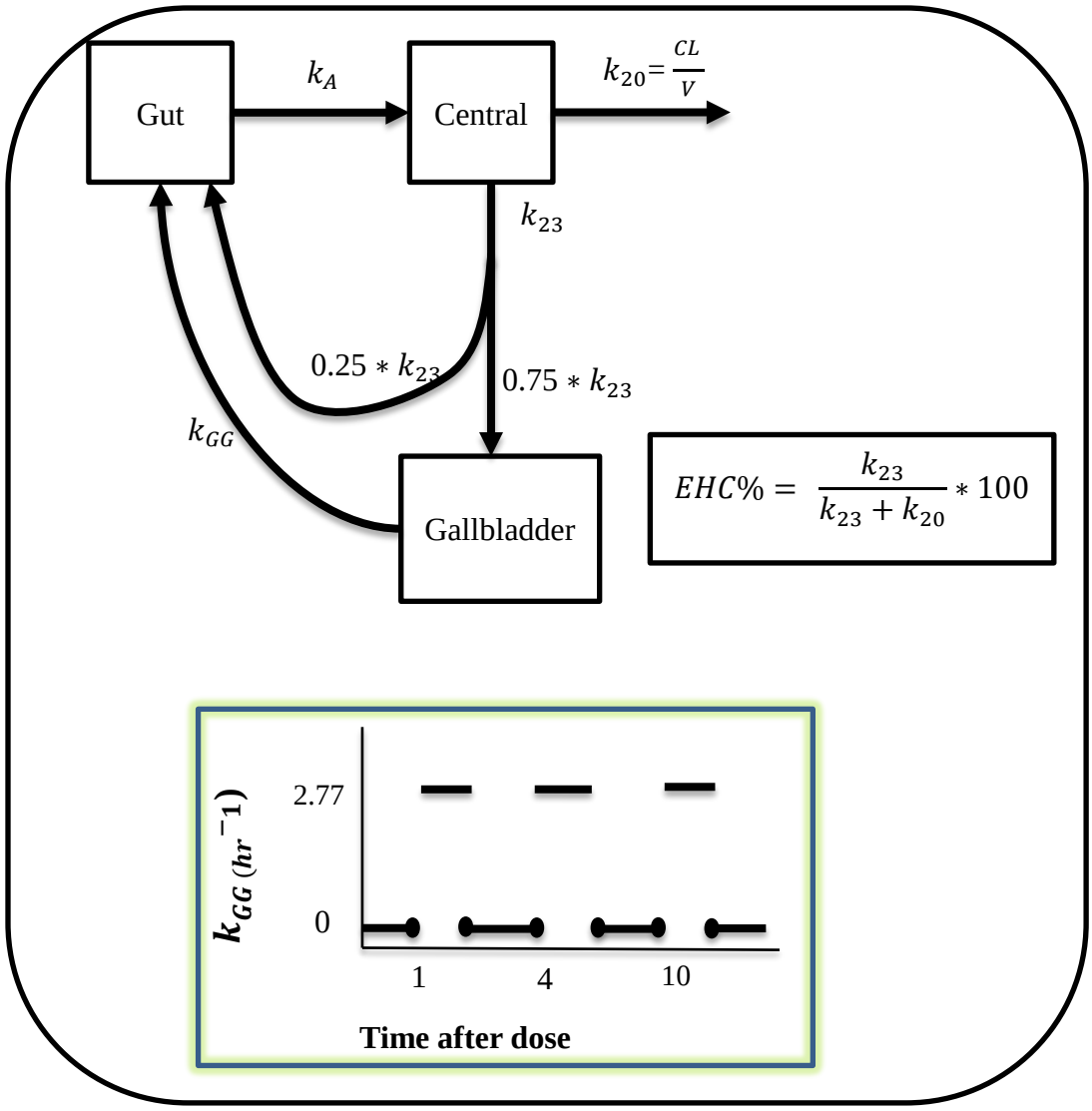

Key:

Compartments: Gut: gut compartment, Central: central compartment, Gallbladder: represents the gallbladder

Rate constants: k_A : absorption rate constant, CL: clearance, V: volume of distribution, K20: elimination rate constant, k_{23}: EHC distribution rate constant, k_{GG}: gallbladder emptying rate constant.

Figure 2-2: Sampling Schemes for the NCA Evaluation

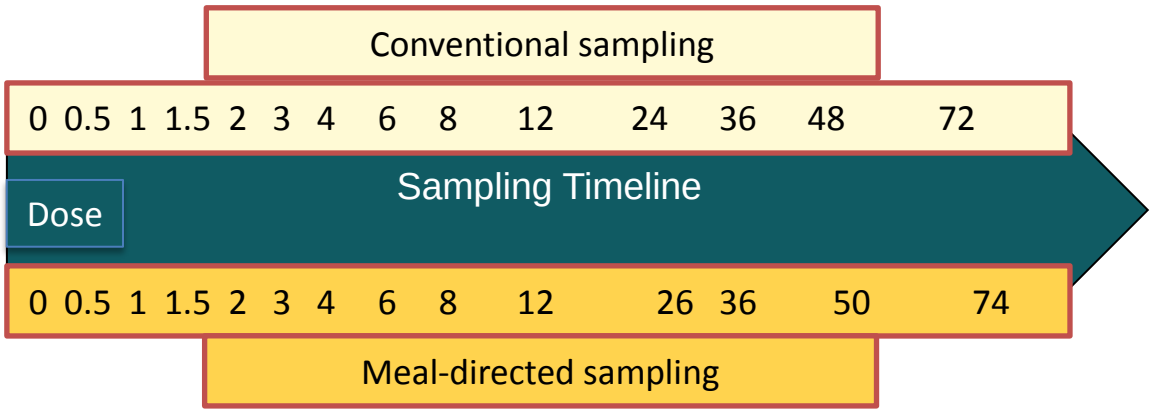

Figure 2-3: Linear Concentration Time Profiles after Intravenous and Oral Dosing

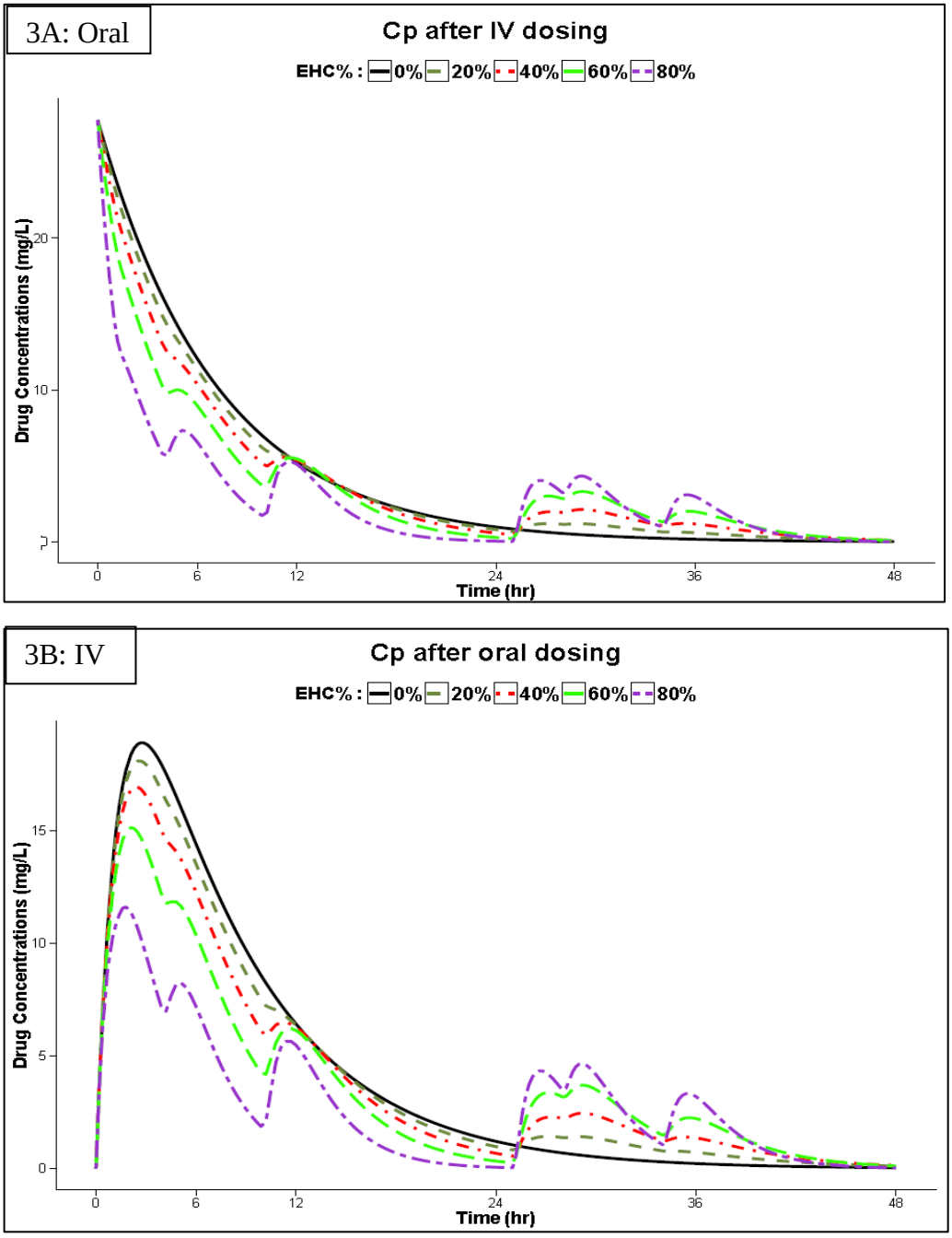

Cp: Concentration, IV: Intravenous

Figure 2-4: Semi-Log Linear Concentration Time Profiles after Intravenous and Oral Dosing

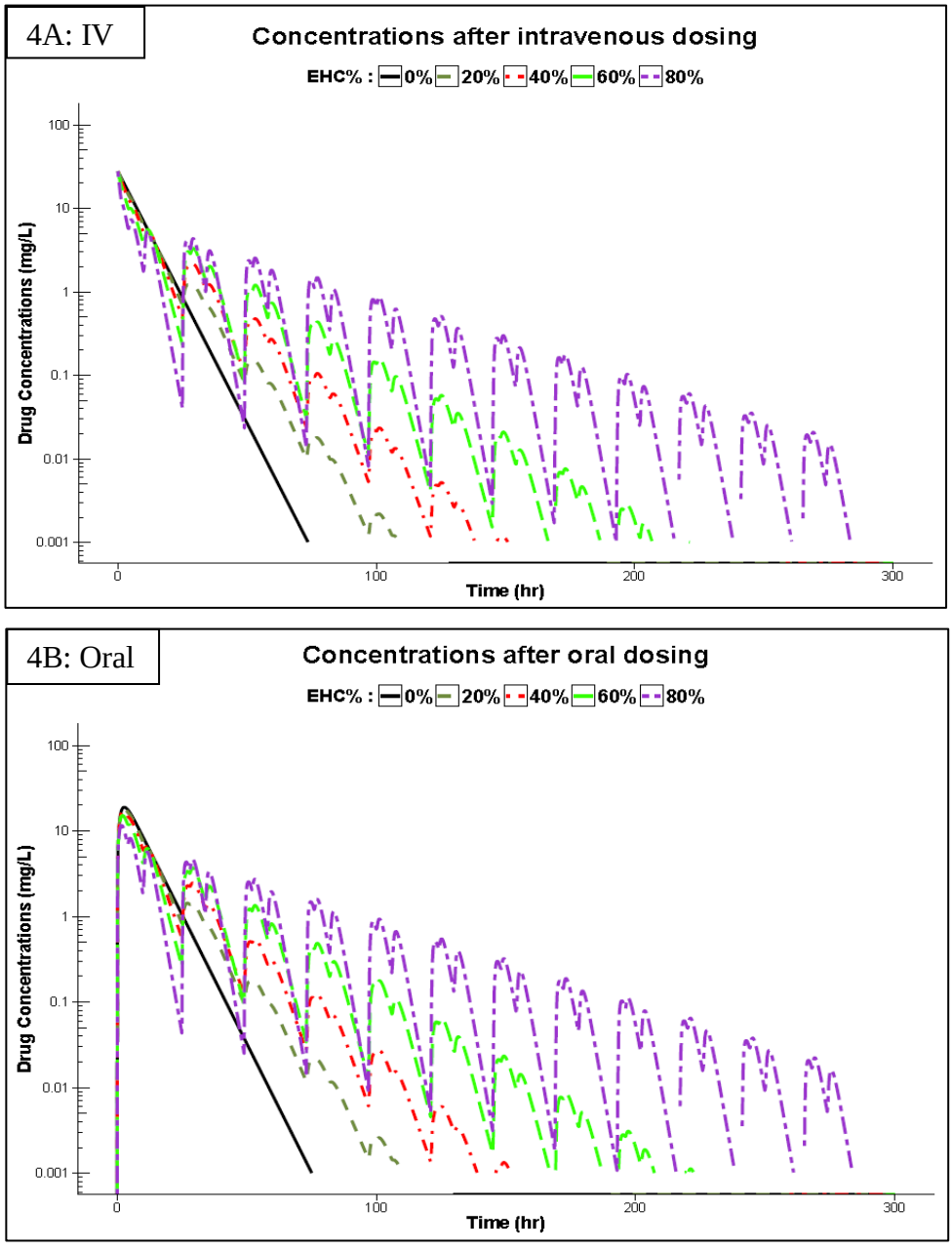

Cp: Concentration, IV: Intravenous

Figure 2-5: Drug Amount Eliminated versus Time Assuming Various EHC%

5A: IV

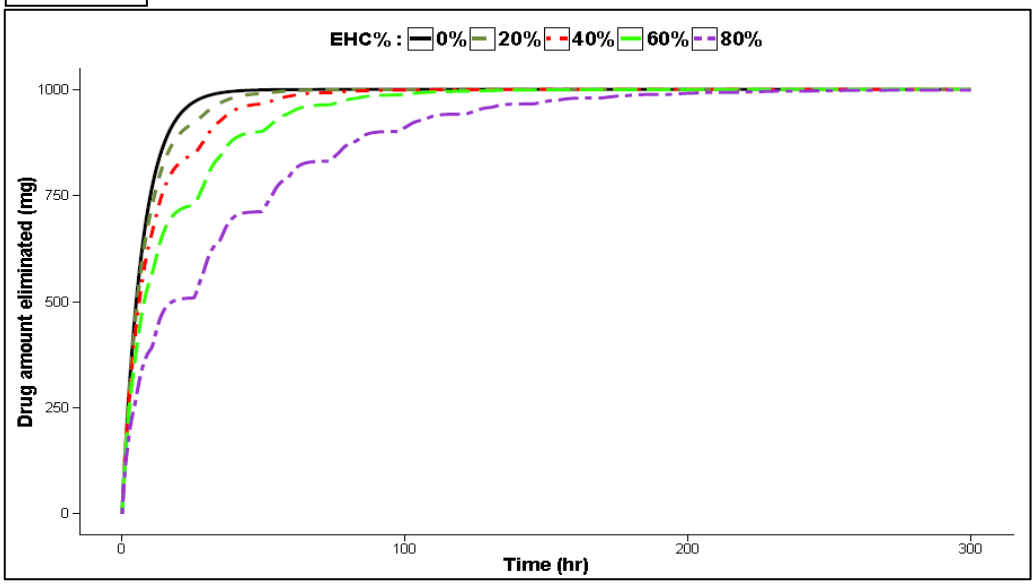

5B: Oral

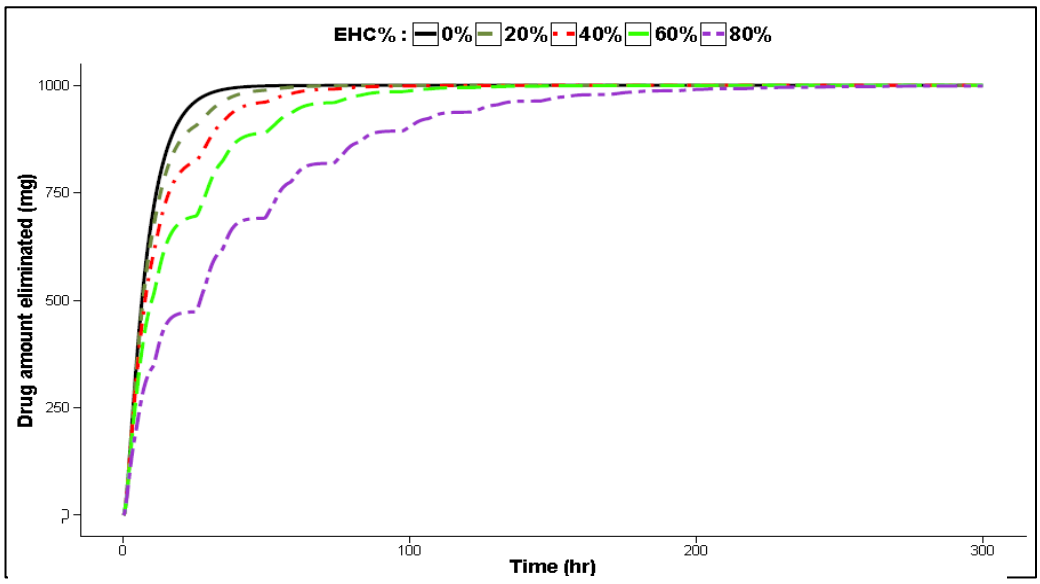

IV: Intravenous

Figure 2-6: Instantaneous Half-Life versus Time after Intravenous and Oral Dosing

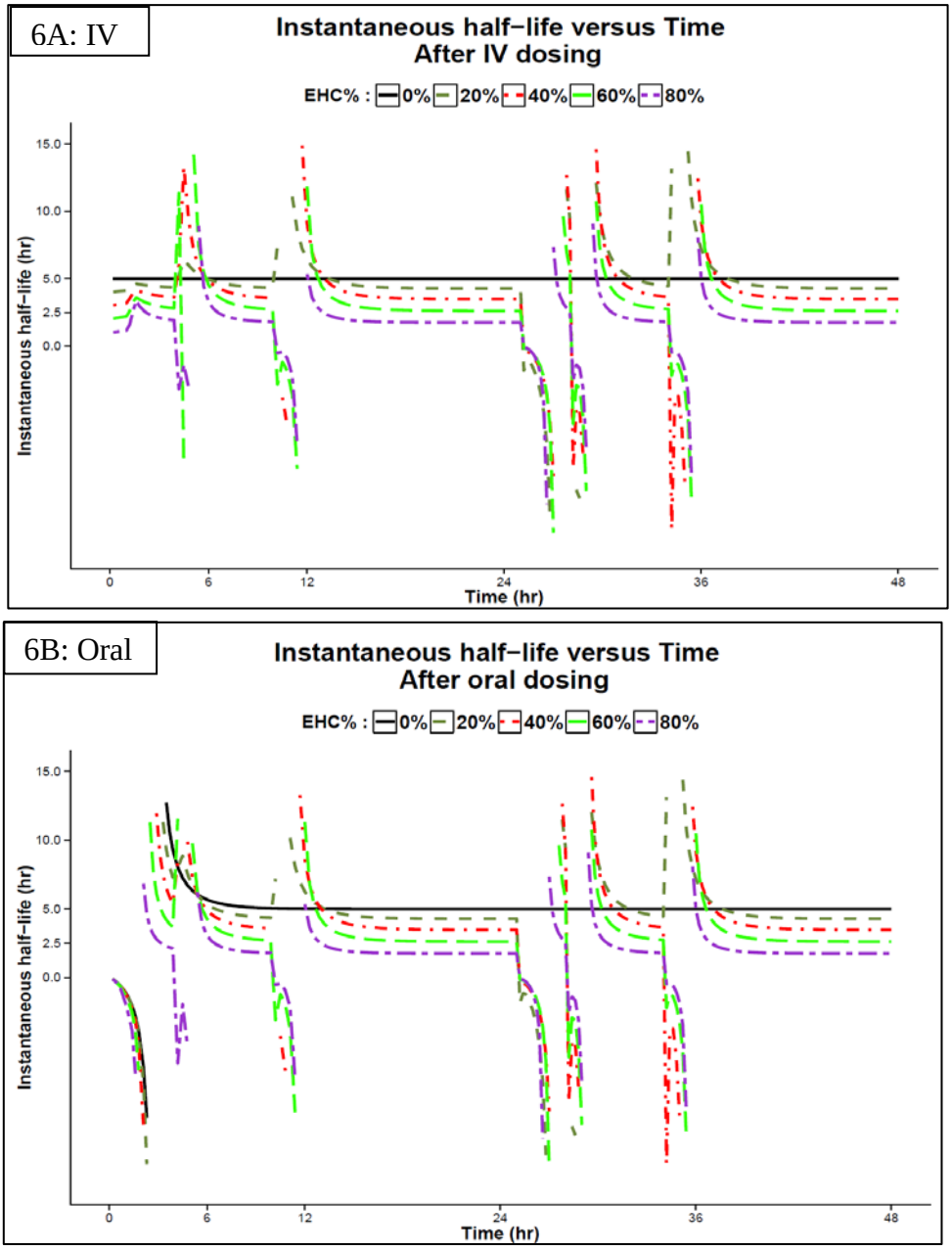

IV: Intravenous

Figure 2-7: Apparent Half-Lives based on Linear Regression Slopes of Logconcentrations Assuming Various EHC%, After Intravenous and Oral Dosing

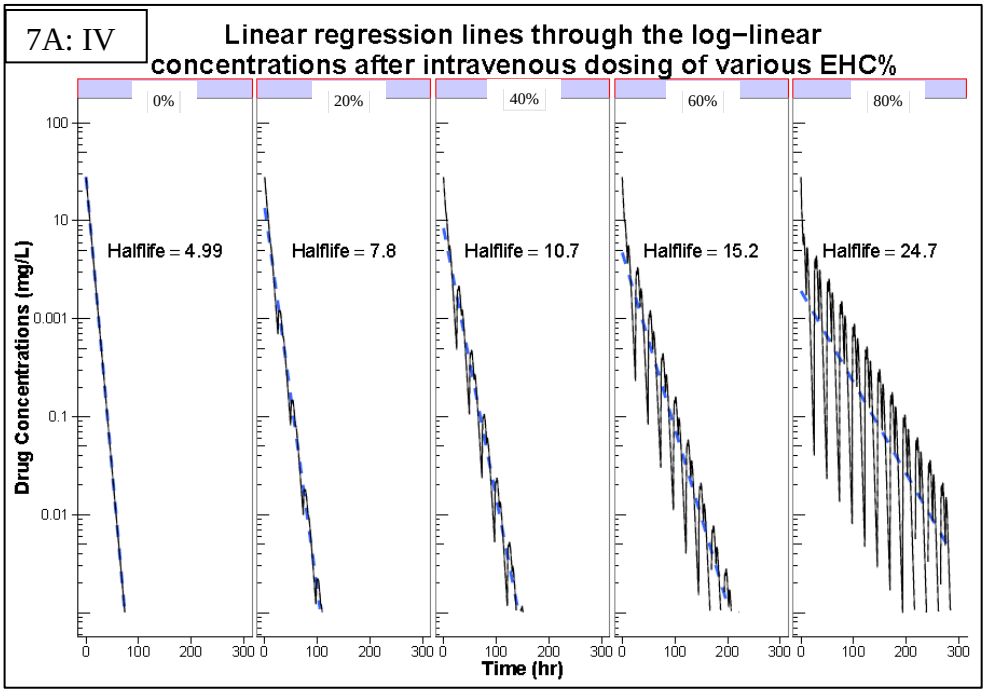

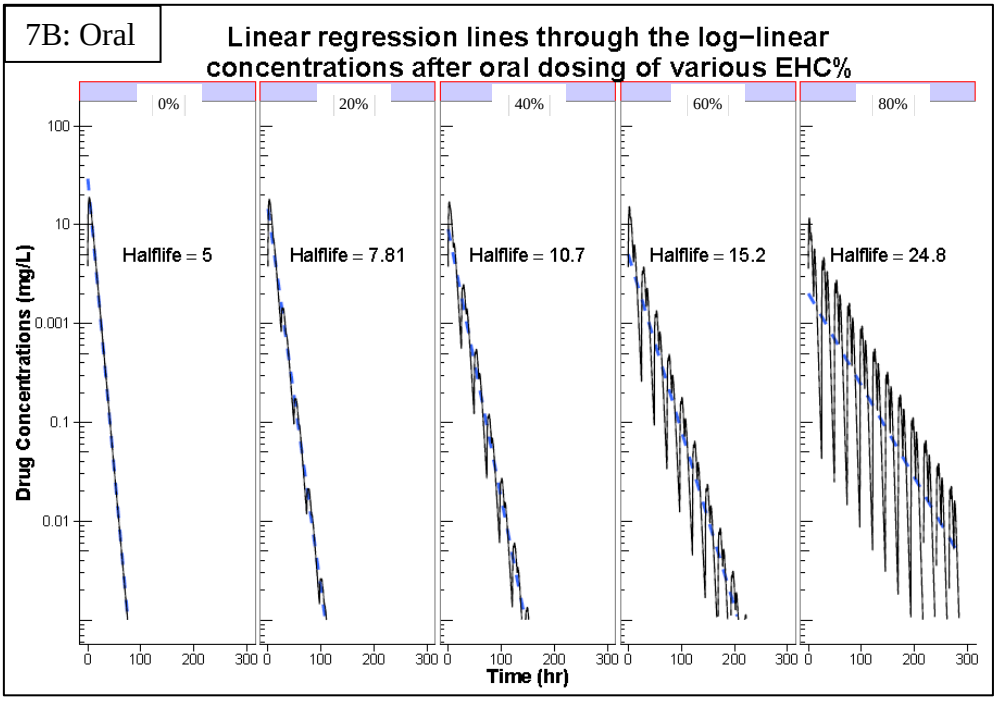

Figure 2-8: The Cumulative Area Under the Concentration versus Time Curve (AUC) of the Various EHC%, after Intravenous and Oral Dosing

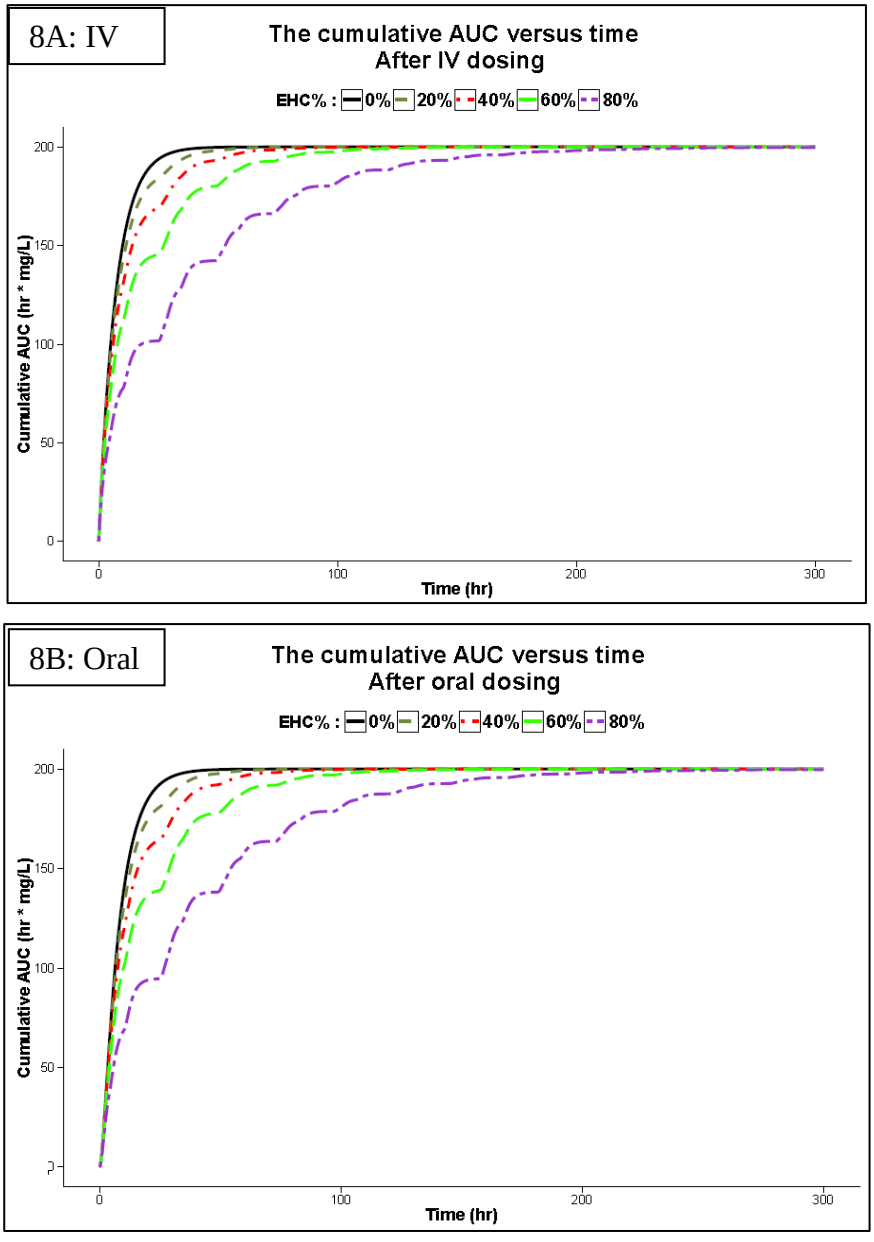

IV: Intravenous

Figure 2-9: Sampling Times of Conventional and Meal-Based Schemes for the Various EHC%

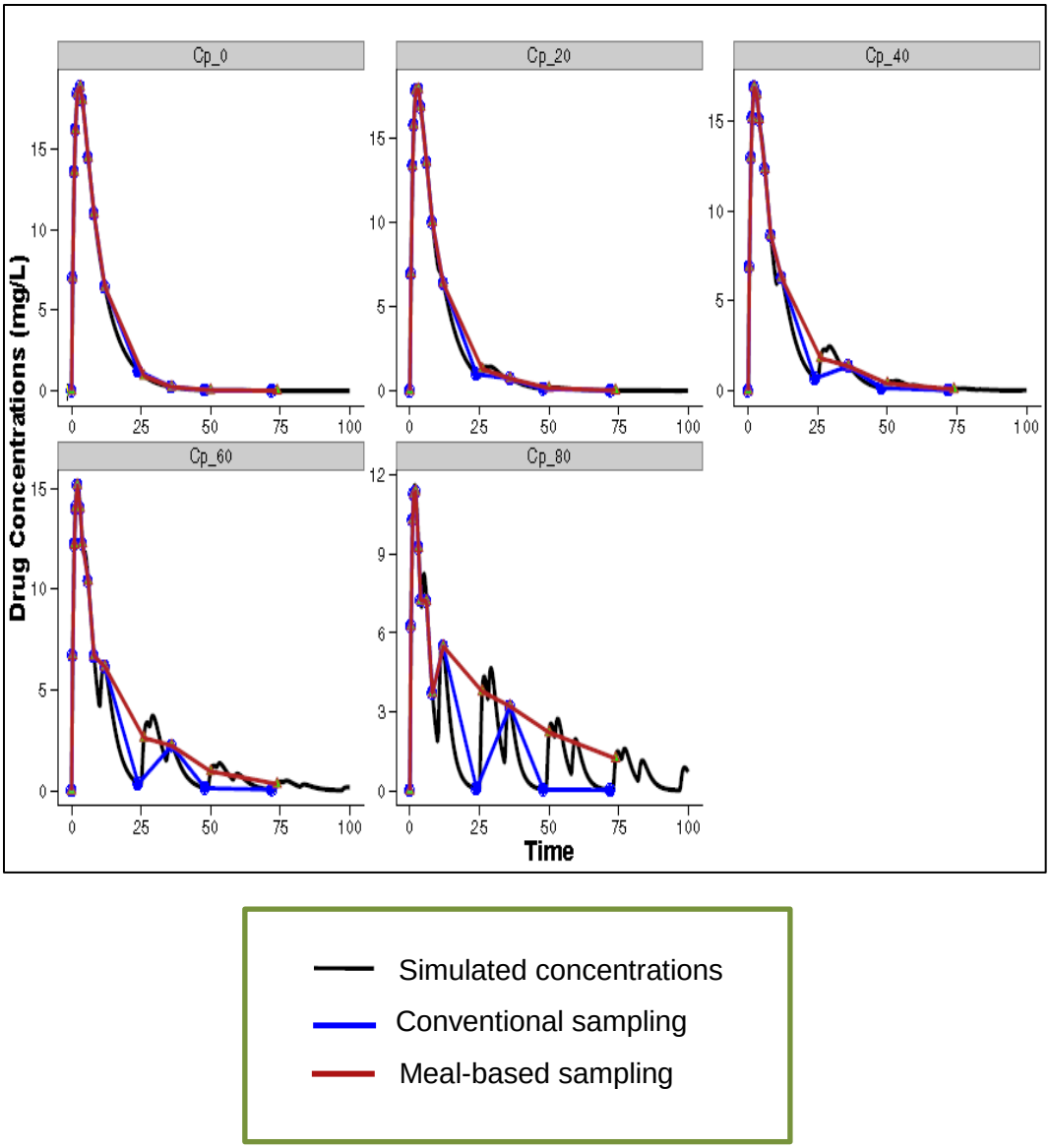

3.1 Introduction

Various Compartmental pharmacokinetic models have been developed to account for the EHC process and predict concentrations of drugs that undergo EHC. Inclusion of EHC in the models represented by a gallbladder compartment usually allows the capture of multiple peaks in the concentration time profiles and the prolonged half-life associated with EHC (1). Mycophenolic (MPA), for example, shows multiple peaks and has a reported half-life of 17.9±6.5 hours (86).

Following the example case of MPA, several models incorporated the effect of EHC on MPA pharmacokinetics (63, 68, 87, 88). Most of these models included an additional compartment to represent the gallbladder in the EHC process. The drug transfer from the gallbladder compartment to the gut compartment was usually assumed to occur at mealtimes, where the number of modeled mealtimes varied (67, 68, 88). In another approach, the drug transfer from the gallbladder to the gut was implemented as a continuous drain from a central compartment to the gut (89); however, this approach does not represent the physiology of EHC in humans and animals that have a gallbladder. Several other studies were not successful in characterizing the EHC process for MPA, and most of these studies used a simple one-compartment or two-compartment disposition model (90-93). The inability to model the EHC process may be attributed to insufficiency or inadequacy of sampling schedules and complexity of MPA pharmacokinetics (94). Variations in models may result in differences in the reported parameter estimates. For example, the reported values of the oral clearance of total MPA vary between 13-37 L/hr (94, 95).

These overall results demonstrate the need to systematically evaluate the various EHC models to determine the models ability to characterizes the effect of EHC on pharmacokinetics, and provide accurate and precise estimates of parameters. Therefore, the objectives of the current study were to evaluate and compare parameter estimates from several EHC models following a single dose of a drug undergoing EHC. Further, steady-state simulations were conducted to assess the predictive ability of these models when used to simulate steady-state concentrations.

3.2 Methods

3.2.1 Simulation Model

The model developed in chapter 2 was used as a simulation model (Figure 3-1). The structure of this model is based on the physiological concepts related to the hepatobiliary system and the gallbladder filling and emptying processes (1, 35-38). The parameter values used in the simulation model are tabulated in in Table 3-1. The model assumes an oral route of administration, where the first order rate constant (k_A) characterizes the absorption process. Elimination from the central compartment is defined using the rate constant k_{20} that is calculated as the ratio of clearance (CL) divided by volume of distribution in the central compartment (V), i.e., $k_{20} = \frac{CL}{V}$. The rate constant k_{23} describes the distributive EHC out of central compartment and it was assumed that approximately 75% of the drug transferred via the k_{23} rate constant goes to the gallbladder, while the remaining 25% leaks and drains directly to the gut compartment (leaking fraction) (35, 36, 39). As shown in Table 3-1, different values of the rate constant k_{23} were used to simulate varying extents of EHC%, where EHC% represents

the percentage of drug amount in central compartment distributed via EHC, and is described according to the following equation:

$$EHC\% = \frac{k_{23}}{k_{23} + k_{20}} * 100$$

The simulation model assumes that subjects receive three meals a day at mealtimes (mt) 1, 4, and 10 hrs after dosing. At these meal times, approximately 75% of the drug stored in the gallbladder is discharged to the gut within a duration (D) of 30 minutes (1, 37, 38). The transfer rate from the gallbladder to the gut is determined by the rate constant k_{GG} according to the following equation:

$$k_{GG} = k_{31} * switch$$

where k_{31} is a rate constant and $switch$ is a function that accounts for multiple cycles of gallbladder emptying. $k_{31}$was fixed to the value 2.77 hr^{-1} based on a simulation analysis which showed that this value results in eliminating 75% of the drug from the gallbladder, within the assumed duration of 30 minutes, see Figure 3-2. The $switch$ function was defined according to the following equations:

$$Hill1 = \exp(-20 * (time - mt1))$$

$$Hill2 = \exp(-20 * (time - \mathrm{E}ndmt1))$$

$$Switch = \frac{1}{1 + Hill1} - \frac{1}{1 + Hill2}$$

where $mt1$ represents the beginning of gallbladder emptying (occurs at the time of mealtime); E$ndmt1$ represents the end of gallbladder emptying (after ~30 min) and calculated as E$ndmt1 = mt1 + D$.

The $Switch$ function uses a double sigmoid function to regulate the gallbladder release rate constant (k_{GG}) allowing a rapid change in the k_{GG} rate constant from zero to almost 2.77 around the time $mt1$. After approximately 30 minutes, $Switch$ causes a rapid decline in k_{GG} back to zero around time E$ndmt1$, see Figure 3-3A. This rapid change of $k_{GG}$was achieved by using a value of 20 in $Hill1$ and $Hill2$ in an attempt to mimic the toggle nature of gallbladder emptying. To represent the multiple cycles of gallbladder emptying, this set of equations was reapplied for each cycle at mealtimes (Figure 3-3B).

A between subject variability (BSV) of 20% was modeled on k_A, CL, and V parameters assuming a lognormal distribution according to the following equation:

$$P_j = TVP * e^{\eta_j}$$

where TVP is the Typical Value of the Parameter in the population and η_j is the difference between the j^{th} individual parameter value (P_j) and TVP on a lognormal scale. It was assumed that η_j values are independent and identically normally distrusted with a mean of zero and a variance ω^2, i.e. $\eta \sim N(0, \omega^2)$.

An additive BSV model (Meal-BSV) was used to allow the mealtimes (mt) to vary normally around the population value, according to the following equation:

$$mt_j = mt + \eta_j$$

where mt is the typical Value of mealtime in the population as described previously; and η_j is the difference between the j^{th} individual mealtime (mt_j) and mt . Again, it was assumed that η_j values follow a normal distribution with a mean of zero and a variance ω^2, which was fixed to a value of 0.06 i.e. $\eta \sim N(0,0.06)$. This variance was chosen to constrain around 95% of the population within ± one-half hour of the fixed effect mealtimes, while retaining the assumption of a normal distribution. For example, when the mealtime equals 4 hrs post-dose, around 95% of the sampled population will fall between 3.5, and 4.5 hours (Figure 3-4).

A proportional error model was included to simulate the residual unexplained variability (RUV) as seen below:

$$C_{ij} = C_{pred,ij} * (1 + \varepsilon_{ij})$$

where C_{ij} is simulated j^{th} central concentration in the i^{th} individual and $C_{pred,ij}$ is the predicted j^{th} central concentration in the i^{th} individual; and ε_{ij} is the j^{th} residual error in the i^{th} individual.

3.2.2 Estimation Models of EHC

A literature review of the EHC modeling strategies revealed the use of various models. Most of these models have the general structure of the gallbladder being represented by a compartment, where the transfer out of this compartment is dependent

upon mealtimes (45, 46, 74, 75, 82).

Seven EHC literature-based estimation models were evaluated in comparison to the previously defined simulation model. Although the structures of these estimation models were based on literature, the gallbladder emptying process was modeled using the rate constant k_{GG} described previously, when applicable. These models include:

Model 1: One-compartment disposition model, without consideration in the model for the EHC process (Figure 3-5)**.**

Model 2: Two-compartment disposition model, without consideration in the model for the EHC process (Figure 3-6)**.** This model allows for capturing a prolonged half-life; however, it does not predict secondary peaks.

Model 3: One-compartment disposition model with a continuous transfer from the central compartment to the gut compartment representing the EHC process (Figure 3-7). This model treats the gut as a peripheral compartment, where the EHC process is modeled as a distribution of a percentage of the drug amount from central compartment to the gut compartment, as described below:

$$EHC\% = \frac{k_{21}}{k_{21} + k_{20}} * 100$$

where k_{20} is the elimination rate constant from central compartment, and k_{21} is the EHC distribution rate constant from the central to the gut compartment.

This model also allows for capturing a prolonged half-life, without representing the secondary peaks.

Model 4: One compartment disposition model with the addition of a gallbladder compartment (Figure 3-8). In this model, the $EHC\%$ is described as:

$$EHC\% = \frac{k_{23}}{k_{23} + k_{20}} * 100$$

where k_{20} is the elimination rate constant from central compartment, and k_{23} is the EHC distribution rate constant from the central to the gallbladder compartment.

This model assumed no direct drainage of the drug from the central compartment to the gut compartment. Therefore, 100% of EHC mass was assumed to go to the gallbladder. An intake of one meal was assumed in this model; therefore, the gallbladder emptying occurred for one mealtime only. To control the discharge from the gallbladder, the same $Switch$ function described previously for the simulation model was used.

Model 5: This model is the same as model 4, however model 5 assumes two mealtimes rather than one **(Figure 3-9).**

Model 6: This model is the same as model 4, however model 6 assumes three mealtimes rather than one **(Figure 3-10).**

Model 7: This model is the same as the simulation model in all assumptions except the fundamental postulate associated with the EHC process **(Figure 3-11)**. The EHC process in the simulation model is considered distributive. On the other hand, model 7 assumes the EHC process as a fraction of elimination rather than being a distribution process. Therefore, the rate constants k_{23}, and k_{20} in model 7 were defined as:

$$k_{23} = EHC\% * \frac{CL}{V}$$

$$k_{20} = (1 - EHC\%) * \frac{CL}{V}$$

where k_{23} is the biliary elimination rate constant; k_{20} is the non-biliary elimination rate constant; CL is drug clearance; V is the volume of distribution; in this model, the $EHC\%$ is a parameter representing the percentage drug cleared via biliary pathway.

In summary, models 1 through 7 differ in several ways. Some of these models do not include a gallbladder compartment (models 1, 2) while some do (models 3-7). Some assumes a continuous EHC process (model 3), others assume a mealtimes-based EHC process (models 4-6), while others assume both (model 7 and the simulation model). The effect of the number of mealtimes was also evaluated: one meal (model 4), two meals (model 5), and three meals (model 6). Lastly, model 7 shows the effect of parameterizing the EHC process as elimination rather than a distribution process.

3.2.3 Stochastic Simulation and Estimation

A stochastic Simulation and Estimation (SSE) analysis method was used to compare parameter estimates of the various estimation models, in addition to the simulation model. This SSE analysis was composed of two consecutive steps: Monte Carlo simulation of 250 concentration datasets using the simulation model, followed by parameter estimation using the simulation model and the seven described estimation models. SSE analyses were done considering several EHC%: 20%, 40%, 60%, and 80%. NONMEM (version 7.3, ICON Development Solutions), via the SSE module in Perl speaking NONMEM (PsN) (96), was used for these evaluations.

The structure of the simulation datasets imitated an orally administrated single dose of 1000 mg to 50 subjects. In all subjects, an intensive sampling protocol was used

in which 11 concentrations were sampled at times 0, 0.5, 1, 2, 4, 6, 8, 10, 12, 16, and 24 hours post-dosing. The same study design was simulated for the various EHC%.

In order to compare the estimation abilities of the included models, an evaluation of parameters estimates was performed in terms of relative bias and precision. Relative Bias is a metric that shows the deviation of a model parameter estimate from the true value used in the simulation, and is calculated as the average difference between these two values relative to the true value:

$$RelativeBias\% = 100 * \frac{1}{N}\sum \frac{\hat{\theta}_i - \theta}{\theta}$$

where N is number of datasets, which in this analysis $N = 250$ datasets; θ represents the true parameter used in the simulations, and $\hat{\theta}_i$ is the model estimated parameter from the ith dataset. In the current study, each model SSE estimation for a given parameter was considered to be biased if the $RelativeBias\%$ (RelBias%) > 10%. As measure of imprecision, relative Root-Mean-Square Error ($Relative\ RMSE\ \%$) was calculated as the following:

$$Relative\ RMSE\ \% = 100 * \sqrt{\frac{1}{N}\sum \frac{(\hat{\theta}_i - \theta)^2}{\theta^2}}$$

In the current study, each parameter Relative RMSE from each model was qualitatively compared to the simulation model respective parameter, instead of having a

cut-off value.

The relative bias and relative RMSE of volume of distribution (V) parameter in the two compartment model (model 2) were calculated for three volume parameters: the central volume of distribution [Model 2 (Vc)], the peripheral volume of distribution [Model 2 (Vp)], and the steady state volume of distribution [Model 2 (Vss)]. The relative bias and RMSE of these three volume parameters were calculated relative to the true V used in the simulations.

As part of the SSE analysis, the objective function values (OFV) for each model as well as NONMEM runtimes were compared.

3.2.4 Steady-State Simulations

An additional analysis was conducted to evaluate the consequences of the behavior of the various EHC models when used to simulate steady state profiles. In detail, a simulation for each of the models (1 simulation+ 7 estimation models) was performed. In these simulations, fixed-effect parameters were assumed as the averages of the SSE result for each corresponding model. BSV and RUV were fixed to zero in these deterministic simulations. These simulations imitated a multiple dose regimen where a 1000 mg dose was given orally every 24 hours for 10 days to meet the steady-state assumption.

Simulated samples from the steady-state profiles were analyzed using NCA module in WinNonlin version 6.4 (Pharsight Corporation, CA, USA). For each of these simulations, the maximum concentration at steady state (Css_{max}) and the minimum concentration at steady state (Css_{min}) were identified. Additionally, the linear trapezoidal rule was used to calculate the area under the curve at steady state from 0 to 24 hours post-

dose (AUCss). The respective values of relative bias of these variables were also calculated according to the same relative bias equation mentioned above.

3.3 Results

SSE were successfully completed. This analysis was performed on the seven EHC models (Models 1-7) and the simulation model. Boxplots of distributions for each parameter determined using various EHC% are presented in Figures 3-12, 3-13, 3-14, 3-15. Each of these boxplot represents a distribution of parameter estimates based on an EHC model used with an assumed EHC%.

The mean, median, relative bias and relative RMSE were used to summarize the estimation ability of the models. Tables (3-2, 3-3, 3-4, 3-5) show the calculated statistics for each of the EHC models when considering the various EHC%.

3.3.1 Relative Bias

The relative bias values of all the parameters with the several models are plotted across the various EHC% as demonstrated in Figure 3-16. Results for each parameter are discussed below.

Clearance (CL; Figure 3-16A)

As EHC% is increased to 40, 60, and 80%, models 1-3 have an average relative bias values around 20%, 45%, and 110%, respectively. Modeling 1 mealtime without a leaking fraction (model 4) resulted in a relative bias that was larger than 10% when EHC% is 60% and 80%. Model 5 that included two mealtimes but no leaking fraction

was marginally biased (~15%) only for 80% EHC. Model 6 which included three meals with no leaking fraction resulted in unbiased (<10%) estimates of CL regardless of the EHC%. Model 7 had the greatest relative bias in CL across the various EHC%, where this relative bias increased as EHC% escalated.

Volume of distribution (V; Figure 3-16B)

The one-compartment model (model 1) showed the highest relative bias in V, where this bias increased with increasing ECH%. Additionally, all volume parameters for the two-compartment model (model 2) were biased; however, the steady state volume of distribution (Vss) was the least biased. Excluding 20% EHC, Model 3 resulted in biased V. In general, the various numbers of meals (models 4-6) showed no biased V, except at ≥ 60% EHC. Assuming EHC is a fraction of elimination (model 7) showed no bias in V estimation regardless of the EHC%.

Absorption parameter (k_A; Figure 3-16C)

Model 1 resulted in unbiased k_A when EHC% ≤40%, however, it became highly biased at ≥60% EHC. k_A was particularly biased for models 2 and 3 where bias increased as EHC% increased. At lower EHC%, models 4-6 resulted in unbiased k_A; while at EHC% > 40%, k_A was highly biased for these models. Model 7 did not show bias in k_A.

EHC% (Percent; Figure 3-16D)

Models 3-7 included an estimated parameter of the EHC% named “Percent”. Model 3 estimated an unbiased Percent parameter with the 20%, and 40% EHC; however, biased results were observed with 60%, and 80% EHC. Estimations of Percent parameter with models 4-6 were generally biased regardless of the EHC%. However, including two or

three mealtimes (models 5 and 6) resulted in less bias when compared to modeling 1 mealtime only (model 4). Model 7 resulted in an unbiased Percent parameter for all EHC%.

BSV parameters (Figures 3-16E-H)

Models 1-4 generally resulted in biased (>10%) BSV on CL (BSV-CL) (Figure 3-16E). Modeling two or three mealtimes (models 5, 6) showed unbiased BSV-CL estimates regardless of EHC%. Assuming EHC as a fraction of elimination (model 7) resulted in unbiased BSV-CL except at 80% EHC.

Except at 20% EHC, models 1-6 led to biased BSV on V (BSV-V) regardless of EHC%. The one-compartment model (model 1) and the two-compartment model (model 2) resulted in the highest bias in BSV-V (Figure 3-16F). Unbiased BSV-V was estimated with model 7.

The BSV parameter on k_A (BSV-k_A) was generally biased when estimated using any of models 1-4 (Figure 3-16G). Modeling two or three mealtimes (models 5 and 6) resulted in unbiased BSV-K_A estimates only when EHC% is $\leq$ 40%. Model 7 did not cause bias in BSV-k_A regardless of EHC%.

Lastly, estimates of BSV-Meal included in models 4-7 were usually biased regardless of EHC% (Figure 3-16H).

RUV parameter (Figure 3-16I)

Bias in the estimated RUV was very prominent with models 1-3 (Figure 3-16I). With EHC% > 20%, modeling 1 mealtime (model 4) exhibited bias as well. Principally, models 1-4 showed an increased bias with increasing EHC%. On the other hand, models

5-7 produced unbiased RUV parameter estimates.

3.3.2 Relative RMSE

Plots of the Relative RMSE for the various EHC% are shown in Figure 3-17. Results are discussed below.

Clearance (CL; Figure 3-17A)

Models 1-4 resulted in imprecise CL estimates when EHC% ≥ 60%. On the other hand, models 5 and 6 precisions were comparable to the simulation model across the various EHC%. Model 7 resulted in highly imprecise CL, where this imprecision escalated with increased EHC%.

Volume of distribution (V; Figure 3-17B)

Generally, models 1-3 caused highly imprecise estimation of V. With respect to model 2, Vss parameter was associated with a lower impression when compared to Vc and Vp. Models 4-6 resulted in more precise estimates with lower EHC%; however, imprecision increased at higher EHC%. Model 7 demonstrated similar precision of V estimation as the simulation model.

Absorption parameter (k_A; Figure 3-17C)

With model 1, the k_A parameter showed similar precision to the simulation model at EHC% ≤ 40%. On the other hand, models 2 and 3 demonstrated high imprecision in k_A estimation, where this imprecision increased with increased EHC%. Model 4 resulted in imprecise estimates of k_A at EHC% ≥ 40%, while model 5 and 6 at EHC% = 80%. Model

7 showed similar precision of k_A estimation as the simulation model.

EHC% (Percent; Figure 3-17D)

Estimates of the Percent parameter were generally imprecise when modeled using models 3 and 4. Models 5 and 6 caused marginally imprecise estimate of percent, where this imprecision is higher at lower EHC%. Except at 20% EHC, model 7 showed precise estimates.

BSV parameters (Figure 3-17 E-H)

Imprecision in random effect parameters was also related to EHC%, where higher EHC% led to less precise estimations. Added to that, models 1-3 resulted in more imprecision in comparison to gallbladder-based models (models 4-7).

RUV parameter (Figure 3-17I)

Estimation of the RUV parameter was highly imprecise with models 1-4 at EHC% $\geq$ 40%. On the other hand, models 5-7 provided precision of RUV similar to simulation model regardless of EHC%.

3.3.3 OFV and Runtimes

During the SSE analysis, the OFV and the estimation runtime of each NONMEM run were recorded. Analysis of the means of the OFVs across the various EHC% showed contrary results for models 1-3 versus models 4-7 (Figures 3-18). With increasing EHC%, the OFVs increased with models 1-3 and decreased with models 4-7. Also, models that included two or three mealtimes (models 5 and 6) resulted in improved data fit (lower OFV) compared to one mealtime only (model 4).

When evaluating the runtimes, models 1-3 required estimation runtimes that were

much shorter than that required by models 4-7 (Figure 3-19). Added to that, the higher EHC% was associated with longer runtimes.

3.3.4 Steady-State Simulations

Steady state concentrations based on multiple dosing strategies were simulated using the aforementioned EHC models. For the various EHC%, the simulations using the various EHC models are shown in Figure 3-20. Table 3-6 shows the following exposure metrics: Css_{max}, Css_{min}, AUCss, and their respective relative bias calculations. These metrics were plotted using two plotting methods: line plots and bar plots, Figures 3-21, 3-22, respectively.

-Css_{max}

When EHC% is 20%, the Css_{max} was not biased except with model 2. For higher EHC%, all models except models 6 and 7 were associated with biased Css_{max}. This bias showed an increasing trend with higher EHC%.

-Css_{min}

At 20% EHC, Css_{min} was only biased with model 2. However, at higher EHC%, models 1-4 caused biased Css_{min}.

-AUCss

Calculated AUCss showed bias with models 1-3 when EHC% ≥40%. Again, bias increased as EHC% was increasing. With models 4 and 5, bias was also observed starting at 60% and 80% EHC, respectively.

3.4 Discussion

This is the first study to compare various EHC models and the contribution of EHC% after a single dose of a drug that undergoes EHC. Models were evaluated based on the bias and precision in the estimated pharmacokinetic parameters. Models were also compared in terms of their predictive performance of simulated steady state concentrations.

The physiology of EHC includes a cycle of bile secretion followed by gut reabsorption. During fasting, around 75% of secreted bile gets stored in the gallbladder while the remaining 25% drains directly to the duodenum (35, 36). On the sight, smell, or ingestion of food, the gallbladder contracts while the sphincter of Oddi relaxes causing the release of around 75% of bile stored in the gallbladder to the duodenum (1, 35-39). Once the meal is finished, the gallbladder relaxes and the sphincter of Oddi contracts causing a restart in the cycle of the gallbladder bile storage.

Overall, the choice of the EHC model, used to represent the EHC process, influences the degree of bias and precision of the estimated fixed and random effect parameters. Modeling strategies that do not account for the EHC process (models 1, 2) result in high bias and imprecision in these parameters. This would be expected as the model structures do not include a distributive phase representing the EHC process. Using a continuous leak (model 3) to represent this distributive EHC results in large bias and imprecision as well, suggesting the model incorrectly represents the above-mentioned EHC process. The modeling technique in model 3 takes on minimal complexity among the EHC models; however, it does not accurately depict the toggle nature of the

gallbladder emptying process. The EHC process involves gallbladder storing and emptying which behaves nonlinearly rather than as a continuous process. Moreover, models 1-3 are crucially disadvantaged as they do not capture the secondary peaks observed in the EHC process, which could lead to inaccurate estimation of pharmacokinetic parameters.

Lower bias and imprecision is observed when utilizing models that include a gallbladder compartment with a various number of modeled mealtimes (models 4-6). The addition of the gallbladder compartment allows for a better portrayal of the EHC process in human and animals containing a gallbladder. This reflects the fractional storage and subsequent release of a given drug dose in the gallbladder. Additionally, the more similar the number of modeled mealtimes to the true number, the lower bias and imprecision is in the estimated parameters.

The assumption of EHC as a fraction of elimination (model 7) rather than as a distributive process does not affect parameters estimates except CL. Model 7 assumes that EHC is a fraction of the elimination process and therefore results in an overestimation of the CL parameter. This may not be clinically significant at lower EHC% (for example 20%); however, at higher EHC%, it may results in large overestimation.

The EHC% often impacts model performance. In general, a higher EHC% is associated with higher bias and imprecision in parameters. This EHC% effect is significantly more prominent with models 1-3 versus models 4-7. Nevertheless, lower EHC% is associated with minor differences are seen between the various models in terms

of bias and precision. This could be attributed to the insignificance of the EHC process at lower EHC%; therefore, less effect of EHC model mis-representation is observed in terms or parameter estimation. On the other hand, the EHC process seems to have a significant effect with higher EHC% and therefore caution should be taken to avoid using models 1-3 at high EHC%, i.e., EHC% ≥40%.

Comparison of the models in terms their ability to capture the data also supports the superiority of the gallbladder-based models over the other models. The OFVs across the various EHC% show different results for models 1-3 versus models 4-7. With increasing EHC%, the OFVs of models 1-3 increased while decreased for models 4-6. In addition, models that included two and three mealtimes (models 5, 6) had better fits than when only one mealtime is included (model 4). These observations demonstrate that the ability of a model to better fit the data improves with higher EHC%. However, this is only true when using an EHC model that involves a gallbladder compartment with a close to true number of mealtimes. As stated previously, non-gallbladder based models result in fits that are generally poor. Such an observation is important as it indicates the presence of high model misspecification when considering models 1-3 for drugs undergoing significant EHC. These results confirm the importance of fitting the data using gallbladder-based models.

The current study evaluated the predictive ability of the various EHC models when used to simulate steady state concentrations. The consequences of the EHC process on the steady state pharmacokinetic profiles of the various models varied based on the EHC%. Additionally, steady-state simulations demonstrated various outcomes depending

on the studied pharmacokinetic exposure metric. At 20% EHC, all estimation models resulted in unbiased AUCss; and all models but model 2 resulted in unbiased Css_{max} and Css_{min}. This result could be attributed to the SSE results of Model 2 showing a combination of overestimating CL and underestimating V and k_A. Based on that, utilizing any of the tested models except model 2 would be appropriate at lower EHC%, i.e., 20%. At higher EHC%, steady-state metrics start to be influenced by the used EHC modeling strategy. Only models that use the exact number of meal times as the truth would result in unbiased steady-state metrics; otherwise, a varying degree of bias should be expected. Overall, the use of gallbladder-based models with as close to truth number of mealtimes results in unbiased (or marginally biased) pharmacokinetic exposure metrics, and using non-gallbladder based models produce biased metrics, where this bias increases with increased EHC%.

3.5 Conclusion

This study was able to demonstrate several characteristics of the EHC process. When a drug undergoes EHC, it is important to model the data using a gallbladder-based EHC model where the number of mealtimes is as close to the truth as possible. In this model, including a fraction of the EHC process that drains directly from the central compartment to the gut is important as it help reducing bias in some parameters like volume of distribution. Contrastingly, the use of non-gallbladder based models, like simple one-compartment or two-compartment model, introduces more bias and imprecision in the estimated parameters. Additionally, bias and imprecision are related to

the EHC%, where the higher the EHC% is, the greater the bias and imprecision get. Moreover, assuming that EHC is a fraction of the elimination process results in similar conclusions to the simulation model except inflating the clearance parameter estimate, where higher inflation is associated with higher EHC%.

Different effects on the steady state exposure metrics are seen when using various EHC modeling strategies. In general, the non-gallbladder based models produce biased steady-state metrics that increase with increasing EHC%. Gallbladder based models, on the other hand, produce unbiased or minimally biased exposure metrics. In these gallbladder-based models, the number of included mealtimes significantly influences the ability to capture the exposure metrics.

Table 3-1: Parameters Used in the Simulation of Various EHC%

Parameter	**Value (unit)**
Clearance (CL)	5 (L/hr)
Volume of distribution (V)	36 (L)
Absorption rate constant (k_A)	0.75 (hr^{-1})
Gallbladder to gut rate constant (k_{GG})	2.77 (hr^{-1})
Mealtimes	1, 4 , 10 (hours)
Duration of gallbladder emptying (D)	30 (minutes)
BSV-CL	0.04
BSV -V	0.04
BSV-k_A	0.04
BSV-Meal	0.06
RUV	0.01

EHC Percent (%)	**k_{23} (hr^{-1})**
0 %	0
20 %	0.035
40 %	0.093
60 %	0.208
80 %	0.556

Table 3-2: Statistics of SSE Outputs with 20% EHC

Parameter	EHC Model	Mean	Median	Relative RMSE%	Relative Bias%
Estimation time	Model 1	27.955	25.135	-	-
	Model 2	59.584	56.645	-	-
	Model 3	57.474	55.060	-	-
	Model 4	275.911	266.040	-	-
	Model 5	476.446	414.015	-	-
	model 6	682.988	636.850	-	-
	Model 7	660.329	638.035	-	-
	Simulation model	678.532	586.290	-	-
OFV	Model 1	762.618	761.676	-	-
	Model 2	745.698	746.302	-	-
	Model 3	759.141	758.944	-	-
	Model 4	662.680	652.549	-	-
	Model 5	628.889	628.305	-	-
	model 6	630.678	626.006	-	-
	Model 7	630.259	629.573	-	-
	Simulation model	624.023	623.499	-	-
k_A	Model 1	0.757	0.756	3.199	0.993
	Model 2	0.530	0.531	30.342	-29.316
	Model 3	0.691	0.692	9.897	-7.830
	Model 4	0.728	0.718	5.859	-2.923
	Model 5	0.749	0.747	3.632	-0.144
	model 6	0.757	0.759	4.152	0.994
	Model 7	0.735	0.736	4.860	-1.940
	Simulation model	0.746	0.745	3.379	-0.467

CL	Model 1	5.367	5.355	7.900	7.335
	Model 2	5.399	5.387	8.516	7.984
	Model 3	5.371	5.359	7.966	7.419
	Model 4	5.066	5.085	6.103	1.315
	Model 5	5.036	5.029	3.129	0.717
	model 6	5.022	5.019	3.285	0.435
	Model 7	6.179	6.191	24.195	23.580
	Simulation model	5.008	5.001	3.024	0.168
V	Model 1	37.306	37.257	4.632	3.628
	Model 2 (Vc)	24.661	24.588	32.600	-31.498
	Model 2 (Vp)	9.199	9.353	74.587	-74.446
	Model 2 (Vss)	33.860	33.892	7.712	-5.944
	Model 3	34.063	34.128	8.415	-5.382
	Model 4	35.818	35.375	4.787	-0.505
	Model 5	36.257	36.181	3.457	0.715
	model 6	36.552	36.486	4.009	1.533
	Model 7	35.687	35.763	3.933	-0.870
	Simulation model	35.966	35.894	3.165	-0.095
Percent	Model 3	0.216	0.231	50.979	7.855
	Model 4	0.103	0.102	55.110	-48.686
	Model 5	0.147	0.151	28.926	-26.580
	model 6	0.156	0.159	25.680	-22.180
	Model 7	0.185	0.194	20.574	-7.698
	Simulation model	0.208	0.208	9.883	3.966
	Model 1	0.029	0.029	35.575	-26.288
	Model 2	0.017	0.017	63.389	-58.135

	Model 3	0.033	0.033	34.161	-16.730
	Model 4	0.033	0.032	29.594	-18.404
BSV- k_A	Model 5	0.036	0.036	25.770	-9.954
	model 6	0.037	0.036	26.292	-8.354
	Model 7	0.037	0.037	25.725	-7.230
	Simulation model	0.039	0.039	24.901	-3.437
	Model 1	0.034	0.034	23.778	-13.764
	Model 2	0.035	0.035	23.166	-12.039
	Model 3	0.035	0.034	23.331	-12.455
	Model 4	0.037	0.037	22.132	-7.793
BSV-CL	Model 5	0.039	0.039	21.889	-2.962
	model 6	0.039	0.038	22.085	-2.289
	Model 7	0.039	0.039	21.620	-3.216
	Simulation model	0.040	0.039	22.143	-1.188
	Model 1	0.034	0.033	24.847	-14.461
	Model 2	0.076	0.076	103.354	91.021
	Model 3	0.039	0.038	27.150	-1.270
	Model 4	0.040	0.040	24.019	-0.287
BSV-V	Model 5	0.039	0.038	21.929	-2.913
	model 6	0.038	0.038	22.099	-4.518
	Model 7	0.040	0.039	22.769	0.481
	Simulation model	0.040	0.039	22.404	-1.086
	Model 4	0.342	0.000	5334.445	470.407
	Model 5	0.072	0.000	240.948	20.530
	model 6	0.073	0.000	249.769	21.545
BSV-Meal	Model 7	0.070	0.000	216.642	17.081

	Simulation model	0.098	0.000	299.596	63.074
RUV	Model 1	0.015	0.014	47.416	45.839
	Model 2	0.014	0.014	45.930	44.246
	Model 3	0.015	0.015	48.390	46.829
	Model 4	0.011	0.010	21.505	11.005
	Model 5	0.010	0.010	9.865	0.324
	model 6	0.010	0.010	11.588	0.934
	Model 7	0.010	0.010	9.773	0.668
	Simulation model	0.010	0.010	7.728	-1.147

Table 3-3: Statistics of SSE Outputs with 40% EHC

Parameter	EHC Model	Mean	Median	Relative RMSE%	Relative Bias%
Estimation time	Model 1	22.407	20.630	-	-
	Model 2	52.075	44.135	-	-
	Model 3	63.142	57.420	-	-
	Model 4	333.114	317.110	-	-
	Model 5	489.167	433.240	-	-
	model 6	796.632	686.580	-	-
	Model 7	819.109	738.930	-	-
	Simulation model	703.973	593.350	-	-
OFV	Model 1	976.986	978.384	-	-
	Model 2	892.792	896.320	-	-
	Model 3	965.393	967.369	-	-
	Model 4	594.927	589.776	-	-
	Model 5	515.418	513.888	-	-
	model 6	514.552	513.227	-	-
	Model 7	513.768	512.498	-	-
	Simulation model	513.049	511.680	-	-
k_A	Model 1	0.778	0.778	5.502	3.793
	Model 2	0.281	0.300	63.021	-62.594
	Model 3	0.565	0.564	25.534	-24.638
	Model 4	0.660	0.656	12.726	-12.008
	Model 5	0.764	0.762	4.246	1.882
	model 6	0.784	0.780	6.344	4.485
	Model 7	0.749	0.746	4.600	-0.152

	Simulation model	0.751	0.747	4.474	0.102
CL	Model 1	5.969	5.959	19.656	19.387
	Model 2	6.087	6.080	22.009	21.748
	Model 3	5.993	5.982	20.133	19.861
	Model 4	5.309	5.309	7.010	6.186
	Model 5	5.073	5.069	3.482	1.464
	model 6	5.024	5.018	3.227	0.484
	Model 7	8.397	8.387	68.204	67.948
	Simulation model	5.012	5.010	3.239	0.235
V	Model 1	39.850	39.874	11.079	10.693
	Model 2 (Vc)	12.438	13.084	65.852	-65.449
	Model 2 (Vp)	12.130	12.752	66.504	-66.305
	Model 2 (Vss)	24.569	26.396	33.989	-31.754
	Model 3	28.894	28.860	20.860	-19.739
	Model 4	33.960	33.855	6.810	-5.667
	Model 5	37.104	37.080	4.334	3.066
	model 6	37.809	37.859	6.120	5.024
	Model 7	36.117	36.110	3.503	0.326
	Simulation model	36.190	36.264	3.480	0.528
Percent	Model 3	0.418	0.422	9.512	4.403
	Model 4	0.206	0.205	48.523	-48.416
	Model 5	0.315	0.315	21.438	-21.226
	model 6	0.335	0.335	16.927	-16.341
	Model 7	0.401	0.401	4.933	0.368
	Simulation model	0.404	0.404	4.898	1.086
	Model 1	0.009	0.001	84.673	-77.380

	Model 2	0.017	0.003	74.808	-56.567
	Model 3	0.024	0.001	86.319	-38.854
	Model 4	0.023	0.026	52.978	-41.491
BSV- k_A	Model 5	0.036	0.035	29.285	-10.097
	model 6	0.037	0.037	29.138	-6.283
	Model 7	0.040	0.040	31.008	0.637
	Simulation model	0.041	0.040	31.443	1.403
	Model 1	0.027	0.027	36.537	-33.054
	Model 2	0.031	0.031	27.980	-22.096
	Model 3	0.030	0.030	30.538	-25.515
	Model 4	0.034	0.034	23.982	-15.281
BSV-CL	Model 5	0.038	0.038	21.406	-5.023
	model 6	0.039	0.039	21.437	-3.496
	Model 7	0.039	0.039	22.978	-2.433
	Simulation model	0.039	0.039	21.584	-2.731
	Model 1	0.029	0.029	34.449	-26.401
	Model 2	0.080	0.097	172.485	99.652
	Model 3	0.037	0.039	59.548	-8.618
	Model 4	0.045	0.044	29.334	12.892
BSV-V	Model 5	0.036	0.036	22.503	-9.371
	model 6	0.035	0.035	23.537	-12.259
	Model 7	0.038	0.038	22.933	-3.808
	Simulation model	0.038	0.038	22.825	-4.258
	Model 4	0.017	0.000	395.980	-71.499
	Model 5	0.036	0.014	92.257	-39.822
	model 6	0.051	0.034	98.850	-15.246

BSV-Meal	Model 7	0.043	0.020	96.579	-28.381
	Simulation model	0.054	0.036	95.347	-10.579
RUV	Model 1	0.035	0.035	253.286	250.766
	Model 2	0.029	0.029	190.472	187.970
	Model 3	0.035	0.034	248.004	245.669
	Model 4	0.013	0.012	37.046	26.791
	Model 5	0.010	0.010	7.636	-1.084
	model 6	0.010	0.010	7.589	-1.524
	Model 7	0.010	0.010	7.618	-0.853
	Simulation model	0.010	0.010	7.607	-1.542

Table 3-4: Statistics of SSE Outputs with 60% EHC

Parameter	EHC Model	Mean	Median	Relative RMSE%	Relative Bias%
Estimation time	Model 1	53.721	48.630	-	-
	Model 2	100.392	89.510	-	-
	Model 3	134.749	124.325	-	-
	Model 4	363.211	350.450	-	-
	Model 5	488.607	470.165	-	-
	model 6	896.225	803.880	-	-
	Model 7	1186.278	1117.540	-	-
	Simulation model	868.640	733.260	-	-
OFV	Model 1	1185.522	1186.521	-	-
	Model 2	1079.230	1079.674	-	-
	Model 3	1169.171	1170.490	-	-
	Model 4	573.991	577.030	-	-
	Model 5	333.438	333.019	-	-
	model 6	330.933	331.768	-	-
	Model 7	326.603	327.326	-	-
	Simulation model	323.968	323.245	-	-
k_A	Model 1	0.875	0.873	18.038	16.727
	Model 2	0.243	0.243	67.662	-67.657
	Model 3	0.347	0.309	56.044	-53.669
	Model 4	0.554	0.556	26.364	-26.099
	Model 5	0.791	0.792	6.286	5.480
	model 6	0.815	0.814	9.602	8.632
	Model 7	0.737	0.737	4.922	-1.744
	Simulation model	0.736	0.737	4.728	-1.899

CL	Model 1	7.195	7.200	44.063	43.891
	Model 2	7.340	7.334	46.963	46.803
	Model 3	7.245	7.246	45.079	44.903
	Model 4	5.846	5.852	17.282	16.923
	Model 5	5.173	5.179	4.874	3.453
	model 6	5.062	5.048	3.827	1.239
	Model 7	12.417	12.434	148.631	148.336
	Simulation model	5.025	5.018	3.604	0.499
V	Model 1	47.172	47.147	31.232	31.034
	Model 2 (Vc)	10.394	10.373	71.146	-71.126
	Model 2 (Vp)	13.484	13.451	62.562	-62.544
	Model 2 (Vss)	23.879	23.834	33.753	-33.670
	Model 3	18.786	16.794	51.202	-47.816
	Model 4	30.825	31.001	15.147	-14.375
	Model 5	39.049	38.982	8.973	8.470
	model 6	40.063	39.995	11.829	11.285
	Model 7	36.088	35.932	3.745	0.243
	Simulation model	36.053	35.954	3.722	0.146
Percent	Model 3	0.399	0.405	35.065	-33.453
	Model 4	0.310	0.310	48.362	-48.335
	Model 5	0.495	0.496	17.506	-17.419
	model 6	0.517	0.517	14.105	-13.811
	Model 7	0.594	0.594	2.955	-0.945
	Simulation model	0.595	0.595	2.929	-0.888
	Model 1	0.035	0.028	91.570	-11.764
	Model 2	0.015	0.016	70.004	-62.042

	Model 3	0.006	0.000	95.043	-84.619
	Model 4	0.008	0.006	82.841	-80.113
BSV- k_A	Model 5	0.031	0.031	32.432	-21.655
	model 6	0.033	0.032	30.653	-18.028
	Model 7	0.038	0.037	32.020	-4.290
	Simulation model	0.039	0.037	31.429	-3.737
	Model 1	0.015	0.015	63.003	-61.986
	Model 2	0.022	0.022	46.264	-44.007
	Model 3	0.023	0.023	44.883	-41.900
	Model 4	0.031	0.031	27.182	-21.374
BSV-CL	Model 5	0.038	0.038	20.402	-5.443
	model 6	0.038	0.038	20.298	-3.980
	Model 7	0.039	0.039	20.732	-1.810
	Simulation model	0.039	0.039	20.456	-1.862
	Model 1	0.004	0.000	92.151	-90.997
	Model 2	0.052	0.037	137.578	30.141
	Model 3	0.047	0.048	66.605	17.067
	Model 4	0.051	0.051	39.382	27.700
BSV-V	Model 5	0.034	0.033	24.341	-16.187
	model 6	0.032	0.032	26.022	-19.065
	Model 7	0.039	0.038	23.626	-3.023
	Simulation model	0.039	0.038	23.119	-3.055
	Model 4	0.003	0.000	95.316	-94.893
	Model 5	0.030	0.027	61.450	-50.760
	model 6	0.037	0.032	56.236	-37.628
BSV-Meal	Model 7	0.034	0.030	63.541	-42.536

	Simulation model	0.039	0.034	55.678	-35.220
RUV	Model 1	0.095	0.095	851.938	848.281
	Model 2	0.073	0.073	637.205	633.474
	Model 3	0.091	0.091	811.326	808.023
	Model 4	0.020	0.020	105.173	103.433
	Model 5	0.010	0.010	7.280	-0.210
	model 6	0.010	0.010	7.418	-1.193
	Model 7	0.010	0.010	8.367	0.968
	Simulation model	0.010	0.010	7.283	-0.527

Table 3-5: Statistics of SSE Outputs with 80% EHC

Parameter	EHC Model	Mean	Median	Relative RMSE%	Relative Bias%
Estimation time	Model 1	63.604	58.815	-	-
	Model 2	102.314	94.505	-	-
	Model 3	274.003	265.100	-	-
	Model 4	416.699	391.695	-	-
	Model 5	856.029	762.035	-	-
	model 6	1697.479	1539.805	-	-
	Model 7	1743.273	1453.870	-	-
	Simulation model	1394.241	990.095	-	-
OFV	Model 1	1228.708	1228.622	-	-
	Model 2	1149.354	1149.971	-	-
	Model 3	1220.626	1220.195	-	-
	Model 4	589.842	587.728	-	-
	Model 5	-60.762	-67.619	-	-
	model 6	-79.221	-90.728	-	-
	Model 7	-95.227	-122.229	-	-
	Simulation model	-133.303	-133.776	-	-
k_A	Model 1	1.478	1.476	97.865	97.105
	Model 2	0.245	0.245	67.328	-67.325
	Model 3	0.192	0.134	78.917	-74.357
	Model 4	0.490	0.490	34.773	-34.728
	Model 5	0.956	0.958	28.274	27.527
	model 6	1.032	1.041	39.272	37.553
	Model 7	0.741	0.734	8.969	-1.239

	Simulation model	0.750	0.748	7.059	0.059
CL	Model 1	10.542	10.537	111.006	110.831
	Model 2	10.795	10.808	116.082	115.907
	Model 3	10.682	10.684	113.815	113.634
	Model 4	8.246	8.306	65.420	64.927
	Model 5	5.769	5.734	16.578	15.376
	model 6	5.204	5.097	12.699	4.077
	Model 7	24.729	24.752	406.019	394.589
	Simulation model	5.025	5.016	4.586	0.502
V	Model 1	79.041	79.016	119.776	119.559
	Model 2 (Vc)	8.618	8.811	76.210	-76.061
	Model 2 (Vp)	10.131	7.089	77.538	-71.859
	Model 2 (Vss)	28.809	28.848	20.231	-19.975
	Model 3	47.245	47.379	31.844	31.235
	Model 4	50.367	50.907	41.463	39.908
	Model 5	35.914	36.088	8.096	-0.239
	model 6	36.412	36.426	6.508	1.145
	Model 7	22.857	22.677	36.885	-36.507
	Simulation model	31.475	31.414	13.595	-12.568
Percent	Model 3	0.081	0.005	92.962	-89.875
	Model 4	0.373	0.368	53.517	-53.376
	Model 5	0.689	0.690	13.939	-13.867
	model 6	0.736	0.741	8.461	-7.950
	Model 7	0.790	0.798	6.432	-1.276
	Simulation model	0.797	0.797	1.328	-0.383
	Model 1	0.001	0.000	98.062	-97.303

	Model 2	0.000	0.000	99.985	-99.985
	Model 3	0.000	0.000	99.990	-99.990
	Model 4	0.012	0.009	77.431	-71.085
BSV- k_A	Model 5	0.028	0.027	41.329	-30.625
	model 6	0.032	0.031	38.514	-19.903
	Model 7	0.040	0.040	50.451	-0.173
	Simulation model	0.040	0.041	47.577	0.687
	Model 1	0.001	0.000	97.231	-97.120
	Model 2	0.007	0.007	84.105	-83.393
	Model 3	0.011	0.011	73.299	-71.366
	Model 4	0.022	0.022	46.705	-44.289
BSV-CL	Model 5	0.037	0.035	34.887	-8.654
	model 6	0.040	0.036	140.450	0.642
	Model 7	0.071	0.039	464.169	76.679
	Simulation model	0.039	0.039	21.990	-2.716
	Model 1	0.000	0.000	99.990	-99.990
	Model 2	168.112	0.000	6643053.776	420181.250
	Model 3	0.001	0.000	99.191	-98.635
	Model 4	0.031	0.031	41.138	-21.742
BSV-V	Model 5	0.032	0.032	28.111	-19.526
	model 6	0.031	0.031	31.839	-22.348
	Model 7	0.039	0.037	50.740	-2.966
	Simulation model	0.038	0.037	41.539	-5.042
	Model 4	0.005	0.004	91.713	-91.152
	Model 5	0.061	0.028	373.948	1.643
	model 6	0.046	0.038	66.719	-23.211

BSV-Meal	Model 7	0.053	0.038	138.859	-11.944
	Simulation model	0.042	0.041	39.698	-29.520
RUV	Model 1	0.253	0.253	2432.512	2428.643
	Model 2	0.232	0.232	2222.929	2218.272
	Model 3	0.243	0.243	2330.843	2327.522
	Model 4	0.070	0.068	609.256	600.424
	Model 5	0.011	0.011	20.283	9.632
	model 6	0.010	0.010	24.886	4.513
	Model 7	0.012	0.010	95.951	16.260
	Simulation model	0.010	0.010	7.929	-0.484

Table 3-6: Steady-State CssMax, Cssmin, AUCss and their Relative Bias

Percent (%)	Model	Css_{max} mg/L	Css_{min} mg/L	AUC_{ss} hr*mg/L	Relative Bias Css_{max}	Relative Bias Css_{min}	Relative Bias AUC_{ss}
	Simulation Model	19.7	1.11	199.57	-	-	-
	Model-1	18.87	1.08	185.94	-4.21	-2.7	-6.83
	Model-2	17.19	2.11	184.77	-12.74	90.09	-7.42
20	Model-3	18.96	1.05	185.77	-3.76	-5.41	-6.91
	Model-4	19.06	1.19	197.02	-3.25	7.21	-1.28
	Model-5	18.79	1.13	198.23	-4.62	1.8	-0.67
	Model-6	19.31	1.04	198.74	-1.98	-6.31	-0.42
	Model-7	19.83	1.09	198.05	0.66	-1.8	-0.76
	Simulation Model	19.71	0.87	199.58	-	-	-
	Model-1	17.53	0.88	167.12	-11.06	1.15	-16.26
	Model-2	16.39	0.66	163.81	-16.84	-24.14	-17.92
40	Model-3	17.61	0.84	166.46	-10.65	-3.45	-16.59
	Model-4	18.23	1.04	188.2	-7.51	19.54	-5.7
	Model-5	17.32	0.94	196.75	-12.13	8.05	-1.42
	Model-6	19.61	0.87	198.62	-0.51	0	-0.48
	Model-7	19.62	0.86	198.52	-0.46	-1.15	-0.53

	Simulation Model	19.98	0.53	199.88	-	-	-
	Model-1	15.12	0.67	138.5	-24.32	26.42	-30.71
	Model-2	13.56	0.48	135.76	-32.13	-9.43	-32.08
60	Model-3	15.42	0.58	137.64	-22.82	9.43	-31.14
	Model-4	16.62	0.67	171.4	-16.82	26.42	-14.25
	Model-5	16.57	0.61	193.61	-17.07	15.09	-3.14
	Model-6	19.75	0.54	197.38	-1.15	1.89	-1.25
	Model-7	19.84	0.53	198.36	-0.7	0	-0.76
	Simulation Model	21.46	0.16	202.82	-	-	-
	Model-1	10.38	0.59	94.48	-51.63	268.75	-53.42
	Model-2	9.37	0.27	92.08	-56.34	68.75	-54.6
80	Model-3	11.87	0.3	93.23	-44.69	87.5	-54.03
	Model-4	13.28	0.18	121.79	-38.12	12.5	-39.95
	Model-5	18.15	0.18	175.95	-15.42	12.5	-13.25
	Model-6	20.59	0.16	194.53	-4.05	0	-4.09
	Model-7	20.73	0.14	194.88	-3.4	-12.5	-3.91

Figure 3-1: Depiction of the Simulation Model Used in the SSE Analysis

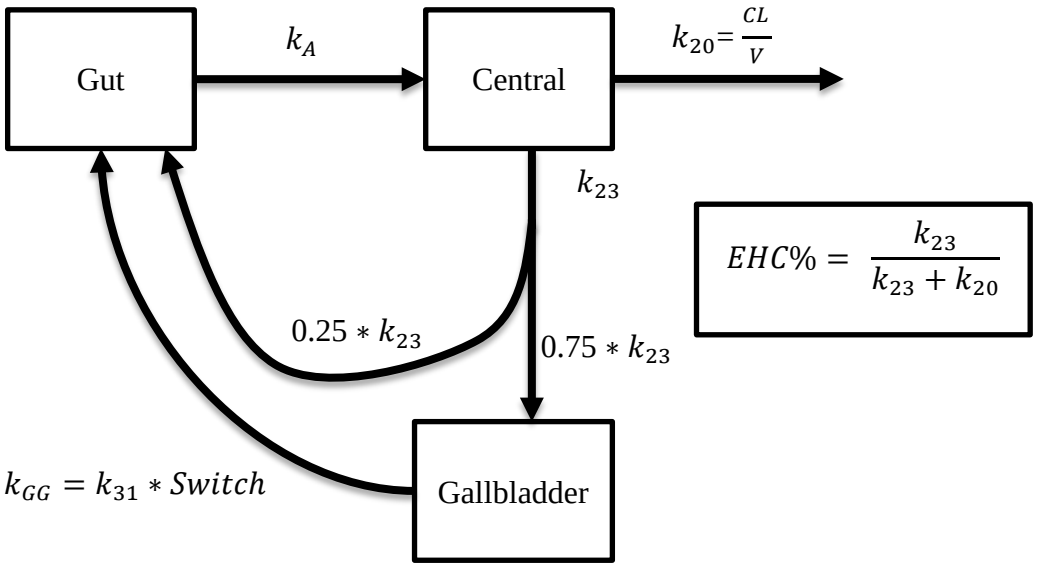

Key:

- **Compartments**: Gut: gut compartment, Central: central compartment, Gallbladder: represents the gallbladder
- **Rate constants:** k_A : absorption rate constant, CL: clearance, V: volume of distribution, K20: elimination rate constant, k_{23}: EHC distribution rate constant, k_{GG}: gallbladder emptying rate constant.

Figure 3-2: Plot of Gallbladder Drug Removal at k_{GG} = 2.77 hr^{-1}

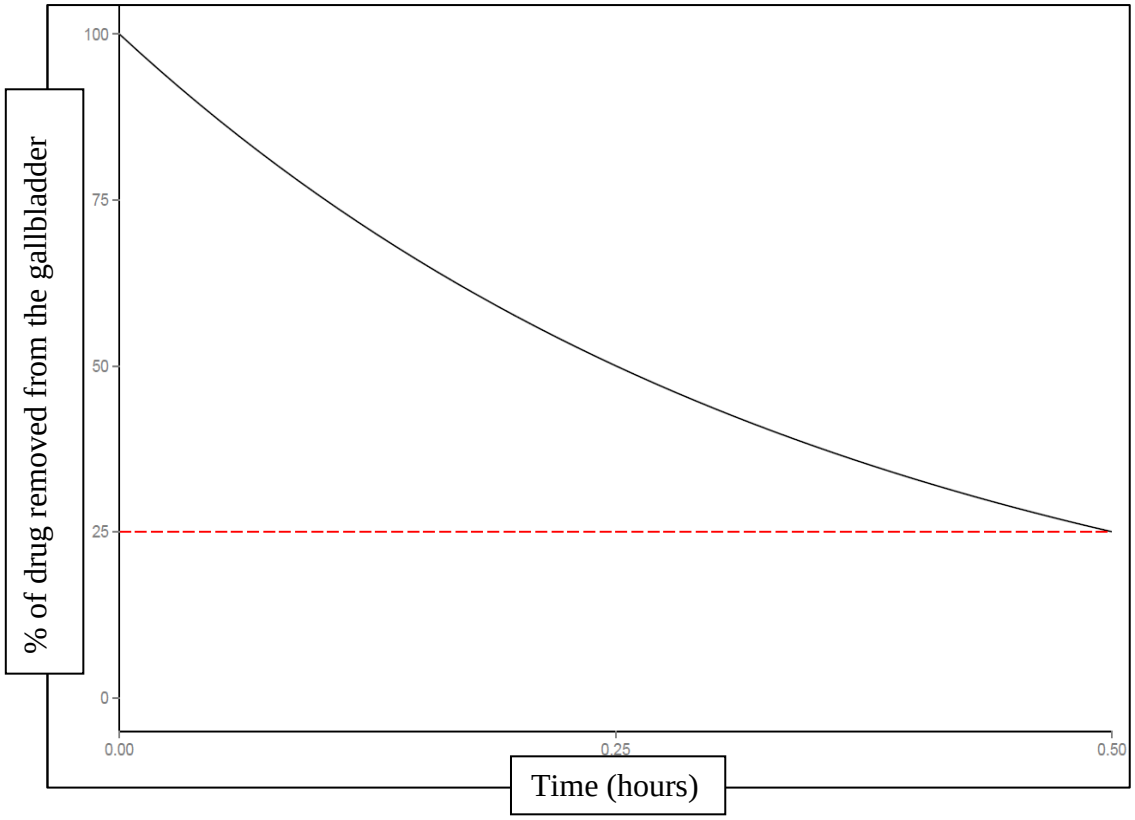

Figure 3-3: The Shape of the Switch Function

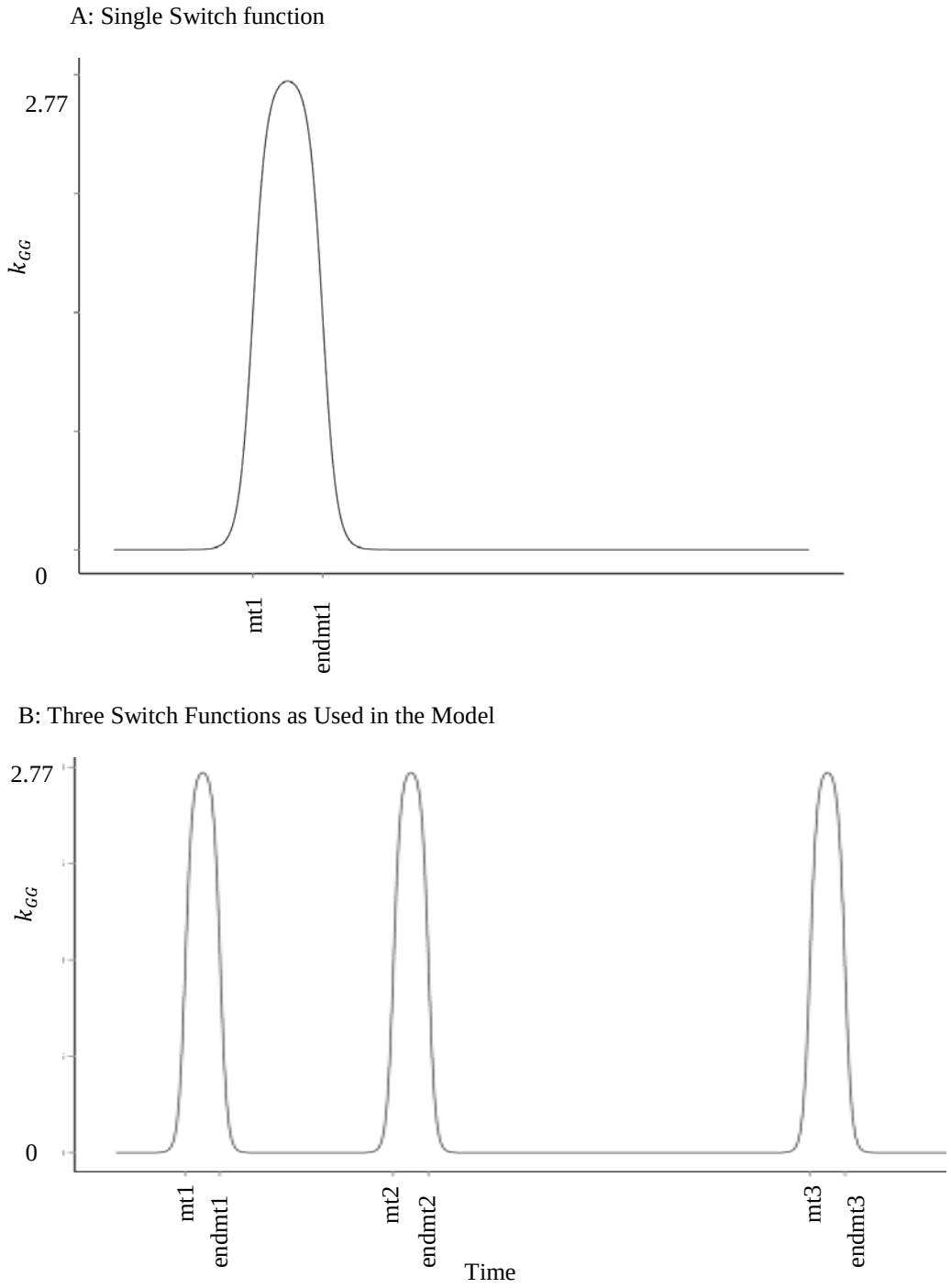

In the current study, mt1, mt2, and mt3 were 1, 4, and 10 hrs, respectively. As the duration of gallbladder emptying (D) was assumed 0.5 hr, endmt1, endmt2, endmt3 were 1.5, 4.5, and 10.5 hrs, respectively.

Figure 3-4: Normal Density Plot of Simulated Sampled Mealtime Distribution when BSV-Meal= 0.06

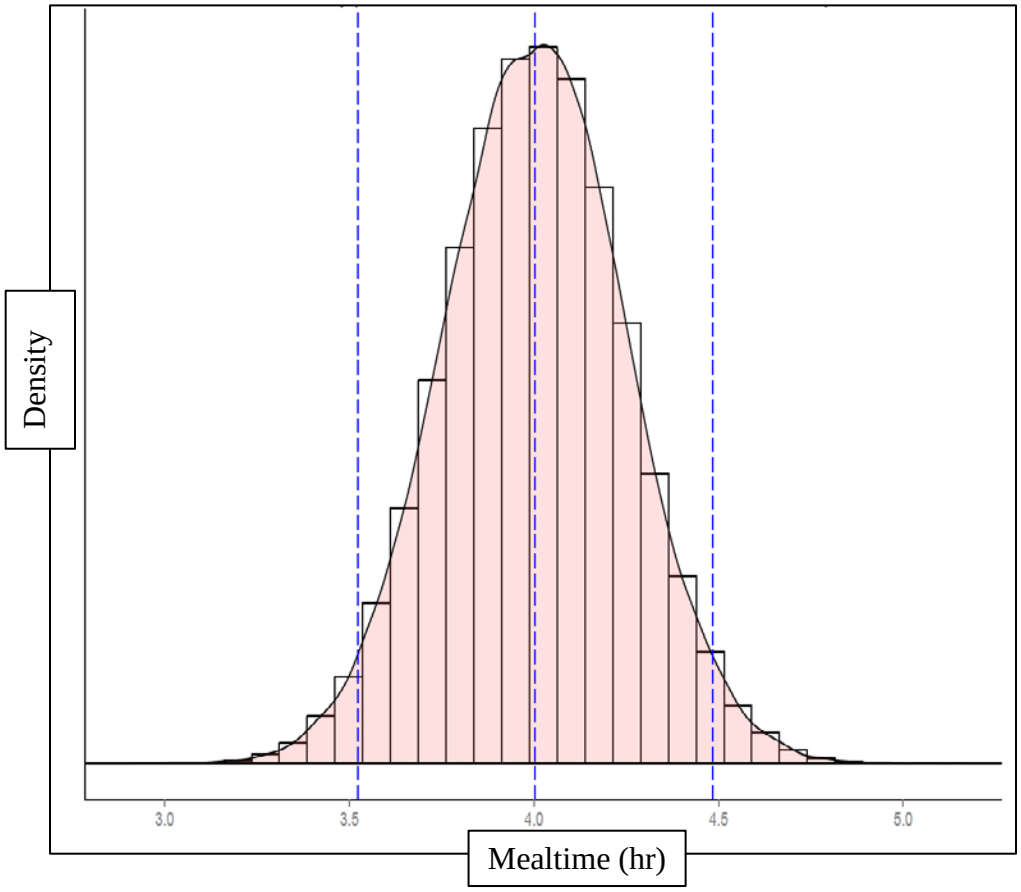

This distribution covers around 95% of the population. Vertical dashed lines represent the 2.5 and 97.5 quantiles.

Figure 3-5: Estimation Model-1

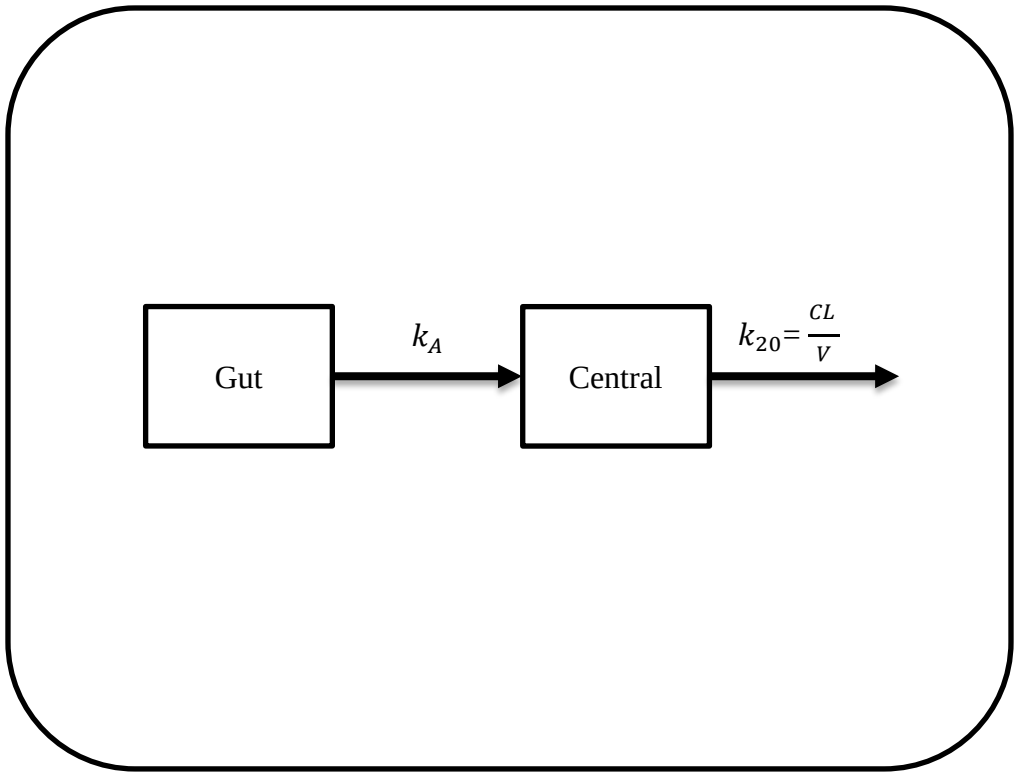

Key:

Compartments: Gut: gut compartment, Central: central compartment

Rate constants: k_A : absorption rate constant, CL: clearance, V: volume of distribution, K_{20}: elimination rate constant.

Figure 3-6: Estimation Model-2

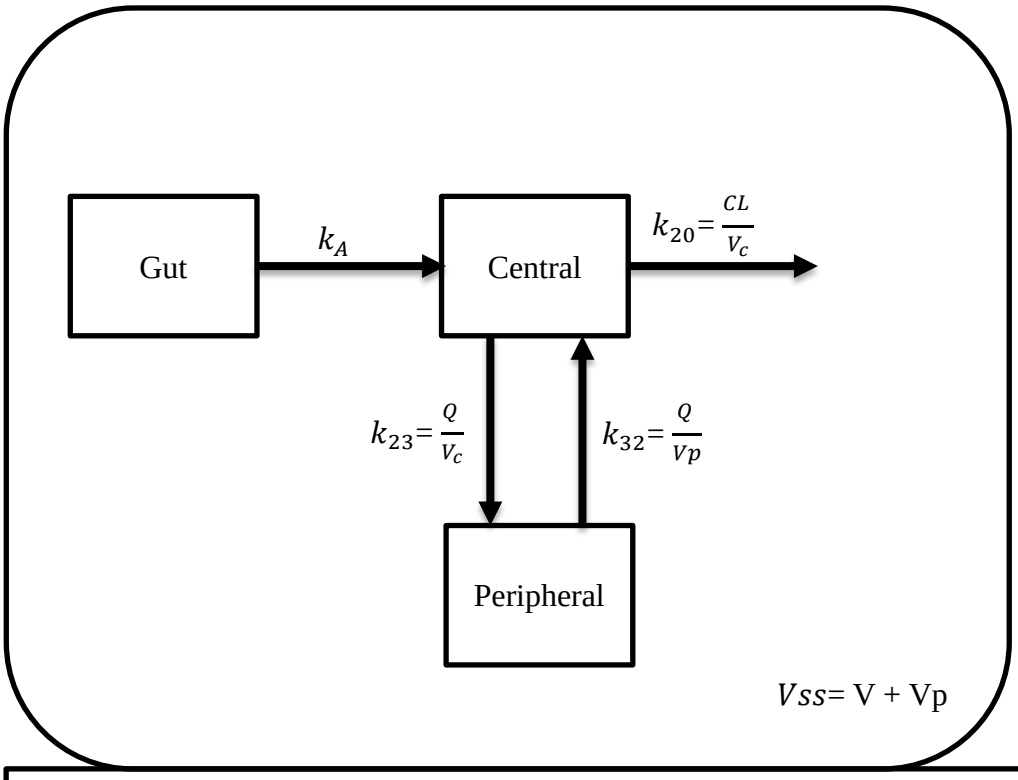

Key:

Compartments: Gut: gut compartment, Central: central compartment

Rate constants: k_A : absorption rate constant, CL: clearance, V_c: central volume of distribution, K_{20}: elimination rate constant, k_{23} and k_{32}: intercompartmental transfer rate constant, Q: intercompartmental clearance , Vp: Peripheral volume of distribution, Vss: Steady state volume of distribution.

Figure 3-7: Estimation Model-3

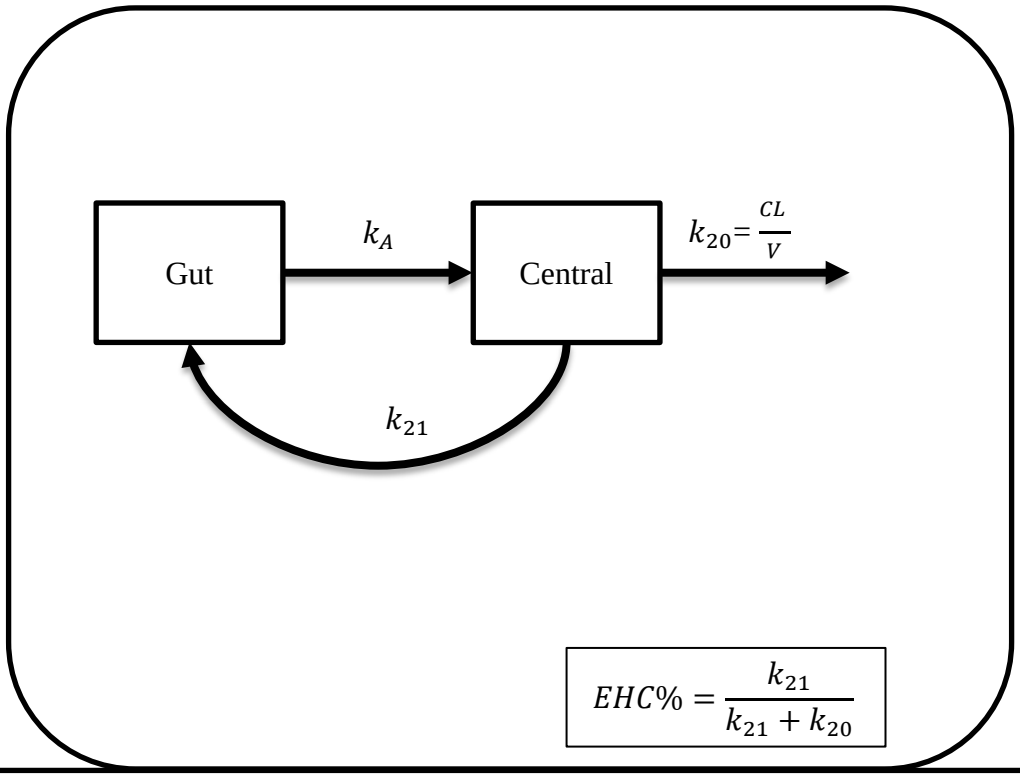

Key:

Compartments: Gut: gut compartment, Central: central compartment

Rate constants: k_A : absorption rate constant, CL: clearance, V: volume of distribution, K_{20}: elimination rate constant, k_{21}: EHC distribution rate constant, $EHC\%$: percent of drug undergoing EHC.

Figure 3-8: Estimation Model-4

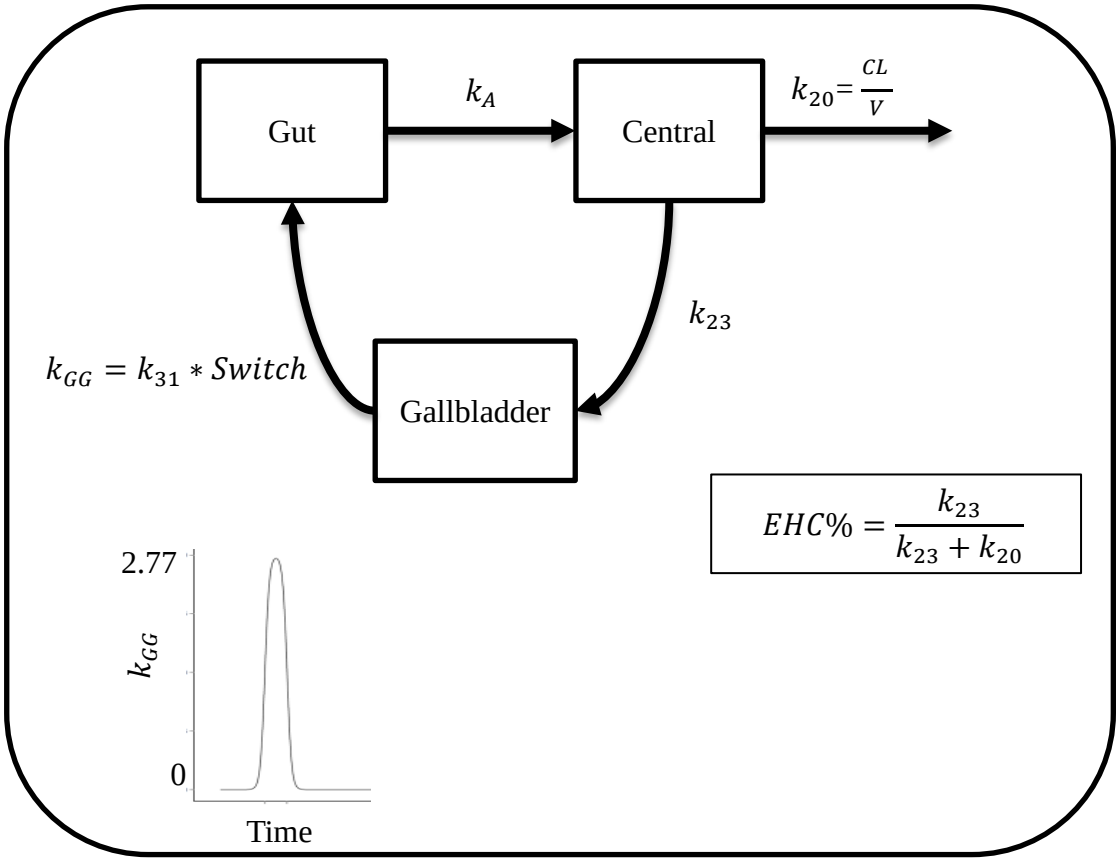

Key:

Compartments: Gut: gut compartment, Central: central compartment, Gallbladder: Gallbladder compartment

Rate constants: k_A : absorption rate constant, CL: clearance, V: volume of distribution, K_{20}: elimination rate constant, k_{23}: EHC distribution rate constant, $EHC\%$: percent of drug undergoing EHC , k_{GG}: transfer rate constant from gallbladder to gut.

Figure 3-9: Estimation Model-5

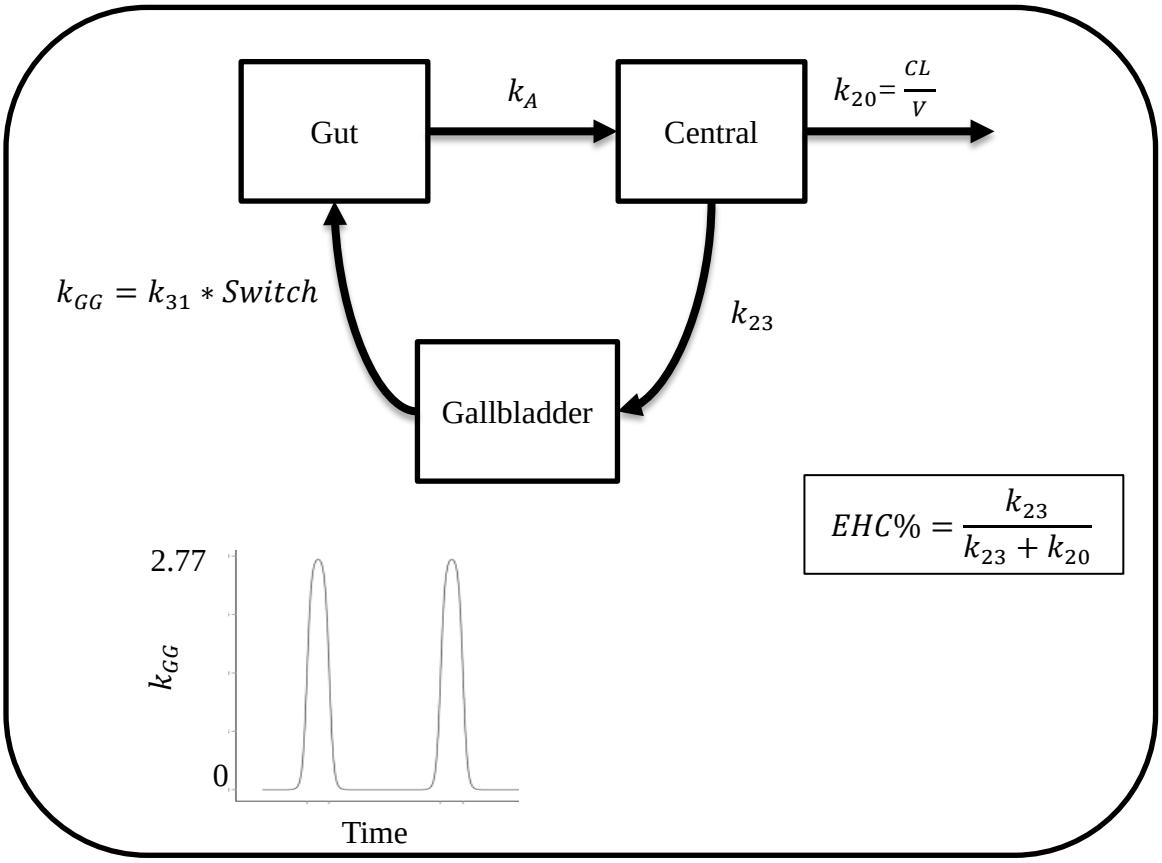

Key:

Compartments: Gut: gut compartment, Central: central compartment, Gallbladder: Gallbladder compartment

Rate constants: k_A : absorption rate constant, CL: clearance, V: volume of distribution, K_{20}: elimination rate constant, k_{23}: EHC distribution rate constant, $EHC\%$: percent of drug undergoing EHC , k_{31}: rate constant fixed to 2.77 hr-1, k_{GG}: transfer rate

Figure 3-10: Estimation Model-6

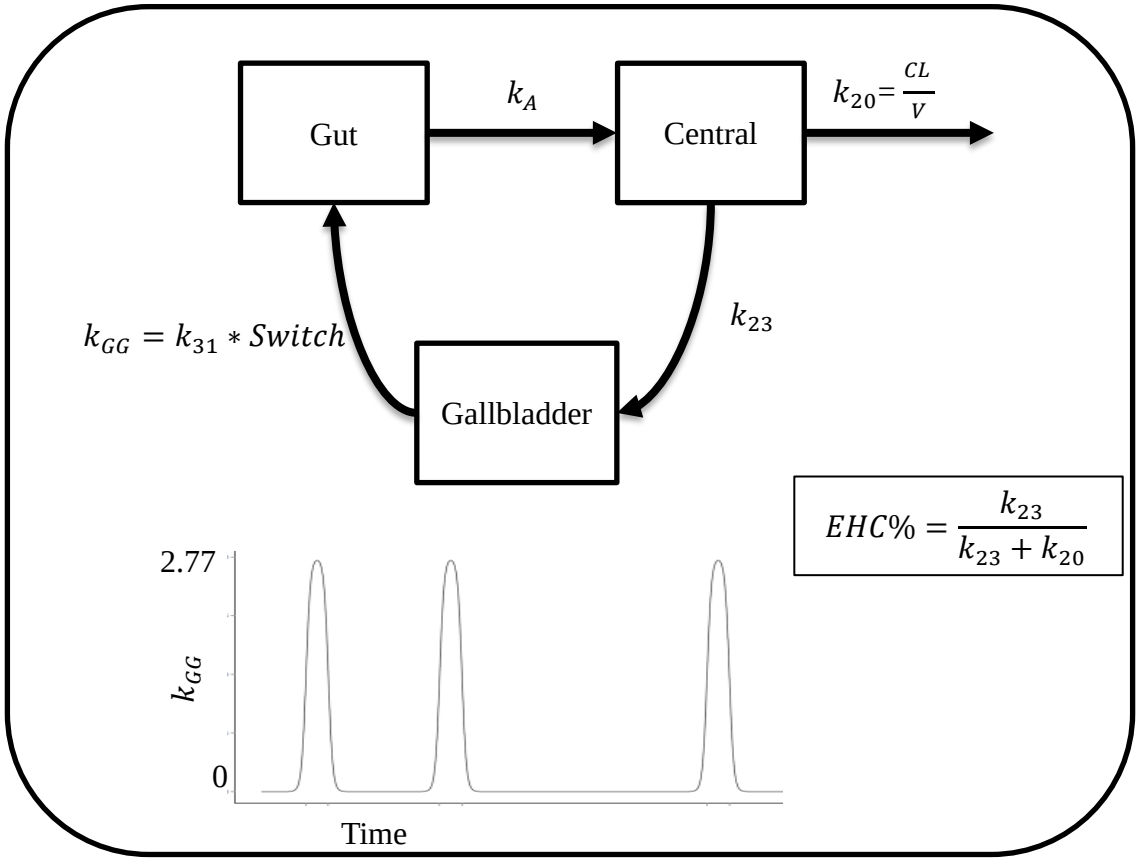

Key:

Compartments: Gut: gut compartment, Central: central compartment, Gallbladder: Gallbladder compartment

Rate constants: k_A : absorption rate constant, CL: clearance, V: volume of distribution, K_{20}: elimination rate constant, k_{23}: EHC distribution rate constant, $EHC\%$: percent of drug undergoing EHC , k_{31}: rate constant fixed to 2.77 hr-1, k_{GG}: transfer rate

Figure 3-11: Estimation Model-7

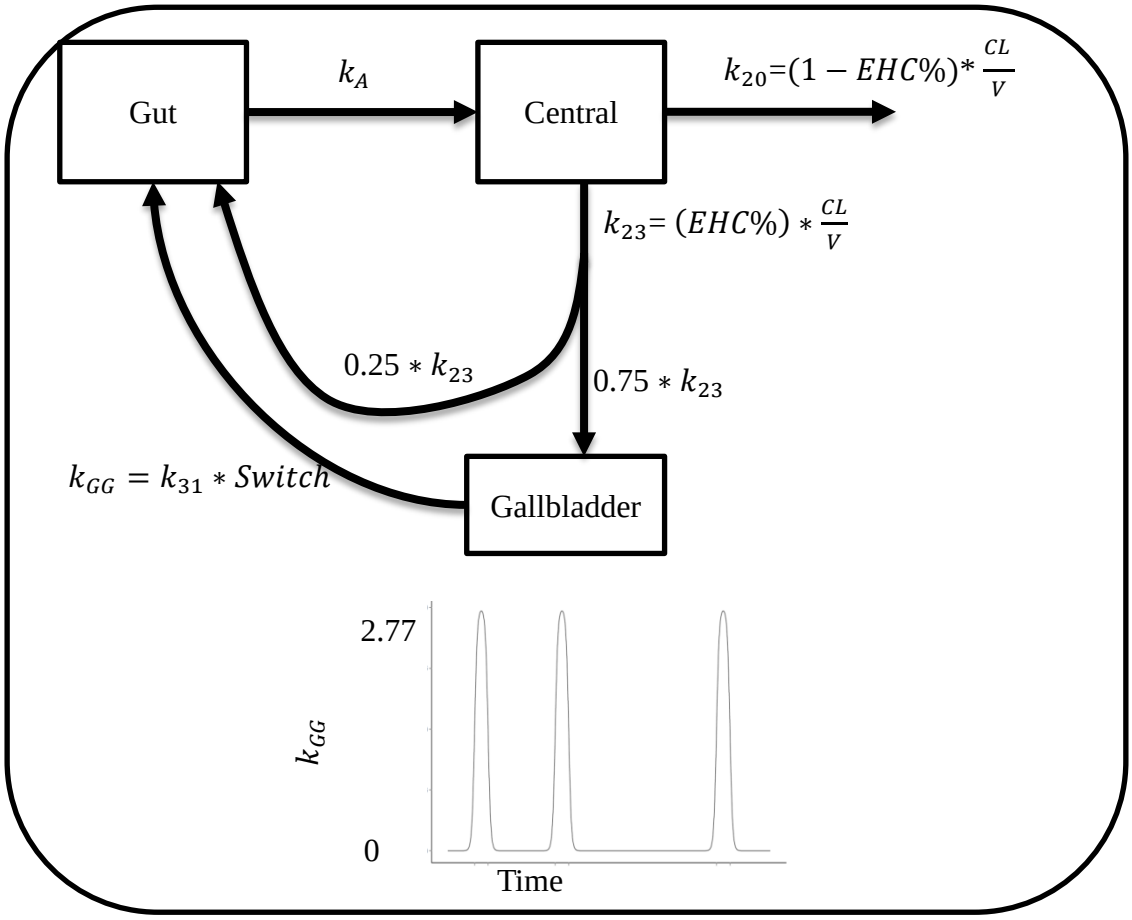

Key:

Compartments: Gut: gut compartment, Central: central compartment, Gallbladder: represents the gallbladder

Rate constants: k_A : absorption rate constant, CL: clearance, V: volume of distribution, K_{20}: Non biliary elimination rate constant, k_{23}: Biliary elimination rate constant, k_{31}: rate constant fixed to 2.77 hr^{-1}, k_{GG}: transfer rate constant from

Figure 3-12: Boxplots of Parameter Estimate of Various EHC Models with 20% EHC

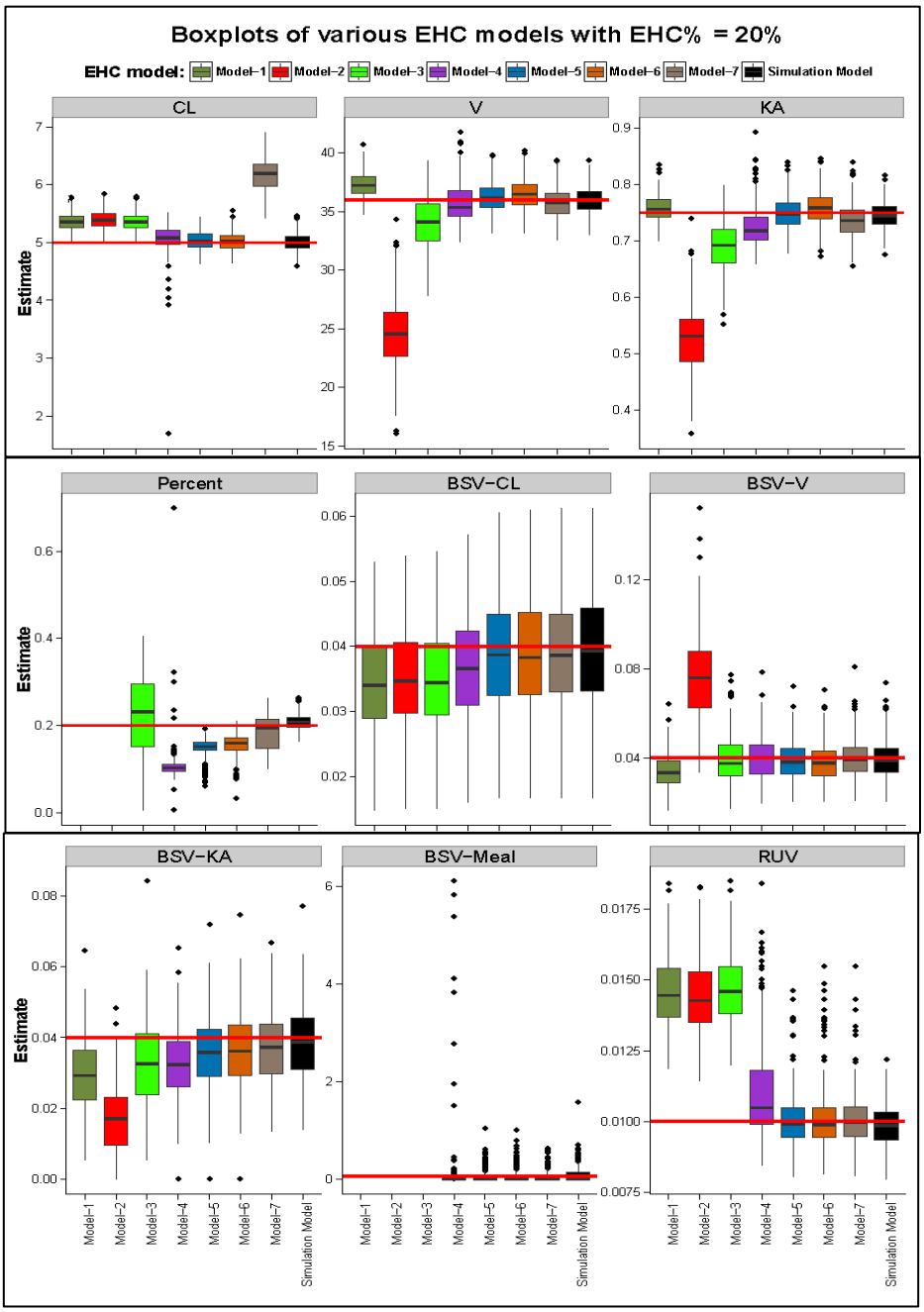

Note:
-Redline in each figure represent the true value used in the simulation
-The upper and lower hinges of the boxplot denote the first and third quartiles, where the distance between them is called inter- quartile range (IQR). Whiskers covers 1.5* IQR, starting from each hinge, and any data point beyond them is considered an outlier and represented by a point.

Figure 3-13: Boxplots of Parameter Estimate of Various EHC Models with 40% EHC

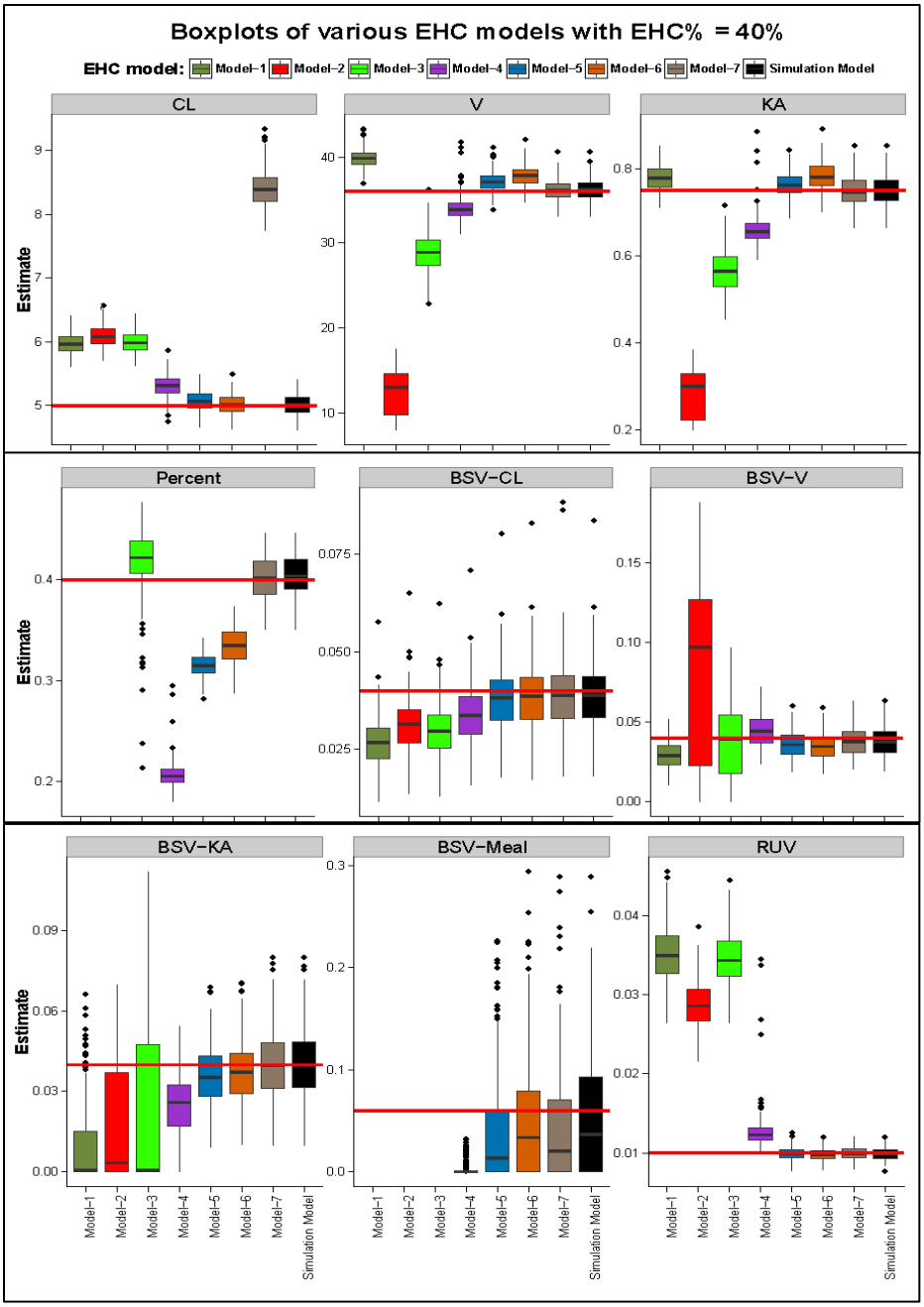

Note:
-Horizontal red line in each figure represents the true value used in the simulation
-The upper and lower hinges of the boxplot denote the first and third quartiles, where the distance between them is called inter- quartile range (IQR). Whiskers covers 1.5* IQR, starting from each hinge, and any data point beyond them is considered an outlier and represented by a point.

Figure 3-14: Boxplots of Parameter Estimate of Various EHC Models with 60% EHC

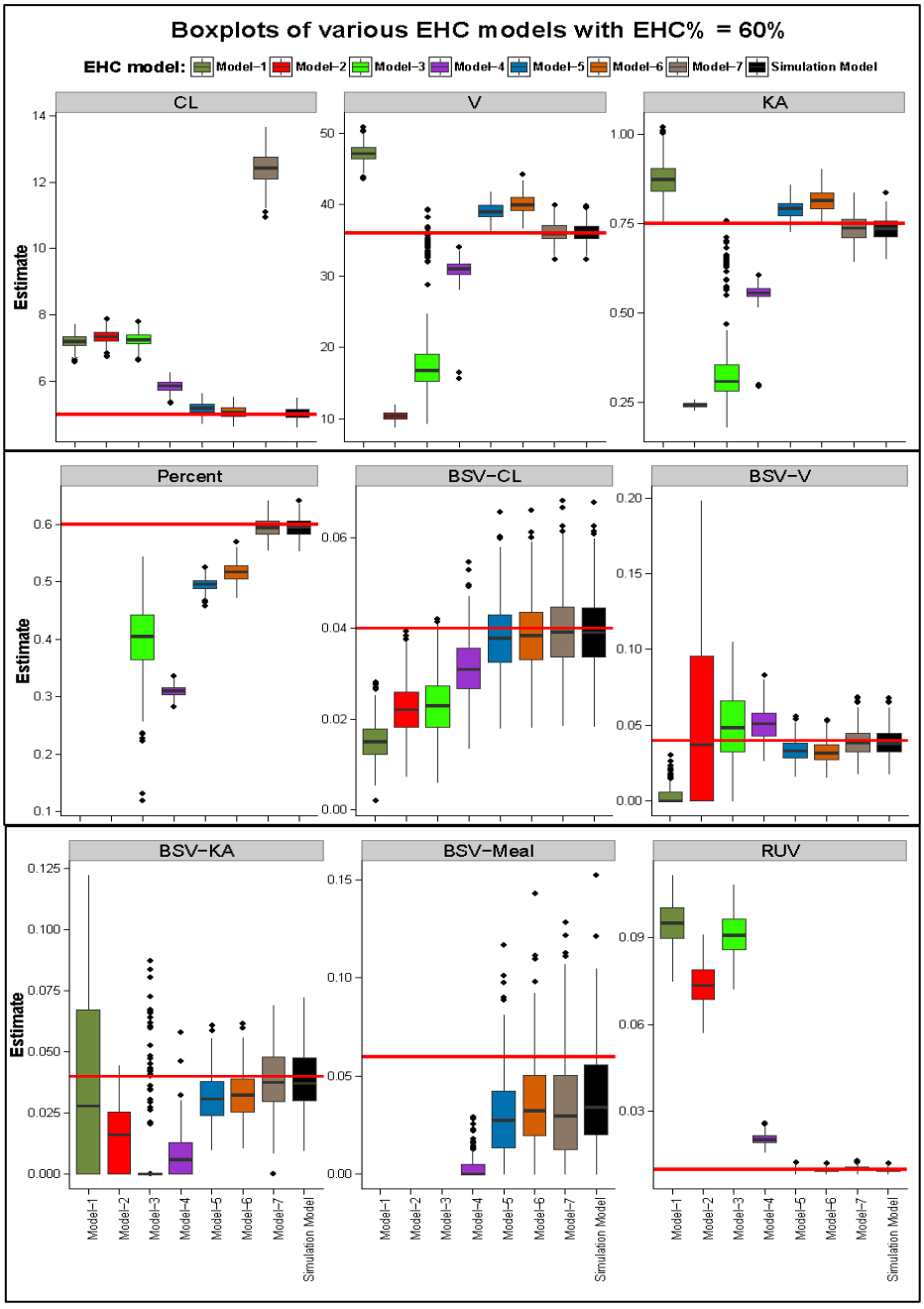

Note:
- Horizontal red line in each figure represents the true value used in the simulation
-The upper and lower hinges of the boxplot denote the first and third quartiles, where the distance between them is called inter- quartile range (IQR). Whiskers covers 1.5* IQR, starting from each hinge, and any data point beyond them is considered an outlier and represented by a point.

Figure 3-15: Boxplots of Parameter Estimate of Various EHC Models with 80% EHC

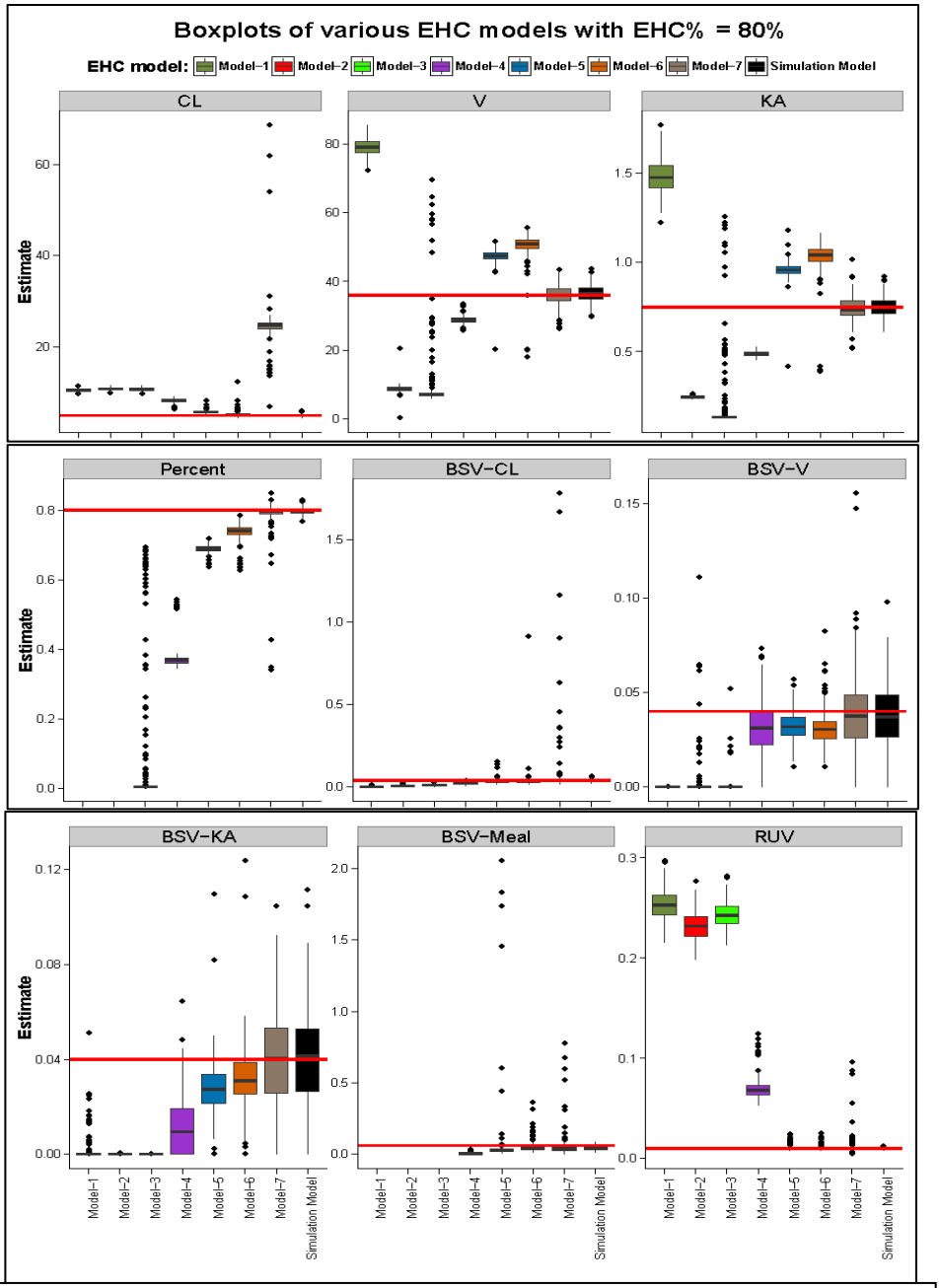

Note:
- Horizontal red line in each figure represents the true value used in the simulation
-The upper and lower hinges of the boxplot denote the first and third quartiles, where the distance between them is called inter- quartile range (IQR). Whiskers covers 1.5* IQR, starting from each hinge, and any data point beyond them is considered an outlier and represented by a point.

Figure 3-16: The Relative Bias Values for All the EHC Models Plotted Across Various EHC%

16A: Relative Bias of CL Parameter Estimates

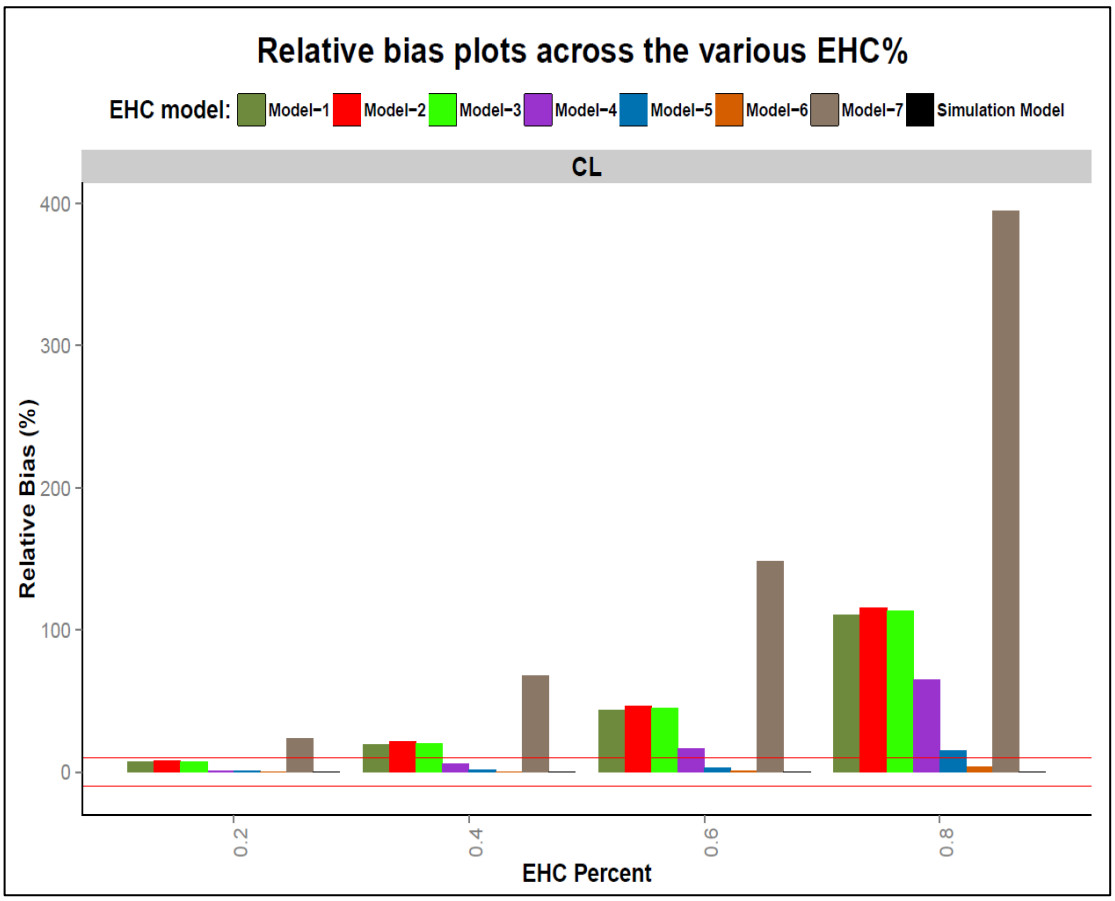

Note:
- Horizontal red lines in each figure represent the upper and lower 10% relative bias values

16B: Relative Bias of V Parameter Estimates

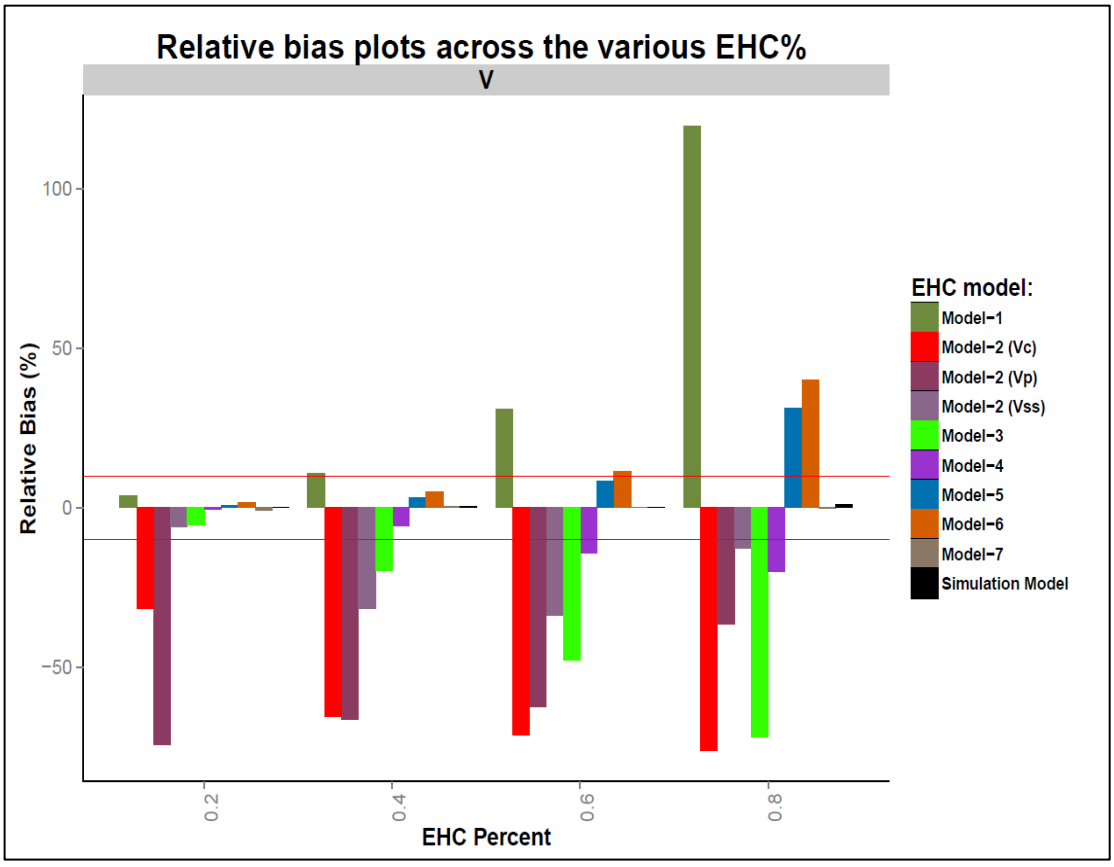

16C: Relative Bias of k_A Parameter Estimates

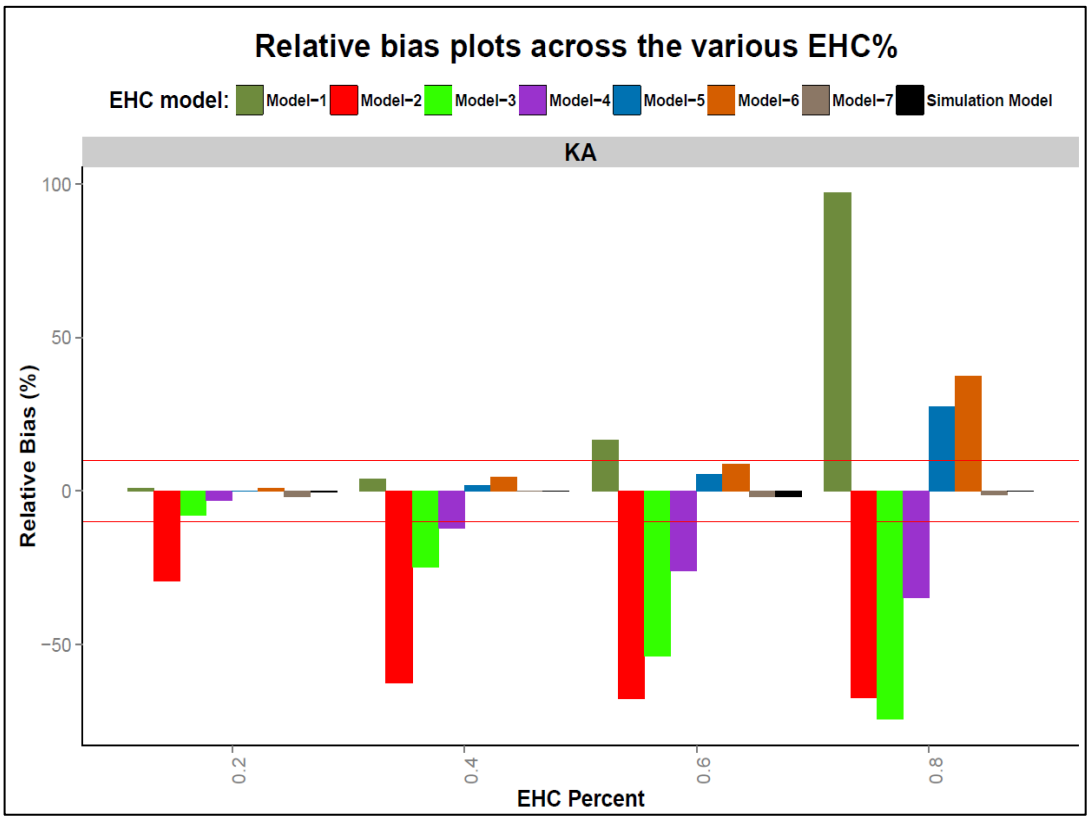

16D: Relative Bias of "Percent" Parameter Estimates

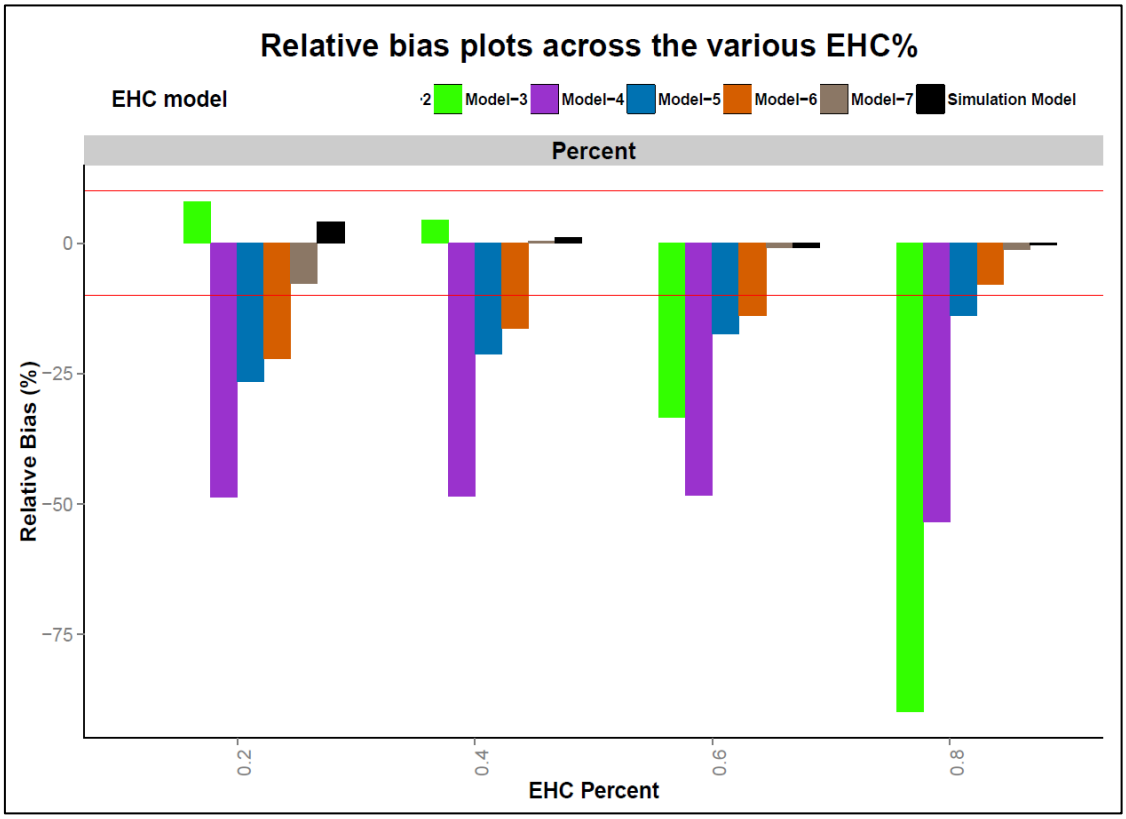

16E: Relative Bias of BSV-CL Parameter Estimates

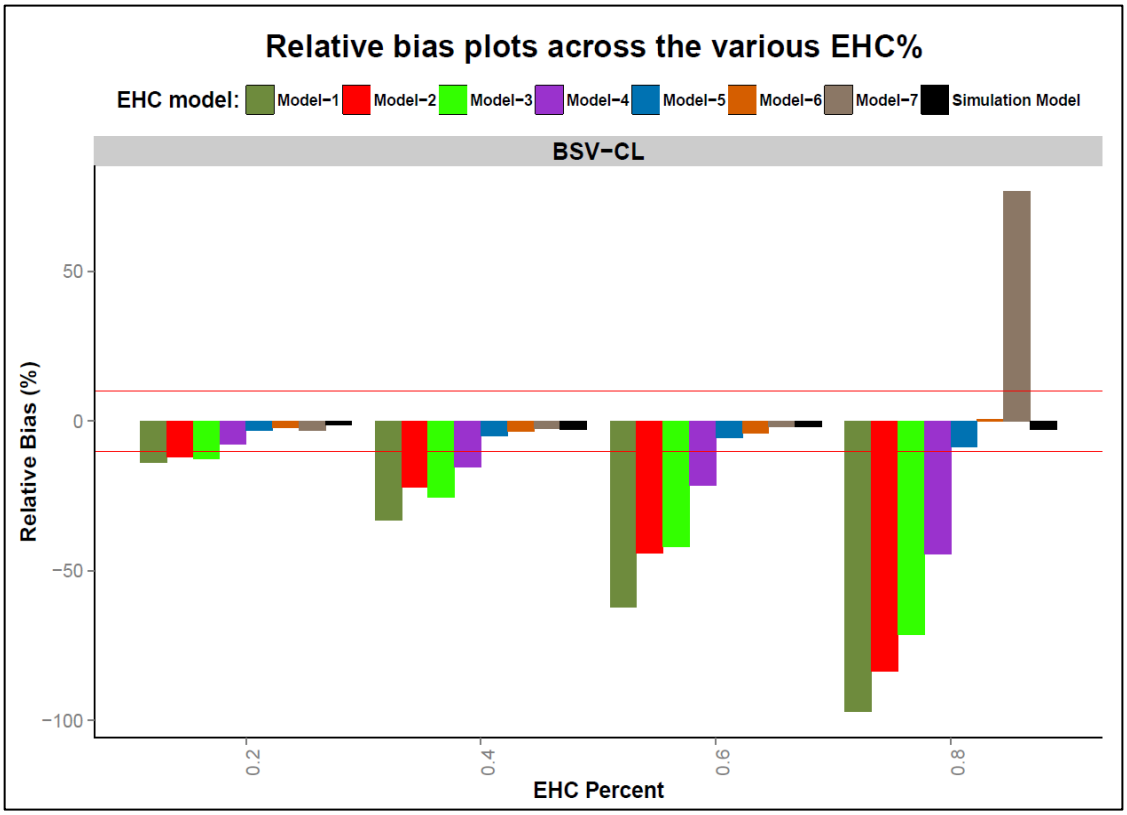

16F: Relative Bias of BSV-V Parameter Estimates

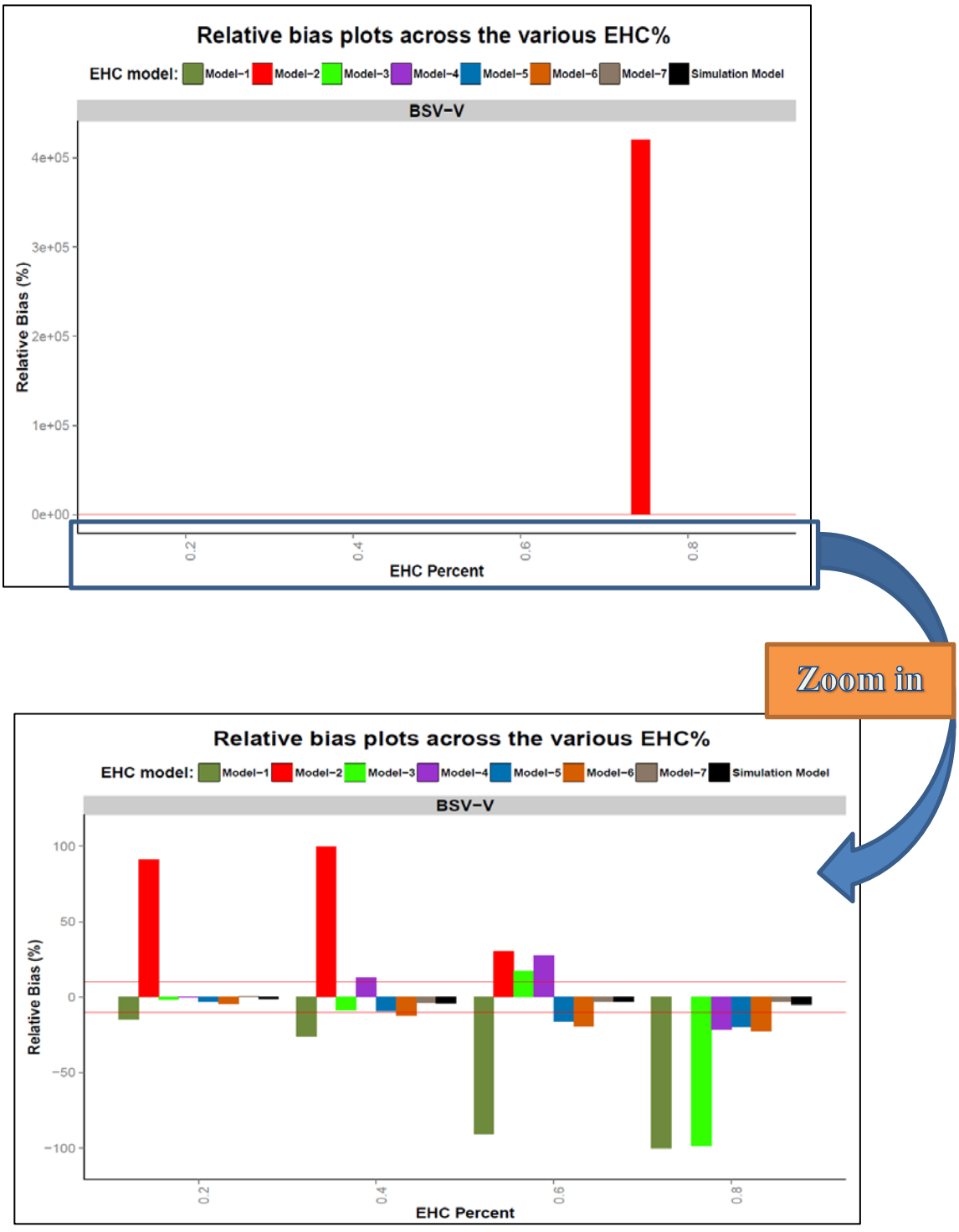

16G: Relative Bias of BSV-k_A Parameter Estimates

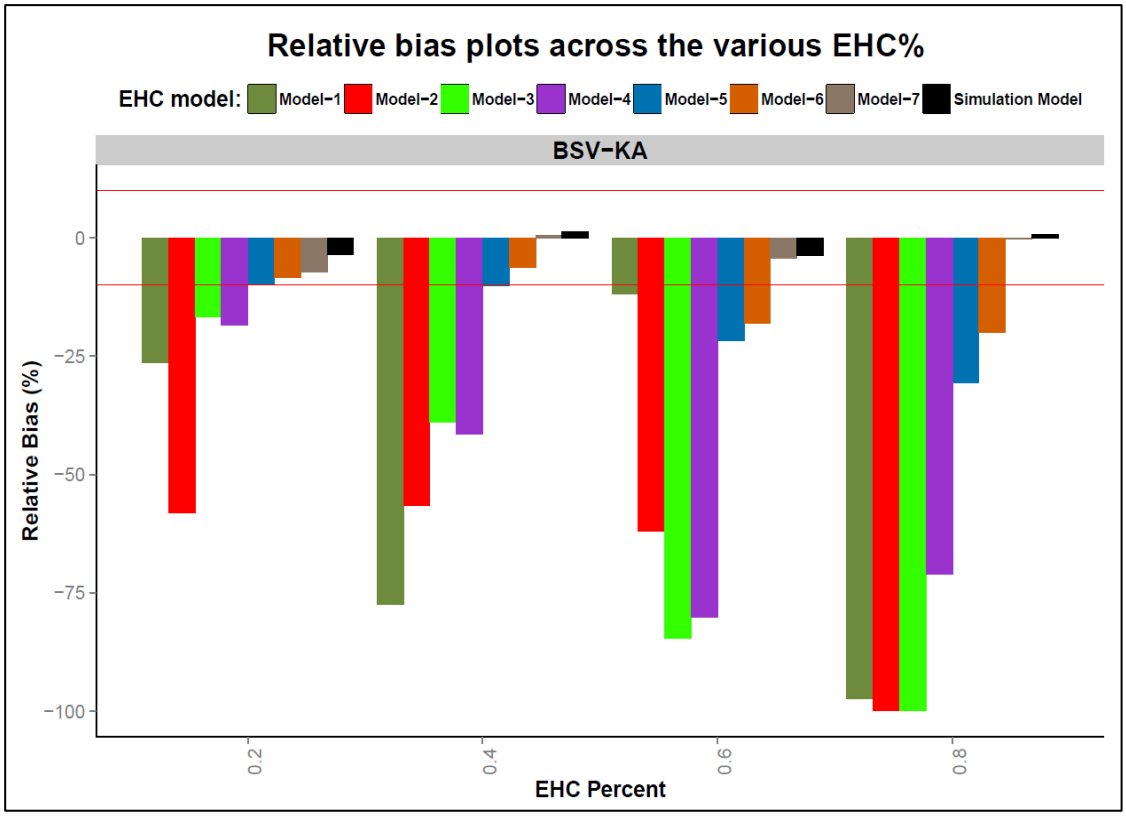

16H: Relative Bias of BSV-Meal Parameter Estimates

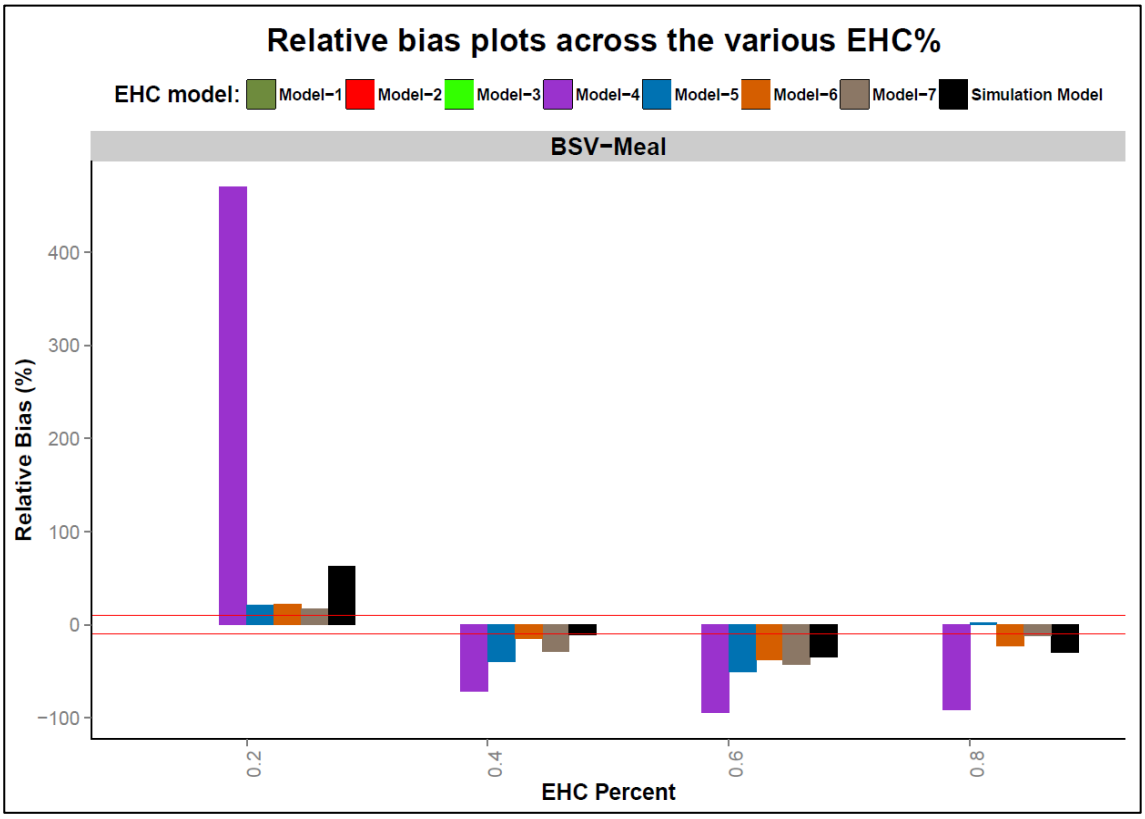

16I: Relative Bias of RUV Parameter Estimates

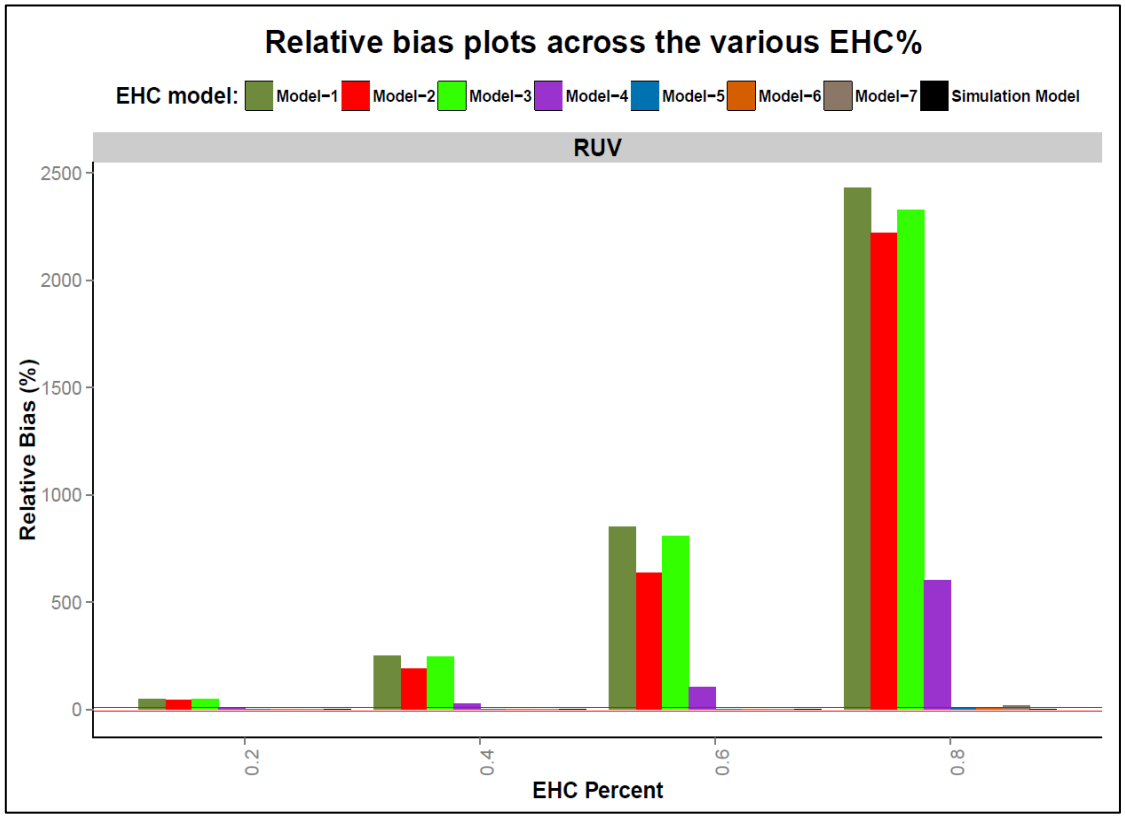

Figure 3-17: The Relative RMSE Values for All the EHC Models Plotted Across Various EHC%

17A: Relative RMSE of CL parameter estimates:

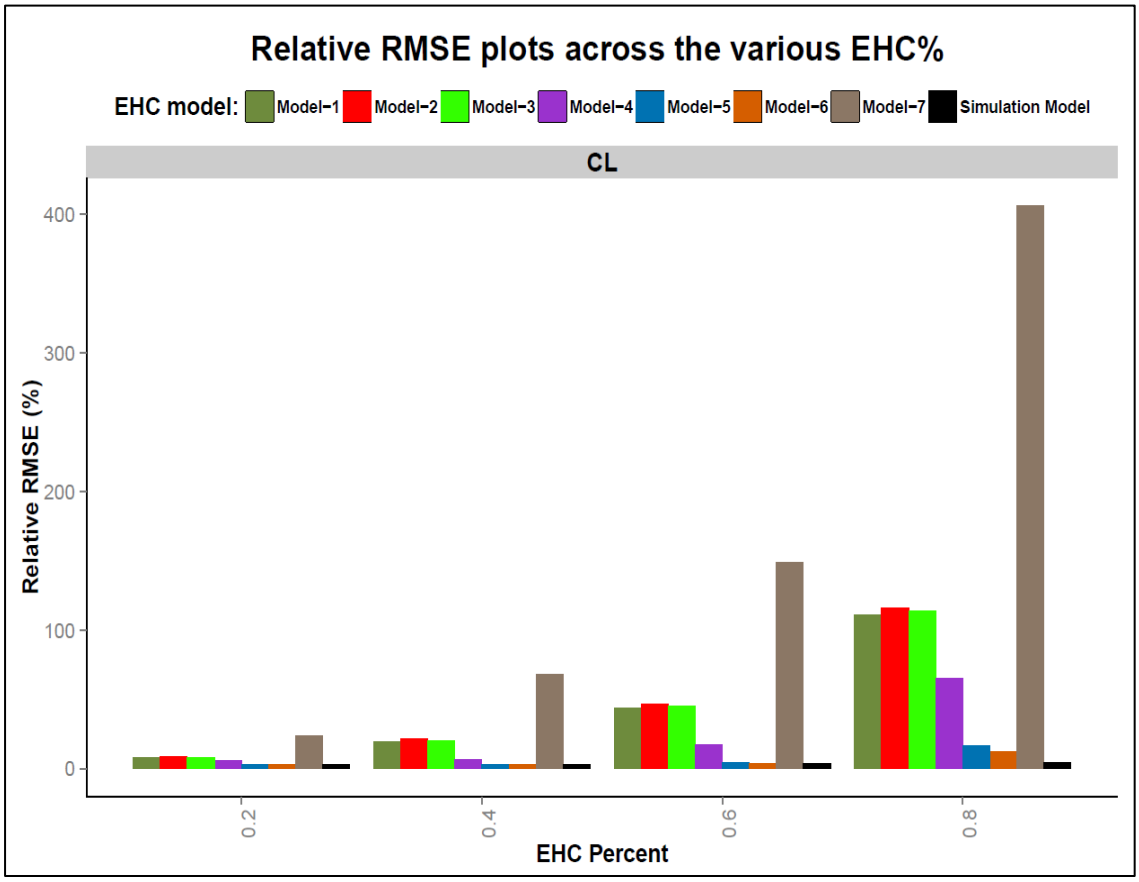

17B: Relative RMSE of V Parameter Estimates:

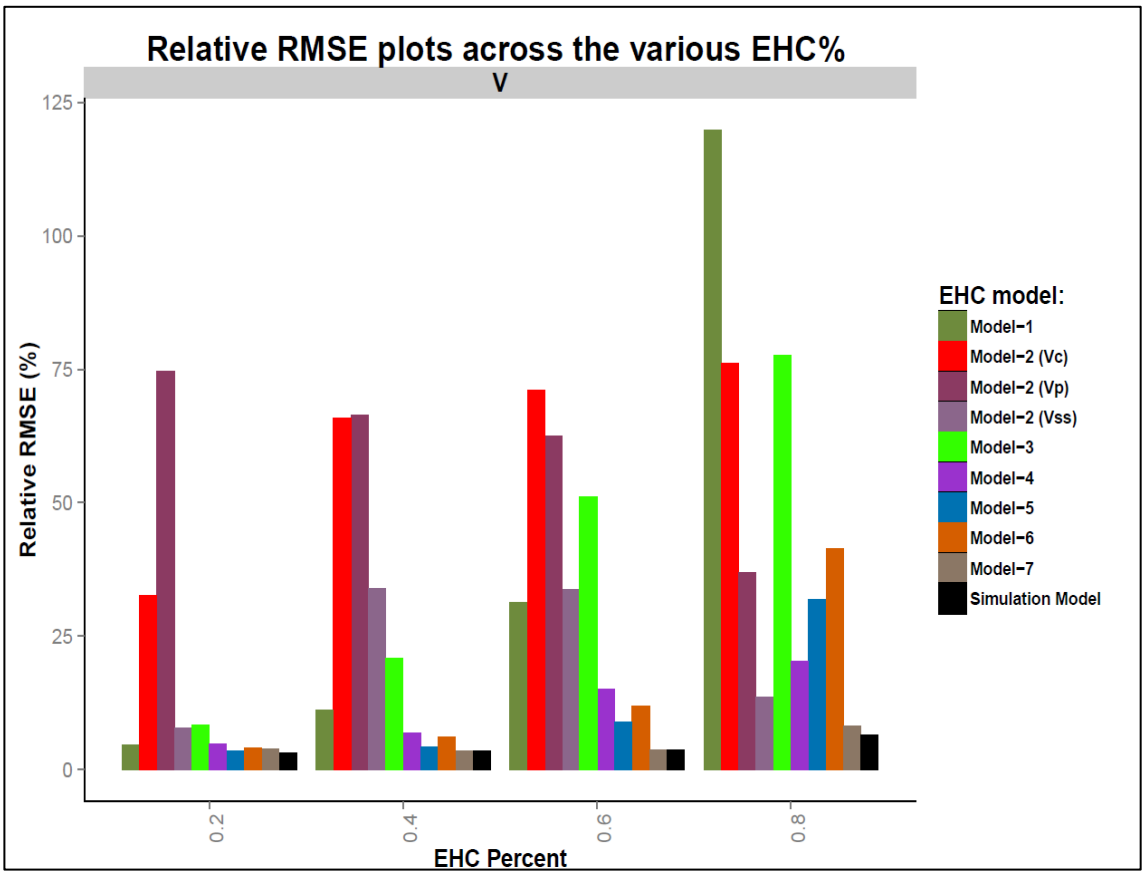

17C: Relative RMSE of k_A Parameter Estimates:

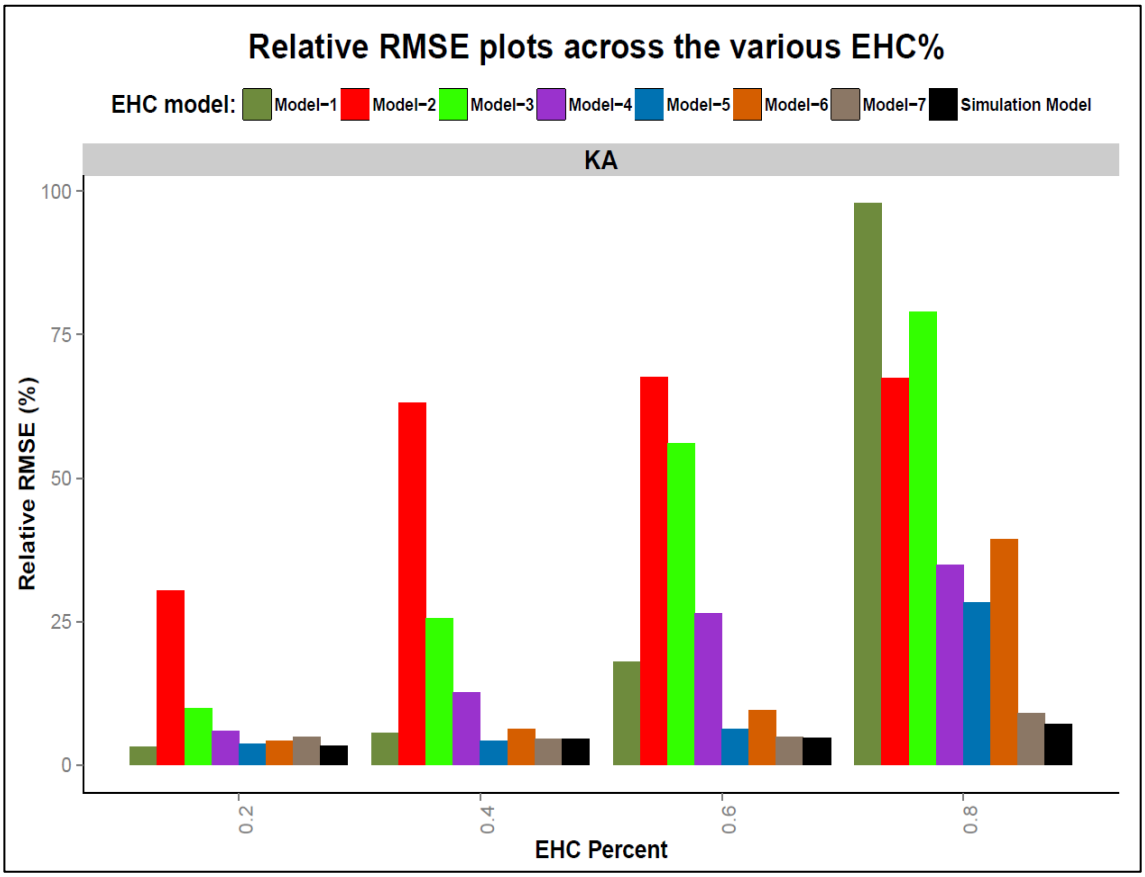

17D: Relative RMSE of "Percent" Parameter Estimates:

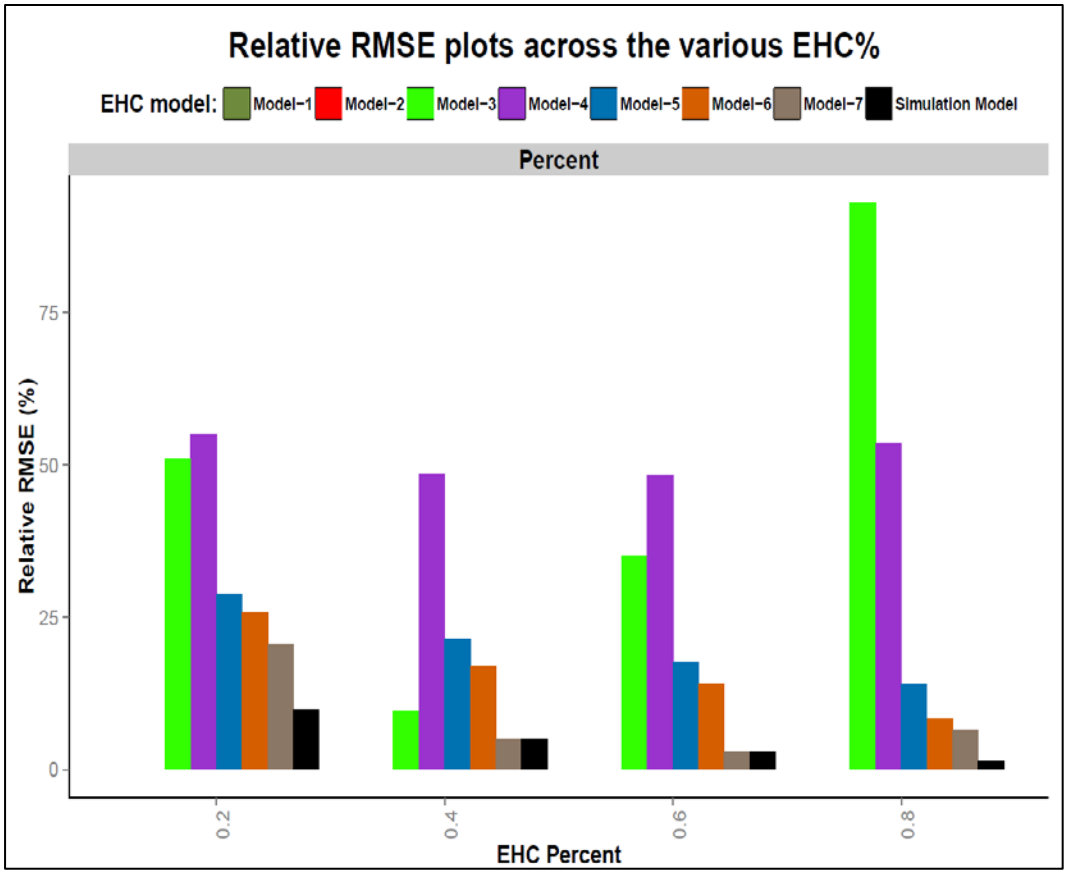

17E: Relative RMSE of BSV-CL Parameter Estimates:

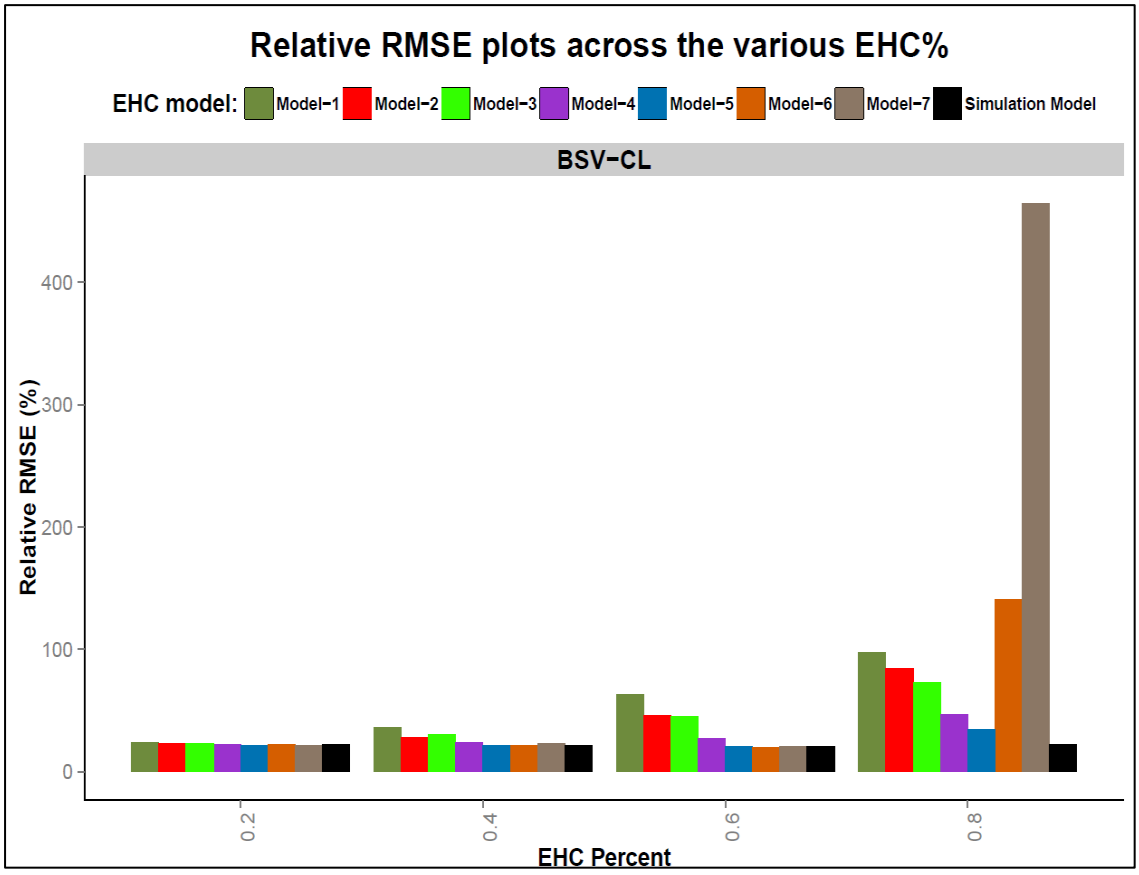

17F: Relative RMSE of BSV-V Parameter Estimates:

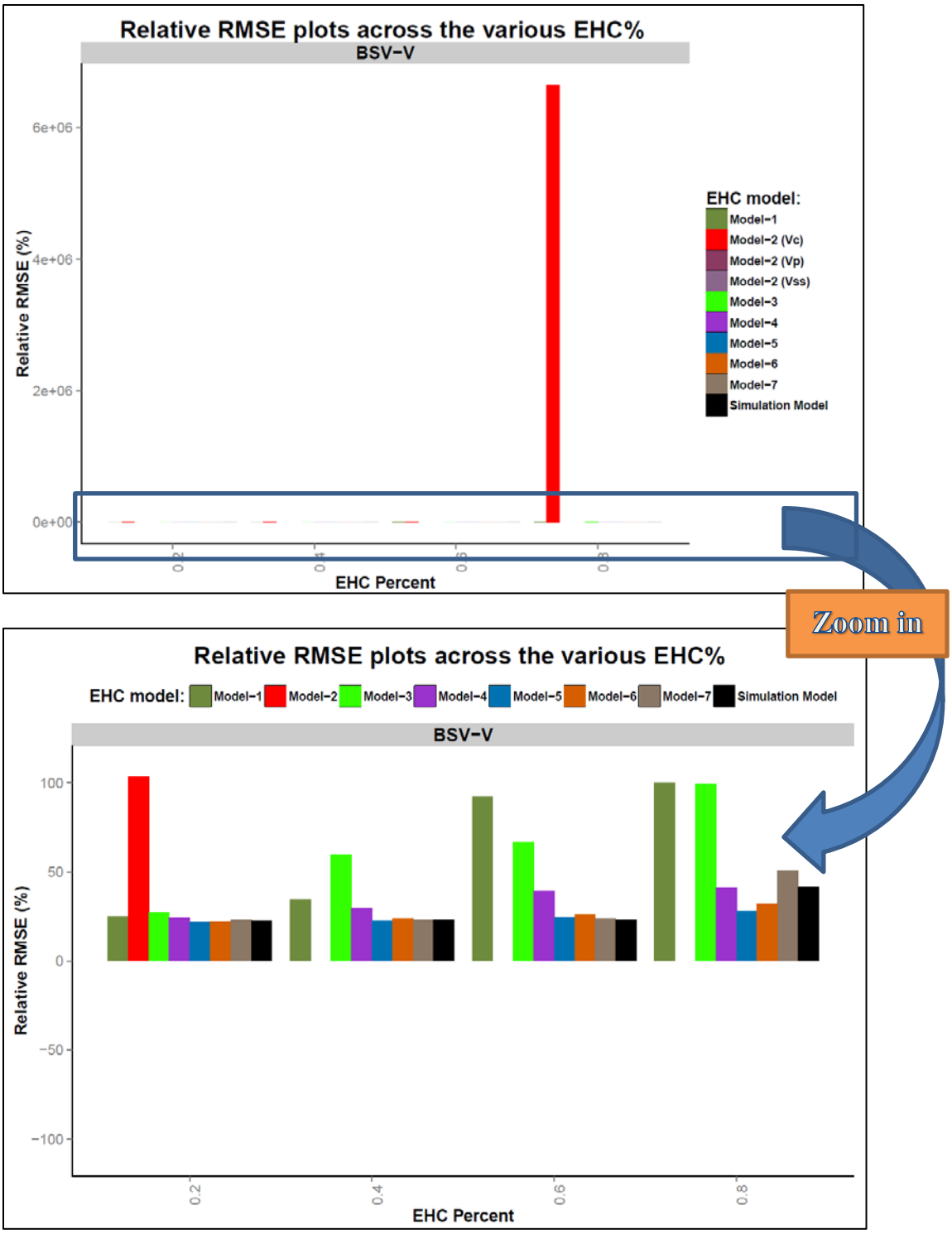

17G: Relative RMSE of BSV-k_A Parameter Estimates:

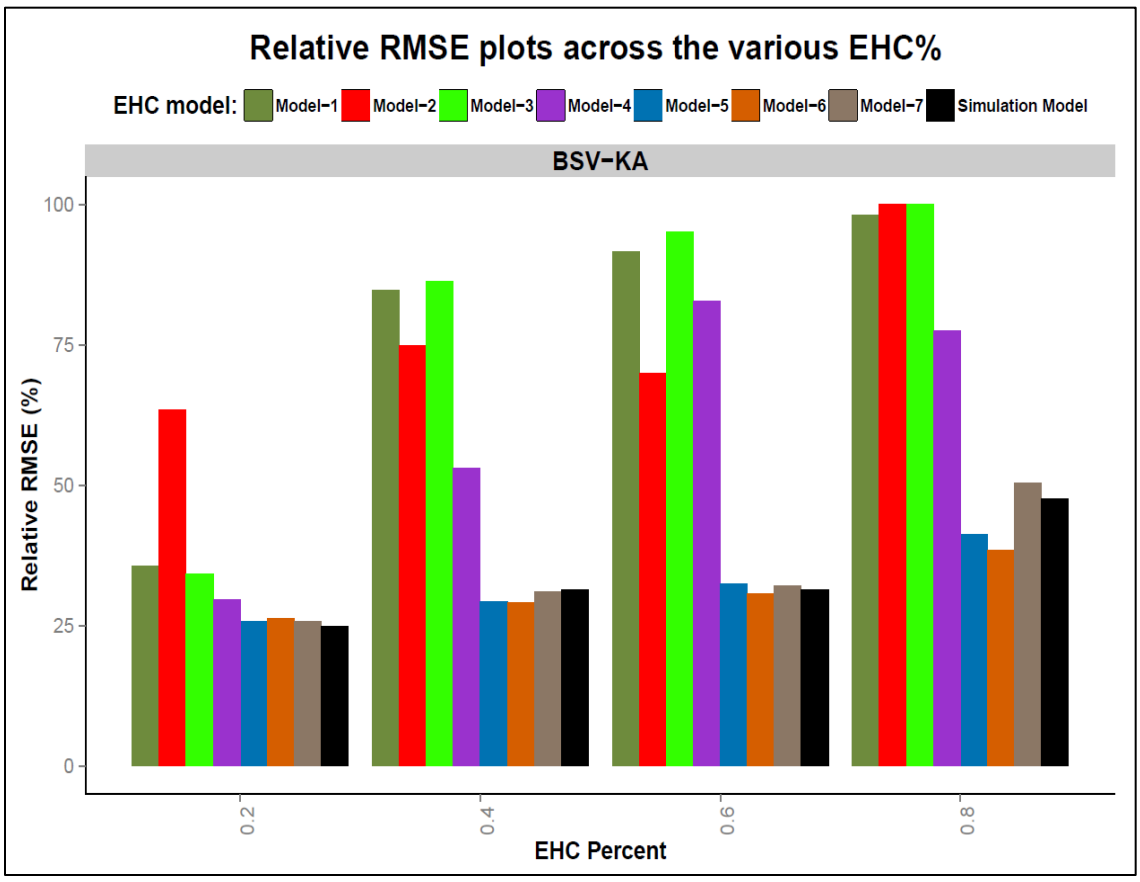

17H: Relative RMSE of BSV-V Parameter Estimates:

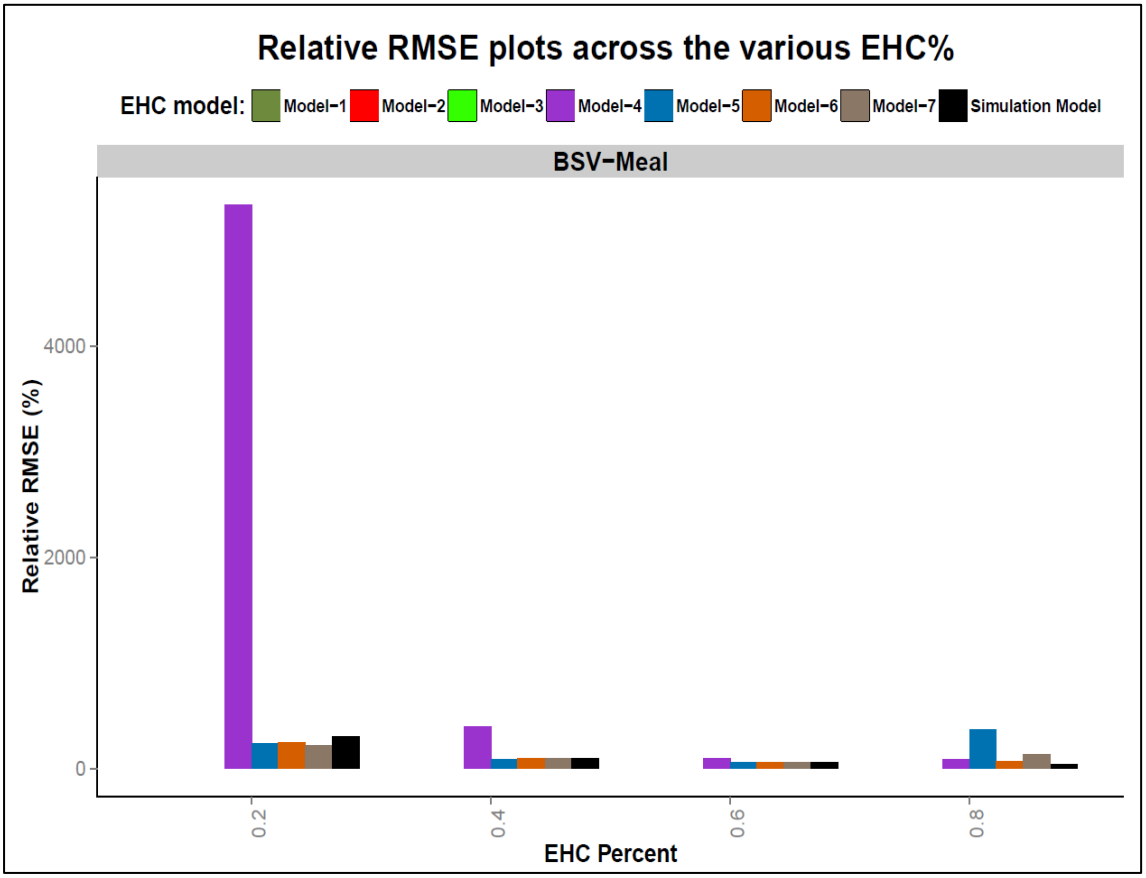

17I: Relative RMSE of RUV Parameter Estimates:

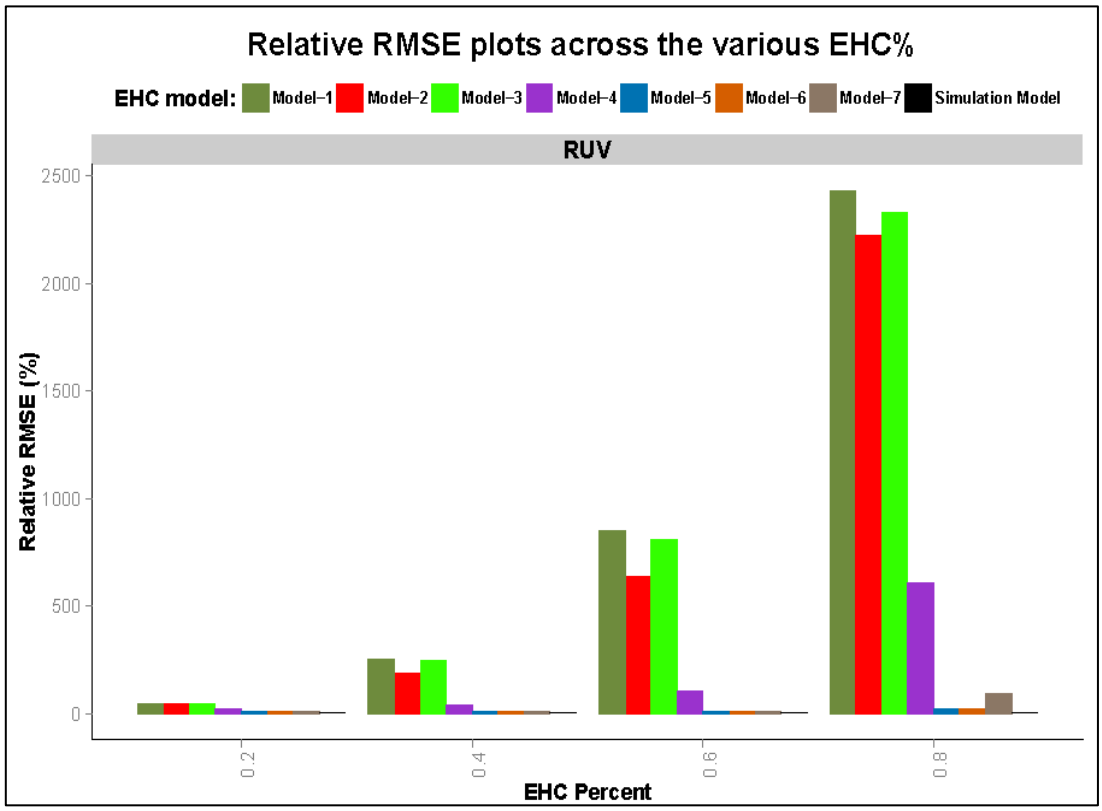

Figure 3-18: The OFV Mean Values For All the EHC Models Plotted Across Various EHC%

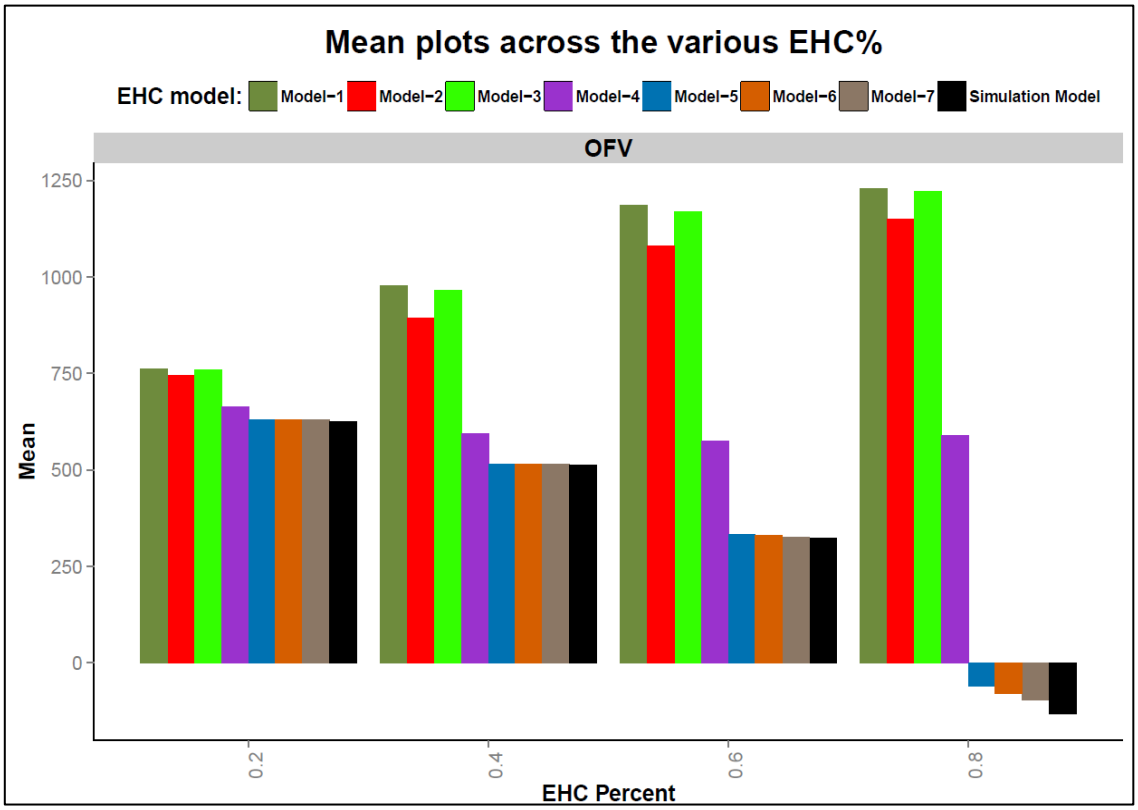

Figure 3-19: The Estimation Runtimes Mean Values (in Seconds), for All the EHC Models, Plotted Across Various EHC%

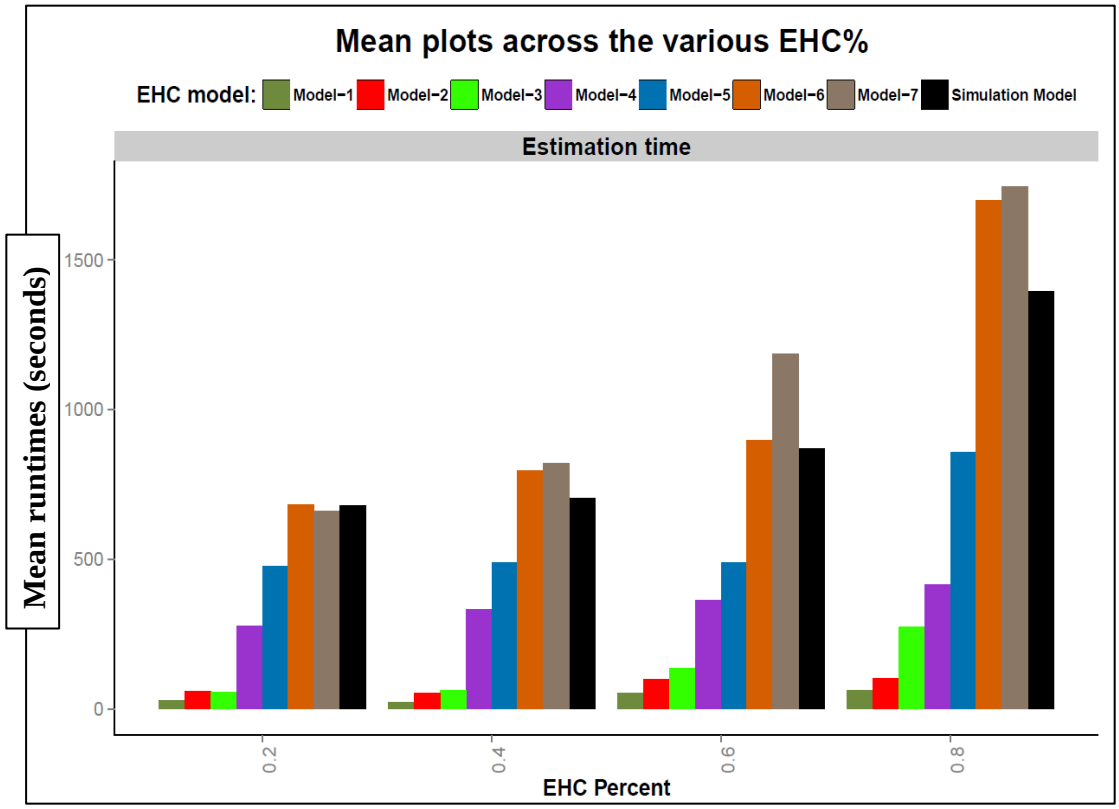

Figure 3-20: Steady-State Simulations Based on the SSE Output of the Various EHC%, and EHC models

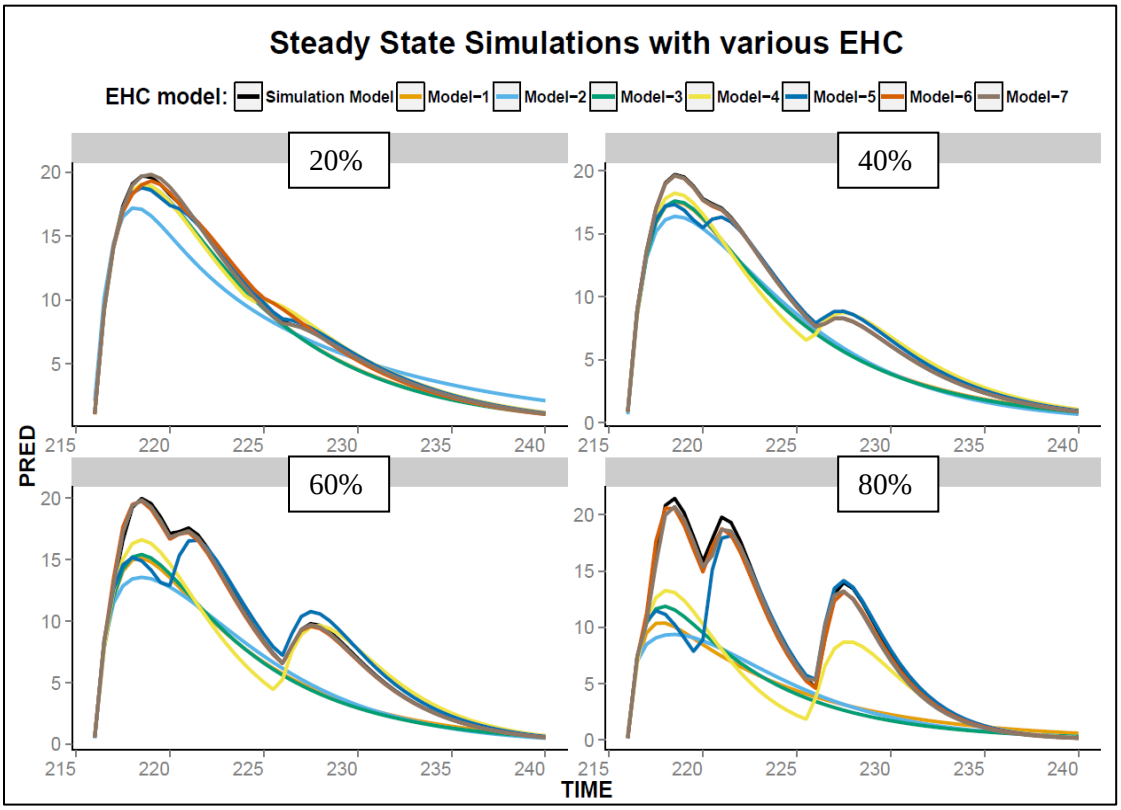

Figure 3-21: Lineplots of Steady State exposure metrics and their relative Bias values across various EHC

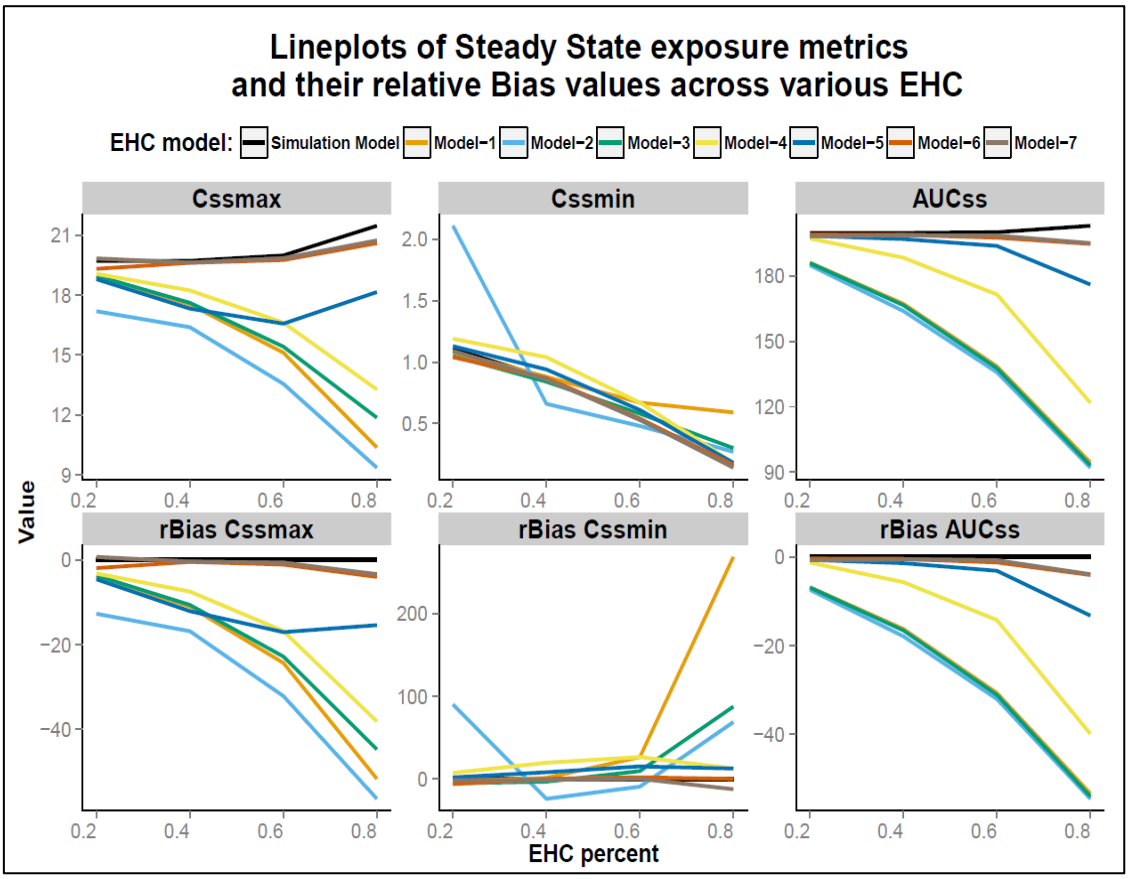

Figure 3-22: Barplots of Steady State exposure metrics and their relative Bias values across various EHC

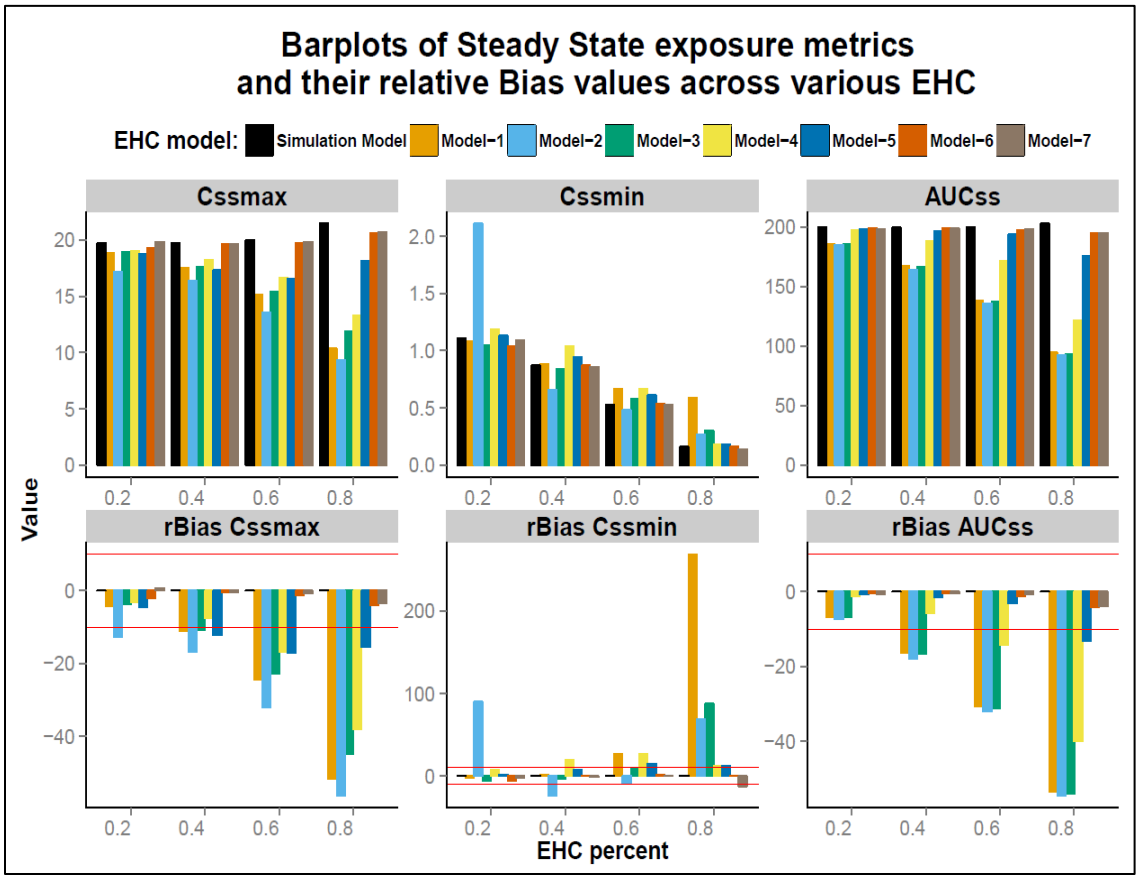

Note:
- Horizontal red lines in the rBias figures represents the upper and lower 10% relative bias values

CHAPTER 4

4 POPULATION PHARMACOKINETICS ANALYSIS OF MYCOPHENOLATE IN KIDNEY TRANSPLANT PATIENTS

4.1 Introduction

Mycophenolic acid (MPA) is a potent immunosuppressive agent used as maintenance prophylactic therapy to prevent allograft rejection after organ transplantation (97). Current kidney post-transplantation maintenance regimens include a combination of an anti-proliferative agent (MPA or azathioprine) and a calcineurin inhibitor (tacrolimus or cyclosporine), with or without corticosteroids (98). The clinical use of MPA has increased exponentially since the Food and Drug Administration (FDA) approval in 1995(99). MPA is currently considered as the anti-proliferative of choice in solid organ post-transplant maintenance regimens (99). In a recent report of the organ procurement and transplantation network (OPTN/SRTR), it was shown that around 94% of adults and pediatric kidney transplant recipients were prescribed MPA along with steroids and tacrolimus (100).

MPA is marketed as mycophenolate mofetil (MMF, CellCept®) which as an MPA ester pro-drug, or as Myfortic (EC-MPS, Myfortic®) which is a sodium salt of MPA (101, 102). Generally, the dosing regimen of MMF in kidney transplant adult recipients is an oral fixed dose of 1000 mg every 12 hours.

4.1.1 The Mechanism of Action of MPA

MPA selectively and reversibly binds and inhibits inosine monophosphate dehydrogenase (IMPDH) enzyme; which is the rate limiting enzyme in the de novo synthesis pathway of purines (103). This pathway is essential for T and B lymphocytes proliferation, where an inhibition of this pathway results in reduced proliferation of lymphocytes and therefore diminished immunity. Additionally, MPA depletes guanosine

triphosphate leading to inhibition of glycosylation and reduction in the recruitment of leukocytes to inflammation sites (103). These actions give MPA its immunosuppressive effects, which are exploited to prevent rejection in kidney transplant patients.

4.1.2 The Pharmacokinetics of MPA

Upon oral administration, MMF is rapidly and extensively pre-systemically metabolized to MPA via carboxyl esterases, CES1 and CES2, expressed in the liver and intestine (104). The bioavailability of MPA after MMF administration to renal transplant recipients is around 81% (105-107). MPA binding to blood cellular components is negligible (<0.01%); however, it is highly bound to serum albumin (around 98%) (108, 109).

MPA is metabolized in the liver primarily by uridine 5'-diphosphate glucuronosyltransferase (UGTs) enzymes producing metabolites including 7-0-MPA-ß-glucuronide (MPAG) and acyl -glucuronide (Acyl-MPAG) (110, 111). The primary enzyme involved in the metabolism of MPA to MPAG is UGT1A9 (112-114). Other isoforms involved in MPAG production include UGT1A7, UGT1A8 and UGT1A10 (112, 114). The enzyme UGT2B7 was demonstrated to be the major isoform involved in the metabolism of MPA to Acyl-MPAG (112, 114).

The metabolite MPAG is the major product of MPA metabolism; however, it has no pharmacological effect with regards to inhibiting IMPDH (115). Unlike MPAG, the metabolite Acyl-MPAG has similar pharmacological potency as MPA (110).

Radiolabel studies demonstrated that renal clearance of MPA is small (~0.6% of

radioactivity) in healthy subjects (104). The metabolites MPAG and Acyl-MPAG are readily excreted into urine by glomerular filtration and active tubular secretion (107). Transporters involved in the renal active secretion of the metabolites include organic anion transporting polypeptides (OATPs) and multidrug resistant protein-2 (MRP-2) (107, 116, 117).

MPAG undergoes enterohepatic circulation (EHC), which is discussed in next section. The efflux transporter (MRP-2) has been demonstrated to be involved in the biliary excretion of MPAG into bile (107). The role of MRP2 was demonstrated by decreased biliary excretion of MPAG in MRP-2 deficient Eisai hyperbilirubinemic rats (EHBRs) (116).

4.1.3 The Enterohepatic Circulation (EHC) Process of MPA

The concentration-time profile of MPA exhibits multiple secondary peaks, which usually occur 4-8 hours after taking an MMF dose (104, 118). These secondary peaks result from the EHC process that involves the excretion of the metabolite MPAG into the bile and from there to the gut. In the gut, MPAG is deconjugated back to MPA by the intestinal microflora. This step is followed by reabsorption of the resulting MPA to the systemic circulation (118). The effect of EHC is significant, where it has been shown that EHC account for around 40-60% of the MPA AUC (86). Therefore, it becomes critical to adequately characterize the EHC process in modeling strategies that describe the pharmacokinetics of MPA.

4.1.4 The Objectives of the Study

MPA has been shown to be effective in preventing the occurance of acute transplant rejection (97). Studies have demonstrated a correlation between MPA concentrations and reduction of acute rejection (119-121). An association between MPA concentrations and hematologic and gastrointestinal side effects has also been established (122, 123). Such association has been shown to be stronger when unbound MPA rather than total MPA concentrations are considered (122).

The presence of these associations along with the high variability demonstrated in MPA concentrations, due to its complex pharmacokinetics, support the need for therapeutic drug monitoring (TDM). Conducting TDM can help in the optimization of MMF therapy by keeping plasma concentrations within the therapeutic window.

The objectives of the current analysis are: 1) to bulid a population pharmacokinetic model of unbound MPA, total MPA, MPAG and acyl-MPAG; 2) to evaluate patient characteristics, co-medication, and genetic polymorphisms as potential sources of variability in MPA pharmacokinetics; and 3) to develop an equation that can be used for dose individualization of MPA in kidney transplant recipients to achieve a desired starting AUC prior to TDM.

4.2 Methods

4.2.1 Subjects and Study Design

92 subjects were enrolled in this study which was part of the Deterioration of Kidney Allograft Function (DeKAF) genomics study conducted in the period of 2006-

2008. DeKAF was a multicenter observational trial aimed to evaluate the effect of individual genetic variability on clinical outcomes of kidney transplantation. Additional information regarding this study is available from government sources (http://www.clinicaltrials.gov) (Identifier: NCT00270712).

Enrolled subjects had end-stage renal failure and underwent kidney or kidney-pancreas transplantation. Inclusion criteria were an age of ≥18 years and functioning kidney graft at the time of the pharmacokinetics visit with an estimated glomerular filtration rate (GFR) >50 ml/min/1.73m^2, within two weeks prior to the pharmacokinetics visit. Exclusion criteria included simultaneously receiving another organ (other than the pancreas) with the qualifying kidney transplant, or if subjects had post-transplant active gastroparesis or liver disease. Institutional Review Board (IRB) approval was obtained at each participating center and all patients provided informed, written consents prior to enrollment.

Subjects received prophylactic oral mycophenolate mofetil (MMF) (Cellcept®) in equal doses (ranging between 500-1500 mg) every 12 hours. Blood samples were collected from patients during the pharmacokinetic visit, which occurred at least 48 hours after starting MMF dosing in which the concentrations were at steady state. Sampling times include pre-dose and 1, 2, 4, 6, 8, and 12 hours following the MMF dose.

4.2.2 Clinical Covariates Collection

Several patient characteristics and clinical factors were collected from recipients and donors, as summarized in Table 4-1. Characteristics collected from both kidney

recipients and donors included: age, gender and race. Additionally, laboratory measurements were collected from recipients and included serum creatinine, bilirubin, albumin, alanine transaminase and alkaline phosphatase. Recipients' relevant concomitant drug therapies were recorded and they comprise of calcineurin Inhibitor (tacrolimus or cyclosporine), steroid and proton pump inhibitors. Other data collected from recipient medical records were height, weight, time to blood collection for pharmacokinetic study since initiating MMF dosing, prior kidney transplant, primary cause of kidney disease, preemptive transplantation[5], deceased or living donor, number of Human leukocyte antigen (HLA) mismatch, diabetes at time of transplantation, and previous antibody induction**.** creatinine clearance (CRCL) was calculated based on recipients serum creatinine levels using Cockcroft and Gault equation (124).

4.2.3 Genotype Data

DNA samples were extracted for the purpose of genotype analysis from peripheral blood lymphocytes collected from both donors and recipients. Lymphocytes were isolated by centrifugation after red blood cell (RBC) lysis. Next, the DNA was isolated and quantified at 260nm absorbance. The platforms SNPlex (Applied Biosystems Inc, Foster City, California, USA) and Sequenom (Sequenom, Inc, San Diego, CA, USA) were used in genotyping the single nucleotide polymorphisms (SNPs). Details of the candidate gene selection and genotyping analysis are reported in a previously published manuscript (125). Briefly, SNPs selection was based on pathways related to MPA

[5] Preemptive kidney transplantation: is transplantation before initiating any dialysis treatment

pharmacokinetics and pharmacodynamics. Based on that, genotyping was conducted on 88 SNPs form both recipients and donors, as listed in Table 4-2.

4.2.4 MPA and Metabolites Bioanalysis in Plasma

Plasma samples collected from patients were processed within 30-60 minutes of blood withdrawal. Concentrations of total and unbound MPA, MPAG, and acyl-MPAG were measured in each sample using an Agilent 1100 series HPLC system (Agilent Technologies, Wilmington, DE). An aliquot of each sample underwent membrane ultrafiltration to extract unbound MPA. Analytes were separated using Phenomenex Polar-RP, 4.6 x 250 mm, reverse phase C-18 column (Phenomenex, Torrance, CA), and detected using a variable wavelength UV detector. Further details about the used bioanalysis technique were previously described by Jacobson et al. (126).

4.2.5 Population Pharmacokinetic Modelling

Nonlinear mixed effects modeling software, NONMEM (Version 7.2, GloboMax, Maryland, USA), was used to perform the population pharmacokinetic analysis. First-order conditional estimation with η, ε-interaction (FOCE-I) was utilized throughout the modeling process. The software Pirana (http://www.pirana-software.com) was utilized as a frontend-modeling environment, and R 3.1.0 was used to conduct the statistical analyses and generate the graphical plots. The Visual Predictive Check (VPC) and Stepwise Covariate Modeling (SCM) were performed using PsN modules (http://psn.sourceforge.net/).

4.2.5.1 Base Model Building

Population model development of unbound MPA, total MPA, MPAG, and acyl-MPAG was conducted as a series of steps that led eventually to a simultaneous population pharmacokinetic model of all the four chemical entities together.

The structure of the final model is displayed in Figure 4-1. The initial modeling step evaluated compartmental models of unbound MPA concentrations including oral one-compartment and two-compartment models, with or without a lag-time term. Several absorption models were tested including first order, zero order, mixed first order and zero order, and transit compartment model.

4.2.5.1.1 Inclusion of Metabolites

The model of unbound MPA was further extended by including the MPAG and Acyl-MPAG metabolites, each in a separate compartment. The fraction metabolized of unbound MPA to MPAG was assumed to be 0.87 while the fraction metabolized to Acyl-MPAG was fixed to 0.13 (104). Therefore, the model assumed no renal elimination of unbound MPA.

4.2.5.1.2 Inclusion of the EHC Process

After incorporating the metabolites, evaluation of the EHC process starting from the MPAG compartment was performed using a gallbladder-based EHC model.

The used gallbladder-based EHC model was built based on the physiological concepts related to the hepatobiliary system and the gallbladder filling and emptying processes. In the model, a gallbladder compartment was connected to MPAG and gut compartments. The extent of EHC (EHC%) which represents the percentage of the

amount of MPAG that gets distributed via EHC was described according to the following equation:

$$EHC\% = \frac{k_{DG}}{k_{DG} + k_{30}}$$

where k_{DG} is the rate constant that describes the EHC distribution process out of the MPAG compartment, and k_{30} is MPAG elimination rate constant.

Another contemplation of the gallbladder-based model is the inclusion of a continuous leak of a percentage of EHC% from the MPAG compartment to the gut. The occurrence of this leak was conveyed by assuming that 75% of the EHC% goes to the gallbladder, while the remaining 25% drains directly from MPAG compartment to the gut compartment.

The gallbladder emptying process was assumed to be triggered by meals, where various numbers of meals was assumed and evaluated, i.e., one meal, two meals, and three meals. Additionally, the timing of meals [mealtimes (mt)] was estimated.

At each mealtime (mt), approximately 75% of the drug stored in the gallbladder is discharged to the gut within a duration (D) of 30 minutes (1, 37, 38). The transfer rate from the gallbladder to the gut was determined by the rate constant k_{GG} according to the following equation:

$$k_{GG} = k_{31} * switch.$$

where k_{31} is a rate constant and $switch$ is a function that accounts for multiple cycles of gallbladder emptying. k_{31} was fixed to 2.77 hr^{-1} based on a simulation analysis which showed that this value results in eliminating 75% of the drug from the gallbladder, within the duration of 30 minutes. The $switch$ function was defined according to the following

equations:

$$Hill1 = \exp(-20 * (time - mt1))$$

$$Hill2 = \exp(-20 * (time - Endmt1))$$

$$Switch = \frac{1}{1 + Hill1} - \frac{1}{1 + Hill2}$$

where $mt1$ represents the beginning of gallbladder emptying (occurs at the same time of mealtime); and $Endmt1$ represents the end of gallbladder emptying (and calculated as $Endmt1 = mt1 + D$, where D was fixed to 30 minutes.

The $Switch$ function applies a double sigmoid function to regulate the gallbladder release rate constant (k_{GG}). The equation $Switch$ allows a rapid change in the k_{GG} rate constant from zero to almost 2.77 around the time $mt1$. After approximately 30 minutes, $Switch$ causes a rapid decline in k_{GG} back to zero around time $Endmt1$. This rapid change of k_{GG} was achieved by using a value of 20 in $Hill1$ and $Hill2$ in an attempt to mimic the toggle nature of gallbladder emptying. To represent the multiple cycles of gallbladder emptying, this set of equations was reapplied at each mealtime.

4.2.5.1.3 Inclusion of Total MPA

A representation of Total MPA concentrations was included using a binding model that estimates MPA fraction unbound (FU) using the equation below:

$$C_{total,ij} = \frac{C_{unbound,ij}}{FU}$$

where $C_{total,ij}$ is j[th] total MPA concentration in the i[th] individual, and $C_{unbound,ij}$ is the j[th] unbound MPA concentration in the i[th] individual

4.2.5.1.4 Inclusion of Concomitant Calcineurin Inhibitor (CNI)

The concomitant CNI drug therapy (*Cdrug*) was included as part of the base model based on previous reports showing clinical significance on MPA pharmacokinetics (127-129). *Cdrug* was modeled on the unbound MPA clearance parameter as the following equation:

$$TVCL = \theta_1 * (1 + \theta_2 * Cdrug)$$

where TVCL is the typical value of unbound MPA clearance; *Cdrug* equals 1 when the concomitant CNI therapy is cyclosporine, and 0 when it is tacrolimus; $\theta_1$represents TVCL when *Cdrug* is tacrolimus , and $(1 + \theta_2)$ represents the fractional change in TVCL when having a concomitant cyclosporine rather than tacrolimus.

4.2.5.1.5 Error Models

Modeling the between-subject variability (BSV) in the structural parameters was included using an exponential model as shown in the following equation:

$$P_j = TVP * e^{\eta_j}$$

where TVP is the typical value of the parameter in the population and η_j is the difference between the j^{th} individual parameter value (P_j) and TVP on a lognormal scale. It was assumed that η_j values are independent and identically normally distributed with a mean of zero and a variance ω^2, i.e. $\eta \sim N(0, \omega^2)$.

Additive, proportional, and combined error models were tested to characterize the residual unexplained variability (RUV) in the model. The equations below describe each one of these models.

- Additive error model:

$$C_{ij} = C_{pred,ij} + \varepsilon_{ij,1}$$

- Proportional error model:

$$C_{ij} = C_{pred,ij} * (1 + \varepsilon_{ij,2})$$

- Combined error model:

$$C_{ij} = C_{pred,ij} * (1 + \varepsilon_{ij,2}) + \varepsilon_{ij,1}$$

where C_{ij} is the observed j^{th} plasma concentration in the i^{th} individual and $C_{pred,ij}$ is the predicted j^{th} plasma concentration in the i^{th} individual. Additionally, ε_{ij} represents the discrepancy between C_{ij} and $C_{pred,ij}$, additively ($\varepsilon_{ij,1}$) and proportionally ($\varepsilon_{ij,2}$). In these models, it is assumed that ε_{ij} are normally distributed with a mean of zero and a variance σ^2; i.e. $\varepsilon \sim N(0, \sigma^2)$.

Eta (η) and epsilon (ε) shrinkage estimates were calculated. A shrinkage value of less than 30% was necessary to justify covariate testing and that the empirical bayesian

estimates (EBEs) mimic the true individual parameters (130, 131). The equation below was used to calculate Eta (η) shrinkage:

$$\eta_{sh} = 1 - \frac{SD(\hat{\eta}_p)}{\omega}$$

where $SD(\hat{\eta}_p)$ is the standard deviation of individual estimated η ($\hat{\eta}_p$) vector related to the population parameter (P); The parameter ω is the model-estimated standard deviation of the random effect parameter associated with the parameter P.

Epsilon shrinkage was calculated as the following:

$$\varepsilon_{sh} = 1 - SD(IWRES)$$

where $SD(IWRES)$ is the standard deviation of the individual weighted residuals vector ($IWRES$), which is calculated according to the following equation:

$$\text{IWRES} = \frac{\text{DV}_{ij} - IPRED_{ij}}{\sigma}$$

where DV is the j^{th} observed concentration in the i^{th} individual; IPRED is the j^{th} prediction in the i^{th} individual; σ is the standard deviation of the residual variability.

4.2.5.2 Covariates Reduction and Modeling

After building the base model, the next step was to evaluate the effect of covariates on the model. The incorporation of influencing covariates allows for higher

predictive performance of the model as it takes into account significant clinical covariates and genotypes.

The starting covariate dataset was composed 25 clinical covariates and 176 SNPs (88 SNPs from recipients and 88 from donors). While the clinical covariates subset included both continuous and categorical variables, the SNP dataset was all categorical.

The large number of covariates included in the study precludes traditional methods used to perform covariate analysis. For instance, by having "N" bivariate covariates[6], there would be 2^N possible combination models, and this number will grow larger with more covariates that have more levels. Furthermore, The Generalized Additive Modeling (GAM) package in R is only able to conduct covariate selection for a maximum of 25 covariates at each run. The Stepwise Covariate Modeling (SCM) method would be impractical to use with this large numbers of covariates as it would demand unreasonably long computing times. Therefore, data reduction steps were conducted in order to be able to limit the number of covariates in a practical manner.

Data reduction methods used in this analysis were contingent on the type of the covariates. The SNPs reduction steps were established based on the pharmacogenomic concepts of minor allele frequency (MAF) and linkage disequilibrium (LD), as described in section 4.2.5.2.1. The reduction of categorical clinical covariates was based the frequencies of categorical levels, see section 4.2.5.2.2.

After the data reduction steps, SNPs and categorical clinical covariates underwent a "levels lumping" step explained in section 4.2.5.3. Next, univariate regression analysis was performed on the resultant SNPs and categorical clinical covariates combined with

[6] N represents the number of covariates

continuous clinical covariates data, as explained in section 4.2.5.4. This was followed by a backward SCM analysis, as described in section 4.2.5.5.

4.2.5.2.1 SNPs Data Reduction

For each SNP, a patient would have one of the SNP three variants: homozygous major for the major allele (wild type), heterozygous, or homozygous minor for the minor allele.

4.2.5.2.1.1.1 SNPs Data Reduction Based on Minor Allele Frequency (MAF)

Minor Allele Frequency (MAF) is defined as the frequency of the homozygous minor allele in the population. The calculation of MAF is performed using the following equation:

$$MAF\% = \frac{N_{hetero} + 2 * N_{homo}}{2 * N_{total}} * 100$$

where N_{hetero} is the number of patients with heterozygous SNP variant, N_{homo} is the number of patients with homozygous SNP variant, and N_{total} is the total number of patients in the study.

The MAF calculation was done for all the SNPs, and a SNP with MAF ≤ 5% was excluded from any further analysis. This cutoff value was selected as it is generally used in the literature.

4.2.5.2.1.1.2 SNPs Data Reduction Based on Linkage Disequilibrium (LD)

The second step of SNP data reduction was based on LD. LD is defined as the presence of a non-random association between two or more genotypes (SNPs) present on

the same chromosome in the population (132). In other words, LD refers to the occurrence of alleles combinations, in the same individual, that would be different from what would be expected from a random process.

The correlation coefficient (R^2) is a measure used to quantify the degree of LD between two SNPs. Interpreting R^2 is relatively straightforward, a value of 0 demonstrates that the examined SNPs are independent of each other, while a value of 1 indicates complete dependency between the two SNPs. It follows that, values ranging between these bounds, as they grow closer to 1, indicate increasing dependency between SNPs. In an example where we have 2 SNPs, SNP x and SNP y, where these SNPs have high LD (high R^2), knowing what variant SNP "x" is, would tell us what variant SNP "y" to expect in the same person. From a statistical point of view, this means that there is high redundancy in the information between SNP x and SNP y which may result in a multicollinearity issue. Therefore, SNPs that have high LD needs to be reduced by removing one of the 2 SNPs.

The SNPs dataset was tested for LD using SNAP website (133, 134). SNAP performs SNPs pair-wise LD analysis using pre-calculated association values from the international HAPMAP and the 1000 Genomes Projects (135, 136). In SNAP analysis, an $R^2 \geq 0.8$ was considered as cutoff point to define high LD. When a pair of SNPs have an $R^2 \geq 0.8$, one SNP was removed from the analysis, and one SNP was kept. The decision of which SNP to remove was based on the type and degree of importance of the SNP, i.e., Non-synonymous SNP is more important than synonymous SNP, which is more important than intronic SNP.

4.2.5.2.2 Categorical Clinical Covariates Data Reduction

Sometimes a categorical covariate will have one level that contains almost all the sample patients. Such a scenario results in minimal information to use in discriminating the effect of the different levels. Such covariate should not be included in the analysis. In the current study, a covariate was removed from any further analysis when that covariate has a level that contained ≥ 90% of the sample patients.

4.2.5.3 Categorical Covariates Levels Lumping

Analyzing categorical covariates (SNPs and clinical) presents another problem caused by levels that rarely occur. Such issue has the potential of inflating the variance for the parameter estimates of the rarely occurring levels. A solution to this problem is to lump levels that rarely occur (Infrequent levels) with each other or with other more frequent ones, based on levels' frequencies.

To perform lumping of levels, a definition of "Infrequent level" was established; a level that has ≤10% of the sample patients. The determination of which "other level" the infrequent level should be lumped to was based on the clinical and the physiological definitions of the levels. For example, if the infrequent level in a SNP was the "Homogenous minor", it was lumped with the "Heterogeneous" level rather than the wild type.

4.2.5.4 Univariate Regression Analysis

Categorical covariates, both SNPs and clinical, that passed the previous data reduction steps, in addition to the continuous clinical covariates were all univariately regressed against the Empirical Bayes Estimates (EBEs) of the following structural fixed

effect parameters from the base model: Unbound MPA Clearance (CL/F), MPAG Clearance (CL_{m1}), and EHC percent (EHC%). A linear regression model was used to conduct the analysis for each covariate parameter pair, where p-value ≤0.01 was considered significant. Covariates that had insignificant p-values were removed from any further analysis.

4.2.5.5 Stepwise Backward Elimination

The significant covariates from the previous step were further investigated using stepwise backward elimination method within the context of NONMEM. The SCM module in Perl Speaks NONMEM (PsN) was used to perform this analysis in an automated fashion. Specifically, all covariates were included and the OFV was calculated. In the next steps, covariates were excluded one at a time and the OFV was calculated. A covariate is removed when its exclusion result in the smallest insignificant increase in the OFV [OFV change < 7.87 (chi- square test, p=0.005, df=1)]. This process is repeated until all remaining covariates are significant.

In this analysis, continuous and categorical covariates were evaluated using different models. Categorical covariates were evaluated using a linear proportional covariate model, as the following:

$$TVP = \theta_1 * (1 + \theta_2 * COV)$$

where TVP is the typical value of the fixed effect parameter; θ_1 is the population estimate of the structural parameter when the covariate is the reference level; $(1 + \theta_2)$

represents the population fractional change in TVP when the covariate is a non-reference level; COV is the categorical covariate value.

Continuous covariates were evaluated using linear model according to the following equation:

$$TVP = \theta_1 * (1 + \theta_2 * (COV - COV_{median}))$$

Where TVP is the typical value of the fixed effect parameter; θ_1 is the population estimate of the structural parameter when the covariate has the median value; θ_2 is the population proportional estimate of the covariate fixed effect; COV is the continuous covariate value; COV_{median} is the median of the COV in the study sample.

4.2.6 Model Qualification

Model qualification was guided by a combination of diagnostic plots, clinical and statistical significance of parameter estimates, precision of the parameter estimates and the objective function value (OFV).

Diagnostic plots were generated using Xpose4 package in R via Rstudio (137-139). These plots include observations (DV) versus population predictions (PRED), DV versus individual predictions (IPRED), conditional weighted residuals (CWRES) versus IPRED, and CWRES versus time.

The standard error (SE) of parameter estimates were calculated as square roots of the diagonals of the variance-covariance matrix estimated using $COV. Relative

Standard Error (RSE%) of the parameter estimates were calculated according to the following equation:

$$RSE\% = \frac{SE}{P} * 100$$

where SE is the standard error of the parameter, and P is the population parameter estimate.

To compare models, Akaike Information Criteria (AIC) was used as defined below, where a lower AIC is generally indicative of better fitting model.

$$\mathrm{AIC} = -2\mathrm{loglikelihood} + 2\mathrm{p}$$

where p is the number of parameters used in the model.

Additionally, Visual Predictive Checks (VPCs) were simulated. The concept of VPC is based on the degree of similarity between model-based simulated data, and observed data that was used to build the model (140). At each observation time, the quantiles (95^{th}, 50^{th}, 5^{th}) were calculated from the observed data and the simulated data. Simulations were conducted 1000 times allowing constructing 95% prediction interval for each of the 3 quantiles. A concentration-time plot was then generated where each 95% prediction interval of the 3 simulated data quantiles, at each observation time, was superimposed over the corresponding observed data quantile. A good VPC should show consistency between simulated data prediction intervals and observed data quantiles.

4.3 Results

4.3.1 Data Summary

Data from the 92 kidney or kidney-pancreas transplant recipients were included in this analysis. From these recipients, a total number of 644 unbound MPA, 644 total MPA, 644 MPAG, and 644 acyl-MPAG concentrations were analyzed. The concentrations-time profiles of unbound MPA, total MPA, MPAG, and acyl-MPAG are shown in Figure 4-2.

Recipients' clinical characteristics are summarized in Table 4-1. Most of the recipients were males (n=62) and white (n=83). The age of the recipients ranged between 20 -73 years with a mean of 51 years. On average, the pharmacokinetic blood sampling was conducted 36 days post-transplant, and 95% of patients had full pharmacokinetic sampling 15-58 days post-transplant, as shown in Figure 4-3. The mean (SD) of CRCL was 82.8 (24.9) ml/min, and the mean (SD) of recipient weights was 82 (17) kg. Diabetes at the time of transplant existed in around one third (29%) of the recipients. Around two thirds (65%) of the sample population received tacrolimus as a concomitant calcineurin inhibitor, while the remaining one third (34%) received cyclosporine. Concomitant steroid and proton pump inhibitor were taken by 60% and 72% of the recipients, respectively.

Genotyping was conducted on the selected 176 SNPs. A summary of all the evaluated SNPs in the study sample is shown in Table 4-2. This table contains the number of patients and frequencies of each SNP considering the three variants: homozygous major, heterozygous, and homozygous minor. Additionally, minor allele frequencies (MAF) of all the SNPs are listed in the same table.

4.3.2 Final Population Model

4.3.2.1 Model Structure

A five-compartment model with first-order absorption from the gastrointestinal tract into an unbound MPA compartment connected to the MPAG, acyl-MPAG, with an additional gallbladder compartments best fitted the data (Figure 4-1). Important features of the model included: one compartment disposition models for unbound MPA, MPAG and Acyl-MPAG; the inclusion of total MPA in the model using a constant fraction unbound (FU); the addition of concomitant calcineurin inhibitors (CNI) drug therapy (*Cdrug*) in the model. A summary of the model parameter estimates are listed in Table 4-3. The table includes parameter estimates and their relative standard error (RSE).

The EHC process was represented using the additional gallbladder compartment that forms a loop between MPAG and gut compartments. Modeling two mealtimes did not improve the fit over one mealtime; therefore, parameters assuming one mealtime were estimated.

Between Subject variability (BSV) was estimated for several structural parameters. Unbound MPA oral clearance (CL/F) had a coefficient of variation (CV) estimate of 30.1% and the volume of distribution of unbound MPA (V/F) demonstrated a CV of 35.5%. Other BSV parameters were also estimated and are summarized in (Table 4-4). The η-shrinkage values estimated for the following structural parameters were k_A = 16.4%, CL/F =8.8%, V/F=23.2%, EHC%=11.8%, CL_{m1}=1.1%, CL_{m2}=2.2%, and

FU=17.5%. These small η-shrinkage value (<30%) validate the use of EBEs in diagnostics and covariate analysis.

Residual unexplained variability (RUV) of unbound MPA, total MPA, MPAG, and acyl-MPAG concentrations were modeled using proportional error models (Table 4-5). The CV for these RUVs were estimated to be 40.49%, 35.8%, 12.2%, and 24.8% for unbound MPA, total MPA, MPAG, and acyl-MPAG concentrations, respectively. In the same table, calculations of ε-shrinkage values are presented.

4.3.2.2 Covariates Analysis

4.3.2.2.1 Covariate Data Reduction

SNP data reduction performed based on MAF resulted in excluding 41 SNPs out of the total 176 SNPs (Table 4-6). Subsequent linkage disequilibrium (LD) analysis conducted on the remaining SNPs showed the presence of high association ($R^2 \geq 0.8$) between two SNPs only: rs7662029 and rs7438135. Both of these SNPs present on the UGT2B7 gene as intronic mutations. Therefore, the process of excluding one of them was performed on a random basis. The same high association also applies to donor SNPs, i.e., donor_ rs7662029 and donor_ rs7438135. Based on that, rs7662029 and donor_rs7662029 were excluded from any further analysis.

Data reduction of categorical clinical covariates resulted in eliminating recipient race, donor race and donor status covariates from any further analysis. Most of the recipients were white, while only 5 were black and 1 was Asian. Around 98% of the donors were living, leaving less than 2% for the other level, deceased. Regarding the

donor race covariate, most of the patients had this covariate information missing (n=62), which would cause high imbalance between the levels.

4.3.2.2.2 Levels Lumping for Categorical Covariates

Next, levels lumping of "infrequent levels" was performed on SNPs and categorical clinical covariates. No clinical covariates needed levels lumping, while level lumping was done in 82 SNPs (Table 4-7). In all These SNPs, heterozygous and homozygous minor were lumped into each other forming one level.

4.3.2.3 Univariate Regression

Univariate regression analysis was conducted to evaluate the remaining covariates, i.e., 133 SNPs and 21 clinical covariates. The analysis resulted in a handful of covariates being significant; refer to Table 4-8. These significant covariates were carried to the next step, which is the backward covariate elimination within the context of NONMEM.

4.3.2.4 Stepwise Backward Elimination

The stepwise backward was performed within NONMEM on the population model. Final significant covariates on the parameters: unbound MPA clearance (CL/F), MPAG clearance(CL_{m1}) and percent (EHC%) are shown in Table 4-9.

4.3.2.5 Final Covariates Results

Unbound MPA oral clearance (CL/F) was found to be significantly affected by CRCL. CL/F was estimated to be 1450 L/hr in patients who had tacrolimus as a concomitant CNI when CRCL was at the median value (=77.37 ml/min). In patients with

the same CRCL however taking cyclosporine instead of tacrolimus, unbound MPA oral clearance increased 14.8% (CL/F=1665 L/hr). The equation below shows the relation between unbound MPA oral clearance, concomitant CNI treatment and CRCL:

$$\frac{\mathrm{CL}}{F} = \mathbf{1450}\frac{L}{hr} * \left(1 + \mathbf{0.0076} * (CRCL - 77.37)\right) * (1.148), \; if \; cyclosporine \; instead \; of \; tacrolimus$$

With respect to the EHC% parameter, only the hepatic nuclear Factor 1 alpha (HNF1A) SNP (rs2393791) was found to be significant. The EHC% of MPAG was estimated as 37.4% in patients with homogenous major (wild type) of the HNF1A SNP rs2393791. Patients who carried one or two alleles (heterogeneous and homogenous minor) of this SNP had 16.5% increase in EHC%, i.e., EHC%=43.6%.

Oral clearance of MPAG was demonstrated to be affected by several covariates including: IMPDH1 SNP rs2288553, diabetes at the time of transplant, and donor gender. If the donor was a male, and the recipient did not have diabetes at the time of transplant, and carried a wild type of the IMPDH1 SNP rs2288553; then, oral clearance of MPAG was estimated as 0.959 L/hr. Having a female donor, instead of male, resulted in 18% reduction in this parameter estimate. If the recipient had diabetes at the time of transplant, MPAG oral clearance decreased by 19.2%. Additionally, a recipient who had 1 or 2 IMPDH1 rs2288553 alleles was estimated to show 32.7% increase in oral clearance of MPAG.

4.3.2.6 Model Qualification

Diagnostic plots of unbound MPA, total MPA, MPAG, and acyl-MPAG are shown in Figures 4-4, 4-5, 4-6, 4-7, respectively. In these plots, IPRED versus DV plots show reliable consistency between predictions and observations around the line of identity. Similar conclusions can be elucidated when comparing PRED versus DV. CWRES vs PRED plots demonstrate random scatter of the points around the zero line, which suggests adequacy of the variability models used. CWRES versus time plots show no specific trend or pattern suggesting structural model adequacy. Overall, the diagnostic plots suggest adequacy of the model. Additional individual plots for the unbound MPA, total MPA, MPAG and acyl-MPAG concentrations can be seen in the appendix.

The Visual Predicative Check (VPC) plots for unbound MPA, total MPA, MPAG, and acyl-MPAG are shown in Figure 4-8. These plots demonstrated that the simulations (n=1000), based on the model fixed and random effect parameters (including significant covariates), result in concentration distributions that are similar and consistent with the observed concentration distribution. In general, these VPC plots show that 95% of the data largely falls within the 95% prediction intervals of the simulated data. Based on that, the VPC plots indicate the model adequacy in describing the general trend and variability in the observed data.

4.3.3 Dosing Equation

Given the estimated oral clearance of unbound MPA (CL/F), the recommended MPA dose can be calculated, assuming a target unbound MPA AUC, as the following:

$$MMF\ Dose\ (mg) = Target\ Unbound\ AUC * \frac{CL}{F}$$

To calculate a target unbound MPA AUC, the following equation can be used:

$$Target\ Unbound\ MPA\ AUC\ = FU\ *\ Target\ Total\ AUC$$

where desired total MPA AUC falls within the range of 30-60 mg*hr/L (121, 141); FU is the Fraction Unbound of MPA and was estimated to be 0.024.

4.4 Discussion

A population pharmacokinetic model that simultaneously describes the concentrations of unbound MPA, total MPA, MPAG, and acyl-MPAG in kidney transplant recipients was established. The EHC process was successfully represented using a more physiologic gallbladder-based model. Utilizing unbound MPA concentrations, the final model provided an equation that can be used in calculating initial doses of MMF administered to kidney transplant recipients.

In literature, several models were built to describe the EHC of MPA using a gallbladder-based model (63, 68, 87, 88). However, these models did not provide a complete representing of the physiology of EHC in their modeling assumptions. The current study utilizes a more physiologic model of the EHC process that is build based on

the physiological concepts related to the hepatobiliary system and the gallbladder filling and emptying processes (1, 35-38). Major assumptions in the current EHC model are based on gallbladder cholescintigraphy studies, which showed that around 75% of bile enters the gallbladder after fasting. These studies also demonstrated that the gallbladder releases around 75% of its content after 30 minutes of cholecystokinin[7] infusion (35, 39).

As a result of the existing high between-patients variability in the MPA pharmacokinetics, TDM of MPA is essential for dose individuation (107, 142) . Current guidelines suggest the use of a total MPA AUC between 30-60 mg*h/L as recommended target ranges in TDM (121, 141-145). However, the utilization of total MPA could be faulty in clinical situations where protein binding may change, as in severe renal impairment (CRCL< 25 mL/min) and hypoalbuminemia (<31 g/L) (69, 146). Renal impairment reduces excretion of MPAG metabolite, which in turn displaces MPA from binding sites(147). Reduction in MPA protein binding result in increased FU which causes higher total MPA clearance and therefore lower concentrations (69).Therefore, changing MPA FU may result in nonlinear relation between total MPA and unbound MPA concentrations. In these situations, total MPA AUC may not represent exposure to the active component in all patients, and monitoring unbound MPA concentrations may be beneficial.

The ability to perform TDM based on unbound MPA AUC requires establishing a window of values of a target exposure of unbound MPA. In the current study, it is justifiable to utilize total MPA target AUC values in predicting a target unbound AUC

[7] Cholecystokinin is the enteric hormone that causes gallbladder emptying

values, and therefore designing the dosing equation. This conclusion came as a result of several reasons. Currently, assays used to measure unbound MPA concentrations are not routinely available in most centers. As a result, there is no information in the literature regarding such target exposure. In addition, the data used in the current analysis does not support evaluating changing FU as blood concentrations were sampled within 12-hour duration. Moreover, patients were sampled after an average of 35 days post-transplantation, time at which FU is considered more stable in renal transplant recipients (104, 148).

The pharmacokinetic process of MPA has been reported to be complex and unpredictable (94). Several factors have been shown to influence the pharmacokinetics of MPA. These factors include concomitant drug therapy, clinical characteristics and genotypes (1, 64). In the current analysis, we have attempted to reduce the unpredictability of MPA pharmacokinetics by evaluating a large number of clinical covariates, concomitant drug therapy, and genotypes from donors and recipients for their significance in the model. To our knowledge, this is the first population pharmacokinetic analysis of unbound MPA that evaluates large number of donor genotypes as potential covariates.

Concomitant CNI treatment was included in the model as a covariate on the oral clearance (CL/F) of unbound MPA. This inclusion is based on the historical knowledge of the clinical effect of concomitant CNI on MPA pharmacokinetics (107). Specifically, it has been shown that cyclosporine results in increased MPA clearance in comparison to concomitant tacrolimus (149). The concentrations of MPA had been shown to be higher

when the concomitant CNI is tacrolimus, rather than cyclosporine (107). In the current study, cyclosporine co-administration instead of tacrolimus caused a 14.8% increase in the oral clearance of unbound MPA (CL/F). This result comes in consistence with the literature where several studies reported similar effect (90, 150, 151).

CRCL was found to be a significant covariate on unbound MPA clearance. The same result was also observed in several other studies (149) (91, 152). Such result indicates the possible presence of significant renal clearance pathway for MPA in kidney transplant recipients. This challenges previous report of irrelevance of renal clearance for MPA; however, that study was conducted in healthy volunteers (104). In the present study, the statistical effect of CRCL was minimal; however, significant. The clinical implication however can be demonstrated when comparing two patients who take tacrolimus, one with CRCL=50 mL/min and another with CRCL=120 mL/min. In the patient with CRCL=50 mL/min, the respective unbound MPA clearance is 1148 L/h. on the other hand, the unbound MPA clearance almost doubles (1920 L/h) in the patient with CRCL=120 mL/min.

The time after transplant did not have a significant effect on unbound MPA exposure. However, previous studies demonstrated 30–50% reduction in total MPA AUC in the first weeks when compared to later times (1-6 months) (104, 153, 154). The inability to observe this effect in the current study can be attributed to the fact that patients are sampled later times after transplantation (more than 2 weeks).

The only covariate that demonstrated an effect on the parameter EHC% was the HNF1A SNP rs2393791. Having a heterozygous or homozygous minor allele variants of

this SNP, instead of the wild type, increased EHC% by 16.5%. HNF1A is a transcription factor expressed in the liver, as well as the kidneys. This transcription factor regulates the expression of several genes including bile acid transporters (155, 156). Therefore, changes in the coding of HNF1A could result in altered transcription and/or functionality of the bile acid transporters and therefore possibly changing the EHC%.

Several covariates were found to be significant on MPAG clearance and they include the IMPDH1 SNP rs2288553, donor gender and diabetes at the time of transplant. Recipients who received kidney from a male donor, and had a wild type rs2288553 and diabetes at the time of transplantation demonstrated 19% lower MPAG clearance when compared to similar patients but without diabetes. The presence of diabetes has been shown to affect UGT enzymes and therefore the pharmacokinetics of MPA metabolites (157). Compared to a male donor, female donor caused 18% decrease in the oral clearance of MPAG in a recipient who had wild type rs2288553 and no diabetes at the time of transplantation. A probable justification involves the differences in the transporters activity between male and female kidneys. The mRNA expression of renal organic anion transporting polypeptide (OATP) had been demonstrated to be less in female rat kidney than in male rat kidney (158). Another study showed 40% reduction of the expression of rat OATP1 protein in kidney cortex of female rat, when compared to the kidney cortex of male rats (159).Therefore, it is speculated that OATP expression in the kidney could be important for the tubular secretion of conjugated drugs in the kidney. Another possible explanation is the related to the differences between male and female kidney sizes. Male kidneys are generally bigger in size and therefore could accomplish

more clearance than female donor kidney. Lastly, no clear understanding of the association between IMPDH1 SNP rs2288553 and MPAG clearance could be concluded; however, it may be a result of statistical type 1 error. Regardless, the effect of this covariate can be tested in a future study by comparing MPAG clearance in two animal groups, one with the minor allele and the other with a wild type variant.

A limitation of the analysis is related to the use of linear regression analyses in the covariate modeling strategy. Such linear regression models may not be able to catch the covariate parameter association if this association was presented in a nonlinear fashion.

4.5 Conclusion

We successfully developed a population pharmacokinetic model that simultaneously modeled unbound MPA, MPAG, acyl-MPAG concentrations, and took into account the EHC process of the drug. Large numbers of covariates needed evaluation and testing for their significance on the model. Therefore, a multi-step covariate data reduction and modeling was developed and utilized to perform the covariate analysis. The modeling results were then used to create a dosing equation of MMF in kidney transplant recipients. The model results needs to be externally validated in a group of kidney transplant patients.

Table 4-1: Patients' Characteristics and Clinical Covariates

Characteristic	Value
Recipient Gender (Male/Female)	62/27
Recipient Age (Years)[1]	51 (12)
Recipient Race (White / Black /Asian)	83/5/1
Recipient Weight (Kg) [1]	82.3 (17)
Recipient BMI[*] at Transplant[1]	28 (5.7)
Recipient Height (Cm) [1]	173 (8.3)
Time to Pharmacokinetic Analysis[#] (Days) [1]	36 (15)
Preemptive Transplantation [+] (Yes/No)	42/47
Previous Antibody Induction (IL2/ Monoclonal/Polyclonal)	32/19/38
Diabetes at Time of Transplant (Yes/No)	26/63
Number Of HLA[†] Mismatch (1/2/3/4/5/Other)	9/12/27/9/18/13
Prior Kidney Transplant (No/ 1 Prior transplant)	73/16
Primary Cause of Kidney Disease (Glomerular disease/Diabetes/Hypertension/Polycystic kidney disease/Other/Unknown)	21/19/6/21/17/5
Serum Creatinine (mg/dL) [1]	1.2 (0.3)

Serum Albumin (g/dL) [1]	0.5 (0.3)
Serum Alanine Aminotransferase (U/L) [1]	27 (19.4)
Serum Alkaine Phosphatase (U/L) [1]	93.6 (95.8)
Creatinine Clearance (ml/min)[1]	82.8 (24.9)
Concomitant Calcineurin Inhibitor (Tacrolimus/ Cyclosporine)	58/31
Concomitant Steriod (Yes/No)	57/32
Concomitant Proton Pump Inhibitor (Yes/No)	66/23
Donor Status (Living/ Deceased)	88/1
Donor Gender (Male/Female)	52/37
Donor Age[1]	42 (12)
Donor Race (White/ Black)	28/2

[1]: Reported values for these characteristics are mean (Standard deviation)
[*]: Body Mass Index
[+]: Preemptive kidney transplantation is defined as transplantation before initiating any dialysis treatment
[#]: Refers to the duration of time between initiating MMF dosing and the pharmacokinetic visit
[†]: HLA: Human Leukocyte Antigen

Table 4-2: Studied SNPs Variants Listed as Number (Frequency)

SNP	Homozygous Major Variant (Wild Type)	Heterozygous Variant	Homozygous Minor Variant	Minor Allele Frequency (MAF)
rs8187710	82 (92.1)	7 (7.9)	0 (0)	3.93
rs8187707	82 (92.1)	7 (7.9)	0 (0)	3.93
rs8045523	60 (67.4)	27 (30.3)	2 (2.2)	17.42
rs7662029	25 (28.1)	41 (46.1)	23 (25.8)	48.88
rs7608713	48 (53.9)	33 (37.1)	8 (9)	27.53
rs7439366	89 (100)	0 (0)	0 (0)	0.00
rs7438244	25 (28.1)	41 (46.1)	23 (25.8)	48.88
rs7438135	25 (28.1)	41 (46.1)	23 (25.8)	48.88
rs73823859	86 (96.6)	3 (3.4)	0 (0)	1.69
rs7311358	63 (70.8)	23 (25.8)	3 (3.4)	16.29
rs72551325	89 (100)	0 (0)	0 (0)	0.00
rs72551324	89 (100)	0 (0)	0 (0)	0.00
rs717620	66 (74.2)	20 (22.5)	2 (2.2)	13.48
rs7118873	68 (76.4)	19 (21.3)	2 (2.2)	12.92
rs7117473	80 (89.9)	7 (7.9)	2 (2.2)	6.18

rs6760588	56 (62.9)	30 (33.7)	3 (3.4)	20.22
rs6731242	58 (65.2)	26 (29.2)	5 (5.6)	20.22
rs6715325	29 (32.6)	47 (52.8)	13 (14.6)	41.01
rs6714486	79 (88.8)	9 (10.1)	1 (1.1)	6.18
rs66471611	89 (100)	0 (0)	0 (0)	0.00
rs60140950	66 (74.2)	22 (24.7)	0 (0)	12.36
rs58597806	89 (100)	0 (0)	0 (0)	0.00
rs4762802	38 (42.7)	40 (44.9)	11 (12.4)	34.83
rs4731448	51 (57.3)	35 (39.3)	3 (3.4)	23.03
rs45504099	89 (100)	0 (0)	0 (0)	0.00
rs4149117	63 (70.8)	23 (25.8)	3 (3.4)	16.29
rs4149058	50 (56.2)	32 (36)	7 (7.9)	25.84
rs4149056	69 (77.5)	18 (20.2)	2 (2.2)	12.36
rs4149026	47 (52.8)	34 (38.2)	7 (7.9)	26.97
rs4148328	34 (38.2)	44 (49.4)	11 (12.4)	37.08
rs41318031	84 (94.4)	5 (5.6)	0 (0)	2.81
rs3999413	69 (77.5)	20 (22.5)	0 (0)	11.24
rs3890213	83 (93.3)	6 (6.7)	0 (0)	3.37
rs3829310	74 (83.1)	13 (14.6)	1 (1.1)	8.43
rs3740074	39 (43.8)	37 (41.6)	13 (14.6)	35.39
rs3740066	45 (50.6)	33 (37.1)	11 (12.4)	30.90
rs3740065	72 (80.9)	16 (18)	1 (1.1)	10.11

rs3740063	38 (42.7)	37 (41.6)	14 (15.7)	36.52
rs34456559	82 (92.1)	7 (7.9)	0 (0)	3.93
rs2851075	27 (30.3)	42 (47.2)	20 (22.5)	46.07
rs2756112	84 (94.4)	5 (5.6)	0 (0)	2.81
rs2741045	46 (51.7)	37 (41.6)	6 (6.7)	27.53
rs2417955	31 (34.8)	44 (49.4)	14 (15.7)	40.45
rs2393791	39 (43.8)	40 (44.9)	10 (11.2)	33.71
rs2306283	30 (33.7)	42 (47.2)	17 (19.1)	42.70
rs2303218	87 (97.8)	2 (2.2)	0 (0)	1.12
rs2302538	73 (82)	14 (15.7)	2 (2.2)	10.11
rs2291075	31 (34.8)	48 (53.9)	10 (11.2)	38.20
rs2291073	66 (74.2)	21 (23.6)	2 (2.2)	14.04
rs2288553	76 (85.4)	13 (14.6)	0 (0)	7.30
rs2288549	52 (58.4)	34 (38.2)	3 (3.4)	22.47
rs2288548	51 (57.3)	35 (39.3)	3 (3.4)	23.03
rs2278293	24 (27)	47 (52.8)	18 (20.2)	46.63
rs2273697	58 (65.2)	27 (30.3)	4 (4.5)	19.66
rs2241409	60 (67.4)	27 (30.3)	2 (2.2)	17.42
rs2228075	47 (52.8)	37 (41.6)	5 (5.6)	26.40
rs2071190	44 (49.4)	36 (40.4)	9 (10.1)	30.34
rs2002042	41 (46.1)	40 (44.9)	8 (9)	31.46
rs1817154	51 (57.3)	31 (34.8)	7 (7.9)	25.28

rs1789694	48 (53.9)	37 (41.6)	4 (4.5)	25.28
rs17863762	87 (97.8)	2 (2.2)	0 (0)	1.12
rs17388851	34 (38.2)	36 (40.4)	19 (21.3)	41.57
rs17222723	82 (92.1)	7 (7.9)	0 (0)	3.93
rs17216282	82 (92.1)	7 (7.9)	0 (0)	3.93
rs16923519	49 (55.1)	31 (34.8)	9 (10.1)	27.53
rs1604144	45 (50.6)	34 (38.2)	10 (11.2)	30.34
rs12988520	28 (31.5)	42 (47.2)	19 (21.3)	44.94
rs12427353	53 (59.6)	31 (34.8)	5 (5.6)	23.03
rs12233719	89 (100)	0 (0)	0 (0)	0.00
rs11892031	75 (84.3)	12 (13.5)	2 (2.2)	8.99
rs11770116	38 (42.7)	46 (51.7)	5 (5.6)	31.46
rs11706052	74 (83.1)	15 (16.9)	0 (0)	8.43
rs1169307	37 (41.6)	39 (43.8)	13 (14.6)	36.52
rs1169306	41 (46.1)	39 (43.8)	9 (10.1)	32.02
rs1169303	26 (29.2)	37 (41.6)	26 (29.2)	50.00
rs1169302	31 (34.8)	38 (42.7)	20 (22.5)	43.82
rs1169293	76 (85.4)	11 (12.4)	2 (2.2)	8.43
rs1169288	49 (55.1)	32 (36)	8 (9)	26.97
rs1169286	31 (34.8)	48 (53.9)	10 (11.2)	38.20
rs11568311	78 (87.6)	11 (12.4)	0 (0)	6.18
rs11563251	74 (83.1)	14 (15.7)	1 (1.1)	8.99

rs1137968	82 (92.1)	7 (7.9)	0 (0)	3.93
rs10929303	63 (70.8)	26 (29.2)	0 (0)	14.61
rs1077858	35 (39.3)	45 (50.6)	9 (10.1)	35.39
rs10501421	69 (77.5)	19 (21.3)	1 (1.1)	11.80
rs10187694	89 (100)	0 (0)	0 (0)	0.00
rs10176426	72 (80.9)	16 (18)	1 (1.1)	10.11
rs10167119	36 (40.4)	42 (47.2)	11 (12.4)	35.96
donor_rs8187710	81 (91)	7 (7.9)	0 (0)	3.93
donor_rs8187707	81 (91)	7 (7.9)	0 (0)	3.93
donor_rs8045523	60 (67.4)	27 (30.3)	1 (1.1)	16.29
donor_rs7662029	31 (34.8)	41 (46.1)	16 (18)	41.01
donor_rs7608713	51 (57.3)	30 (33.7)	6 (6.7)	23.60
donor_rs7439366	88 (98.9)	0 (0)	0 (0)	0.00
donor_rs7438244	31 (34.8)	41 (46.1)	16 (18)	41.01
donor_rs7438135	31 (34.8)	41 (46.1)	16 (18)	41.01
donor_rs73823859	82 (92.1)	6 (6.7)	0 (0)	3.37
donor_rs7311358	62 (69.7)	24 (27)	2 (2.2)	15.73
donor_rs72551325	88 (98.9)	0 (0)	0 (0)	0.00
donor_rs72551324	88 (98.9)	0 (0)	0 (0)	0.00
donor_rs717620	52 (58.4)	27 (30.3)	9 (10.1)	25.28
donor_rs7118873	68 (76.4)	19 (21.3)	1 (1.1)	11.80
donor_rs7117473	81 (91)	7 (7.9)	0 (0)	3.93

donor_rs6760588	43 (48.3)	39 (43.8)	6 (6.7)	28.65
donor_rs6731242	59 (66.3)	25 (28.1)	3 (3.4)	17.42
donor_rs6715325	32 (36)	43 (48.3)	13 (14.6)	38.76
donor_rs6714486	85 (95.5)	3 (3.4)	0 (0)	1.69
donor_rs66471611	88 (98.9)	0 (0)	0 (0)	0.00
donor_rs60140950	67 (75.3)	20 (22.5)	0 (0)	11.24
donor_rs58597806	88 (98.9)	0 (0)	0 (0)	0.00
donor_rs4762802	41 (46.1)	34 (38.2)	13 (14.6)	33.71
donor_rs4731448	53 (59.6)	30 (33.7)	5 (5.6)	22.47
donor_rs45504099	87 (97.8)	1 (1.1)	0 (0)	0.56
donor_rs4149117	62 (69.7)	24 (27)	2 (2.2)	15.73
donor_rs4149058	52 (58.4)	29 (32.6)	7 (7.9)	24.16
donor_rs4149056	65 (73)	20 (22.5)	3 (3.4)	14.61
donor_rs4149026	54 (60.7)	27 (30.3)	7 (7.9)	23.03
donor_rs4148328	29 (32.6)	45 (50.6)	14 (15.7)	41.01
donor_rs41318031	82 (92.1)	6 (6.7)	0 (0)	3.37
donor_rs3999413	66 (74.2)	22 (24.7)	0 (0)	12.36
donor_rs3890213	79 (88.8)	9 (10.1)	0 (0)	5.06
donor_rs3829310	74 (83.1)	14 (15.7)	0 (0)	7.87
donor_rs3740074	29 (32.6)	40 (44.9)	19 (21.3)	43.82
donor_rs3740066	30 (33.7)	39 (43.8)	19 (21.3)	43.26
donor_rs3740065	73 (82)	14 (15.7)	1 (1.1)	8.99

donor_rs3740063	25 (28.1)	38 (42.7)	25 (28.1)	49.44
donor_rs34456559	81 (91)	7 (7.9)	0 (0)	3.93
donor_rs2851075	30 (33.7)	39 (43.8)	18 (20.2)	42.13
donor_rs2756112	82 (92.1)	6 (6.7)	0 (0)	3.37
donor_rs2741045	51 (57.3)	30 (33.7)	7 (7.9)	24.72
donor_rs2417955	37 (41.6)	41 (46.1)	10 (11.2)	34.27
donor_rs2393791	33 (37.1)	38 (42.7)	17 (19.1)	40.45
donor_rs2306283	37 (41.6)	42 (47.2)	9 (10.1)	33.71
donor_rs2303218	87 (97.8)	1 (1.1)	0 (0)	0.56
donor_rs2302538	65 (73)	21 (23.6)	2 (2.2)	14.04
donor_rs2291075	37 (41.6)	41 (46.1)	10 (11.2)	34.27
donor_rs2291073	73 (82)	13 (14.6)	2 (2.2)	9.55
donor_rs2288553	72 (80.9)	16 (18)	0 (0)	8.99
donor_rs2288549	53 (59.6)	31 (34.8)	4 (4.5)	21.91
donor_rs2288548	53 (59.6)	30 (33.7)	5 (5.6)	22.47
donor_rs2278293	27 (30.3)	36 (40.4)	25 (28.1)	48.31
donor_rs2273697	61 (68.5)	24 (27)	3 (3.4)	16.85
donor_rs2241409	58 (65.2)	29 (32.6)	1 (1.1)	17.42
donor_rs2228075	48 (53.9)	34 (38.2)	5 (5.6)	24.72
donor_rs2071190	48 (53.9)	33 (37.1)	7 (7.9)	26.40
donor_rs2002042	45 (50.6)	38 (42.7)	5 (5.6)	26.97
donor_rs1817154	49 (55.1)	37 (41.6)	2 (2.2)	23.03

donor_rs1789694	50 (56.2)	34 (38.2)	4 (4.5)	23.60
donor_rs17863762	87 (97.8)	1 (1.1)	0 (0)	0.56
donor_rs17388851	23 (25.8)	43 (48.3)	22 (24.7)	48.88
donor_rs17222723	80 (89.9)	7 (7.9)	0 (0)	3.93
donor_rs17216282	81 (91)	7 (7.9)	0 (0)	3.93
donor_rs16923519	53 (59.6)	28 (31.5)	7 (7.9)	23.60
donor_rs1604144	48 (53.9)	32 (36)	7 (7.9)	25.84
donor_rs12988520	26 (29.2)	46 (51.7)	15 (16.9)	42.70
donor_rs12427353	56 (62.9)	27 (30.3)	5 (5.6)	20.79
donor_rs12233719	88 (98.9)	0 (0)	0 (0)	0.00
donor_rs11892031	78 (87.6)	10 (11.2)	0 (0)	5.62
donor_rs11770116	42 (47.2)	36 (40.4)	10 (11.2)	31.46
donor_rs11706052	69 (77.5)	18 (20.2)	1 (1.1)	11.24
donor_rs1169307	37 (41.6)	38 (42.7)	13 (14.6)	35.96
donor_rs1169306	37 (41.6)	39 (43.8)	11 (12.4)	34.27
donor_rs1169303	27 (30.3)	38 (42.7)	23 (25.8)	47.19
donor_rs1169302	26 (29.2)	37 (41.6)	25 (28.1)	48.88
donor_rs1169293	73 (82)	14 (15.7)	1 (1.1)	8.99
donor_rs1169288	43 (48.3)	35 (39.3)	10 (11.2)	30.90
donor_rs1169286	30 (33.7)	44 (49.4)	14 (15.7)	40.45
donor_rs11568311	77 (86.5)	10 (11.2)	1 (1.1)	6.74
donor_rs11563251	75 (84.3)	11 (12.4)	2 (2.2)	8.43

donor_rs1137968	81 (91)	7 (7.9)	0 (0)	3.93
donor_rs10929303	54 (60.7)	30 (33.7)	4 (4.5)	21.35
donor_rs1077858	32 (36)	47 (52.8)	9 (10.1)	36.52
donor_rs10501421	71 (79.8)	16 (18)	1 (1.1)	10.11
donor_rs10187694	88 (98.9)	0 (0)	0 (0)	0.00
donor_rs10176426	69 (77.5)	19 (21.3)	0 (0)	10.67
donor_rs10167119	42 (47.2)	39 (43.8)	7 (7.9)	29.78

Notes:

- The values are presented in this table as: the Number of patients (frequencies of SNP variants)
- The SNPs that starts with “rs” are from the recipients while the ones starting with “donor_rs” are from the donors

Table 4-3: A Summary of the Model Parameter Estimates

Theta	Estimate	RSE
k_A (hr^{-1})	2	18.4%
CL/F (L/hr)	1450	6.5%
V/F (L)	5630	7.9%
EHC% (fraction)	0.374	5.9%
Mealtime (mt1) (hr)	7.73	0.1%
CL_{m1} (L/hr)	0.959	4.8%
V_{m1} (L)	5.72	4.9%
CL_{m2} (L/hr)	32.3	7.6%
V_{m2} (L)	17.9	9.4%
FU (fraction)	0.0239	5.2%
The marginal effect of CDRUG (cyclosporine instead of tacrolimus) on CL/F	0.148	61.1%
The marginal effect of CRCL on CL/F	0.0076	30.5%
The marginal effect of having diabetes at time of transplant (versus not) on CL_{m1}	-0.192	31.6%
The marginal effect of donor gender (female instead of male) on CL_{m1}	-0.181	34.4%
The marginal effect of the IMPDH1 SNP rs2288553* (Heterozygous instead of Wild Type) on CL_{m1}	0.327	37.0%
The effect of the HNF1A SNP rs2393791 (Heterozygous or Homozygous Minor instead of wild type) on EHC%	0.165	55.0%

Key:
k_A: absorption rate constant, Cl/F: unbound MPA clearance, V/F: unbound MPA volume of distribution, EHC%: EHC percentage, CL_{m1}:MPAG clearance, V_{m1}:MPAG volume of distribution, CL_{m2}: Acyl-MPAG clearance, V_{m2}:Acyl-MPAG volume of distribution, FU: MPA fraction unbound
Notes:
*: No patient in the study sample had a homozygous minor variant of rs2288553
CDRUG: concomitant calcineurin inhibitor
CRCL: Creatinine clearance
IMPDH1: Inosine-5'-monophosphate dehydrogenase 1
HNF1A: Hepatic Nuclear Factor 1 Alpha

Table 4-4: Estimates of the Between Subject Variability (BSV) Parameters

BSV Parameter	CV Estimate (%)	RSE (%)	η-shrinkage (%)
kA	108.6	29.3	16.4
CL/F	30.1	25.4	8.8
V/F	35.5	33.6	23.2
EHC%	27.8	29.4	11.8
CL_{m1}	27.2	20.6	1.1
CL_{m2}	46.3	19.8	2.2
FU	24	24.3	17.5

Table 4-5: Estimates of Residual Unexplained Variability (RUV) Parameters

RUV Parameter	CV Estimate (%)	Shrinkage (%)
Unbound MPA	40.49	5.9%
Total MPA	35.8	8.1%
MPAG	12.2	11%
Acyl-MPAG	24.8	10.2%

Table 4-6: Excluded SNPs Based on Minor Allele Frequency (MAF) Analysis

SNP	Homozygous major variant (Wild Type)	heterozygous variant	Homozygous minor variant	Minor Allele Frequency (%)
rs7439366	89 (100)	0 (0)	0 (0)	0.00
rs72551325	89 (100)	0 (0)	0 (0)	0.00
rs72551324	89 (100)	0 (0)	0 (0)	0.00
rs66471611	89 (100)	0 (0)	0 (0)	0.00
rs58597806	89 (100)	0 (0)	0 (0)	0.00
rs45504099	89 (100)	0 (0)	0 (0)	0.00
rs12233719	89 (100)	0 (0)	0 (0)	0.00
rs10187694	89 (100)	0 (0)	0 (0)	0.00
rs2303218	87 (97.8)	2 (2.2)	0 (0)	1.12
rs17863762	87 (97.8)	2 (2.2)	0 (0)	1.12
rs73823859	86 (96.6)	3 (3.4)	0 (0)	1.69
rs41318031	84 (94.4)	5 (5.6)	0 (0)	2.81
rs2756112	84 (94.4)	5 (5.6)	0 (0)	2.81
rs3890213	83 (93.3)	6 (6.7)	0 (0)	3.37
rs8187710	82 (92.1)	7 (7.9)	0 (0)	3.93
rs8187707	82 (92.1)	7 (7.9)	0 (0)	3.93
rs34456559	82 (92.1)	7 (7.9)	0 (0)	3.93
rs17222723	82 (92.1)	7 (7.9)	0 (0)	3.93
rs17216282	82 (92.1)	7 (7.9)	0 (0)	3.93
rs1137968	82 (92.1)	7 (7.9)	0 (0)	3.93
donor_rs7439366	88 (98.9)	0 (0)	0 (0)	0.00
donor_rs72551325	88 (98.9)	0 (0)	0 (0)	0.00
donor_rs72551324	88 (98.9)	0 (0)	0 (0)	0.00
donor_rs66471611	88 (98.9)	0 (0)	0 (0)	0.00
donor_rs58597806	88 (98.9)	0 (0)	0 (0)	0.00

donor_rs12233719	88 (98.9)	0 (0)	0 (0)	0.00
donor_rs10187694	88 (98.9)	0 (0)	0 (0)	0.00
donor_rs45504099	87 (97.8)	1 (1.1)	0 (0)	0.56
donor_rs2303218	87 (97.8)	1 (1.1)	0 (0)	0.56
donor_rs17863762	87 (97.8)	1 (1.1)	0 (0)	0.56
donor_rs6714486	85 (95.5)	3 (3.4)	0 (0)	1.69
donor_rs73823859	82 (92.1)	6 (6.7)	0 (0)	3.37
donor_rs41318031	82 (92.1)	6 (6.7)	0 (0)	3.37
donor_rs2756112	82 (92.1)	6 (6.7)	0 (0)	3.37
donor_rs8187710	81 (91)	7 (7.9)	0 (0)	3.93
donor_rs8187707	81 (91)	7 (7.9)	0 (0)	3.93
donor_rs7117473	81 (91)	7 (7.9)	0 (0)	3.93
donor_rs34456559	81 (91)	7 (7.9)	0 (0)	3.93
donor_rs17222723	80 (89.9)	7 (7.9)	0 (0)	3.93
donor_rs17216282	81 (91)	7 (7.9)	0 (0)	3.93
donor_rs1137968	81 (91)	7 (7.9)	0 (0)	3.93

Table 4-7: List of SNPs that Underwent Lumping of Levels

SNP	SNP	SNP
rs8045523	rs12427353	donor_rs2288553
rs7608713	rs11892031	donor_rs2288549
rs7311358	rs11770116	donor_rs2288548
rs717620	rs11706052	donor_rs2273697
rs7118873	rs1169293	donor_rs2241409
rs7117473	rs1169288	donor_rs2228075
rs6760588	rs11568311	donor_rs2071190
rs6731242	rs11563251	donor_rs2002042
rs6714486	rs10929303	donor_rs1817154
rs60140950	rs10501421	donor_rs1789694
rs4731448	rs10176426	donor_rs16923519
rs4149117	donor_rs8045523	donor_rs1604144
rs4149058	donor_rs7608713	donor_rs12427353
rs4149056	donor_rs7311358	donor_rs11892031
rs4149026	donor_rs7118873	donor_rs11706052
rs3999413	donor_rs6760588	donor_rs1169293
rs3829310	donor_rs6731242	donor_rs11568311
rs3740065	donor_rs60140950	donor_rs11563251
rs2741045	donor_rs4731448	donor_rs10929303

rs2302538	donor_rs4149117	donor_rs10501421
rs2291073	donor_rs4149058	donor_rs10176426
rs2288553	donor_rs4149056	donor_rs10167119
rs2288549	donor_rs4149026	-
rs2288548	donor_rs3999413	-
rs2273697	donor_rs3890213	-
rs2241409	donor_rs3829310	-
rs2228075	donor_rs3740065	-
rs2002042	donor_rs2741045	-
rs1817154	donor_rs2302538	-
rs1789694	donor_rs2291073	-

Table 4-8: Significant Covariates after Univariate Regression Analysis

Parameter	Significant covariates
Unbound MPA Clearance (CL/F)	Recipient Weight, CRCL, donor_rs12988520
MPAG Clearance (CL_{m1})	Donor Gender, Recipient Age, Diabetes at Time of Transplant,rs2288553
Percent (EHC%)	rs3829310, rs2393791, donor_rs1169306, donor_rs1169288, donor_rs2291073

Table 4-9: Final List of Significant Covariates

Parameter	Significant covariates
Unbound MPA Clearance (CL/F)	CRCL
MPAG Clearance (CL_{m1})	Donor Gender, Diabetes at Time of Transplant, rs2288553
Percent (EHC%)	rs2393791

Figure 4-1: Schematic Representation of the Model

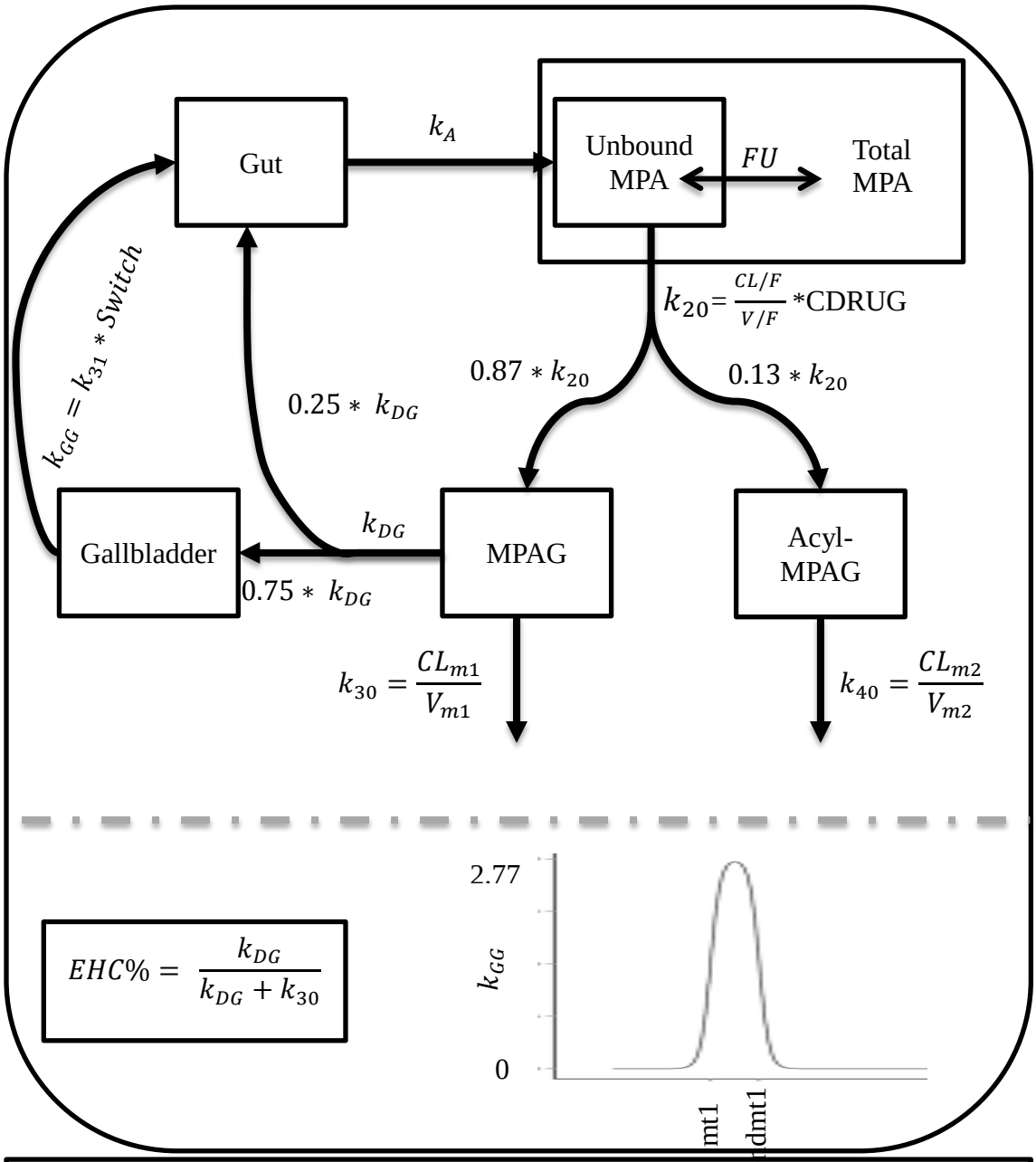

Key:

k_A : absorption rate constant; FU: fraction unbound; CL/F: apparent oral clearance; V/F: apparent volume of distribution; K_{20}: unbound MPA elimination rate constant; k_{DG}: EHC distribution rate constant; k_{GG}: gallbladder emptying rate constant; CL_{m1}:MPAG oral clearance; V_{m1}:MPAG volume of distribution; k_{30}: MPAG elimination rate constant; CL_{m2}: Acyl-MPAG oral clearance; V_{m2}: Acyl-MPAG volume of distribution; k_{40}: Acyl-MPAG elimination rate constant; mt1: represents a mealtime (beginning of gallbladder emptying); endmt1: represents the end of gallbladder emptying

Figure 4-2: The Concentration-Time Profile of Unbound MPA, Total MPA, MPAG, and Acyl-MPAG

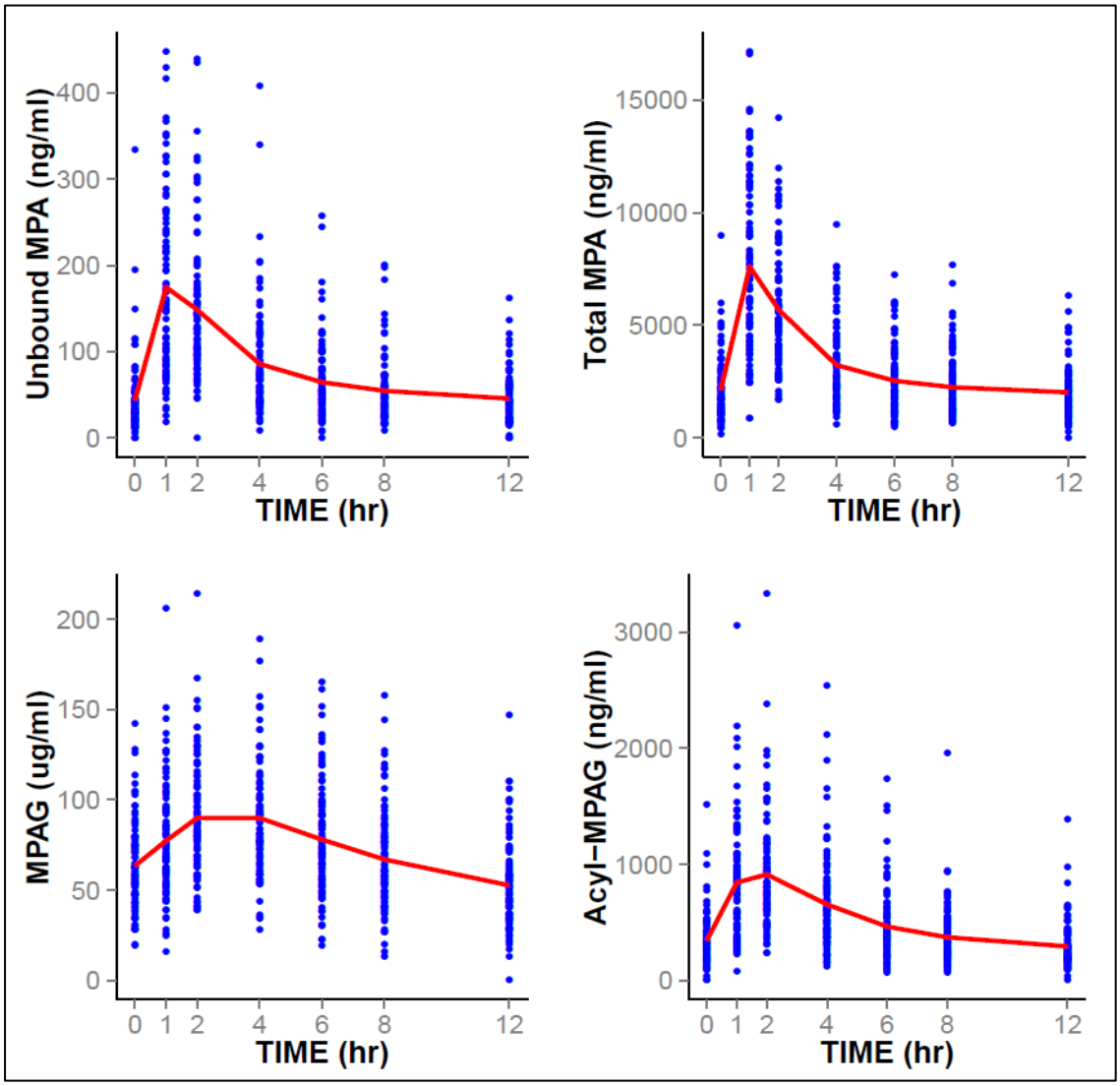

Note:
Points are the observed concentrations. Lines are the means of these concentrations.

Figure 4-3: Density Plot of Time to Pharmacokinetic Analysis

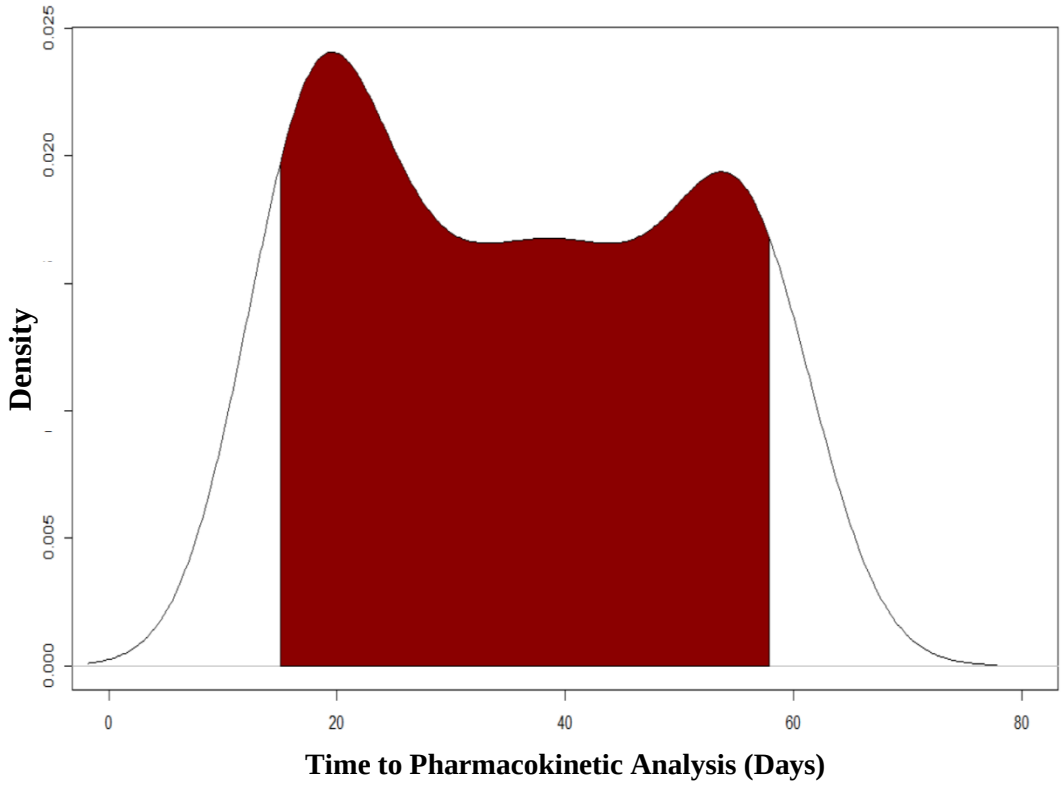

Note: Shaded area represents the 95% of the population around the mean (36 days). This area is demarcated by the 5th quantile and the 95th quantile, which correspond to 15 and 58 days to pharmacokinetic analysis, respectively.

Figure 4-4: Goodness of Fit Plots for Unbound MPA

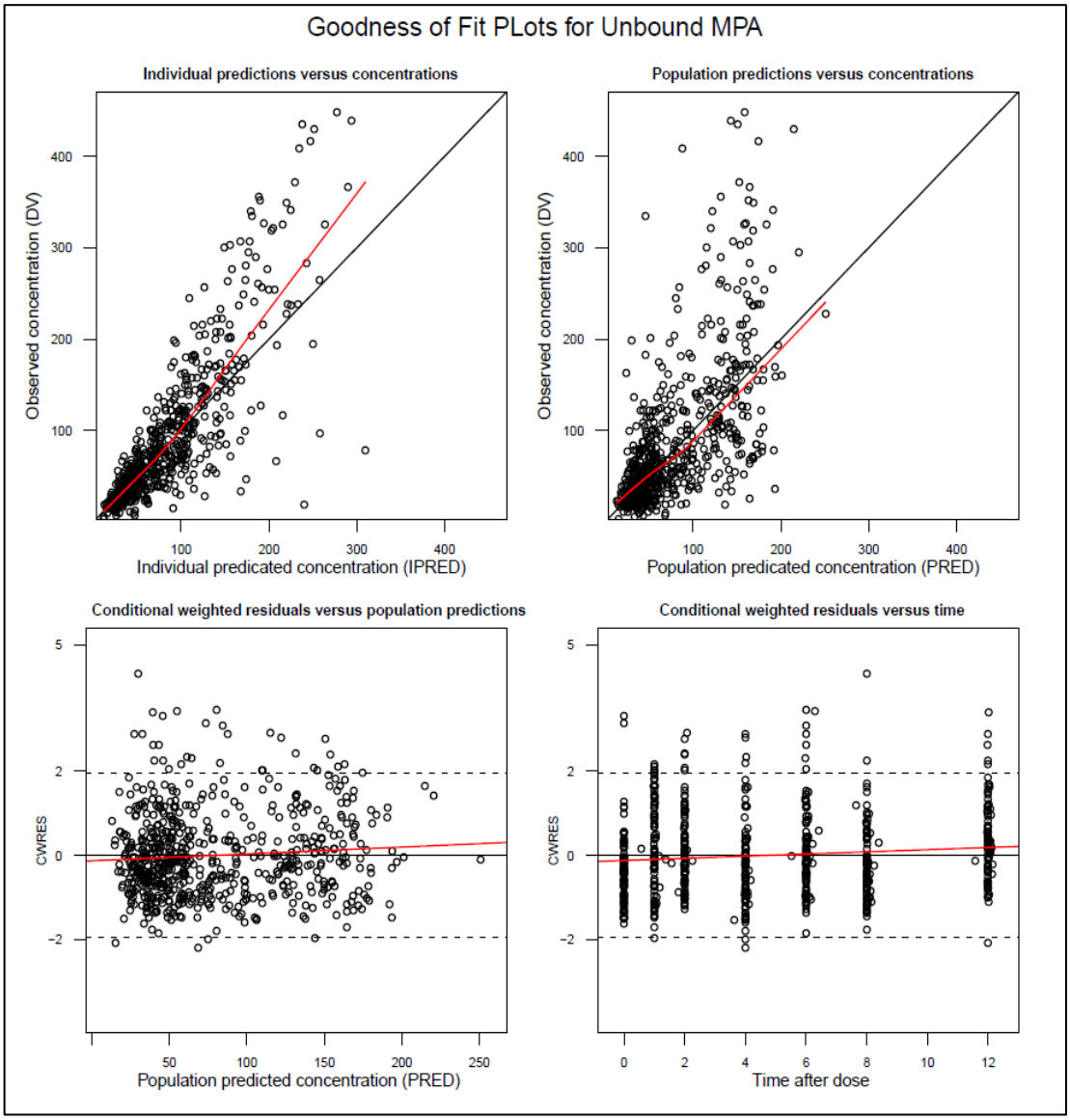

Note: Black lines represent the line of identity; Red lines represent loess smooth

Figure 4-5: Goodness of Fit Plots for Total MPA

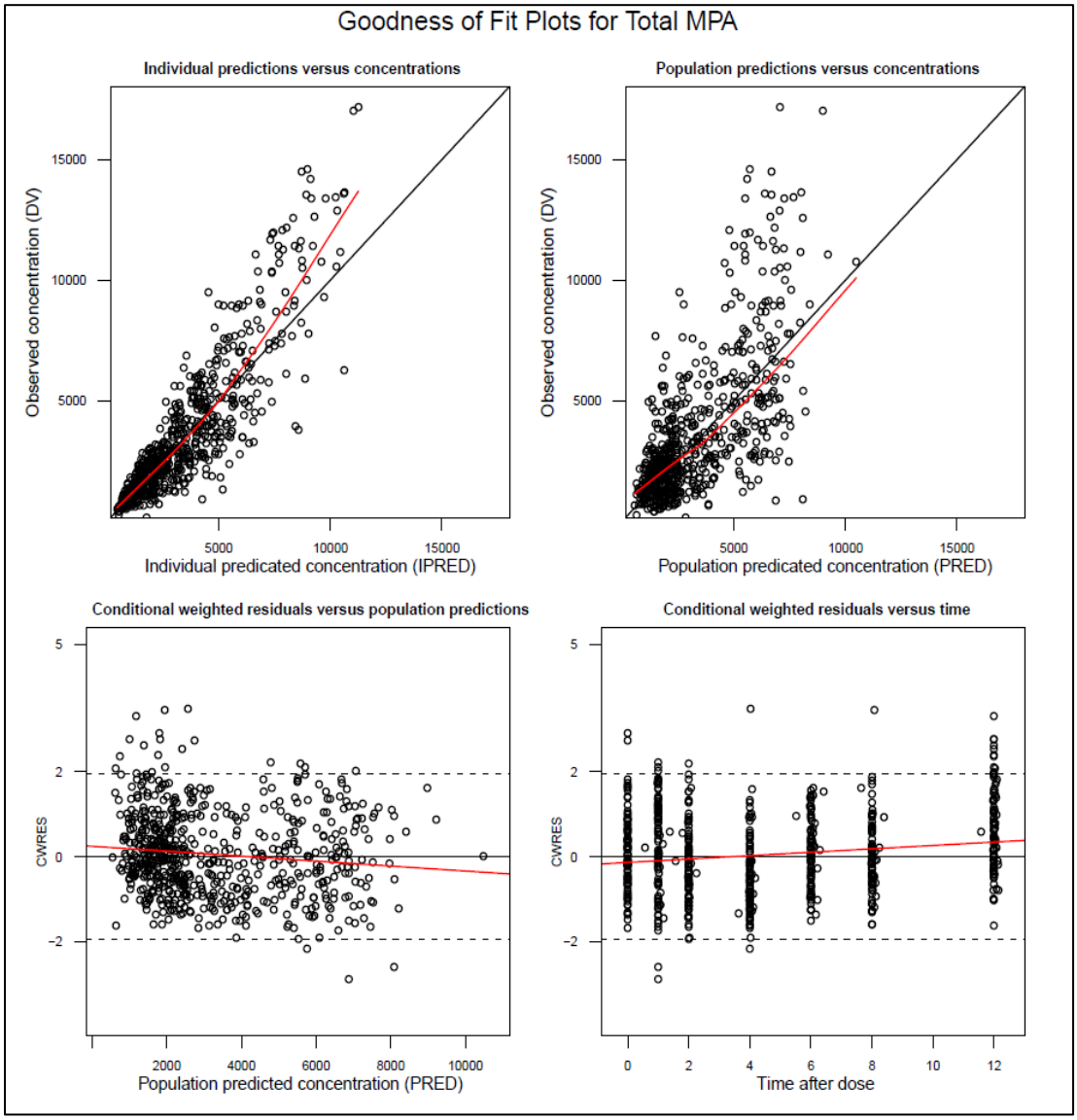

Note: Black lines represent the line of identity; Red lines represent loess smooth

Figure 4-6: Goodness of Fit Plots for MPAG

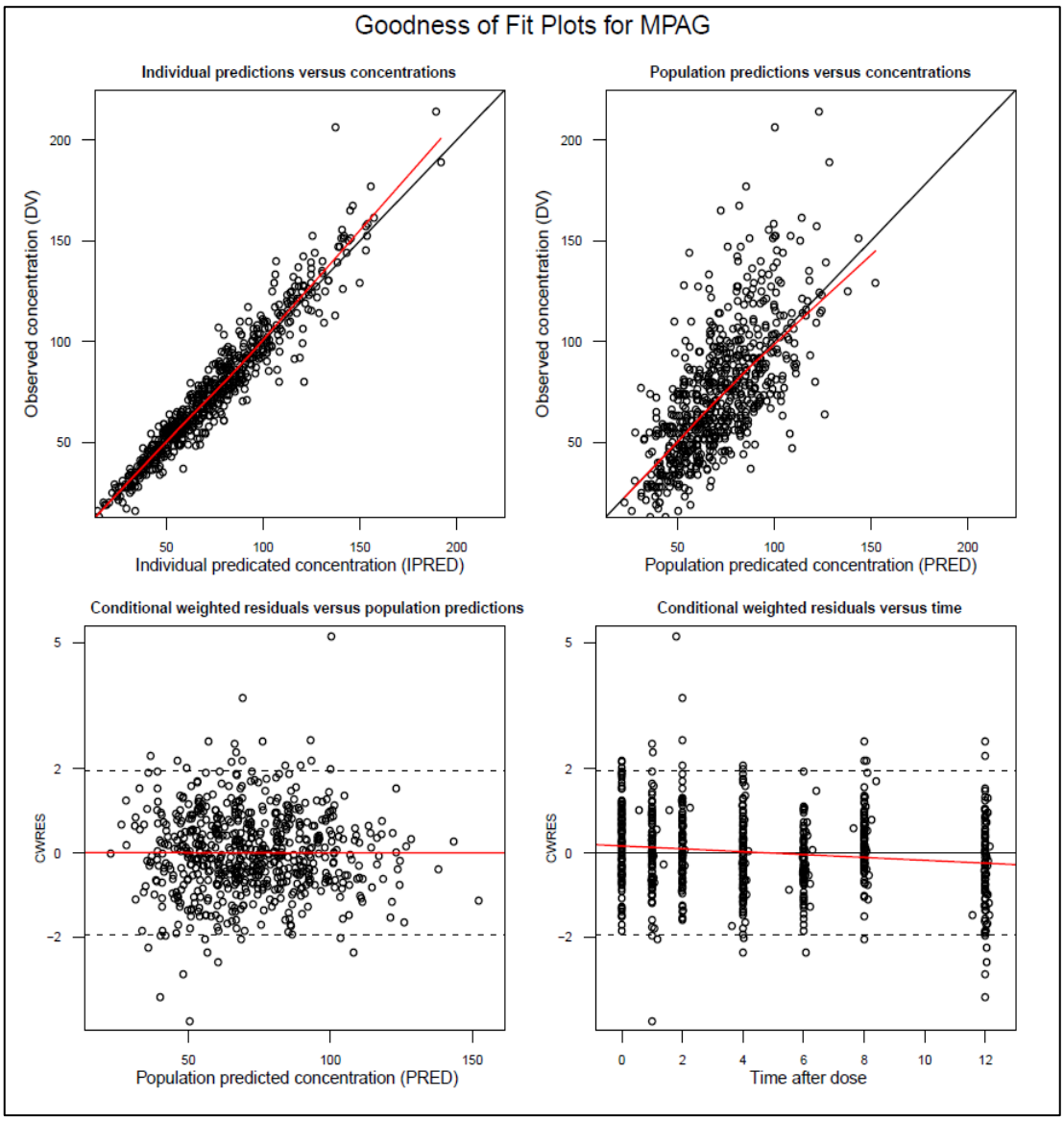

Note: Black lines represent the line of identity; Red lines represent loess smooth

Figure 4-7: Goodness of Fit Plots for acyl-MPAG

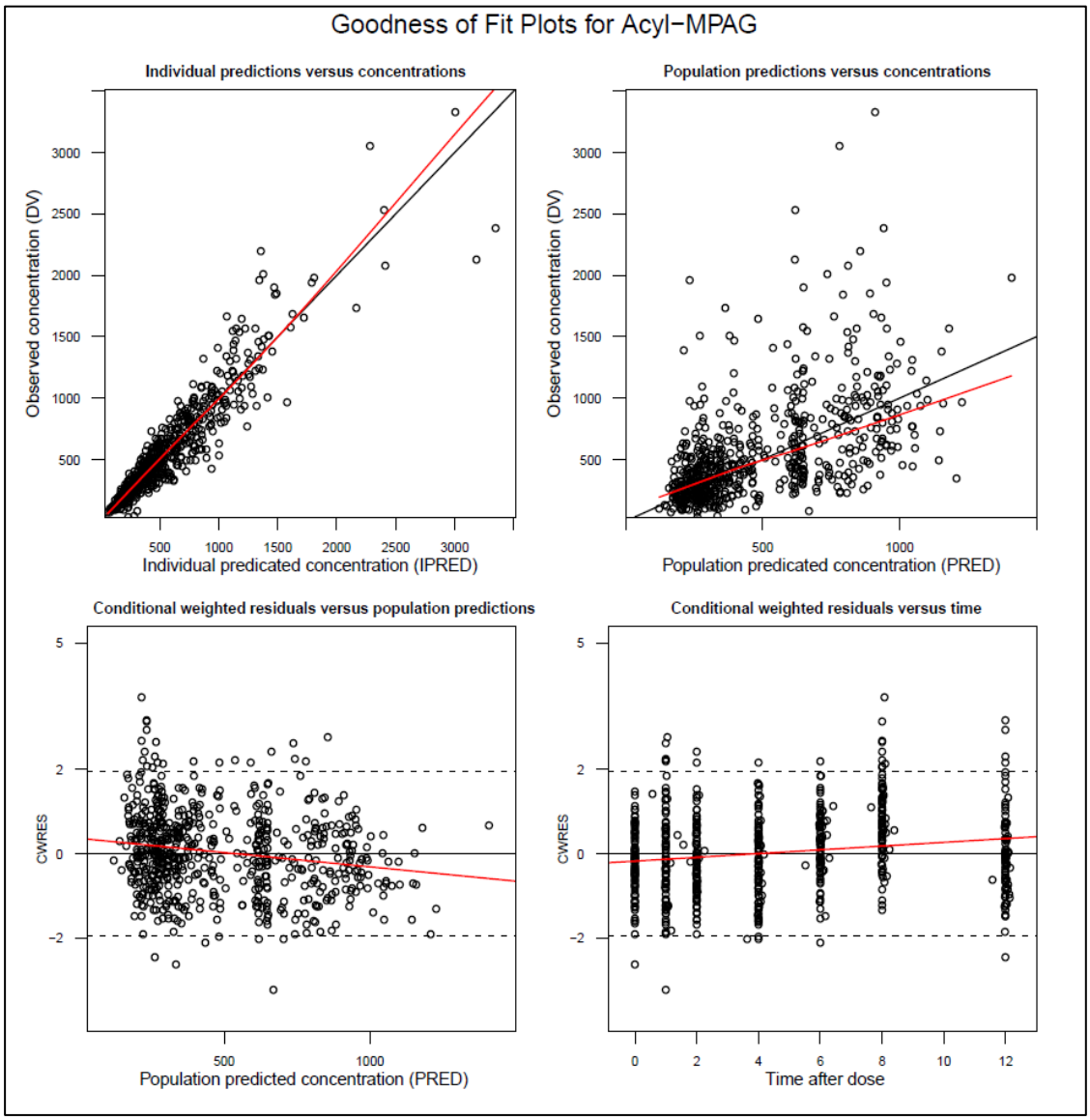

Note: Black lines represent the line of identity; Red lines represent loess smooth

Figure 4-8: Visual Predicative Check (VPC) Plots for Unbound MPA, Total MPA, MPAG, and Acyl-MPAG

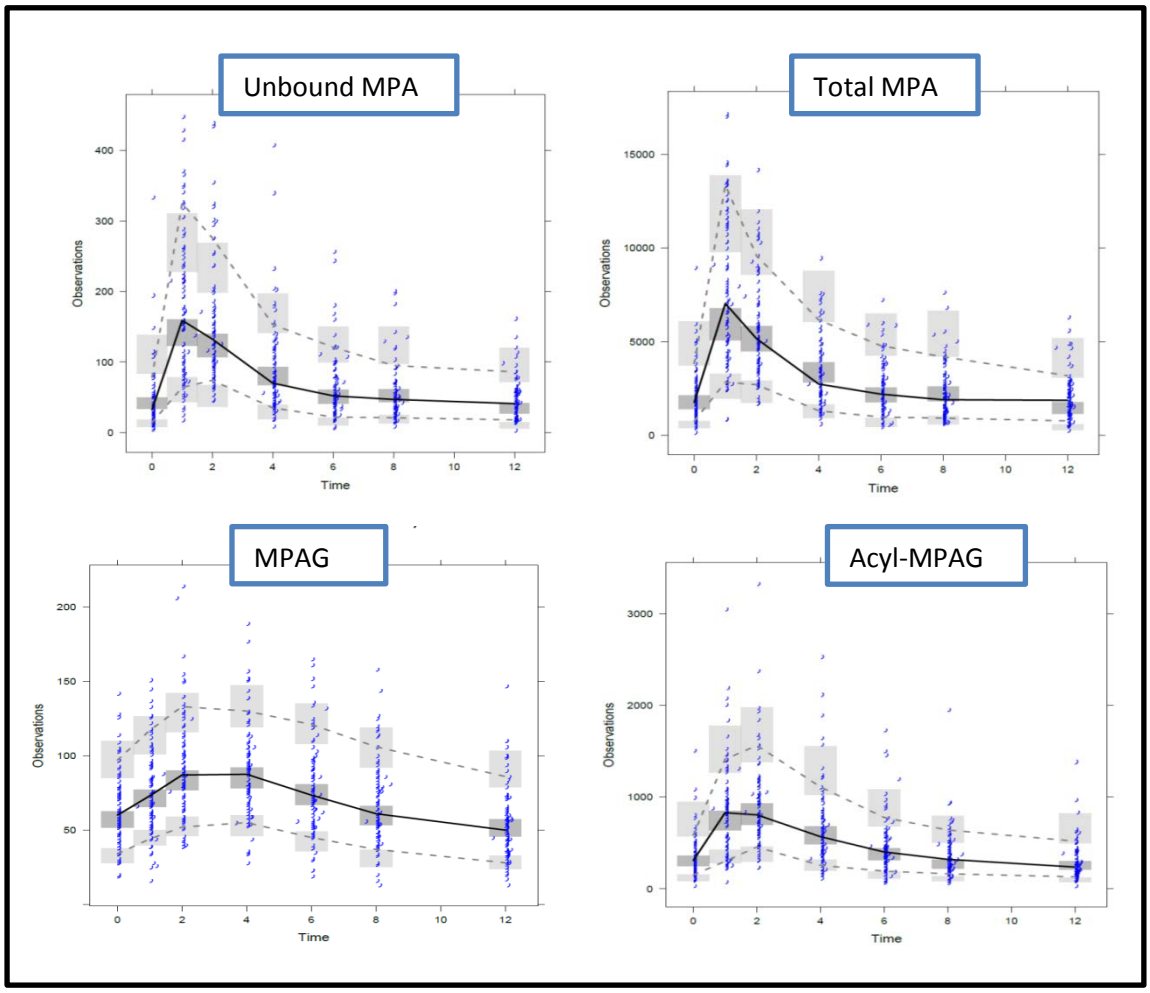

Note: Solid black lines represent the medians of the observed data; dashed black lines represent the 5th and 95th quantiles of the observed data; shaded areas represent the 95% prediction intervals for corresponding simulated data.

CHAPTER 5

5 EXPOSURE-RESPONSE MODELING OF MPA-ASSOCIATED EFFICACY AND TOXICITY IN KIDNEY TRANSPLANT RECIPIENTS

5.1 Introduction

MPA is an immunosuppressive drug used to prevent acute rejection; however, it is associated with several side effects. Extracted from *Penicillium brevicompactum* in 1969, MPA demonstrated strong antimitotic activity in mammalian cells, in addition to its antibacterial and antifungal activities (160). In the same year, it was shown that daily doses of MPA exhibit immunosuppressive effect on the antibody formation process in mice (161). In vitro studies demonstrated that MPA causes inhibition of antigen formation, lymphocyte adhesion, and cytotoxic T-cell generation (162, 163). In an animal study that was conducted on 33 canine renal transplants, MPA was found to significantly increase graft survival; however, gastrointestinal side effects including gastritis, diarrhea, and anorexia were observed (164). An early phase 1 trial included 48 human kidney transplants demonstrated MPA efficacy in reducing acute rejection; nevertheless, gastrointestinal and myelotoxicity side effects were also observed (165).

Results from all the above mentioned studies led to the conduct of 3 major phase III clinical trials with the purpose of evaluating the efficacy and safety of MPA in transplant patients (97, 119, 120). These studies demonstrated comparable results; the addition of MPA to the treatment regimen, compared to azathioprine or placebo, causes 50% reduction in rates of acute rejection resulting in an overall acute rejection cumulative incidence of 20%. These studies also demonstrated the association between MPA exposure and several side effects, most commonly gastrointestinal and leukopenia.

In the literature, several exposure metrics has been utilized to evaluate the association between MPA exposure and acute rejection and/or toxicities. Some of these

studies used the area under the curve for 12 hours (AUC_{12}) (144), others used the minimum concentration (Ctrough) (128), while other studies evaluated the maximum concentration (C_{max}) (64).

Most exposure-response studies were conducted considering total MPA, and there seems to be less understanding of the response relationship to unbound MPA and the active metabolite acyl-MPAG. Therefore, the objective of this analysis is to quantitatively evaluate the MPA exposure-response relationship by building a model that helps to describe the relationships between total MPA, unbound MPA and acyl-MPAG exposure variables and the probability of acute rejection and leukopenia.

5.2 Methods

In the current analysis, several exposure metrics were evaluated. These metrics were calculated from the three concentration-time profiles: total MPA, unbound MPA and acyl-MPAG. Additionally, dichotomization of the continuous exposure metrics was performed and resulted in categorized variables. Using logistic regression, both of the original continuous and dichotomized variables were univariately examined for their effect on the response variables acute rejection and leukopenia.

5.2.1 Pharmacokinetic Exposure Data

Blood concentrations were obtained from 92 individuals who were enrolled in the DeKAF study discussed in details in chapter 4. Briefly, subjects received prophylactic oral mycophenolate mofetil (MMF; Cellcept®) ranging between 500-1500 mg every 12 hours. Blood samples were collected from patients during the pharmacokinetic visit,

which occurred at least 48 hours after starting MMF dosing in which the concentrations were at steady state. Sampling times include pre-dose and 1, 2, 4, 6, 8, and 12 hours following the MMF dose. Total MPA, unbound MPA and acyl-MPAG concentrations were measured in each sample using an Agilent 1100 series HPLC system (Agilent Technologies, Wilmington, DE)

For each subject, exposure metrics were calculated for unbound MPA, total MPA and acyl-MPAG concentrations. These metrics were calculated using WinNonlin (Pharsight Corporation, CA, USA) and they included AUC at steady state between 0 and 12 hours (AUCss), the maximum concentration at steady state (Cssmax), and the minimum concentration at steady state (Cssmin).

5.2.2 Pharmacodynamic Response Data

Response variables evaluated in this analysis included acute rejection and leukopenia. Each of these two variables was coded using a binary system of [0] and [1]. The [0] value indicated that the individual did not develop the event, while the [1] value indicated that the patient had developed the event. For the acute rejection response variable, [0] meant that the patient did not develop acute rejection and [1] meant that the patient did. An individual leukopenia response variable of [0] meant that the patient did not have leukopenia while [1] meant the opposite.

5.2.3 Dichotomization of Exposure Metrics

Considering each response variable separately, each exposure metric was categorized into two groups, "*low*" and "*high*", using a cutoff point. The selection of the value for this cutoff point was done using Youden index in the R package

"*OptimalCutpoints*" (166, 167). Optimal cutoff points were determined for the AUCss, Css_{max}, Css_{min} exposure metrics for unbound MPA, total MPA, and Acyl-MPAG.

5.2.4 Logistic Regression

Logistic regression was conducted for each combination of the exposure metric and the response variable. Each exposure metric was regressed univariately, both in the continuous and the dichotomized forms, against acute rejection and leukopenia. The analysis of the continuous variable of each exposure metric was performed independently of the dichotomized variable.

The generalized linear model (GLM) was used in the logistic analysis. These models are defined by three components: the random component, the systematic component, and the link function. The random component defines the distribution of the outcome variable. The systematic component relates the exposure variable (x) to the intercept, i.e., $\boldsymbol{\alpha + \beta X}$. Lastly, the link function connects the random and systematic components.

When applied to the current logistic regression, GLM was used with a binomial distribution random component, and the logit canonical link was used as a link function throughout the whole analysis. A p value ≤0.05 was considered significant.

The general form of the GLM used in the analysis is described by the equation below:

$$\mathbf{logit}(\boldsymbol{\pi_i}) = \boldsymbol{\alpha} + \boldsymbol{\beta} * \boldsymbol{exposure_i}$$

where $\boldsymbol{\pi_i}$ is the probability of having the response event in subject *i*. i.e., $\boldsymbol{P(Y = 1)}$; the variable $\boldsymbol{exposure_i}$ represent the exposure metric in the i^{th} subject; the parameter $\boldsymbol{\alpha}$ represents the logit of the success probability (having the response) when the exposure metric is zero in the continuous exposure metric variable or *low* group in the dichotomized variable; the parameter $\boldsymbol{\beta}$ describes the linear relation between the exposure metric and the response variable.

The logistic analysis was done using the R function glm (168)**.** The R packages ggplot2 (169) and dplyr (170) were used for plotting and data manipulation.

5.3 Results

5.3.1 Pharmacokinetic and Pharmacodynamic Data

Summaries of the exposure data are presented in Table 5-1. The table includes the mean, median, standard deviation (SD) and range of values calculated for each exposure variable. Density plots of the exposure metrics of unbound MPA, total MPA, and acyl-MPAG, were created and can be seen in Figures 5-1, 5-2, 5-3. With respect to the pharmacodynamic response data, 16 patients developed acute rejection during the duration of the study, while leukopenia occurred in 9 patients only.

5.3.2 Dichotomization Analysis

Results of the dichotomization analysis can be seen in Table 5-2. Included in the table are the cutoff values for each exposure metric. Taking the acute rejection response as an example, the analysis identifies 37060 hr*ng/ml (37.06 hr*mg/L) as a cutoff point of the total MPA AUCss exposure metric. Patients with total MPA AUCss greater or equal than this cutoff point have a greater likelihood of experiencing acute rejection and

vice versa for patients with total MPA AUCss values lower than the cutoff point. Considering the other response, leukopenia, the total MPA AUCss cutoff value is defined at 44520 hr*ng/ml (44.52 hr*mg/L). Tables 5-3 and 5-4 are the contingency tables that show the number of patients in each category for acute rejection and Leukopenia, respectively.

5.3.3 Logistic Regression

The results of the univariate logistic regression analyses for all the exposure metrics against acute rejection and leukopenia are listed in Tables 5-5 and 5-6, respectively.

With respect to acute rejection, none of the exposure metrics was found to be significant at the specified p value. However, dichotomized Css_{min} of acyl- MPAG was marginally insignificant (p value=0.51). For this exposure metric, the $\boldsymbol{\beta}$ parameter estimate was 1.148, which represents the log odds that a patient will have acute rejection versus a patient not having acute rejection. Interpreted as an odds ratio, there is 215% increase in the odds of acute rejection with the *high* acyl- MPAG Css_{min} group, compared to the *low* group.

When considering the leukopenia response, no exposure metric except dichotomized Total MPA AUCss was found significant. Other metrics including continuous Total MPA Css_{min}, and dichotomized Unbound MPA AUCss showed trends of association, however not significant. The $\boldsymbol{\beta}$ parameter estimate for the dichotomized Total MPA AUCss was 1.48, meaning that the *high* Total MPA AUCss group is associated with larger logits of leukopenia than the *low* group. In terms of odds ratio,

there is around 340 % increase in the odds of leukopenia in the *high* Total MPA AUCss group, compared to the *low* group.

5.4 Discussion

The current analysis explored the relationship between the exposure metrics of unbound MPA, total MPA and acyl-MPAG and related outcomes including acute rejection and leukopenia. Evaluated exposure metrics included AUCss, Cssmax and Cssmin. These exposure metrics were also dichotomized and evaluated independently of their respective continuous variables. As response variables were binary, univariate logistic regression analyses were conducted on each combination of the exposure metric and response.

Results demonstrated the absence of significant relationship between acute rejection and any of the exposure metrics, neither in the continuous nor in the dichotomized variables. This result could be due to the confounded non-compartmental calculations of the exposure metrics as a result of enterohepatic circulation process observed with MPA (as demonstrated in chapter 2). Additionally, few acute rejection episodes (n=16) were observed during the study, and this could be hindering the logistic regression (171). Regardless, a trend of association was demonstrated between acute rejection and the dichotomized Cssmin of acyl-MPAG. Being in the *high* group of acyl-MPAG Cssmin (>251 ng/ml) showed a trend of higher odds of acute rejection in comparison to the *low* group. Acyl-MPAG Cssmin has been shown to be significantly

higher during acute rejection episodes (148). A possible explanation is related to the impairment of renal elimination of acyl-MPAG at the times of acute rejection.

The current analysis demonstrated the presence of significant association between leukopenia and dichotomized Total MPA AUCss; higher odds of leukopenia in the *high* Total MPA AUCss group (>43.99 mg/L • h^{-1}), when compared to the *low* group. Similar results were observed in a study conducted by Kuyper et al however at a different cutoff point of Total MPA AUCss, i.e., 60 mg/L • h^{-1} rather than 43.99 mg/L • h^{-1}(172).

It is common in clinical research to dichotomize patient-specific variables in order to simplify decision-making process. As an example, high blood pressure is usually defined as having ≥ 90 mm Hg diastolic blood pressure and/or ≥ 140 mm Hg diastolic blood pressure. Several examples can be also found in the drug development literature when it comes to utilizing dichotomization. For instance, in a phase 2 study that aimed to evaluate efficacy and safety of rilotumumab, the levels of MET[8] in patients were dichotomized into high versus low groups (173). Dichotomization is advantageous as it simplifies the results and makes the interpretation easier and more straightforward. Dichotomization is also helpful when dealing with crude exposure variables (high noise in the data) where it would be difficult to specify a particular model. This could be the reason why no association was observed in the continuous variables of the exposure metrics in the current analysis, while associations and trends were observed in the dichotomized variable.

[8] MET is a tyrosine kinase receptor

In conclusion, the current study suggests that Cssmin of acyl-MPAG could be a possible predictor of acute rejection, and Total MPA AUCss a possible predictor of leukopenia. Further studies that include larger number of patients should be conducted to evaluate these relationships.

Table 5-1: Summaries of Exposure Data (Pharmacokinetic Data)

Exposure variable	Mean	Standard Deviation (SD)	Median	Minimum value	Maximum value
Total MPA AUCss (hr*ng/ml)	38887.2	14330.5	37065.2	15678.7	74697.3
Total MPA Css_{max} (ng/ml)	8831.4	3269.4	8913	2452	17167
Total MPA Css_{min} (ng/ml)	2060	1177.6	1869	258	6334
Unbound MPA AUCss (hr*ng/ml)	946.5	408.2	884.3	296.6	2767.8
Unbound MPA Cssmax (ng/ml)	214.8	90.6	202	54	448
Unbound MPA Cssmin (ng/ml)	49.51	34.73	42	3	201
Acyl-MPAG AUCss (hr*ng/ml)	6227	3407.32	5680.1	1403.5	22677.5
Acyl-MPAG Cssmax (ng/ml)	1044.7	506.1	941	265	3329
Acyl-MPAG Cssmin (ng/ml)	300.9	206	241	31	1388

Table 5-2: Results of Dichotomization Analysis of MPA Exposure Metrics

Exposure Variable	Acute Rejection	Leukemia
Total MPA AUCss (hr*ng/ml)	20606.6	43993.2
Total MPA Css_{max} (ng/ml)	6503	5961
Total MPA Css_{min} (ng/ml)	2082	1765
Unbound MPA AUCss (hr*ng/ml)	423.3	778.3
Unbound MPA Css_{max} (ng/ml)	166	146
Unbound MPA Css_{min} (ng/ml)	62	32
Acyl-MPAG AUCss (hr*ng/ml)	4553.8	14142
Acyl-MPAG Css_{max} (ng/ml)	854	488
Acyl-MPAG Css_{min} (ng/ml)	251	170

Table 5-3: Contingency Table for Acute Rejection

Dichotomized Exposure Variable	Acute rejection (No/Yes)	Number of Patients in Exposure Variable Categories	
		Low	High
Total MPA AUCss	No	8	65
	Yes	0	16
Total MPA Cssmax	No	23	50
	Yes	3	13
Total MPA Cssmin	No	43	30
	Yes	6	10
Unbound MPA AUCss	No	4	69
	Yes	1	15
Unbound MPA Cssmax	No	25	48
	Yes	4	12
Unbound MPA Cssmin	No	59	14
	Yes	10	6
Acyl-MPAG AUCss	No	27	46
	Yes	3	13
Acyl-MPAG Cssmax	No	30	43
	Yes	6	10
Acyl-MPAG Cssmin	No	43	30
	Yes	5	11

Table 5-4: Contingency Table for Leukopenia

Dichotomized Exposure Variable	Leukopenia (No/Yes)	Number of Patients in Exposure Variable Categories	
		Low	High
Total MPA AUCss	No	55	25
	Yes	3	6
Total MPA Cssmax	No	19	61
	Yes	1	8
Total MPA Cssmin	No	41	39
	Yes	2	7
Unbound MPA AUCss	No	35	45
	Yes	1	8
Unbound MPA Cssmax	No	19	61
	Yes	1	8
Unbound MPA Cssmin	No	34	46
	Yes	1	8
Acyl-MPAG AUCss	No	77	3
	Yes	9	0
Acyl-MPAG Cssmax	No	7	73
	Yes	1	8
Acyl-MPAG Cssmin	No	18	62
	Yes	2	7

Table 5-5: Results of Univariate Regression Analyses on Acute Rejection

Exposure Metric	Variable	Intercept	Intercept SE	Slope	Slope SE	Intercept P value	Slope P value	Odds Ratio
Total MPA AUCss	Continuous	-1.354	0.799	-4.2E-6	1.9E-5	0.09	0.829	1
	Dichotomized	-17.566	1398.721	16.164	1398.7	0.990	0.991	1.05E+07
Total MPA Css_{max}	Continuous	-1.769	0.808	2.81E-5	8.4E-5	0.029	0.739	1
	Dichotomized	-2.037	0.614	0.690	0.688	0.001	0.316	1.99
Total MPA Css_{min}	Continuous	-2.277	0.577	3.4E-04	2.1E-4	8.04E-05	0.11	1
	Dichotomized	-1.969	0.436	0.871	0.569	6.21E-06	0.126	2.39
Unbound MPA AUCss	Continuous	-0.93	0.735	-0.001	0.001	0.206	0.404	1
	Dichotomized	-1.386	1.118	-0.140	1.154	0.215	0.904	0.87
Unbound MPA Css_{max}	Continuous	-1.229	0.713	-0.001	0.003	0.085	0.665	1.00
	Dichotomized	-1.833	0.539	0.446	0.628	0.001	0.477	1.56
Unbound MPA Css_{min}	Continuous	-1.765	0.481	0.005	0.007	2.44E-04	0.515	1.005
	Dichotomized	-1.775	0.342	0.928	0.596	2.1E-07	0.120	2.53
Acyl-MPAG AUCss	Continuous	-1.707	0.563	2.98E-5	7.6E-5	0.002	0.695	1
	Dichotomized	-2.197	0.609	0.934	0.685	0.000305	0.173	2.54
Acyl-MPAG Css_{max}	Continuous	-1.925	0.628	3.78E-4	0.001	0.002	0.458	1
	Dichotomized	-1.609	0.447	0.151	0.569	0.00032	0.791	1.16
Acyl-MPAG Css_{min}	Continuous	-1.797	0.479	0.001	0.001	1.75E-04	0.458	1
	Dichotomized	-2.152	0.472	***1.148***	0.589	5.26E-06	***0.051***	3.15

Table 5-6: Results of Univariate Regression Analyses on Leukopenia

Exposure Metric	Variable	Intercept	Intercept SE	Slope	Slope SE	Intercept P value	Slope P value	Odds Ratio
Total MPA AUCss	Continuous	-3.463	1.114	3.E-05	2.4E-5	0.002	0.199	1
	Dichotomized	-2.91	0.59	***1.48***	0.75	9.28E-7	***0.047***	4.40
Total MPA Cssmax	Continuous	-2.298	1.024	1.2E-5	1.0E-4	0.025	0.905	1
	Dichotomized	-2.94	1.03	0.91	1.09	4.10E-03	0.40	2.49
Total MPA Cssmin	Continuous	-3.337	0.758	4.9E-4	2.5E-04	1.08E-05	0.053	1.0005
	Dichotomized	-3.02	0.72	1.30	0.83	3.03E-05	0.12	3.68
Unbound MPA AUCss	Continuous	-3.176	0.873	0.001	0.001	2.74E-04	0.184	1.001
	Dichotomized	-3.56	1.01	1.83	1.08	4.56E-04	0.09	6.22
Unbound MPA Cssmax	Continuous	-2.426	0.915	0.001	0.004	0.008	0.772	1.001
	Dichotomized	-2.94	1.03	0.91	1.09	4.10E-03	0.40	2.49
Unbound MPA Cssmin	Continuous	-2.871	0.627	0.012	0.008	4.74E-06	0.138	1.012
	Dichotomized	-3.53	1.01	1.78	1.08	5.10E-04	0.101	5.91
Acyl-MPAG AUCss	Continuous	-1.592	0.846	-1.E-4	1.4E-4	0.06	0.467	1
	Dichotomized	-2.15	0.35	-15.42	2284	1.10E-09	0.99	2.01E-07
Acyl-MPAG Cssmax	Continuous	-1.168	0.896	-0.001	0.001	0.193	0.255	0.999
	Dichotomized	-1.95	1.07	-0.27	1.13	0.07	0.81	0.77
Acyl-MPAG Cssmin	Continuous	-1.988	0.653	-0.001	0.002	0.002	0.73	0.999
	Dichotomized	-2.20	0.75	0.02	0.85	3.20E-03	0.98	1.02

Figure 5-1: Density Plots of Exposure Metrics of Total MPA

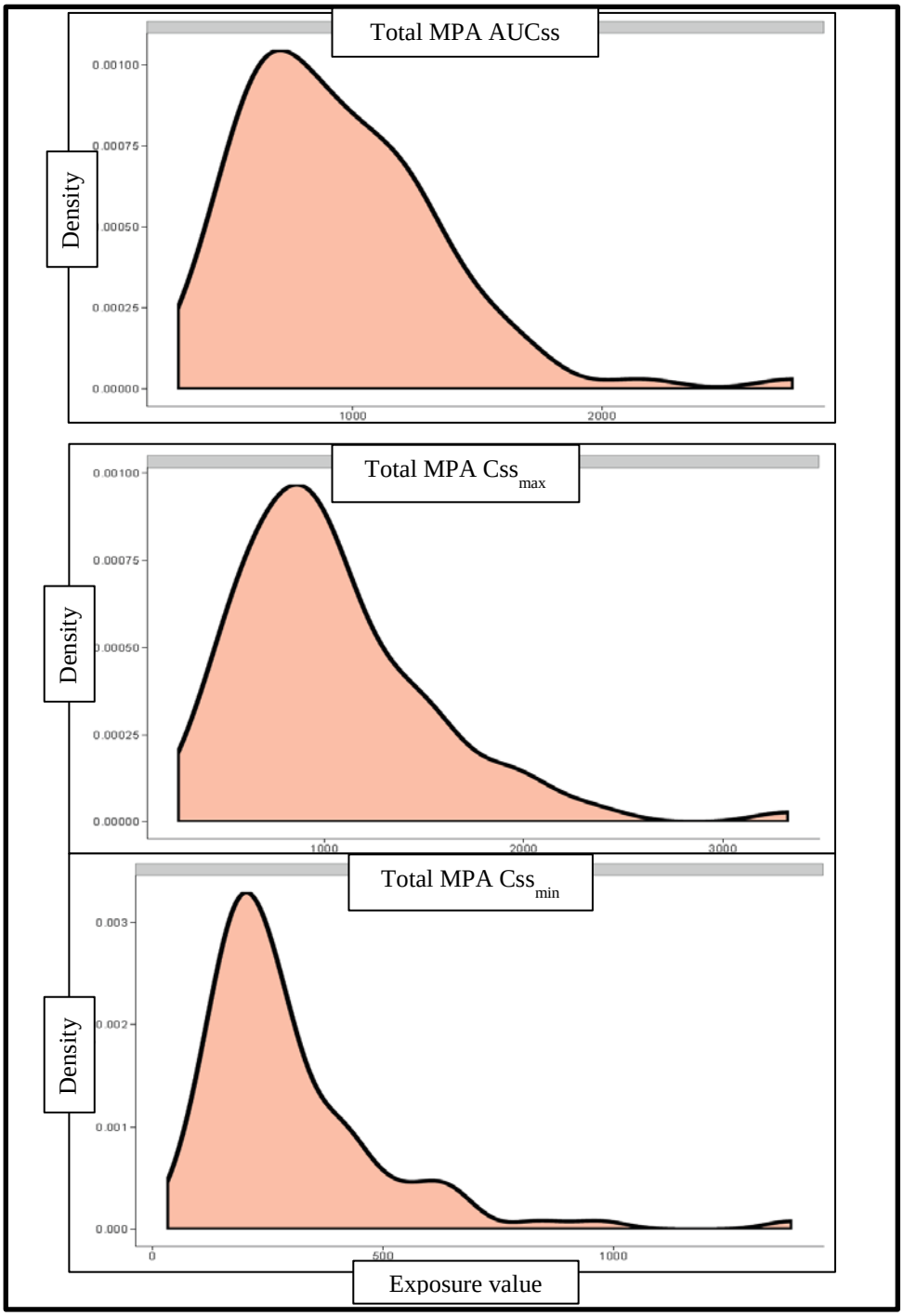

Figure 5-2: Density Plots of Exposure Metrics of Unbound MPA

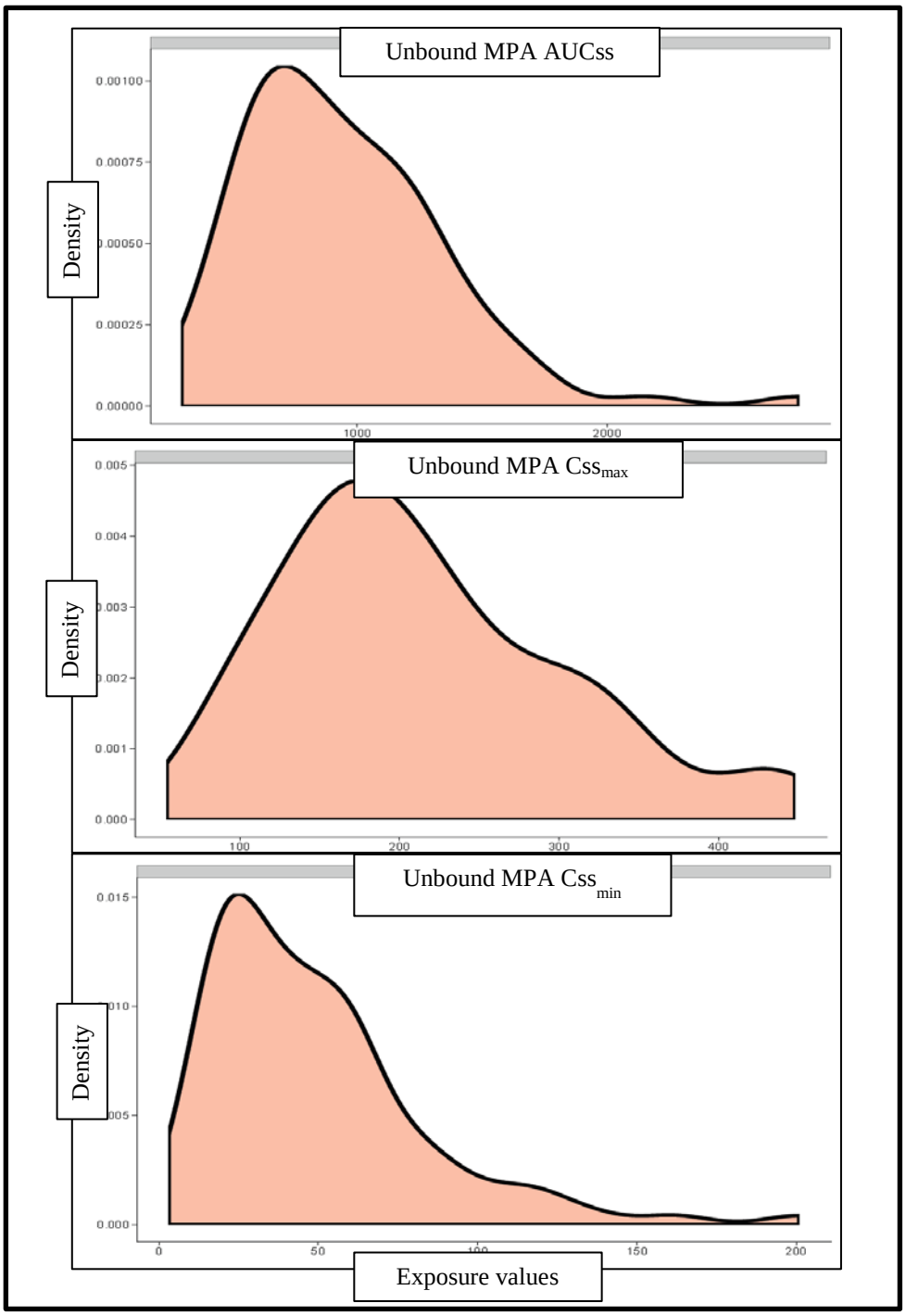

Figure 5-3: Density Plots of Exposure Metrics of Acyl-MPAG

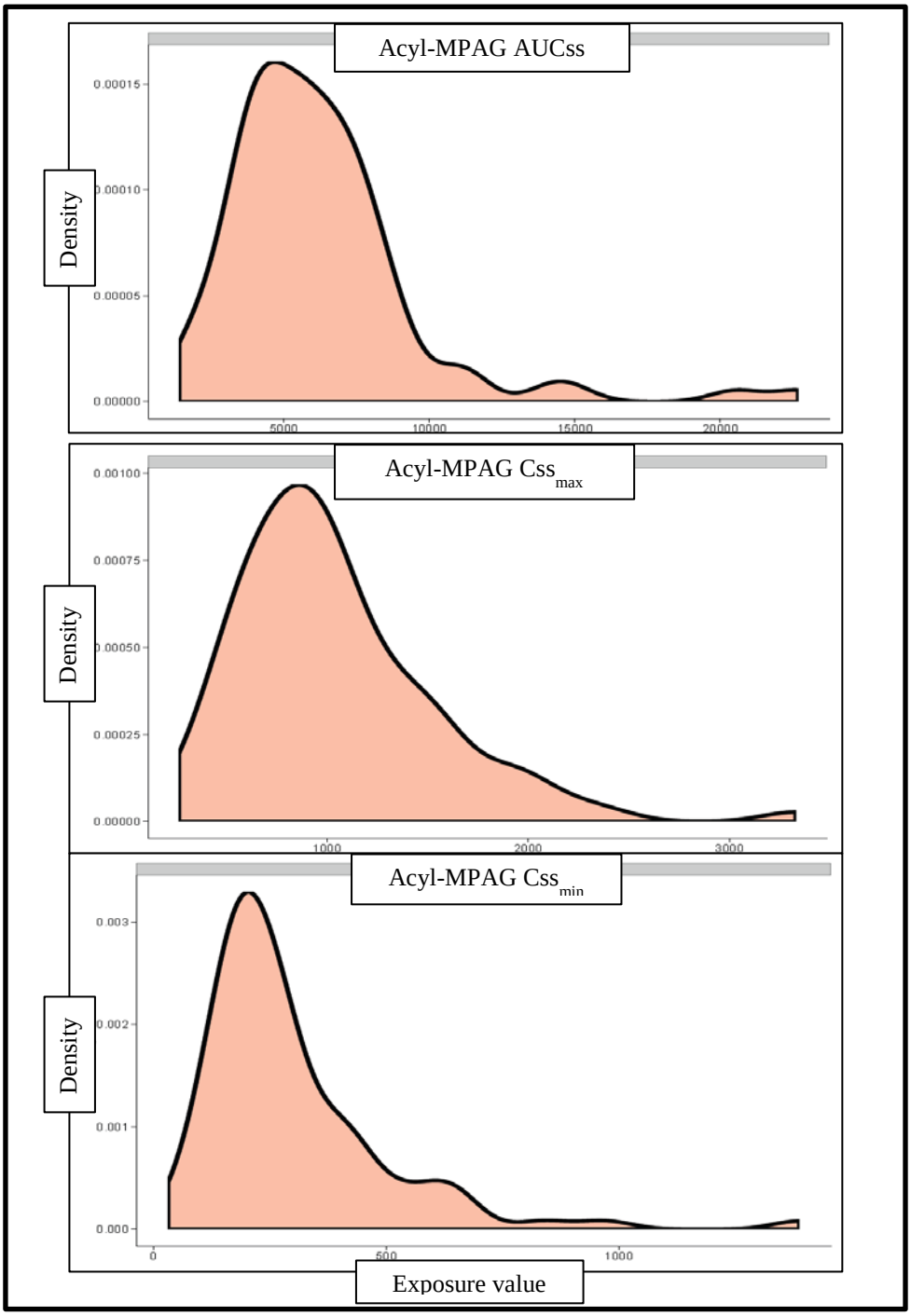

CHAPTER 6

RECAPITULATION

EHC is a complex process; however, it can be broken down into a set of sequential steps. From the hepatocytes, drugs are secreted into the biliary canals in unchanged and/or metabolized forms. Bile and accompanying drug is either stored in the gallbladder until it is ejected at mealtimes, or drained directly to the duodenum. During fasting, it is estimated that around 75% of bile gets to the gallbladder, while the remaining 25% skips the gallbladder and drains directly to the duodenum. The controlling factor in this process is related to the balance between the bile secretory pressure in the liver, the pressure in the cystic duct, and the pressure of the sphincter of Oddi. Upon meal intake, around 75% of bile stored in the gallbladder is secreted into the duodenum as the gallbladder contracts over a duration of 30 minutes. The gallbladder then relaxes and the sphincter of Oddi contracts causing the restart of the gallbladder bile storing cycle. In the intestine, secreted metabolites maybe converted back to the original drug (parent form) via intestinal flora. A fraction of the drug is then absorbed back into the portal circulation to the liver, while the remaining fraction is eliminated via feces. A percentage of the absorbed drug will then be conveyed into the systemic circulation, and the rest will undergo liver metabolism and/or subsequent biliary excretion, after which the EHC cycle repeats.

Several modeling strategies of intended to capture the EHC process have been implemented in the pharmacokinetic literature. Generally, these models were built based on the EHC-related observations of longer drug half-lives and the appearance of multiple secondary peaks. As described in **chapter 1**, the various modeling strategies were classified into simple two-compartment models, Tgap-based models and gallbladder-

based models. Simple two-compartment models were able to account for a longer half-life, but not the secondary peaks. Tgap-based models provided the ability to capture a single secondary peak; however, these models do not represent the physiology of EHC in humans and animals that have a gallbladder. Another disadvantage of Tgap-based models is their inability to account for multiple peaks subsequent to multiple meals. The gallbladder-based models included a specific gallbladder compartment and were classified based on the function used to model the bile release from the gallbladder. These classes are continuous release, single bolus release, switch function release, sigmoid function release, sine function release and other modeling strategies. Briefly, the continuous release models resemble the simple two compartments models, as they were able to account for longer half-life, but not the secondary peaks. Single bolus release models are similar to Tgap-based models as they were capable of predicting one secondary peak only; however, they are more physiologic than Tgap-based models as they included a gallbladder compartment. The third class, the switch function release, are a set of models that are capable of modeling multiple secondary peaks at irregular intervals. However, due to the discontinuous nature of a switch function these models may result in numerical difficulties in the optimization process. The sine function models are able to predict multiple secondary peaks, however these models are crucially disadvantaged as the sine function assumes a regular appearance of secondary peaks. This is not physiological as secondary peaks are related to mealtimes which could be irregular with respect to time, i.e., time periods between breakfast, lunch and dinner meals may not be exact. The sigmoid function models allow predicting multiple

secondary peak, and they have the advantage of being capable of modeling irregular mealtimes.

It is true that gallbladder-based models involve a physiological representation of EHC by incorporating the gallbladder into the model. However, these models were generally not built while considering the physiological aspects of the hepatobiliary system in relation to mealtimes, as previously described. Therefore, the core of this thesis was to build a gallbladder-based model that not only includes an additional gallbladder compartment, but also provide more physiological representation for the parameters and processes related to EHC.

The first project of this thesis (**chapter 2**) involved building the proposed model, followed by using the model to evaluate the effect of EHC on the pharmacokinetic profile and NCA calculations. The evaluation of the effect of EHC on the pharmacokinetic profile was done qualitatively where several parameters and exposure metrics were considered. The model was successful in predicting a longer apparent half-life and the appearance of multiple secondary peaks. It was also shown that the presence of EHC result in lowering the Cmax (primary peak) and the occurrence of earlier Tmax. The instantaneous half-life, which is a term we coined, was no longer constant as a result of EHC. The nature of EHC results in nonlinearity in the instantaneous half-life; therefore, no single value can be used to represent a terminal half-life. The effect of EHC on NCA was then tested by considering two sampling schemes, conventional and meal-directed. Results demonstrated that the presence of EHC causes biased NCA calculations, and that small differences in the sampling times can profoundly influence the NCA results.

After evaluating the effect of EHC on NCA results, we assessed the effect of EHC on compartmental modeling strategies (**chapter 3**). A SSE analysis was performed where several literature models were evaluated. The selection of these literature models was based on the fact these models were applied to drugs that are known to undergo EHC. Results from this analysis demonstrated the importance of using a gallbladder-based model where the number of modeled mealtimes is as close to the truth as possible. It was also shown that including a more physiological representation of the hepatobiliary parameters and processes result in less bias and imprecision of parameter estimates. In contrast, the use of non-gallbladder based models, like simple one-compartment or two-compartment models, introduces more bias and imprecision in the estimated parameters.

The proposed gallbladder-based model was then modified and applied to a simultaneous population pharmacokinetic analysis of steady-state unbound MPA, total MPA, MPAG and acyl-MPAG concentrations in kidney transplant recipients (**chapter 4**). Based on the pharmacology of the drug, a major modification of the model was the inclusion of the MPAG metabolite into the EHC model as the chemical entity that undergoes the EHC process. Additionally, the toggle nature of gallbladder emptying process was modelled using a double sigmoid function. This function was successfully implemented as it was able to provide predictions of secondary peaks of steady-state concentrations without causing numerical difficulties in the optimization process. A secondary objective of this project was to evaluate clinical characteristics and genotypes for their significance on the model. As the number of tested covariates was large, a multi-step covariate data reduction and modeling was developed and utilized to perform the

covariate analysis. The final model results were then used to create a dosing equation of MMF in kidney transplant recipients.

The last chapter of this thesis evaluated the exposure-response of MPA-associated efficacy and toxicity in kidney transplant recipients (**chapter 5**). An NCA was conducted on unbound MPA, total MPA, and acyl-MPAG concentrations to calculate and estimate the AUCss, Cssmax and Cssmin. These metrics were also dichotomized into bivariate categorical variables. Using logistic regression, both of the original continuous and dichotomized variables of the exposure metrics were univariately examined for their effect on the response variables of acute rejection and leukopenia. Results did not demonstrate any significant relationship between acute rejection and any of the exposure metrics, in neither the continuous nor the dichotomized variables. This result could be due to biased non-compartmental calculations of the exposure metrics as a result of EHC process observed with MPA. The current analysis demonstrated the presence of a significant association between leukopenia and dichotomized Total MPA AUCss.

The developed model provided the advantage of being more physiological than current available empirical models. Future studies may enhance the physiological representation by including a liver compartment. However, the current model was adequate in predicting the characteristics associated with EHC.

Clinical implications of the work presented can be summarized in several points. First, higher EHC% causes longer apparent half-life; therefore, and considering the presence of variability between patients in terms of EHC%, patients with longer apparent half-life will need longer interdosing interval to maintain the same level of exposure as

other patients with shorter apparent half-life. Such necessitation could be clinically important only if such variability in EHC% is significant and if the used pharmacokinetic metric depends on the duration of exposure, like AUC. Second, the presence of EHC causes biased NCA calculations especially at higher EHC%. Care should be taken when defining sampling times in studies of drugs that undergo EHC. There is a need for future studies that attempt to identify the best sampling strategies in the presence of EHC. However, it seems that time of meals is an important factor to consider when designing the studies. Third, the use of a gallbladder-based model, rather than simple non-EHC models, appears to be important when the drug EHC% is high (>40%) and therapeutic window is small. In the presence of small EHC%, evaluated compartmental modeling strategies seem to provide similar predictions. In the case of large therapeutic window, variations in the predictions from the different modeling strategies may not result in clinically significant differences, as long as these predictions fall within the therapeutic window. Lastly, the proposed EHC model was utilized for MPA data; however, it was built considering only the physiological aspects of EHC. No parameters related to the MPA drug were used in building the EHC part of the model; therefore, the proposed model is applicable to all drugs that undergo EHC, as long as the studied population sample are healthy subjects with normal EHC physiology.

REFERENCES

References

1. Roberts MS, Magnusson BM, Burczynski FJ, Weiss M. Enterohepatic circulation. Clinical pharmacokinetics. 2002;41(10):751-90.
2. Dobrinska M. Enterohepatic circulation of drugs. The Journal of Clinical Pharmacology. 1989;29(7):577-80.
3. Gao Y, Shao J, Jiang Z, Chen J, Gu S, Yu S, et al. Drug enterohepatic circulation and disposition: constituents of systems pharmacokinetics. Drug discovery today. 2014;19(3):326-40.
4. Adlercreutz H, Martin F, Järvenpää P, Fotsis T. Steroid absorption and enterohepatic recycling. Contraception. 1979;20(3):201-23.
5. Azezli AD, Bayraktaroglu T, Orhan Y. The use of konjac glucomannan to lower serum thyroid hormones in hyperthyroidism. Journal of the American College of Nutrition. 2007;26(6):663-8.
6. Clements M, Chalmers T, Fraser D. Enterohepatic circulation of vitamin D: a reappraisal of the hypothesis. The Lancet. 1984;323(8391):1376-9.
7. Steinberg SE, Campbell CL, Hillman RS. Kinetics of the normal folate enterohepatic cycle. Journal of Clinical Investigation. 1979;64(1):83.
8. Philipps AF, Dvorák B, Kling PJ, Grille JG, Koldovský O. Absorption of milk-borne insulin-like growth factor-I into portal blood of suckling rats. Journal of pediatric gastroenterology and nutrition. 2000;31(2):128-35.
9. DiBaise JK, Islam RS. Bile acids: an underrecognized and underappreciated cause of chronic diarrhea. Practical gastroenterology Nutrition issues in gastroenterology, Series. 2012;110.
10. Vijayvargiya P, Camilleri M, Shin A, Saenger A. Diagnostic Methods for Bile Acid Malabsorption in Clinical Practice. Clinical gastroenterology and hepatology : the official clinical practice journal of the American Gastroenterological Association. 2013;11(10):1232-9.
11. Illing HP. Xenobiotic Metabolism and Disposition: The design of studies on novel compounds. CRC press; 1989.
12. Jason K. Sicklick MDA, Yuman Fong. The Liver. In: Courtney M. Townsend Jr. RDB, B. Mark Evers, Kenneth L. Mattox, editor. Sabiston Textbook of Surgery. 19th ed2012. p. 1411-73.
13. http://www.liver.co.uk/surgical-anatomy-liver.html.
14. Bradley SE. ANESTHESIA AND THE LIVER*. Annals of the New York Academy of Sciences. 1970;170(1):1067.
15. McClusky DA, 3rd, Skandalakis LJ, Colborn GL, Skandalakis JE. Hepatic surgery and hepatic surgical anatomy: historical partners in progress. World journal of surgery. 1997;21(3):330-42.
16. Renz JF, Kinkhabwala M. Chapter 2 - Surgical Anatomy of the Liver. In: Klintmalm RWBBG, editor. Transplantation of the Liver (Third Edition). Philadelphia: W.B. Saunders; 2015. p. 23-39.

17. James Toouli MB. Anatomy and physiology of the biliary tree and gallbladder. In: Pierre-Alain Clavien JB, editor. Diseases of the Gallbladder and Bile Ducts: Diagnosis and Treatment, 2nd Edition: Wiley-Blackwell; 2006. p. 1-20.
18. Rutkauskas S, Gedrimas V, Pundzius J, Barauskas G, Basevicius A. Clinical and anatomical basis for the classification of the structural parts of liver. Medicina (Kaunas, Lithuania). 2006;42(2):98-106.
19. Rossi P, Baert AL, Ricci P, Broglia L. Portal Hypertension: Diagnostic Imaging and Imaging-Guided Therapy: Springer Berlin Heidelberg; 2012.
20. Phillip S. Mushlin SG. Hepatic Physiology and Pathophysiology. In: Miller RD, editor. Miller's anesthesia. 8th ed2015. p. 521-44.
21. Arey, Leslie B. Developmental anatomy. Philadelphia: W. B. Saunders Company, 1940. 612 p. $6.75. Science Education. 1941;25(2):111-.
22. Healey JE, Jr., Schroy PC. Anatomy of the biliary ducts within the human liver; analysis of the prevailing pattern of branchings and the major variations of the biliary ducts. AMA archives of surgery. 1953;66(5):599-616.
23. Lindner HH, Pena VA, Ruggeri RA. A clinical and anatomical study of anomalous terminations of the common bile duct into the duodenum. Annals of surgery. 1976;184(5):626-32.
24. Richard Drake AWV, Adam W. M. Mitchel. Gray's Anatomy for Students2005.
25. Wood M. Presidential address: Eponyms in biliary tract surgery. American journal of surgery. 1979;138(6):746-54.
26. Suriawinata AA TS. Liver. In: Mills SE, editor. Histology for Pathologists Lippincott Williams & Wilkins; 2012.
27. Krishna M. Microscopic anatomy of the liver. Clinical Liver Disease. 2013;2(S1):S4-S7.
28. Haschek WM, Rousseaux CG, Wallig MA. Haschek and Rousseaux's handbook of toxicologic pathology: Academic Press; 2013.
29. Ilett KF, Tee LB, Reeves PT, Minchin RF. Mebolism of drugs and other xenobiotics in the gut lumen and wall. Pharmacology & therapeutics. 1990;46(1):67-93.
30. Hall SD, Thummel KE, Watkins PB, Lown KS, Benet LZ, Paine MF, et al. Molecular and physical mechanisms of first-pass extraction. Drug Metabolism and Disposition. 1999;27(2):161-6.
31. Lecureur V, Courtois A, Payen L, Verhnet L, Guillouzo A, Fardel O. Expression and regulation of hepatic drug and bile acid transporters. Toxicology. 2000;153(1):203-19.
32. Kwon Y, Kamath AV, Morris ME. Inhibitors of P-glycoprotein-mediated daunomycin transport in rat liver canalicular membrane vesicles. Journal of pharmaceutical sciences. 1996;85(9):935-9.
33. Dawson P. Bile secretion and the enterohepatic circulation. Sleisenger and Fordtran’s Gastrointestinal and Liver Disease Philadelphia, PA: Saunders Elsevier Inc. 2010:1075-88.
34. Hohenester S, Maillette de Buy Wenniger L, Paulusma CC, van Vliet SJ, Jefferson DM, Oude Elferink RP, et al. A biliary HCO3− umbrella constitutes a

protective mechanism against bile acid-induced injury in human cholangiocytes. Hepatology. 2012;55(1):173-83.
35. Shaffer E. Review article: control of gall-bladder motor function. Alimentary pharmacology & therapeutics. 2000;14(s2):2-8.
36. Siddiqui AA. Overview of Biliary Function 2013 [updated November 2013]. Available from: https://www.merckmanuals.com/professional/hepatic-and-biliary-disorders/gallbladder-and-bile-duct-disorders/overview-of-biliary-function.
37. Clavien P-A, Baillie J. Diseases of the gallbladder and bile ducts: diagnosis and treatment: John Wiley & Sons; 2008.
38. Takahashi T, May D, Owyang C. Cholinergic dependence of gallbladder response to cholecystokinin in the guinea pig in vivo. American Journal of Physiology-Gastrointestinal and Liver Physiology. 1991;261(4):G565-G9.
39. Shaffer E, McOrmond P, Duggan H. Quantitative cholescintigraphy: assessment of gallbladder filling and emptying and duodenogastric reflux. Gastroenterology. 1980;79(5 Pt 1):899-906.
40. Fisher RS, Stelzer F, Rock E, Malmud LS. Abnormal gallbladder emptying in patients with gallstones. Digestive diseases and sciences. 1982;27(11):1019-24.
41. Parker R, Hirom P, Millburn P. Enterohepatic recycling of phenolphthalein, morphine, lysergic acid diethylamide (LSD) and diphenylacetic acid in the rat Hydrolysis of glucuronic acid conjugates in the gut lumen. Xenobiotica. 1980;10(9):689-703.
42. Drasar BS, Hill MJ. Human intestinal flora: Academic Press (London) Ltd., 24/28 Oval Road, London, NWI; 1974.
43. Lehr T, Staab A, Tillmann C, Trommeshauser D, Schaefer H-G, Kloft C. A Quantitative Enterohepatic Circulation Model. Clinical pharmacokinetics. 2009;48(8):529-42.
44. VREE TB, ANDRÉ J. Clinical consequences of the biphasic elimination kinetics for the diuretic effect of furosemide and its acyl glucuronide in humans. Journal of pharmacy and pharmacology. 1999;51(3):239-48.
45. Colburn WA. Pharmacokinetic and biopharmaceutic parameters during enterohepatic circulation of drugs. Journal of pharmaceutical sciences. 1982;71(1):131-3.
46. Shepard TA, Reuning RH, Aarons LJ. Estimation of area under the curve for drugs subject to enterohepatic cycling. Journal of pharmacokinetics and biopharmaceutics. 1985;13(6):589-608.
47. Pedersen PV, Miller R. Pharmacokinetics and bioavailability of cimetidine in humans. Journal of pharmaceutical sciences. 1980;69(4):394-8.
48. Miller R. Pharmacokinetics and bioavailability of ranitidine in humans. Journal of pharmaceutical sciences. 1984;73(10):1376-9.
49. Ichikawa T, Ishida S, Sakiya Y, Sawada Y, Hanano M. Biliary excretion and enterohepatic cycling of glycyrrhizin in rats. Journal of pharmaceutical sciences. 1986;75(7):672-5.
50. Shepard TA, Reuning RH, Aarons LJ. Interpretation of area under the curve measurements for drugs subject to enterohepatic cycling. Journal of pharmaceutical sciences. 1985;74(2):227-8.

51. Harrison LI, Gibaldi M. Influence of cholestasis on drug elimination: Pharmacokinetics. Journal of pharmaceutical sciences. 1976;65(9):1346-8.
52. Chen HSG, Gross JF. Pharmacokinetics of drugs subject to enterohepatic circulation. Journal of pharmaceutical sciences. 1979;68(6):792-4.
53. Huckle KR, Chipman JK, Hutson DH, Millburn P. Metabolism of 3-phenoxybenzoic acid and the enterohepatorenal disposition of its metabolites in the rat. Drug metabolism and disposition: the biological fate of chemicals. 1981;9(4):360-8.
54. Xiong H, Turner KC, Ward ES, Jansen PL, Brouwer KL. Altered hepatobiliary disposition of acetaminophen glucuronide in isolated perfused livers from multidrug resistance-associated protein 2-deficient TR− rats. Journal of Pharmacology and Experimental Therapeutics. 2000;295(2):512-8.
55. Siegers C-P, Mackenroth T, Wächter S, Younes M. Effects of liver injury and cholestasis on microsomal enzyme activities and metabolism of halothane, enflurane and methoxyflurane in vivo in rats. Xenobiotica. 1981;11(5):293-9.
56. Reichen J, Hoilien C, Le M, Jones RH. Decreased uptake of taurocholate and ouabain by hepatocytes isolated from cirrhotic rat liver. Hepatology. 1987;7(1):67-70.
57. Dumaswala R, Berkowitz D, Setchell KD, Heubi JE. Effect of fasting on the enterohepatic circulation of bile acids in rats. The American journal of physiology. 1994;267(5 Pt 1):G836-42.
58. Soloway RD, Schoenfield LJ. Effects of meals and interruption of enterohepatic circulation on flow, lipid composition, and cholesterol saturation of bile in man after cholecystectomy. The American journal of digestive diseases. 1975;20(2):99-109.
59. Hepner GW, Demers LM. Dynamics of the enterohepatic circulation of the glycine conjugates of cholic, chenodeoxycholic, deoxycholic, and sulfolithocholic acid in man. Gastroenterology. 1977;72(3):499-501.
60. Steimer JL, Plusquellec Y, Guillaume A, Boisvieux JF. A time-lag model for pharmacokinetics of drugs subject to enterohepatic circulation. Journal of pharmaceutical sciences. 1982;71(3):297-302.
61. Colburn WA, Hirom P, Parker RJ, Milburn P. A pharmacokinetic model for enterohepatic recirculation in the rat: phenolphthalein, a model drug. Drug Metabolism and Disposition. 1979;7(2):100-2.
62. Pedersen PV, Miller R. Pharmacokinetics of doxycycline reabsorption. Journal of pharmaceutical sciences. 1980;69(2):204-7.
63. FUNAKI T. Enterohepatic circulation model for population pharmacokinetic analysis. Journal of pharmacy and pharmacology. 1999;51(10):1143-8.
64. Bullingham RE, Nicholls AJ, Kamm BR. Clinical pharmacokinetics of mycophenolate mofetil. Clinical pharmacokinetics. 1998;34(6):429-55.
65. Strandgården K, Höglund P, Grönquist L, Svensson L, Olov Gunnarsson P. Absorption and disposition including enterohepatic circulation of (14C) roquinimex after oral administration to healthy volunteers. Biopharmaceutics & drug disposition. 2000;21(2):53-67.
66. Ide T, Sasaki T, Maeda K, Higuchi S, Sugiyama Y, Ieiri I. Quantitative population pharmacokinetic analysis of pravastatin using an enterohepatic circulation

model combined with pharmacogenomic Information on SLCO1B1 and ABCC2 polymorphisms. The Journal of Clinical Pharmacology. 2009;49(11):1309-17.
67. Jiao Z, Ding Jj, Shen J, Liang Hq, Zhong Lj, Wang Y, et al. Population pharmacokinetic modelling for enterohepatic circulation of mycophenolic acid in healthy Chinese and the influence of polymorphisms in UGT1A9. British journal of clinical pharmacology. 2008;65(6):893-907.
68. Sam WJ, Akhlaghi F, Rosenbaum SE. Population pharmacokinetics of mycophenolic acid and its 2 glucuronidated metabolites in kidney transplant recipients. The Journal of Clinical Pharmacology. 2009;49(2):185-95.
69. de Winter BC, van Gelder T, Sombogaard F, Shaw LM, van Hest RM, Mathot RA. Pharmacokinetic role of protein binding of mycophenolic acid and its glucuronide metabolite in renal transplant recipients. Journal of pharmacokinetics and pharmacodynamics. 2009;36(6):541-64.
70. Yau WP, Vathsala A, Lou HX, Zhou S, Chan E. Mechanism-Based Enterohepatic Circulation Model of Mycophenolic Acid and Its Glucuronide Metabolite: Assessment of Impact of Cyclosporine Dose in Asian Renal Transplant Patients. The Journal of Clinical Pharmacology. 2009;49(6):684-99.
71. Berg AK, Mandrekar SJ, Ziegler KLA, Carlson EC, Szabo E, Ames MM, et al. Population pharmacokinetic model for cancer chemoprevention with sulindac in healthy subjects. The Journal of Clinical Pharmacology. 2013;53(4):403-12.
72. Rosner GL, Panetta J, Innocenti F, Ratain M. Pharmacogenetic pathway analysis of irinotecan. Clinical Pharmacology & Therapeutics. 2008;84(3):393-402.
73. Plusquellec Y, Houin G. Drug recirculation model with multiple cycles occurring at unequal time intervals. Journal of biomedical engineering. 1992;14(6):521-6.
74. Jain L, Woo S, Gardner ER, Dahut WL, Kohn EC, Kummar S, et al. Population pharmacokinetic analysis of sorafenib in patients with solid tumours. British journal of clinical pharmacology. 2011;72(2):294-305.
75. Wajima T, Yano Y, Oguma T. A pharmacokinetic model for analysis of drug disposition profiles undergoing enterohepatic circulation. Journal of pharmacy and pharmacology. 2002;54(7):929-34.
76. Huntjens D, Strougo A, Chain A, Metcalf A, Summerfield S, Spalding D, et al. Population pharmacokinetic modelling of the enterohepatic recirculation of diclofenac and rofecoxib in rats. British journal of pharmacology. 2008;153(5):1072-84.
77. Vane JR. Inhibition of prostaglandin synthesis as a mechanism of action for aspirin-like drugs. Nature: New biology. 1971(231):232-5.
78. Fuchs W, von Nieciecki A, Molz K, Popescu G, Weil A, Barkworth M, et al. [The effect of bile secretion on the pharmacokinetics of a theophylline sustained-release preparation]. Arzneimittel-Forschung. 1998;48(5A):597-604.
79. Ezzet F, Krishna G, Wexler DB, Statkevich P, Kosoglou T, Batra VK. A population pharmacokinetic model that describes multiple peaks due to enterohepatic recirculation of ezetimibe. Clinical therapeutics. 2001;23(6):871-85.
80. Younis IR, Malone S, Friedman HS, Schaaf LJ, Petros WP. Enterohepatic recirculation model of irinotecan (CPT-11) and metabolite pharmacokinetics in patients with glioma. Cancer chemotherapy and pharmacology. 2009;63(3):517-24.

81. Ibarra M, Vázquez M, Fagiolino P. Population pharmacokinetic model to analyze nevirapine multiple-peaks profile after a single oral dose. Journal of pharmacokinetics and pharmacodynamics. 2014;41(4):363-73.
82. Kim TH, Shin S, Landersdorfer CB, Chi YH, Paik SH, Myung J, et al. Population Pharmacokinetic Modeling of the Enterohepatic Recirculation of Fimasartan in Rats, Dogs, and Humans. The AAPS journal. 2015:1-14.
83. Plusquellec Y, Bousquet L. Time-delay for two-compartment models used for study of enterohepatic circulation of drugs. Biomedical Engineering, IEEE Transactions on. 1984(6):469-72.
84. Stella 9ed: http://www.iseesystems.com/.
85. McNaught AD, McNaught AD. Compendium of chemical terminology: Blackwell Science Oxford; 1997.
86. CellCept (Mycophenolate mofetil) [package insert]. Hofmann-La Roche B, Switzerland.
87. Shum B, Duffull S, Taylor P, Tett S. Population pharmacokinetic analysis of mycophenolic acid in renal transplant recipients following oral administration of mycophenolate mofetil. British journal of clinical pharmacology. 2003;56(2):188-97.
88. Sherwin CM, Sagcal-Gironella ACP, Fukuda T, Brunner HI, Vinks AA. Development of population PK model with enterohepatic circulation for mycophenolic acid in patients with childhood-onset systemic lupus erythematosus. British journal of clinical pharmacology. 2012;73(5):727-40.
89. Colom H, Lloberas N, Andreu F, Caldés A, Torras J, Oppenheimer F, et al. Pharmacokinetic modeling of enterohepatic circulation of mycophenolic acid in renal transplant recipients. Kidney international. 2014;85(6):1434-43.
90. Li H, Mager D, Sandmaier B, Maloney D, Bemer M, McCune J. Population pharmacokinetics and dose optimization of mycophenolic acid in HCT recipients receiving oral mycophenolate mofetil. The Journal of Clinical Pharmacology. 2013;53(4):393-402.
91. Frymoyer A, Verotta D, Jacobson P, Long-Boyle J. Population pharmacokinetics of unbound mycophenolic acid in adult allogeneic haematopoietic cell transplantation: effect of pharmacogenetic factors. British journal of clinical pharmacology. 2013;75(2):463-75.
92. Barau C, Furlan V, Debray D, Taburet AM, Barrail-Tran A. Population pharmacokinetics of mycophenolic acid and dose optimization with limited sampling strategy in liver transplant children. British journal of clinical pharmacology. 2012;74(3):515-24.
93. Zhao W, Fakhoury M, Deschenes G, Roussey G, Brochard K, Niaudet P, et al. Population pharmacokinetics and pharmacogenetics of mycophenolic acid following administration of mycophenolate mofetil in de novo pediatric renal-transplant patients. Journal of clinical pharmacology. 2010;50(11):1280-91.
94. Sherwin CM, Fukuda T, Brunner HI, Goebel J, Vinks AA. The evolution of population pharmacokinetic models to describe the enterohepatic recycling of mycophenolic acid in solid organ transplantation and autoimmune disease. Clinical pharmacokinetics. 2011;50(1):1-24.

95. Dong M, Fukuda T, Vinks AA. Optimization of mycophenolic acid therapy using clinical pharmacometrics. Drug metabolism and pharmacokinetics. 2014;29(1):4-11.
96. Lindbom L, Ribbing J, Jonsson EN. Perl-speaks-NONMEM (PsN)—a Perl module for NONMEM related programming. Computer methods and programs in biomedicine. 2004;75(2):85-94.
97. Sollinger HW. Mycophenolate mofetil for the prevention of acute rejection in primary cadaveric renal allograft recipients. U.S. Renal Transplant Mycophenolate Mofetil Study Group. Transplantation. 1995;60(3):225-32.
98. Magee CC, Pascual M. Update in renal transplantation. Archives of internal medicine. 2004;164(13):1373-88.
99. Kaufman DB, Shapiro R, Lucey MR, Cherikh WS, R TB, Dyke DB. Immunosuppression: practice and trends. American journal of transplantation : official journal of the American Society of Transplantation and the American Society of Transplant Surgeons. 2004;4 Suppl 9:38-53.
100. Matas AJ, Smith JM, Skeans MA, Thompson B, Gustafson SK, Schnitzler MA, et al. OPTN/SRTR 2012 Annual Data Report: kidney. American journal of transplantation : official journal of the American Society of Transplantation and the American Society of Transplant Surgeons. 2014;14 Suppl 1:11-44.
101. Staatz CE, Tett SE. Pharmacology and toxicology of mycophenolate in organ transplant recipients: an update. Arch Toxicol. 2014;88(7):1351-89.
102. Allison AC, Eugui EM. The design and development of an immunosuppressive drug, mycophenolate mofetil. Springer Semin Immunopathol. 1993;14(4):353-80.
103. Allison AC. Mechanisms of action of mycophenolate mofetil. Lupus. 2005;14 Suppl 1:s2-8.
104. Bullingham RE, Nicholls AJ, Kamm BR. Clinical pharmacokinetics of mycophenolate mofetil. Clinical pharmacokinetics. 1998;34(6):429-55.
105. Braun KP, Glander P, Hambach P, Bohler T, Waiser J, Mai I, et al. Pharmacokinetics and pharmacodynamics of mycophenolate mofetil under oral and intravenous therapy. Transplantation proceedings. 2002;34(5):1745-7.
106. Pescovitz MD, Conti D, Dunn J, Gonwa T, Halloran P, Sollinger H, et al. Intravenous mycophenolate mofetil: safety, tolerability, and pharmacokinetics. Clinical transplantation. 2000;14(3):179-88.
107. Staatz CE, Tett SE. Clinical pharmacokinetics and pharmacodynamics of mycophenolate in solid organ transplant recipients. Clinical pharmacokinetics. 2007;46(1):13-58.
108. Langman LJ, LeGatt DF, Yatscoff RW. Blood distribution of mycophenolic acid. Therapeutic drug monitoring. 1994;16(6):602-7.
109. Nowak I, Shaw LM. Mycophenolic acid binding to human serum albumin: characterization and relation to pharmacodynamics. Clinical chemistry. 1995;41(7):1011-7.
110. Schutz E, Shipkova M, Armstrong VW, Wieland E, Oellerich M. Identification of a pharmacologically active metabolite of mycophenolic acid in plasma of transplant recipients treated with mycophenolate mofetil. Clinical chemistry. 1999;45(3):419-22.

111. Shipkova M, Armstrong VW, Wieland E, Niedmann PD, Schutz E, Brenner-Weiss G, et al. Identification of glucoside and carboxyl-linked glucuronide conjugates of mycophenolic acid in plasma of transplant recipients treated with mycophenolate mofetil. British journal of pharmacology. 1999;126(5):1075-82.
112. Picard N, Ratanasavanh D, Premaud A, Le Meur Y, Marquet P. Identification of the UDP-glucuronosyltransferase isoforms involved in mycophenolic acid phase II metabolism. Drug metabolism and disposition: the biological fate of chemicals. 2005;33(1):139-46.
113. Bernard O, Guillemette C. The main role of UGT1A9 in the hepatic metabolism of mycophenolic acid and the effects of naturally occurring variants. Drug metabolism and disposition: the biological fate of chemicals. 2004;32(8):775-8.
114. Dupuis R, Yuen A, Innocenti F. The influence of UGT polymorphisms as biomarkers in solid organ transplantation. Clinica chimica acta; international journal of clinical chemistry. 2012;413(17-18):1318-25.
115. Nowak I, Shaw LM. Effect of mycophenolic acid glucuronide on inosine monophosphate dehydrogenase activity. Therapeutic drug monitoring. 1997;19(3):358-60.
116. Kobayashi M, Saitoh H, Kobayashi M, Tadano K, Takahashi Y, Hirano T. Cyclosporin A, but not tacrolimus, inhibits the biliary excretion of mycophenolic acid glucuronide possibly mediated by multidrug resistance-associated protein 2 in rats. The Journal of pharmacology and experimental therapeutics. 2004;309(3):1029-35.
117. Hesselink DA, van Gelder T. Genetic and nongenetic determinants of between-patient variability in the pharmacokinetics of mycophenolic acid. Clinical pharmacology and therapeutics. 2005;78(4):317-21.
118. Bullingham R, Monroe S, Nicholls A, Hale M. Pharmacokinetics and bioavailability of mycophenolate mofetil in healthy subjects after single-dose oral and intravenous administration. Journal of clinical pharmacology. 1996;36(4):315-24.
119. Placebo-controlled study of mycophenolate mofetil combined with cyclosporin and corticosteroids for prevention of acute rejection. European Mycophenolate Mofetil Cooperative Study Group. Lancet. 1995;345(8961):1321-5.
120. A blinded, randomized clinical trial of mycophenolate mofetil for the prevention of acute rejection in cadaveric renal transplantation. The Tricontinental Mycophenolate Mofetil Renal Transplantation Study Group. Transplantation. 1996;61(7):1029-37.
121. van Gelder T, Hilbrands LB, Vanrenterghem Y, Weimar W, de Fijter JW, Squifflet JP, et al. A randomized double-blind, multicenter plasma concentration controlled study of the safety and efficacy of oral mycophenolate mofetil for the prevention of acute rejection after kidney transplantation. Transplantation. 1999;68(2):261-6.
122. Weber LT, Shipkova M, Armstrong VW, Wagner N, Schutz E, Mehls O, et al. The pharmacokinetic-pharmacodynamic relationship for total and free mycophenolic Acid in pediatric renal transplant recipients: a report of the german study group on mycophenolate mofetil therapy. Journal of the American Society of Nephrology : JASN. 2002;13(3):759-68.

123. Mourad M, Malaise J, Chaib Eddour D, De Meyer M, Konig J, Schepers R, et al. Correlation of mycophenolic acid pharmacokinetic parameters with side effects in kidney transplant patients treated with mycophenolate mofetil. Clinical chemistry. 2001;47(1):88-94.
124. Cockcroft DW, Gault MH. Prediction of creatinine clearance from serum creatinine. Nephron. 1976;16(1):31-41.
125. Jacobson PA, Schladt D, Oetting WS, Leduc R, Guan W, Matas AJ, et al. Genetic determinants of mycophenolate-related anemia and leukopenia after transplantation. Transplantation. 2011;91(3):309-16.
126. Jacobson PA, Green KG, Hering BJ. Mycophenolate mofetil in islet cell transplant: variable pharmacokinetics but good correlation between total and unbound concentrations. Journal of clinical pharmacology. 2005;45(8):901-9.
127. de Winter BC, van Gelder T, Glander P, Cattaneo D, Tedesco-Silva H, Neumann I, et al. Population pharmacokinetics of mycophenolic acid : a comparison between enteric-coated mycophenolate sodium and mycophenolate mofetil in renal transplant recipients. Clinical pharmacokinetics. 2008;47(12):827-38.
128. Gaston R, Kaplan B, Shah T, Cibrik D, Shaw L, Angelis M, et al. Fixed-or Controlled-Dose Mycophenolate Mofetil with Standard-or Reduced-Dose Calcineurin Inhibitors: The Opticept Trial. American Journal of Transplantation. 2009;9(7):1607-19.
129. van Gelder T, Klupp J, Barten MJ, Christians U, Morris RE. Comparison of the effects of tacrolimus and cyclosporine on the pharmacokinetics of mycophenolic acid. Therapeutic drug monitoring. 2001;23(2):119-28.
130. Karlsson MO, Savic RM. Diagnosing model diagnostics. Clinical pharmacology and therapeutics. 2007;82(1):17-20.
131. Savic RM, Karlsson MO. Importance of shrinkage in empirical bayes estimates for diagnostics: problems and solutions. The AAPS journal. 2009;11(3):558-69.
132. Reich DE, Cargill M, Bolk S, Ireland J, Sabeti PC, Richter DJ, et al. Linkage disequilibrium in the human genome. Nature. 2001;411(6834):199-204.
133. Johnson AD, Handsaker RE, Pulit SL, Nizzari MM, O'Donnell CJ, de Bakker PI. SNAP: a web-based tool for identification and annotation of proxy SNPs using HapMap. Bioinformatics (Oxford, England). 2008;24(24):2938-9.
134. http://www.broadinstitute.org/mpg/snap/index.php.
135. The International HapMap Project. Nature. 2003;426(6968):789-96.
136. Abecasis GR, Auton A, Brooks LD, DePristo MA, Durbin RM, Handsaker RE, et al. An integrated map of genetic variation from 1,092 human genomes. Nature. 2012;491(7422):56-65.
137. Jonsson EN, Karlsson MO. Xpose--an S-PLUS based population pharmacokinetic/pharmacodynamic model building aid for NONMEM. Computer methods and programs in biomedicine. 1999;58(1):51-64.
138. R Development Core Team (2008). R: A language and environment for statistical computing. R Foundation for Statistical Computing V, Austria. ISBN 3-900051-07-0, URL http://www.R-project.org.
139. RStudio (2012). RStudio: Integrated development environment for R (Version 0.97.551) [Computer software]. Boston M.

140. Holford NV, the visual predictive check— superiority to standard diagnostic (Rorschach) plots [abstr 738]. PAGE14, 2005 <http://www.page-meeting.org/?abstract=738>.
141. Sommerer C, Muller-Krebs S, Schaier M, Glander P, Budde K, Schwenger V, et al. Pharmacokinetic and pharmacodynamic analysis of enteric-coated mycophenolate sodium: limited sampling strategies and clinical outcome in renal transplant patients. British journal of clinical pharmacology. 2010;69(4):346-57.
142. Shaw LM, Figurski M, Milone MC, Trofe J, Bloom RD. Therapeutic drug monitoring of mycophenolic acid. Clinical Journal of the American Society of Nephrology. 2007;2(5):1062-72.
143. Gaston RS, Kaplan B, Shah T, Cibrik D, Shaw LM, Angelis M, et al. Fixed- or controlled-dose mycophenolate mofetil with standard- or reduced-dose calcineurin inhibitors: the Opticept trial. American journal of transplantation : official journal of the American Society of Transplantation and the American Society of Transplant Surgeons. 2009;9(7):1607-19.
144. van Gelder T, Silva HT, de Fijter JW, Budde K, Kuypers D, Tyden G, et al. Comparing mycophenolate mofetil regimens for de novo renal transplant recipients: the fixed-dose concentration-controlled trial. Transplantation. 2008;86(8):1043-51.
145. Le Meur Y, Buchler M, Thierry A, Caillard S, Villemain F, Lavaud S, et al. Individualized mycophenolate mofetil dosing based on drug exposure significantly improves patient outcomes after renal transplantation. American journal of transplantation : official journal of the American Society of Transplantation and the American Society of Transplant Surgeons. 2007;7(11):2496-503.
146. Atcheson BA, Taylor PJ, Kirkpatrick CM, Duffull SB, Mudge DW, Pillans PI, et al. Free mycophenolic acid should be monitored in renal transplant recipients with hypoalbuminemia. Therapeutic drug monitoring. 2004;26(3):284-6.
147. Nowak I, Shaw LM. Mycophenolic acid binding to human serum albumin: characterization and relation to pharmacodynamics. Clinical chemistry. 1995;41(7):1011-7.
148. Kuypers D, Vanrenterghem Y, Squifflet J-P, Mourad M, Abramowicz D, Oellerich M, et al. Twelve-Month Evaluation of the Clinical Pharmacokinetics of Total and Free Mycophenolic Acid and Its Glucuronide Metabolites in Renal Allograft Recipients on Low Dose Tacrolimus in Combination with Mycophenolate Mofetil. Therapeutic drug monitoring. 2003;25(5):609-22.
149. Naito T, Mino Y, Otsuka A, Ushiyama T, Ito T, Ozono S, et al. Impact of calcineurin inhibitors on urinary excretion of mycophenolic acid and its glucuronide in kidney transplant recipients. The Journal of Clinical Pharmacology. 2009;49(6):710-8.
150. de Winter BC, Mathot RA, Sombogaard F, Vulto AG, van Gelder T. Nonlinear relationship between mycophenolate mofetil dose and mycophenolic acid exposure: implications for therapeutic drug monitoring. Clinical Journal of the American Society of Nephrology. 2011;6(3):656-63.
151. Zeng L, Blair EY, Nath CE, Shaw PJ, Earl JW, Stephen K, et al. Population pharmacokinetics of mycophenolic acid in children and young people undergoing blood

or marrow and solid organ transplantation. British journal of clinical pharmacology. 2010;70(4):567-79.
152. Kim H, Long-Boyle J, Rydholm N, Orchard PJ, Tolar J, Smith AR, et al. Population pharmacokinetics of unbound mycophenolic acid in pediatric and young adult patients undergoing allogeneic hematopoietic cell transplantation. The Journal of Clinical Pharmacology. 2012;52(11):1665-75.
153. Hale MD, Nicholls AJ, Bullingham RE, Hene R, Hoitsma A, Squifflet JP, et al. The pharmacokinetic-pharmacodynamic relationship for mycophenolate mofetil in renal transplantation. Clinical pharmacology and therapeutics. 1998;64(6):672-83.
154. Oellerich M, Shipkova M, Schutz E, Wieland E, Weber L, Tonshoff B, et al. Pharmacokinetic and metabolic investigations of mycophenolic acid in pediatric patients after renal transplantation: implications for therapeutic drug monitoring. German Study Group on Mycophenolate Mofetil Therapy in Pediatric Renal Transplant Recipients. Therapeutic drug monitoring. 2000;22(1):20-6.
155. Odom DT, Zizlsperger N, Gordon DB, Bell GW, Rinaldi NJ, Murray HL, et al. Control of pancreas and liver gene expression by HNF transcription factors. Science. 2004;303(5662):1378-81.
156. Shih DQ, Bussen M, Sehayek E, Ananthanarayanan M, Shneider BL, Suchy FJ, et al. Hepatocyte nuclear factor-1α is an essential regulator of bile acid and plasma cholesterol metabolism. Nature genetics. 2001;27(4):375-82.
157. Dostalek M, Hazarika S, Akhlaghi F. Diabetes mellitus reduces activity of human UDP-glucuronosyltransferase 2B7 in liver and kidney leading to decreased formation of mycophenolic acid acyl-glucuronide metabolite. Drug Metabolism and Disposition. 2011;39(3):448-55.
158. Lu R, Kanai N, Bao Y, Wolkoff AW, Schuster VL. Regulation of renal oatp mRNA expression by testosterone. The American journal of physiology. 1996;270(2 Pt 2):F332-7.
159. Cerrutti JA, Brandoni A, Quaglia NB, Torres AM. Sex differences in p-aminohippuric acid transport in rat kidney: role of membrane fluidity and expression of OAT1. Molecular and cellular biochemistry. 2002;233(1-2):175-9.
160. Franklin TJ, Cook JM. The inhibition of nucleic acid synthesis by mycophenolic acid. The Biochemical journal. 1969;113(3):515-24.
161. Mitsui A, Suzuki S. Immunosuppressive effect of mycophenolic acid. The Journal of antibiotics. 1969;22(8):358-63.
162. Allison AC, Hovi T, Watts RW, Webster AD. Immunological observations on patients with Lesch-Nyhan syndrome, and on the role of de-novo purine synthesis in lymphocyte transformation. Lancet. 1975;2(7946):1179-83.
163. Allison AC, Kowalski WJ, Muller CJ, Waters RV, Eugui EM. Mycophenolic acid and brequinar, inhibitors of purine and pyrimidine synthesis, block the glycosylation of adhesion molecules. Transplantation proceedings. 1993;25(3 Suppl 2):67-70.
164. Platz KP, Sollinger HW, Hullett DA, Eckhoff DE, Eugui EM, Allison AC. RS-61443--a new, potent immunosuppressive agent. Transplantation. 1991;51(1):27-31.
165. Sollinger HW, Deierhoi MH, Belzer FO, Diethelm AG, Kauffman RS. RS-61443--a phase I clinical trial and pilot rescue study. Transplantation. 1992;53(2):428-32.

166. Lopez-Raton M, Rodrıguez-Alvarez MX, Cadarso-Suárez C, Gude-Sampedro F. OptimalCutpoints: An R Package for Selecting Optimal Cutpoints in Diagnostic Tests. JOURNAL OF STATISTICAL SOFTWARE. 2014;61(8):1-36.
167. Youden WJ. Index for rating diagnostic tests. Cancer. 1950;3(1):32-5.
168. Team RC, . R: A language and environment for statistical computing. R Foundation for Statistical Computing, Vienna, Austria. 2014.
169. Wickham H. ggplot2: elegant graphics for data analysis: Springer Science & Business Media; 2009.
170. Wickham H, Francois R. dplyr: A grammar of data manipulation. R package version 03 02. 2014.
171. van der Ploeg T, Austin PC, Steyerberg EW. Modern modelling techniques are data hungry: a simulation study for predicting dichotomous endpoints. BMC medical research methodology. 2014;14(1):137.
172. Kuypers DR, de Jonge H, Naesens M, de Loor H, Halewijck E, Dekens M, et al. Current target ranges of mycophenolic acid exposure and drug-related adverse events: a 5-year, open-label, prospective, clinical follow-up study in renal allograft recipients. Clinical therapeutics. 2008;30(4):673-83.
173. Ryan CJ, Rosenthal M, Ng S, Alumkal J, Picus J, Gravis G, et al. Targeted MET inhibition in castration-resistant prostate cancer: a randomized phase II study and biomarker analysis with rilotumumab plus mitoxantrone and prednisone. Clinical cancer research : an official journal of the American Association for Cancer Research. 2013;19(1):215-24.

APPENDIX

Chapter 2:

2. A: Stella Code Used in Simulating the Proposed EHC Model

```
Bile_amount(t) = Bile_amount(t - dt) + (Noname_1) * dt
INIT Bile_amount = 0

INFLOWS:
Noname_1 = central*K23
central(t) = central(t - dt) + (rate_abs - rate_out - centgb - LEAK) * dt
INIT central = 0

INFLOWS:
rate_abs = gut*KA
OUTFLOWS:
rate_out = central*K20
centgb = central*K23*(1-leakfraction)
LEAK = central*K23*leakfraction
CUMAUC(t) = CUMAUC(t - dt) + (INTEGRATOR) * dt
INIT CUMAUC = 0

INFLOWS:
INTEGRATOR = Cp
gallbladder(t) = gallbladder(t - dt) + (centgb - gbgut) * dt
INIT gallbladder = 0

INFLOWS:
centgb = central*K23*(1-leakfraction)
OUTFLOWS:
gbgut = gallbladder*KGG
gut(t) = gut(t - dt) + (gbgut + dosing + LEAK - rate_abs) * dt
INIT gut = 0

INFLOWS:
gbgut = gallbladder*KGG
dosing = IF(TIME<300) THEN pulse(1000,0,24) ELSE 0
LEAK = central*K23*leakfraction
```

```
OUTFLOWS:
rate_abs = gut*KA
Urine(t) = Urine(t - dt) + (rate_out) * dt
INIT Urine = 0

INFLOWS:
rate_out = central*K20
CL = 2.5
Cp = central/V
derivative = derivn(logCp,1)
K20 = CL/V
K23 = (Percnt*K20)/(1-Percnt)
KA = .75
KGG = IF(TIME>=1) AND (TIME<1.5) THEN kgg1 ELSE
IF(TIME>=4) AND (TIME<4.5) THEN kgg1  ELSE
IF(TIME>=10) AND (TIME<10.5) THEN kgg1  ELSE
IF(TIME>=25) AND (TIME<25.5) THEN kgg1   ELSE
IF(TIME>=28) AND (TIME<28.5) THEN kgg1  ELSE
IF(TIME>=34) AND (TIME<34.5) THEN kgg1  ELSE
IF(TIME>=49) AND (TIME<49.5) THEN kgg1  ELSE
IF(TIME>=52) AND (TIME<52.5) THEN kgg1  ELSE
IF(TIME>=58) AND (TIME<58.5) THEN kgg1  ELSE
IF(TIME>=73) AND (TIME<73.5) THEN kgg1  ELSE
IF(TIME>=76) AND (TIME<76.5) THEN kgg1  ELSE
IF(TIME>=82) AND (TIME<82.5) THEN kgg1  ELSE
IF(TIME>=97) AND (TIME<97.5) THEN kgg1  ELSE
IF(TIME>=100) AND (TIME<100.5) THEN kgg1  ELSE
IF(TIME>=106) AND (TIME<106.5) THEN kgg1  ELSE
IF(TIME>=121) AND (TIME<121.5) THEN kgg1  ELSE
IF(TIME>=124) AND (TIME<124.5) THEN kgg1  ELSE
IF(TIME>=130) AND (TIME<130.5) THEN kgg1  ELSE
IF(TIME>=121) AND (TIME<121.5) THEN kgg1  ELSE
IF(TIME>=124) AND (TIME<124.5) THEN kgg1  ELSE
IF(TIME>=130) AND (TIME<130.5) THEN kgg1  ELSE
IF(TIME>=145) AND (TIME<145.5) THEN kgg1  ELSE
IF(TIME>=148) AND (TIME<148.5) THEN kgg1  ELSE
```

IF(TIME>=154) AND (TIME<154.5) THEN kgg1 ELSE
IF(TIME>=169) AND (TIME<169.5) THEN kgg1 ELSE
IF(TIME>=172) AND (TIME<172.5) THEN kgg1 ELSE
IF(TIME>=178) AND (TIME<178.5) THEN kgg1 ELSE
IF(TIME>=193) AND (TIME<193.5) THEN kgg1 ELSE
IF(TIME>=196) AND (TIME<196.5) THEN kgg1 ELSE
IF(TIME>=202) AND (TIME<202.5) THEN kgg1 ELSE
IF(TIME>=217) AND (TIME<217.5) THEN kgg1 ELSE
IF(TIME>=220) AND (TIME<220.5) THEN kgg1 ELSE
IF(TIME>=226) AND (TIME<226.5) THEN kgg1 ELSE
IF(TIME>=241) AND (TIME<241.5) THEN kgg1 ELSE
IF(TIME>=244) AND (TIME<244.5) THEN kgg1 ELSE
IF(TIME>=250) AND (TIME<250.5) THEN kgg1 ELSE
IF(TIME>=265) AND (TIME<265.5) THEN kgg1 ELSE
IF(TIME>=268) AND (TIME<268.5) THEN kgg1 ELSE
IF(TIME>=274) AND (TIME<274.5) THEN kgg1 ELSE
0

kgg1 = 2.77
leakfraction = .25
logCp = LOGN(Cp)
Percnt = 0 ***;Percnt value was changed to 0.2, 0.4, 0.6, 0.8 to reflect the 20%,40%, 60%, and 80% EHC, respectively.***
Thalf = -0.693/derivative
V = 36

Chapter 3:

3.A: NONMEM Code for the Simulation Model Used in the Analysis

```
;; 1. Based on:
;; 2. Description: simulation model(EHC as dist)
;; x1. Author: Malek Okour

;; 3. Label:
$PROBLEM simulation of population data
$INPUT C ID TIME MDV EVID DV AMT
$DATA sim_template.csv IGNORE=@
$SUBROUTINES ADVAN6 TOL=10
$MODEL
COMP=(GUT)
COMP=(CENTRAL)
COMP=(GB)

$PK
KA=THETA(1)* EXP(ETA(1))
TVCL=THETA(2)
CL =TVCL* EXP(ETA(2))
TVV=THETA(3)
V  =TVV* EXP(ETA(3))
S2 = V

;EHC
K20=(CL/V)
PERCNT=THETA(4)
K23= (PERCNT*K20)/(1-PERCNT)
KLEAK=.25*K23
KGG=.75*K23

;times of EHC
;duration of gb emptying
D=.5 ; half an hour
;first meal at 1 hr TAD
mt1=THETA(5)+ETA(4)
```

```
mt2=mt1+D
;2nd meal at 4 hr TAD
mt3=THETA(6)+ETA(4)
mt4=mt3+D
;3rd meal at 10 hr TAD
mt5=THETA(7)+ETA(4)
mt6=mt5+D
;gb empytying rate constant that result in emptying around 75% of gb content
K31=2.77

$DES
hill1=exp(-THETA(8)*(t-mt1))
hill2=exp(-THETA(8)*(t-mt2))
flag1=1./(1+hill1)  ; changes from 0 to 1 at t=mt1
flag2=1./(1+hill2)  ; changes from 0 to 1 at t=mt2
flagA=flag1-flag2

hill3=exp(-THETA(8)*(t-mt3))
hill4=exp(-THETA(8)*(t-mt4))
flag3=1./(1+hill3)  ; changes from 0 to 1 at t=mt3
flag4=1./(1+hill4)  ; changes from 0 to 1 at t=mt4
flagB=flag3-flag4

hill5=exp(-THETA(8)*(t-mt5))
hill6=exp(-THETA(8)*(t-mt6))
flag5=1./(1+hill5)  ; changes from 0 to 1 at t=mt5
flag6=1./(1+hill6)  ; changes from 0 to 1 at t=mt6
flagC=flag5-flag6

gb=K31*A(3)*flagA +K31*A(3)*flagB+K31*A(3)*flagC

DADT(1)=-KA*A(1)+KLEAK*A(2)+gb
DADT(2)=KA*A(1)-K20*A(2) -K23*A(2)
DADT(3) = KGG*A(2)-gb
```

$THETA
(0,.75) ;KA
(0,5) ;CL
(0,36) ;V
(0,.4) ;PERCNT EHC ; ***;Percnt value was changed to 0.2, 0.4, 0.6, 0.8 to reflect the 20%,40%, 60%, and 80% EHC in the simulations, respectively.***
(0,1) ;meal1
(0,4) ;meal2
(0,10) ;meal3
20 FIX ;hill

$OMEGA
0.04 ; IIVKA
0.04 ; IIVCL
0.04 ; IIVV
0.06 ;IIVMEAL

$SIGMA
0.01; ERR

$ERROR
IPRED = F
Y=F+F*ERR(1)
W=IPRED
IRES=DV-IPRED
IWRES=IRES/W
IND = IREP

A1=A(1)
A2=A(2)
A3=A(3)

; half lives
;THALF based on 1COMP CL and V
THALF=(.693*TVV)/TVCL

```
$SIMULATION  (123123) ONLY
;$EST METHOD=1 INTER MAXEVAL=9999 NOABORT SIG=3 PRINT=1 POSTHOC

$TABLE NOPRINT ONEHEADER IND ID AMT TIME EVID FILE=popsim1
$TABLE IND ID TIME DV MDV EVID IWRES IPRED IWRES CWRES IRES PRED NOAPPEND
ONEHEADER NOPRINT FILE=sdtab1
$TABLE IND ID TIME KA CL V PERCNT IPRED DV PRED THALF gb A1 A2 A3 mt1 mt2 mt3
mt4 mt5 mt6 ETA(1) ETA(2) ETA(3) ETA(4) ONEHEADER NOPRINT FILE=patab1
```

3.B: NONMEM Code for the Estimation Model 1 Used in The Analysis (Model 1)

```
;; 1. Based on:
;; 2. Description: est-mod 1comp
;; x1. Author: Malek Okour
;; 3. Label:
$PROBLEM simulation of population data
$INPUT C ID TIME MDV EVID DV AMT

$DATA sim_template.csv IGNORE=@
$SUBROUTINES ADVAN2 TRANS2

$PK
KA=THETA(1)* EXP(ETA(1))
TVCL=THETA(2)
CL =TVCL* EXP(ETA(2))
TVV=THETA(3)
V  =TVV* EXP(ETA(3))
S2 = V

$ERROR
IPRED = F
Y=F+F*ERR(1);+ERR(2)
W=IPRED
IRES=DV-IPRED
IWRES=IRES/W

A1=A(1)
A2=A(2)
; half lives
;THALF based on 1COMP CL and V
THALF=(.693*TVV)/TVCL

$THETA
(0,.75) ;KA
(0,5)   ;CL
(0,36)  ;V
```

```
$OMEGA
0.04 ; IIVKA
0.04 ; IIVCL
0.04 ; IIVV

$SIGMA
0.01; ERR

$EST METHOD=1 INTER MAXEVAL=9999 NOABORT SIG=3 PRINT=1 POSTHOC

; Xpose
$TABLE ID TIME DV MDV EVID IWRES IPRED IWRES CWRES IRES PRED NOAPPEND
ONEHEADER NOPRINT FILE=sdtab2
$TABLE ID TIME CL V THALF KA IPRED ONEHEADER NOPRINT FILE=patab2
```

3.C: NONMEM Code for the Estimation Model 2 Used in The Analysis (Model 2)

```
;; 1. Based on:
;; 2. Description: est-mod 2comp
;; x1. Author: Malek Okour
;; 3. Label:
$PROBLEM simulation of population data
$INPUT C ID TIME MDV EVID DV AMT
$DATA sim_template.csv IGNORE=@
$SUBROUTINES ADVAN4 TRANS4

$PK
KA=THETA(1)* EXP(ETA(1))
TVCL=THETA(2)
CL =TVCL* EXP(ETA(2))
TVV=THETA(3)
V2  =TVV* EXP(ETA(3))
Q  = THETA(4)
V3 = THETA(5)
S2 = V2
VSS=V2+V3
$ERROR
IPRED = F
Y=F+F*ERR(1);+ERR(2)
W=IPRED
IRES=DV-IPRED
IWRES=IRES/W

; half lives
;THALF based on 1COMP CL and V
THALF=(.693*TVV)/TVCL

$THETA
(0,.75) ;KA
(0,5)   ;CL
(0,25)  ;V
(0,10)   ; Q
(0,25)   ; V3
```

```
$OMEGA
0.04 ; IIVKA
0.04 ; IIVCL
0.04 ; IIVV


$SIGMA
0.01; ERR

$EST METHOD=1 INTER MAXEVAL=9999 NOABORT SIG=3 PRINT=1 POSTHOC

; Xpose
$TABLE ID TIME DV MDV EVID IWRES IPRED IWRES CWRES IRES PRED NOAPPEND
ONEHEADER NOPRINT FILE=sdtab3
$TABLE ID TIME  CL  V2 V3 VSS Q  KA IPRED ONEHEADER NOPRINT FILE=patab3
```

3.D: NONMEM Code for the Estimation Model 3 Used in the Analysis (Model 3)

```
;; 1. Based on:
;; 2. Description: est-mod 1COMP+contEHC
;; x1. Author: Malek Okour

;; 3. Label:
$PROBLEM simulation of population data
$INPUT C ID TIME MDV EVID DV AMT
$DATA sim_template.csv IGNORE=@
$SUBROUTINES ADVAN6 TOL=10
$MODEL
COMP=(GUT)
COMP=(CENTRAL)
$PK
KA=THETA(1)* EXP(ETA(1))
TVCL=THETA(2)
CL =TVCL* EXP(ETA(2))
TVV=THETA(3)
V  =TVV* EXP(ETA(3))
S2 = V
K12=KA

;EHC
K20=(CL/V)
PERCNT=THETA(4)
K21= (PERCNT*K20)/(1-PERCNT)

$ERROR
IPRED = F
Y=F+F*ERR(1)
W=IPRED
IRES=DV-IPRED
IWRES=IRES/W

$DES
DADT(1)=-K12*A(1)+K21*A(2)
```

```
DADT(2)=K12*A(1)-K21*A(2) -K20*A(2)

$THETA
(0,.75)  ;KA
(0,5)  ;CL
(0,36) ;V
(0,.5) ;PERCNT EHC

$OMEGA
0.04 ; IIVKA
0.04 ; IIVCL
0.04 ; IIVV

$SIGMA
0.01; ERR

$EST METHOD=1 INTER MAXEVAL=9999 NOABORT SIG=3 PRINT=1 POSTHOC

; Xpose
$TABLE ID TIME DV MDV EVID IWRES IPRED IWRES CWRES IRES PRED NOAPPEND
ONEHEADER NOPRINT FILE=sdtab4
$TABLE ID TIME  CL  V  KA K21 IPRED ONEHEADER NOPRINT FILE=patab4
```

3. E: NONMEM Code for the Estimation Model 4 Used in the Analysis (Model 4)

```
;; 1. Based on:
;; 2. Description:  est-mod 1COMP+gbEHC-1meal
;; x1. Author: Malek Okour
;; 3. Label:
$PROBLEM simulation of population data
$INPUT C ID TIME MDV EVID DV AMT
$DATA sim_template.csv IGNORE=@
$SUBROUTINES ADVAN6 TOL=10
$MODEL
COMP=(GUT)
COMP=(CENTRAL)
COMP=(GB)

$PK
KA=THETA(1)* EXP(ETA(1))
TVCL=THETA(2)
CL =TVCL* EXP(ETA(2))
TVV=THETA(3)
V  =TVV* EXP(ETA(3))
S2 = V
;EHC
K20=(CL/V)
PERCNT=THETA(4)
K23= (PERCNT*K20)/(1-PERCNT)

;times of EHC
;duration of gb emptying
D=.5 ; half an hour
;a meal
mt1=THETA(5)+ETA(4)
mt2=mt1+D
;gb empytying rate constant that result in emptying around 75% of gb content
K31=2.77
```

```
$DES
hill1=exp(-THETA(6)*(t-mt1))
hill2=exp(-THETA(6)*(t-mt2))
flag1=1./(1+hill1)  ; changes from 0 to 1 at t=mt1
flag2=1./(1+hill2)  ; changes from 0 to 1 at t=mt2
flagA=flag1-flag2
gb=K31*A(3)*flagA

DADT(1)=-KA*A(1)+gb
DADT(2)=KA*A(1)-K20*A(2) -K23*A(2)
DADT(3) = K23*A(2)-gb

$THETA
(0,.75)  ;KA
(0,5)  ;CL
(0,36) ;V
(0,.5) ;PERCNT EHC
(0,8)  ;meal1
20 FIX ;hill

$OMEGA
0.04 ; IIVKA
0.04 ; IIVCL
0.04 ; IIVV
0.06 ;IIVMEAL
$SIGMA
0.01; ERR

$ERROR
IPRED = F
Y=F+F*ERR(1)
W=IPRED
IRES=DV-IPRED
IWRES=IRES/W
IND = IREP
A1=A(1)
```

```
A2=A(2)
A3=A(3)

$EST METHOD=1 INTER MAXEVAL=9999 NOABORT SIG=3 PRINT=1 POSTHOC
; Xpose
$TABLE ID TIME DV MDV EVID IWRES IPRED IWRES CWRES IRES PRED NOAPPEND
ONEHEADER NOPRINT FILE=sdtab5
$TABLE ID TIME  CL  V  gb KA A1 A2 A3 IPRED ONEHEADER NOPRINT FILE=patab5
```

3. F: NONMEM Code for the Estimation Model 5 Used in the Analysis (Model 5)

```
;; 1. Based on:
;; 2. Description: est-mod 1COMP+gbEHC-2meal
;; x1. Author: Malek Okour
;; 3. Label:
$PROBLEM simulation of population data
$INPUT C ID TIME MDV EVID DV AMT
$DATA sim_template.csv IGNORE=@
$SUBROUTINES ADVAN6 TOL=10
$MODEL
COMP=(GUT)
COMP=(CENTRAL)
COMP=(GB)

$PK
KA=THETA(1)* EXP(ETA(1))
TVCL=THETA(2)
CL =TVCL* EXP(ETA(2))
TVV=THETA(3)
V  =TVV* EXP(ETA(3))
S2 = V
;EHC
K20=(CL/V)
PERCNT=THETA(4)
K23= (PERCNT*K20)/(1-PERCNT)
;times of EHC
;duration of gb emptying
D=.5 ; half an hour
;a meal
mt1=THETA(5)+ETA(4)
mt2=mt1+D
;2nd meal
mt3=THETA(6)+ETA(4)
mt4=mt3+D
;gb empytying rate constant that result in emptying around 75% of gb content
K31=2.77
```

```
$DES
hill1=exp(-THETA(7)*(t-mt1))
hill2=exp(-THETA(7)*(t-mt2))
flag1=1./(1+hill1)  ; changes from 0 to 1 at t=mt1
flag2=1./(1+hill2)  ; changes from 0 to 1 at t=mt2
flagA=flag1-flag2
hill3=exp(-THETA(7)*(t-mt3))
hill4=exp(-THETA(7)*(t-mt4))
flag3=1./(1+hill3)  ; changes from 0 to 1 at t=mt1
flag4=1./(1+hill4)  ; changes from 0 to 1 at t=mt2
flagB=flag3-flag4
gb=K31*A(3)*flagA +K31*A(3)*flagB

DADT(1)=-KA*A(1)+gb
DADT(2)=KA*A(1)-K20*A(2) -K23*A(2)
DADT(3) = K23*A(2)-gb

$THETA
(0,.75)  ;KA
(0,5)  ;CL
(0,36) ;V
(0,.5) ;PERCNT EHC
(0,4)  ;meal1
(0,10)  ;meal2
20 FIX ;hill

$OMEGA
0.04 ; IIVKA
0.04 ; IIVCL
0.04 ; IIVV
0.06 ;IIVMEAL

$SIGMA
0.01; ERR
```

```
$ERROR
IPRED = F
Y=F+F*ERR(1)
W=IPRED
IRES=DV-IPRED
IWRES=IRES/W
IND = IREP

A1=A(1)
A2=A(2)
A3=A(3)



$EST METHOD=1 INTER MAXEVAL=9999 NOABORT SIG=3 PRINT=1 POSTHOC

; Xpose
$TABLE ID TIME DV MDV EVID IWRES IPRED IWRES CWRES IRES PRED NOAPPEND
ONEHEADER NOPRINT FILE=sdtab6
$TABLE ID TIME CL V gb KA A1 A2 A3 ONEHEADER NOPRINT FILE=patab6
```

3. G: NONMEM Code for the Estimation Model 6 Used in the Analysis (Model 6)

```
;; 1. Based on:
;; 2. Description: est-mod 1COMP+gbEHC-3meal
;; x1. Author: Malek Okour
;; 3. Label:
$PROBLEM simulation of population data
$INPUT C ID TIME MDV EVID DV AMT
$DATA sim_template.csv IGNORE=@
$SUBROUTINES ADVAN6 TOL=10
$MODEL
COMP=(GUT)
COMP=(CENTRAL)
COMP=(GB)

$PK
KA=THETA(1)* EXP(ETA(1))
TVCL=THETA(2)
CL =TVCL* EXP(ETA(2))
TVV=THETA(3)
V  =TVV* EXP(ETA(3))
S2 = V
;EHC
K20=(CL/V)
PERCNT=THETA(4)
K23= (PERCNT*K20)/(1-PERCNT)
;times of EHC
;duration of gb emptying
D=.5 ; half an hour
;a meal
mt1=THETA(5)+ETA(4)
mt2=mt1+D
;2nd meal
mt3=THETA(6)+ETA(4)
mt4=mt3+D
;3rd meal at 10 hr TAD
mt5=THETA(7)+ETA(4)
```

```
mt6=mt5+D

;gb empytying rate constant that result in emptying around 75% of gb content
K31=2.77


$DES
hill1=exp(-THETA(8)*(t-mt1))
hill2=exp(-THETA(8)*(t-mt2))
flag1=1./(1+hill1)  ; changes from 0 to 1 at t=mt1
flag2=1./(1+hill2)  ; changes from 0 to 1 at t=mt2
flagA=flag1-flag2

hill3=exp(-THETA(8)*(t-mt3))
hill4=exp(-THETA(8)*(t-mt4))
flag3=1./(1+hill3)  ; changes from 0 to 1 at t=mt1
flag4=1./(1+hill4)  ; changes from 0 to 1 at t=mt2
flagB=flag3-flag4

hill5=exp(-THETA(8)*(t-mt5))
hill6=exp(-THETA(8)*(t-mt6))
flag5=1./(1+hill5)  ; changes from 0 to 1 at t=mt1
flag6=1./(1+hill6)  ; changes from 0 to 1 at t=mt2
flagC=flag5-flag6

gb=K31*A(3)*flagA +K31*A(3)*flagB+K31*A(3)*flagC

DADT(1)=-KA*A(1)+gb
DADT(2)=KA*A(1)-K20*A(2) -K23*A(2)
DADT(3) = K23*A(2)-gb

$THETA
(0,.75)  ;KA
(0,5)  ;CL
(0,36) ;V
(0,.5) ;PERCNT EHC
```

```
(0,1)  ;meal1
(0,4)  ;meal2
(0,10) ;meal3
20 FIX ;hill

$OMEGA
0.04 ; IIVKA
0.04 ; IIVCL
0.04 ; IIVV
0.06 ;IIVMEAL


$SIGMA
0.01; ERR

$ERROR
IPRED = F
Y=F+F*ERR(1)
W=IPRED
IRES=DV-IPRED
IWRES=IRES/W
IND = IREP

A1=A(1)
A2=A(2)
A3=A(3)



$EST METHOD=1 INTER MAXEVAL=9999 NOABORT SIG=3 PRINT=1 POSTHOC

; Xpose
$TABLE ID TIME DV MDV EVID IWRES IPRED IWRES CWRES IRES PRED NOAPPEND
ONEHEADER NOPRINT FILE=sdtab7
$TABLE ID TIME CL V gb KA A1 A2 A3 IPRED ONEHEADER NOPRINT FILE=patab7
```

3. H: NONMEM Code for the Estimation Model 7 Used in the Analysis (Model 7)

```
;; 1. Based on:
;; 2. Description: est mod- sameASsim BUT EHC as CL
;; x1. Author: Malek Okour
;; 3. Label:
$PROBLEM simulation of population data
$INPUT C ID TIME MDV EVID DV AMT
$DATA sim_template.csv IGNORE=@
$SUBROUTINES ADVAN6 TOL=10
$MODEL
COMP=(GUT)
COMP=(CENTRAL)
COMP=(GB)

$PK
KA=THETA(1)* EXP(ETA(1))
TVCL=THETA(2)
CL =TVCL* EXP(ETA(2))
TVV=THETA(3)
V  =TVV* EXP(ETA(3))
S2 = V

;EHC
PERCNT=THETA(4)
K20=(1-PERCNT)*(CL/V)
K23=(PERCNT)*(CL/V)
KLEAK=.25*K23
KGG=.75*K23
;times of EHC
;duration of gb emptying
D=.5 ; half an hour
;first meal at 1 hr TAD
mt1=THETA(5)+ETA(4)
mt2=mt1+D
;2nd meal at 4 hr TAD
```

```
mt3=THETA(6)+ETA(4)
mt4=mt3+D
;3rd meal at 10 hr TAD
mt5=THETA(7)+ETA(4)
mt6=mt5+D

;gb empytying rate constant that result in emptying around 75% of gb content
K31=2.77

$DES
hill1=exp(-THETA(8)*(t-mt1))
hill2=exp(-THETA(8)*(t-mt2))
flag1=1./(1+hill1)  ; changes from 0 to 1 at t=mt1
flag2=1./(1+hill2)  ; changes from 0 to 1 at t=mt2
flagA=flag1-flag2

hill3=exp(-THETA(8)*(t-mt3))
hill4=exp(-THETA(8)*(t-mt4))
flag3=1./(1+hill3)  ; changes from 0 to 1 at t=mt1
flag4=1./(1+hill4)  ; changes from 0 to 1 at t=mt2
flagB=flag3-flag4

hill5=exp(-THETA(8)*(t-mt5))
hill6=exp(-THETA(8)*(t-mt6))
flag5=1./(1+hill5)  ; changes from 0 to 1 at t=mt1
flag6=1./(1+hill6)  ; changes from 0 to 1 at t=mt2
flagC=flag5-flag6

gb=K31*A(3)*flagA +K31*A(3)*flagB+K31*A(3)*flagC

DADT(1)=-KA*A(1)+KLEAK*A(2)+gb
DADT(2)=KA*A(1)-K20*A(2) -K23*A(2)
DADT(3) = KGG*A(2)-gb

$THETA
(0,.75)  ;KA
```

```
(0,5)  ;CL
(0,36) ;V
(0,.5) ;PERCNT EHC
(0,1)  ;meal1
(0,4)  ;meal2
(0,10) ;meal3
20 FIX ;hill

$OMEGA
0.04 ; IIVKA
0.04 ; IIVCL
0.04 ; IIVV
0.06 ;IIVMEAL

$SIGMA
0.01; ERR

$ERROR
IPRED = F
Y=F+F*ERR(1)
W=IPRED
IRES=DV-IPRED
IWRES=IRES/W
IND = IREP

A1=A(1)
A2=A(2)
A3=A(3)

; half lives
;THALF based on 1COMP CL and V
THALF=(.693*TVV)/TVCL


$EST METHOD=1 INTER MAXEVAL=9999 NOABORT SIG=3 PRINT=1 POSTHOC
```

```
$TABLE NOPRINT ONEHEADER IND ID AMT TIME EVID FILE=popsim8
$TABLE IND ID TIME DV MDV EVID IWRES IPRED IWRES CWRES IRES PRED NOAPPEND
ONEHEADER NOPRINT FILE=sdtab8
$TABLE IND ID TIME KA CL V PERCNT IPRED DV PRED THALF gb A1 A2 A3 mt1 mt2 mt3
mt4 mt5 mt6 ETA(1) ETA(2) ETA(3) ETA(4) ONEHEADER NOPRINT FILE=patab8
```

3. I: The Structure of the Dataset Used in the SSE Analysis

C	ID	TIME	MDV	EVID	DV	AMT	CMT
.	1	0	1	1	.	1000	1
.	1	0.5	0	0	.	.	2
.	1	1	0	0	.	.	2
.	1	2	0	0	.	.	2
.	1	4	0	0	.	.	2
.	1	6	0	0	.	.	2
.	1	8	0	0	.	.	2
.	1	10	0	0	.	.	2
.	1	12	0	0	.	.	2
.	1	16	0	0	.	.	2
.	1	24	0	0	.	.	2
.	2	0	1	1	.	1000	1
.	2	0.5	0	0	.	.	2
.	2	1	0	0	.	.	2
.	2	2	0	0	.	.	2
.	2	4	0	0	.	.	2
.	2	6	0	0	.	.	2
.	2	8	0	0	.	.	2
.	2	10	0	0	.	.	2
.	2	12	0	0	.	.	2
.	2	16	0	0	.	.	2
.	2	24	0	0	.	.	2

Dataset shown here includes only the first 2 subjects while the actual dataset included 50 subjects

Chapter 4:

4.A: NONMEM Code for the Final Model Used in the Population Pharmacokinetic Modeling Analysis of Unbound MPA, Total MPA, MPAG and Acyl-MPAG

```
;; 1. Based on:
;; 2. Description: run5vpc
;; x1. Author: Malek Okour

$PROBLEM    simulation of population data
$INPUT      C ID PID=DROP TIME AMT NTIME CMT DV TYPE SS II MDV
ADDL=DROP EVID CDRUG CRCL WT=DROP GEND AGE=DROP DIAB
GENO1=DROP GENO2 GENO3=DROP GENO4 GENO5=DROP GENO6=DROP
GENO7=DROP
$DATA      cov_dataset.csv IGNORE=@
$SUBROUTINE ADVAN6 TOL=9
$MODEL
COMP=(GUT,INITIALOFF,DEFDOSE)
COMP=(CENTRAL)
COMP=(MPAG)
COMP=(ACYL)
COMP=(GB)

$PK

;;; PERCNTGENO4-DEFINITION START
IF(GENO4.EQ.0) PERCNTGENO4 = 1  ; Most common
IF(GENO4.EQ.1.OR.GENO4.EQ.2) PERCNTGENO4 = ( 1 + THETA(13))
;IF(GENO4.EQ.2) PERCNTGENO4 = ( 1 + THETA(14))
IF(GENO4.EQ.-99) PERCNTGENO4 = 1  ; Missing data
;;; PERCNTGENO4-DEFINITION END

;;; PERCNT-RELATION START
PERCNTCOV=PERCNTGENO4
;;; PERCNT-RELATION END

;;; CLMGENO2-DEFINITION START
IF(GENO2.EQ.0) CLMGENO2 = 1  ; Most common
```

```
IF(GENO2.EQ.1) CLMGENO2 = ( 1 + THETA(12))
IF(GENO2.EQ.-99) CLMGENO2 = 1  ; Missing data
;;; CLMGENO2-DEFINITION END

;;; CLMGEND-DEFINITION START
IF(GEND.EQ.1) CLMGEND = 1  ; Most common
IF(GEND.EQ.0) CLMGEND = ( 1 + THETA(11))
IF(GEND.EQ.-99) CLMGEND = 1  ; Missing data
;;; CLMGEND-DEFINITION END


;;; CLMDIAB-DEFINITION START
IF(DIAB.EQ.0) CLMDIAB = 1  ; Most common
IF(DIAB.EQ.1) CLMDIAB = ( 1 + THETA(10))
IF(DIAB.EQ.-99) CLMDIAB = 1  ; Missing data
;;; CLMDIAB-DEFINITION END

;;; CLM-RELATION START
CLMCOV=CLMDIAB*CLMGEND*CLMGENO2
;;; CLM-RELATION END

;;; CLCRCL-DEFINITION START
IF(CRCL.EQ.-99) THEN
CLCRCL = 1
ELSE
CLCRCL = ( 1 + THETA(9)*(CRCL - 77.37))
ENDIF
;;; CLCRCL-DEFINITION END

;;; CL-RELATION START
CLCOV=CLCRCL
;;; CL-RELATION END

;;; PCDRUG-DEFINITION START
IF(CDRUG.EQ.1) PCDRUG = 1  ; Most common
IF(CDRUG.EQ.0) PCDRUG = ( 1 + THETA(8))
```

```
IF(CDRUG.EQ.-99) PCDRUG = 1  ; Missing data
;;; PCDRUG-DEFINITION END

if (ii>0) then
inter=ii
else
inter=inter
endif

if (newind.le.1) ptime=0
ptime=time ; Must remember previous time. PK is called *before* the advance to the
current record.
if (dostim>0) then
ptime=dostim
else
ptime=time ; Must remember previous time. PK is called *before* the advance to the
current record.
endif

KA=THETA(1)*EXP(ETA(4))
TVCL=THETA(2)*PCDRUG
TVCL = CLCOV*TVCL
CL =TVCL*EXP(ETA(1))
TVV=THETA(3)
V= TVV* EXP(ETA(2))
TVCLM=THETA(4)
TVCLM = CLMCOV*TVCLM
CLM=TVCLM*EXP(ETA(3))
VM=THETA(5)

K20=CL/V
KM=CLM/VM

S2=V/1000
S3=VM
TVPERCNT=THETA(6)
```

```
TVPERCNT = PERCNTCOV*TVPERCNT
PERCNT=TVPERCNT*EXP(ETA(5))
KDG= (PERCNT*KM)/(1-PERCNT)
KLEAK=.25*KDG
KCG=.75*KDG
KGG=2.77

;EHC
D=.5 ; half an hour

;first meal at 1 hr TAD
mt1=inter*INT(ptime/inter)+THETA(7);+ETA(5)
mt2=mt1+D

CLM2=THETA(14)*EXP(ETA(6))
VM2=THETA(15)
KM2=CLM2/VM2
S4=VM2/1000

FU=THETA(16)*EXP(ETA(7))

$DES
hill1=exp(-20*(t-mt1))
hill2=exp(-20*(t-mt2))
flag1=1./(1+hill1)  ; changes from 0 to 1 at t=mt1
flag2=1./(1+hill2)  ; changes from 0 to 1 at t=mt2
flagA=flag1-flag2

gb=KGG*A(5)*flagA

DADT(1)=-KA*A(1)+gb+KLEAK*A(3)
DADT(2)= KA*A(1)-K20*A(2)
DADT(3)= 0.87*K20*A(2)-KM*A(3)-KDG*A(3)
DADT(4)= 0.13*K20*A(2)-KM2*A(4)
DADT(5)= KCG*A(3)-gb
```

```
$ERROR
IF(TYPE.EQ.3) THEN
FCTOT=(F/FU)
ELSE
PRED=F
END IF

IF(TYPE.EQ.2) Z=0
IF(TYPE.EQ.3) Z=1
IF(TYPE.EQ.2) Y1=F*(1+ERR(1))*(1-Z)
IF(TYPE.EQ.3) Y1=FCTOT*(1+ERR(2))*(Z)
Q1=0
IF (CMT.EQ.2) Q1=1
Q2=0
IF (CMT.EQ.3) Q2=1
Y2=F*(1+ERR(3))
Q3=0
IF (CMT.EQ.4) Q3=1
Y3=F*(1+ERR(4))
Y=(Q1*Y1)+(Q2*Y2)+(Q3*Y3)

IF(TYPE.EQ.3) THEN
IPRED=(F/FU)
ELSE
IPRED=F
END IF

W=IPRED
IRES=DV-IPRED
IWRES=IRES/W

A1=A(1)
A2=A(2)
A3=A(3)
```

```
$THETA
(0, 2,10) ; KA
(0.001, 1450) ; CL
(0.001, 5630) ; V
(0, 0.959) ; CLM1
(0, 5.72) ; VM1
(0, 0.374) ; PRCNT
(0, 7.73,12) ; MEAL1
(0, 0.148,1) ; cdrug
(-0.01, 0.00763,0.028) ; CLCRCL1
(-1, -0.192,5) ; CLMDIAB1
(-1, -0.181,5) ; CLMGEND1
(-1, 0.327,5) ; CLMGENO21
(-1, 0.165,5) ; PERCNTGENO4_1or2
(0, 32.3) ;CLacyl
(0, 17.9) ;Vacyl
(0, 0.0239,1) ;FU

$OMEGA
0.0907 ;      IIVCL
 0.126 ;      IIVV
 0.0741 ;     IIVCLM
 1.18 ;      IIVka
 0.0771 ;      prcnt
;0.00441 ;IIVMEAL
 0.214 ; IIVCLacyl
 0.0576 ;IIVFU

$SIGMA
 0.164
 0.128
 0.0149
 0.0614

$ESTIMATION METHOD=1 INTER MAXEVAL=9999 NOABORT SIG=3 PRINT=1 POSTHOC
$COVARIANCE PRINT=E UNCONDITIONAL MATRIX=S
```

```
; Xpose
$TABLE ID TIME NTIME A1 A2 A3 CDRUG TYPE CMT DV MDV EVID CMT
IPRED IWRES CWRES IRES PRED NOAPPEND ONEHEADER NOPRINT FILE=sdtab7
$TABLE ID TIME NTIME CDRUG TYPE CMT KA CL PERCNT V K20 CLM VM KM CLM2 VM2
KM2 FU ETA(1) ETA(2) ETA(3) ONEHEADER NOPRINT FILE=patab7
```

4.B: Individual Plots of Unbound MPA

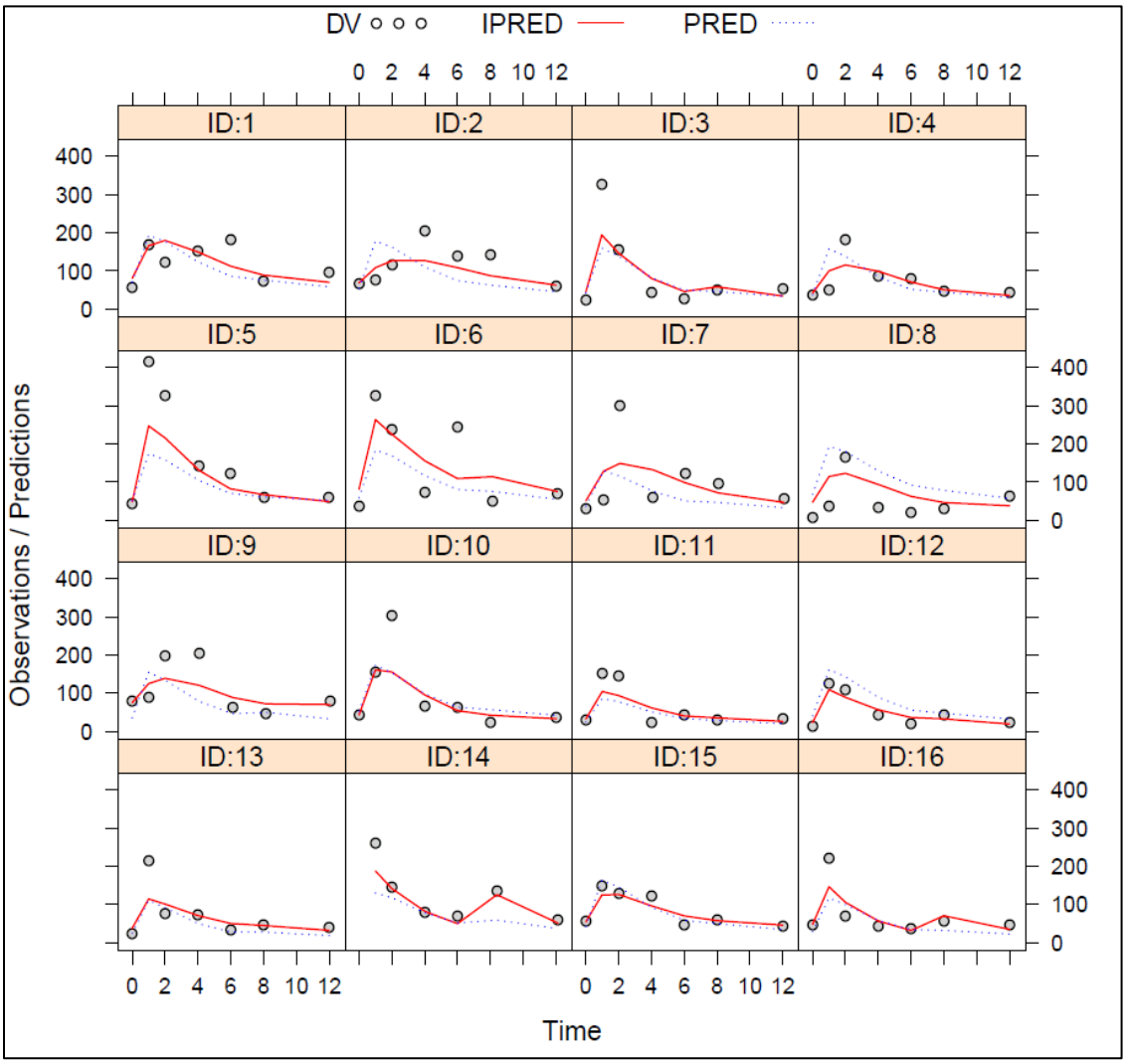

Individual Plots of Unbound MPA

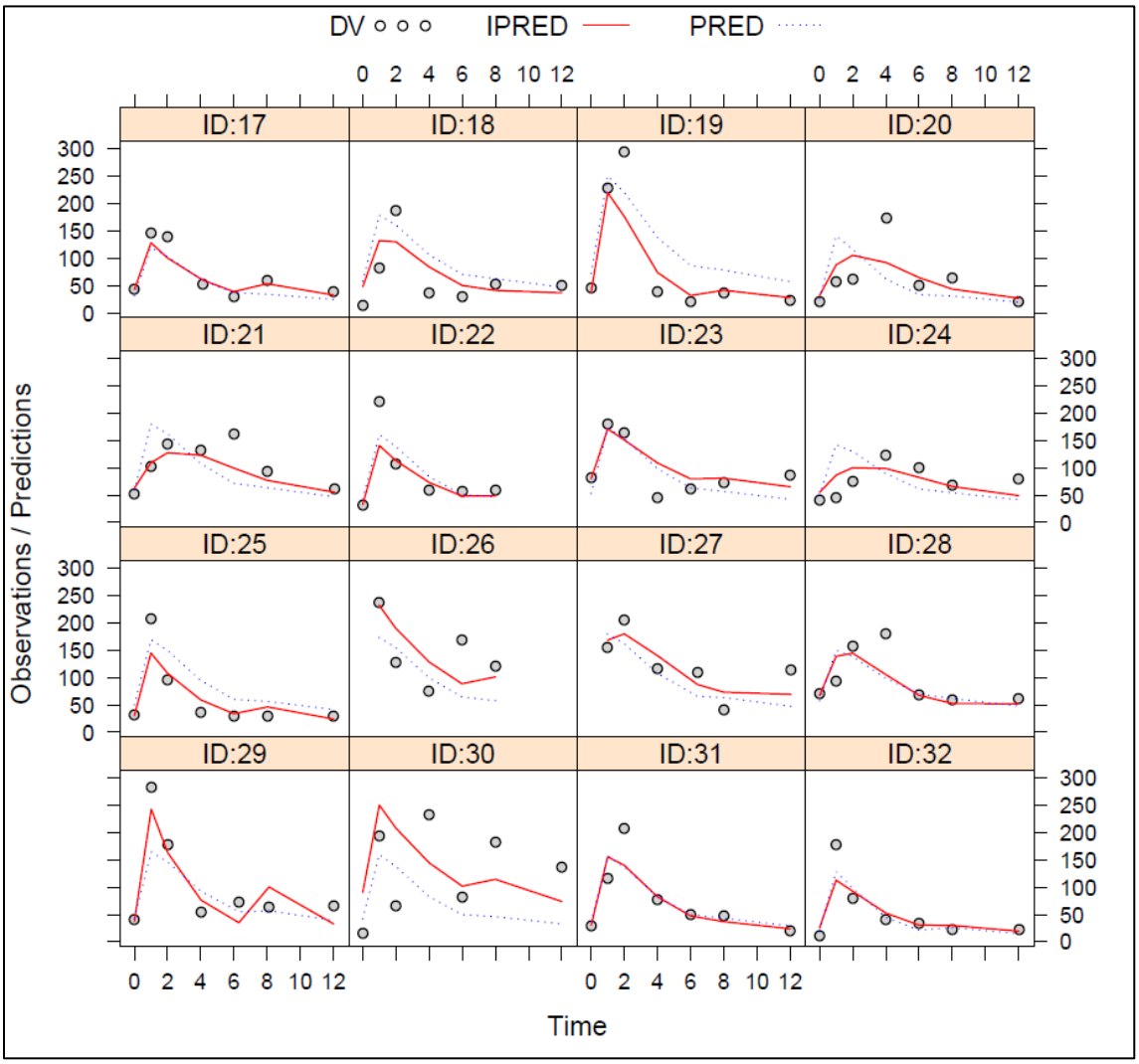

Individual Plots of Unbound MPA

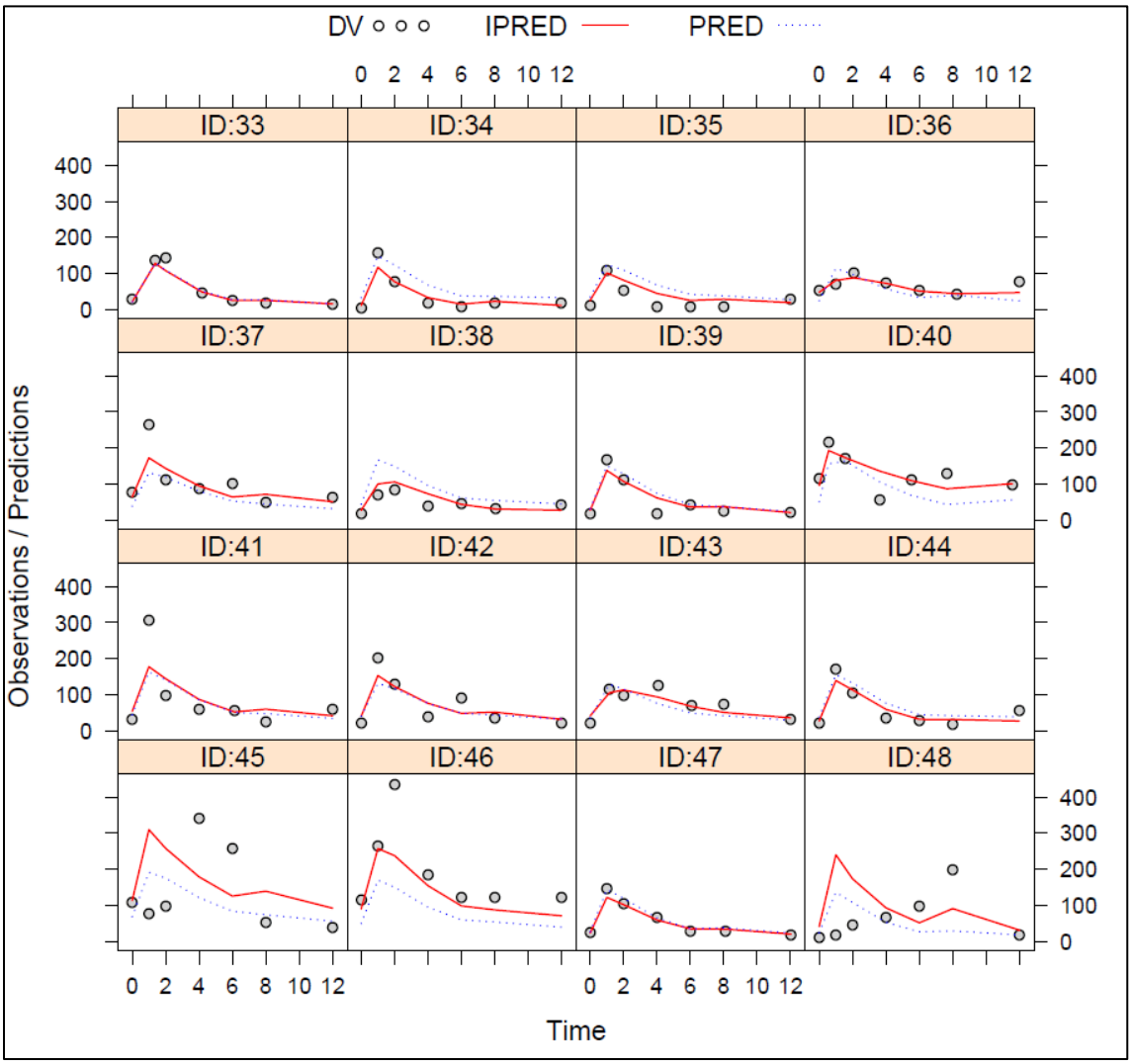

Individual Plots of Unbound MPA

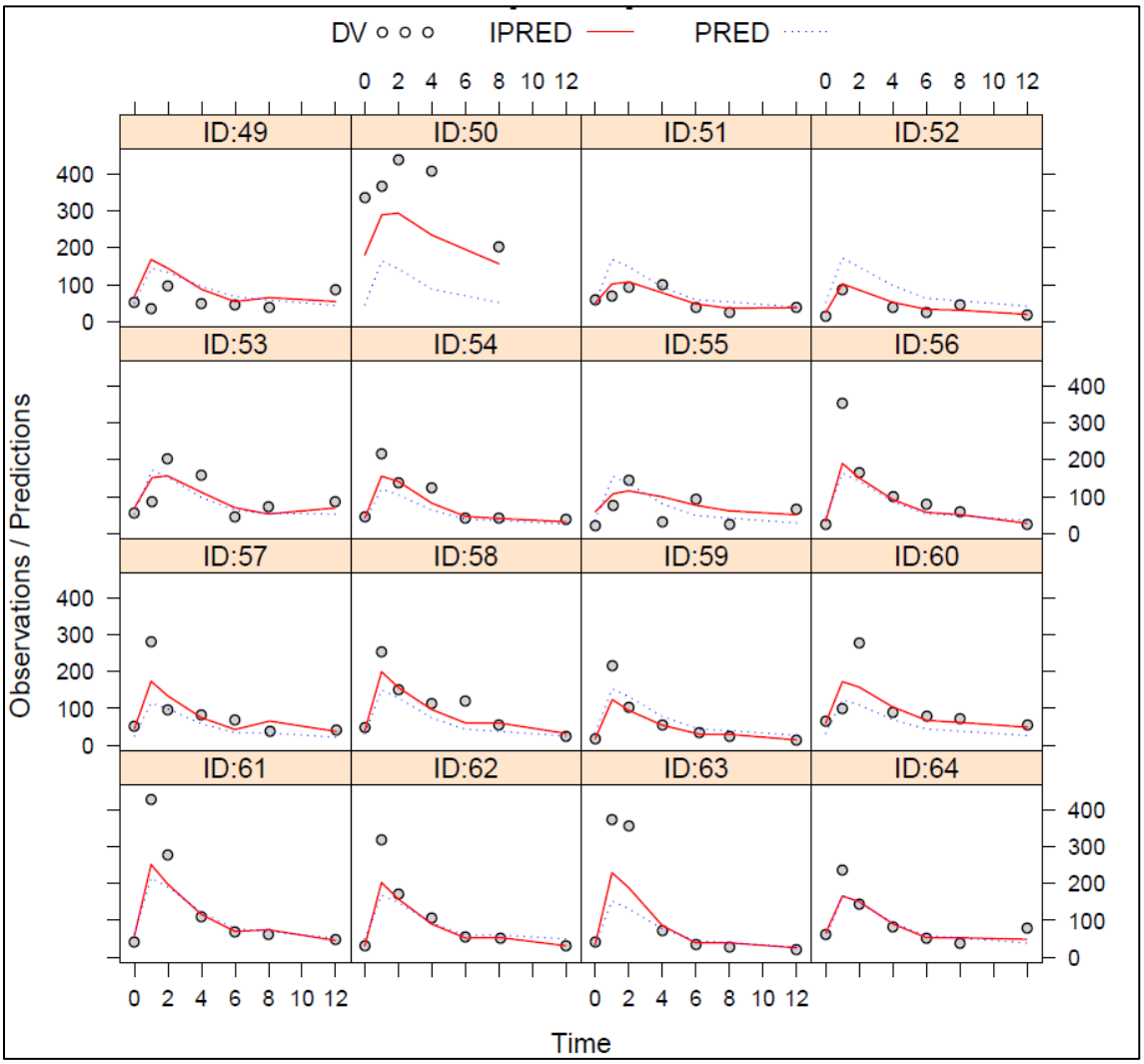

Individual Plots of Unbound MPA

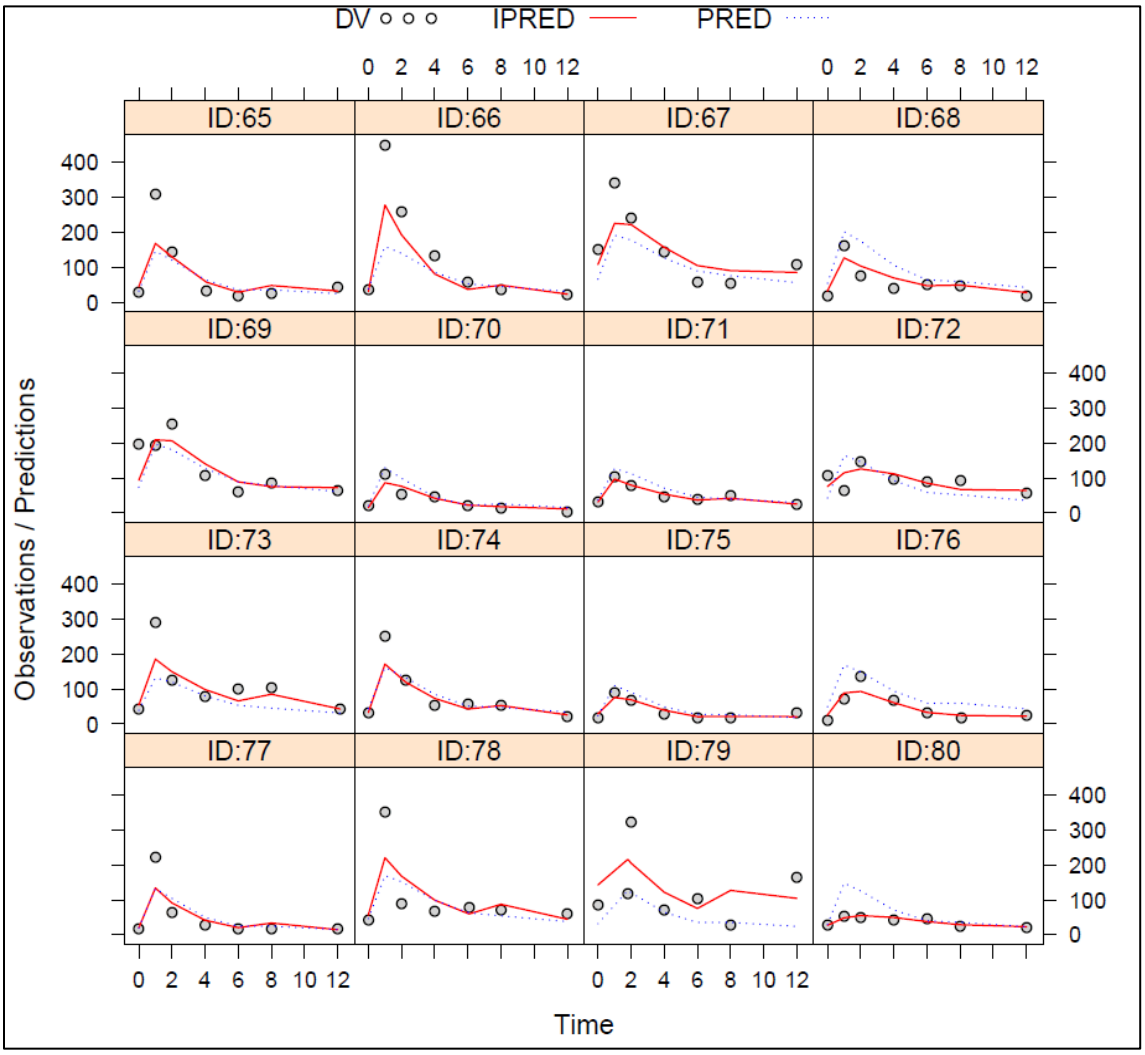

Individual Plots of Unbound MPA

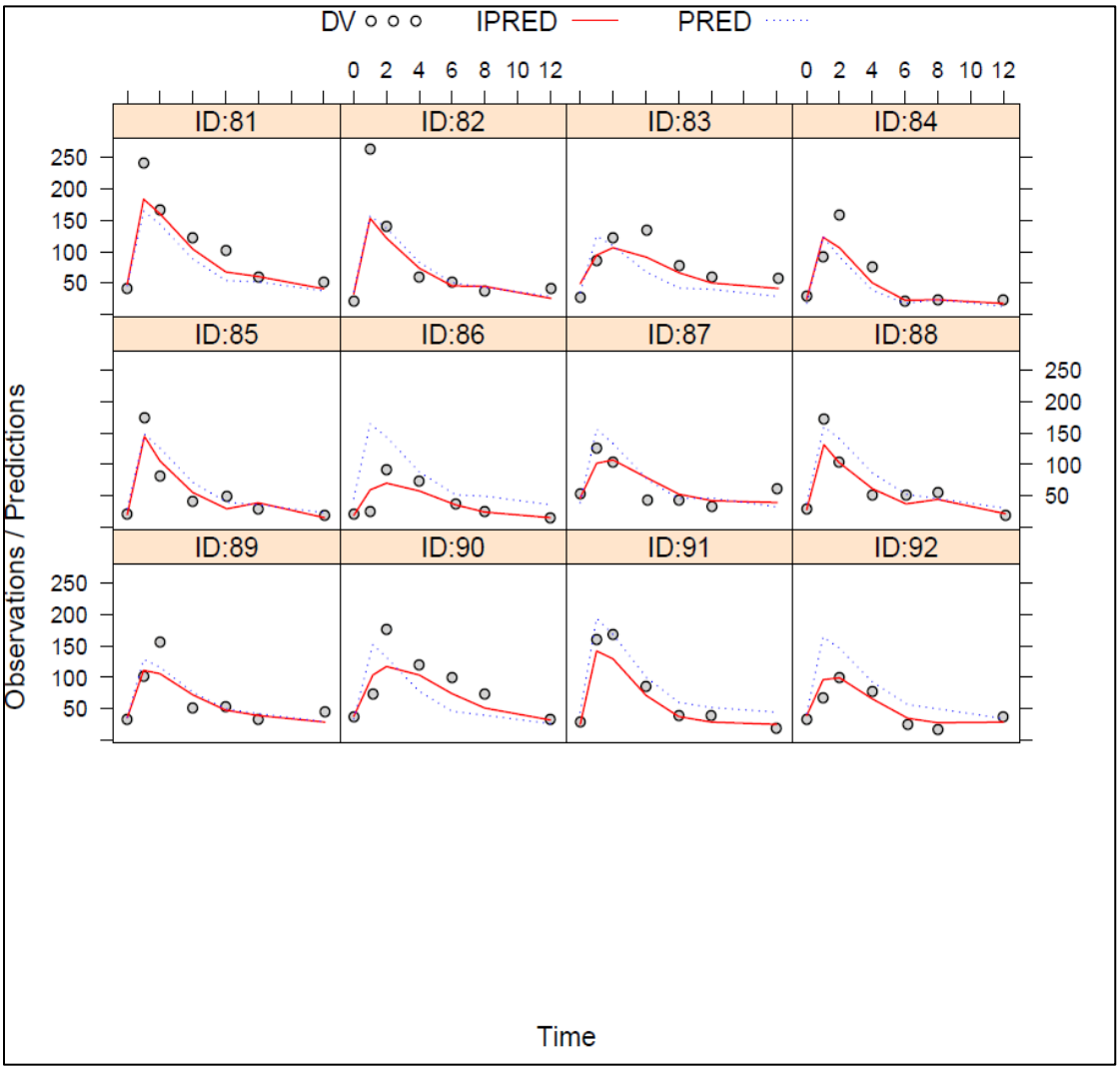

4.C: Individual Plots of Total MPA

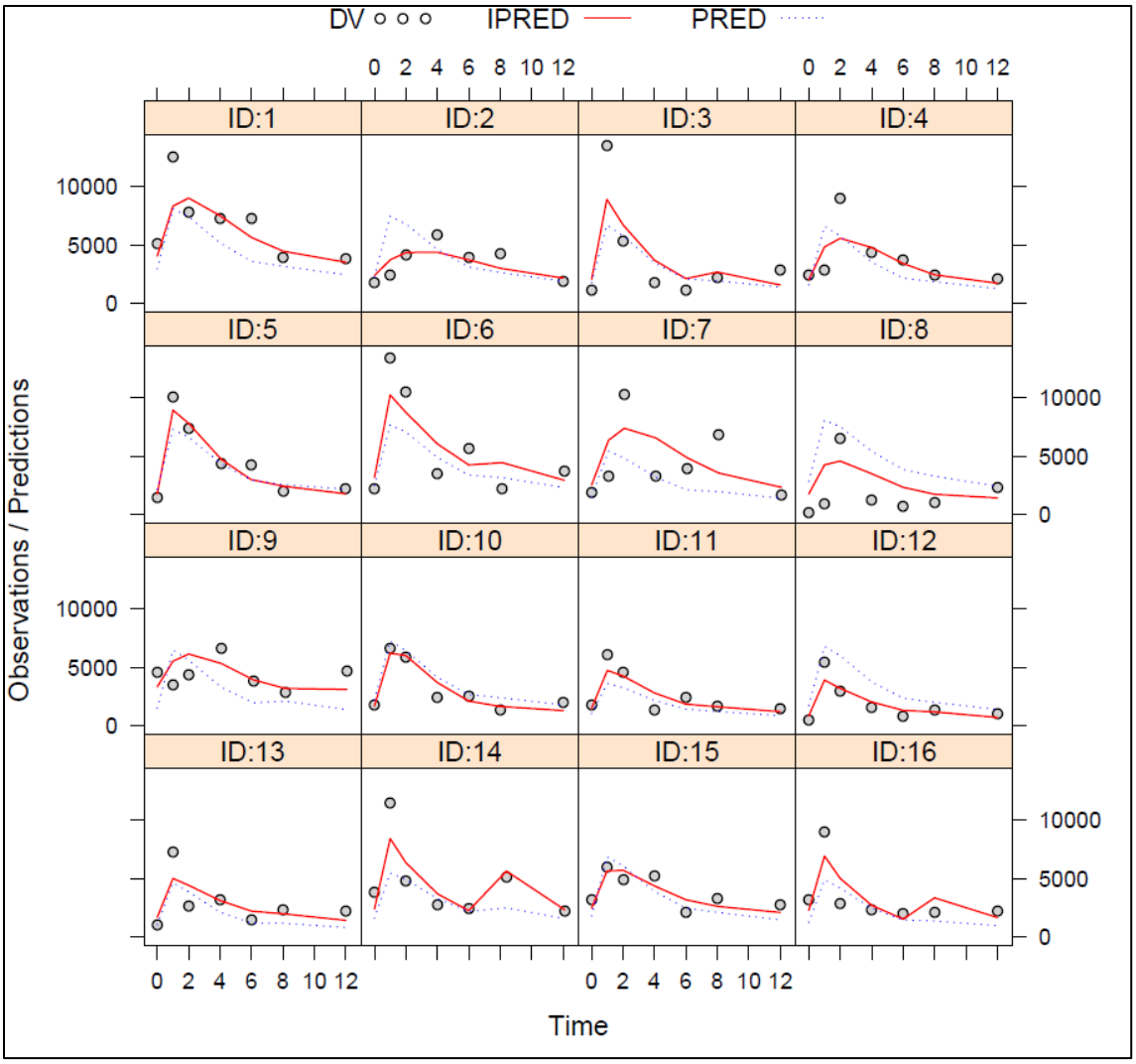

Individual Plots of Total MPA

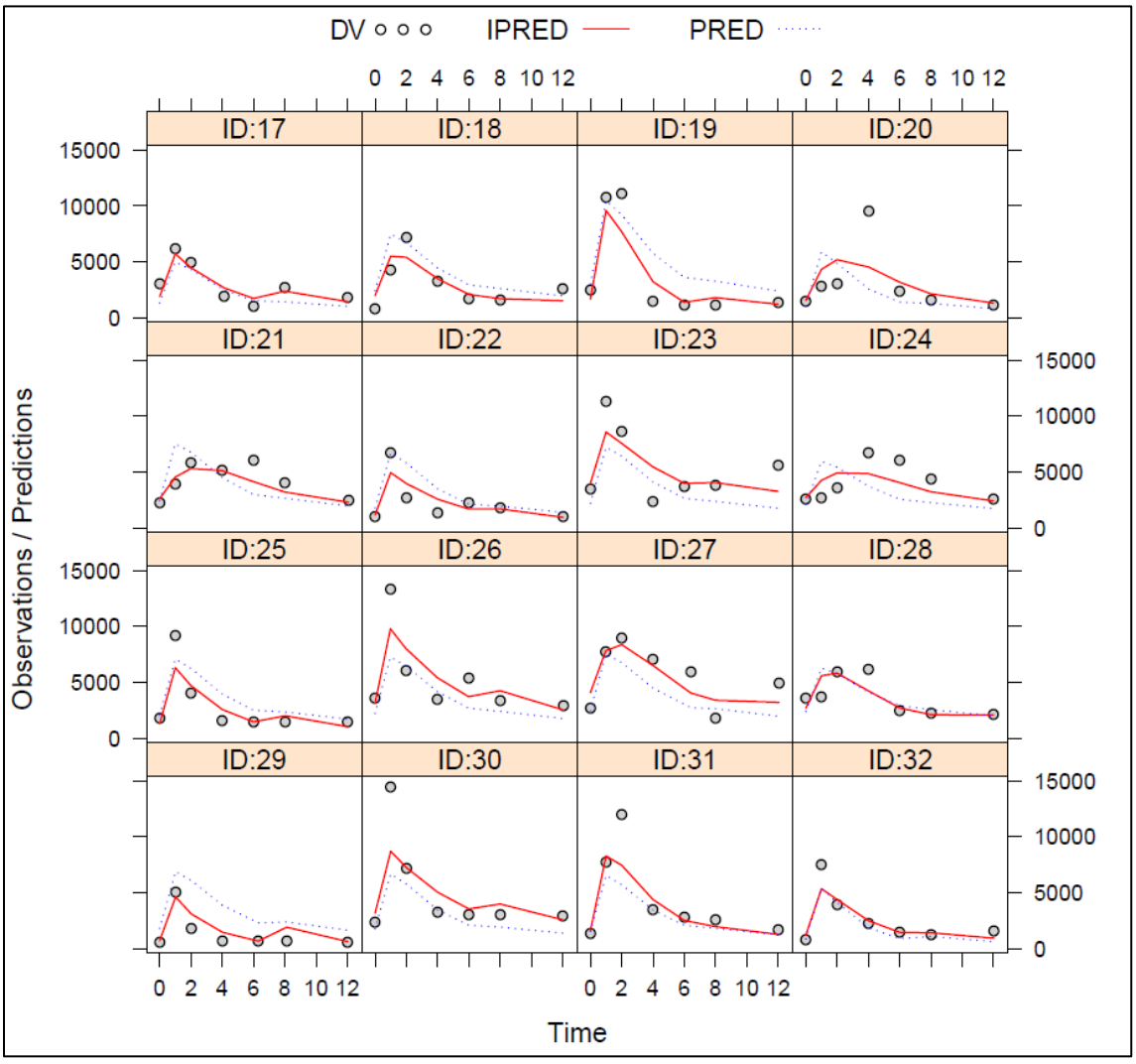

Individual Plots of Total MPA

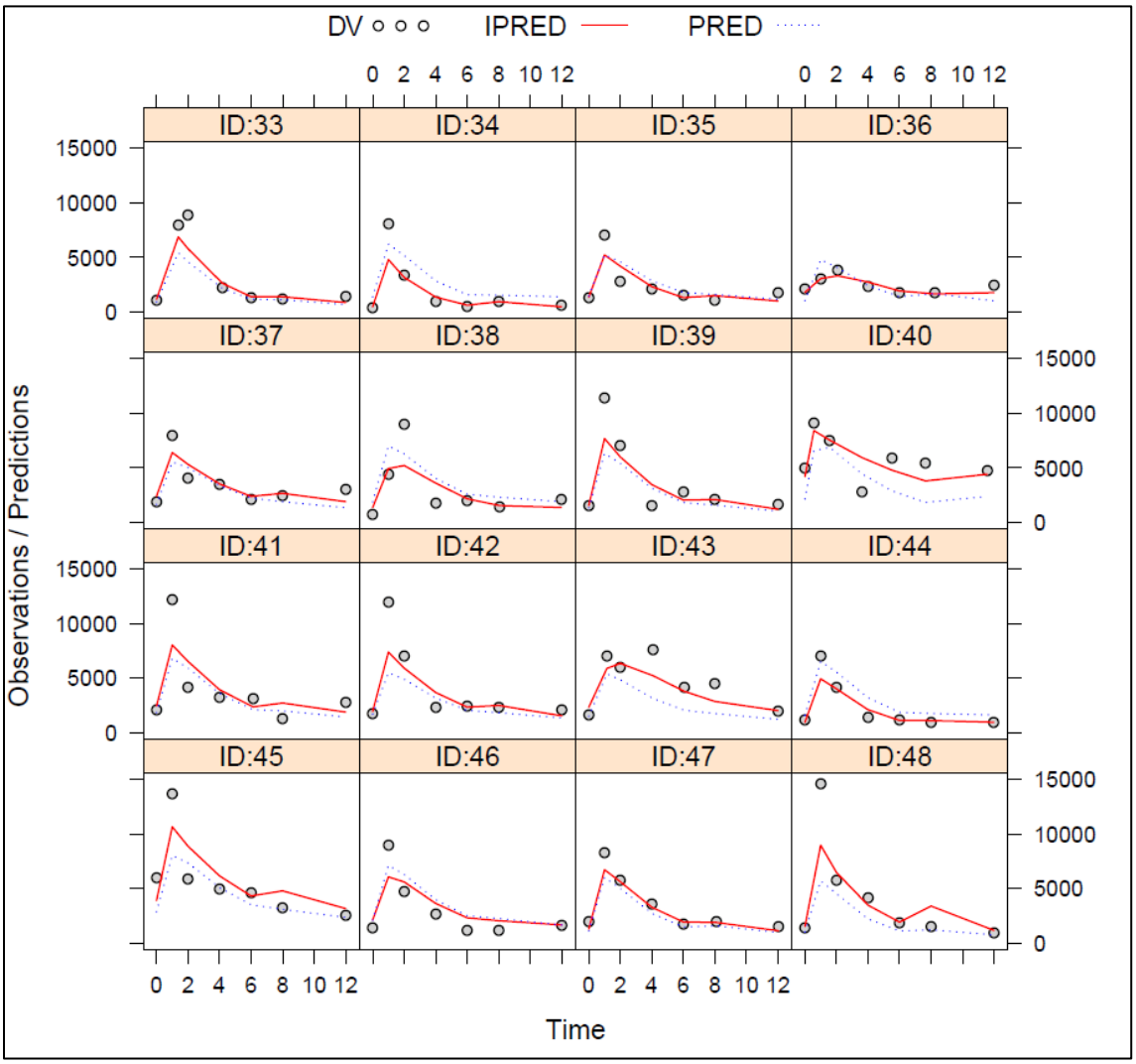

Individual Plots of Total MPA

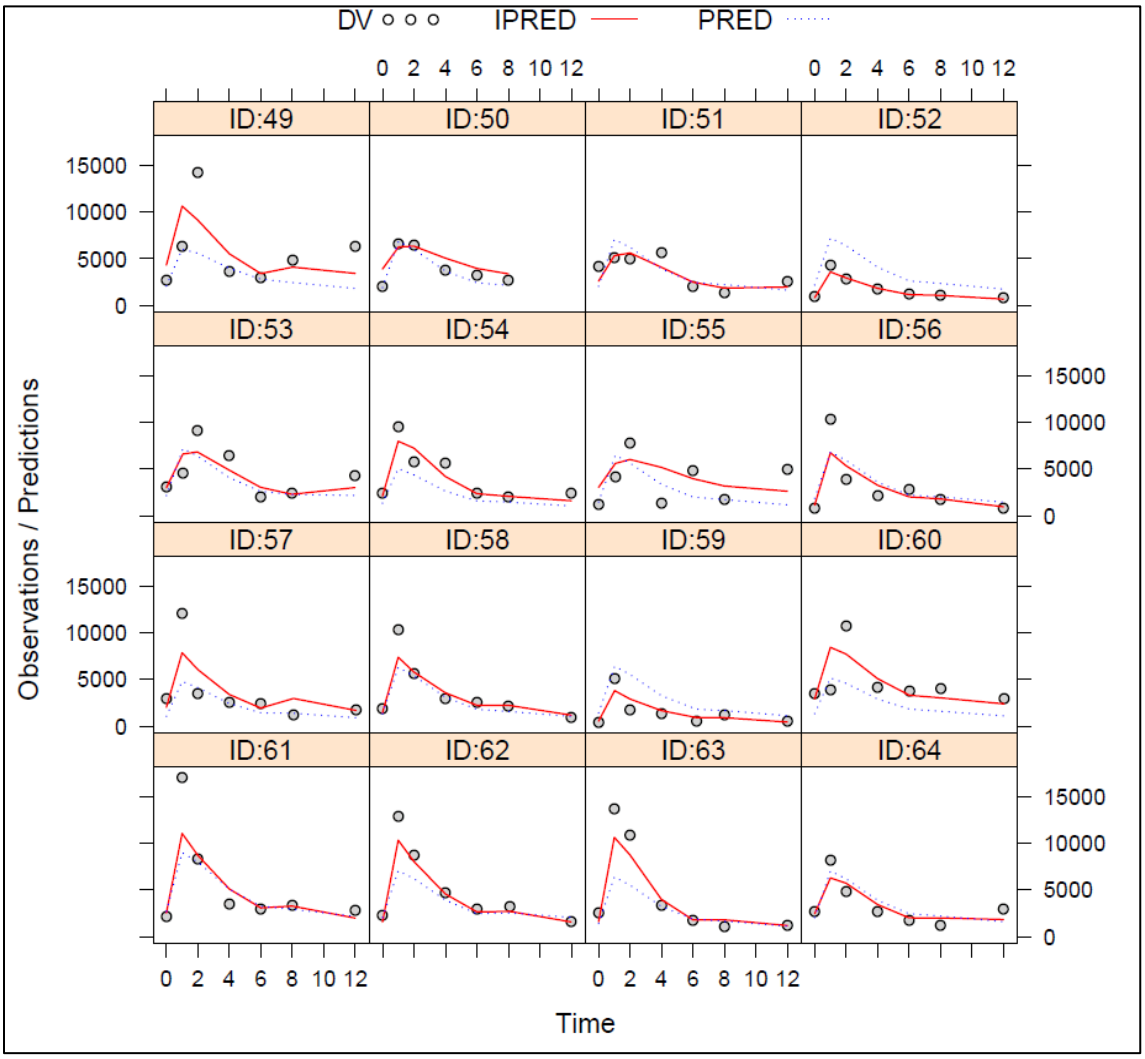

Individual Plots of Total MPA

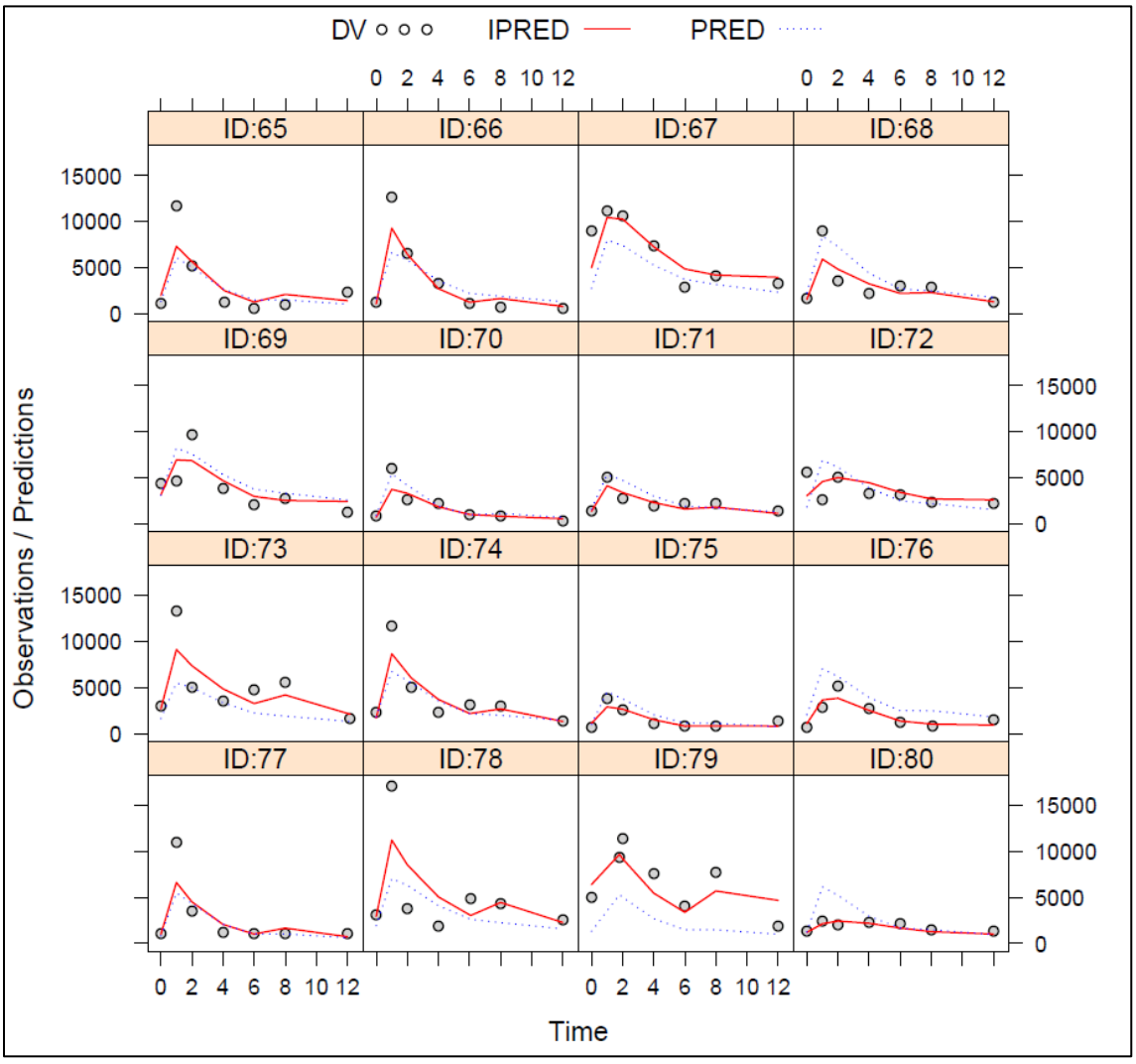

Individual Plots of Total MPA

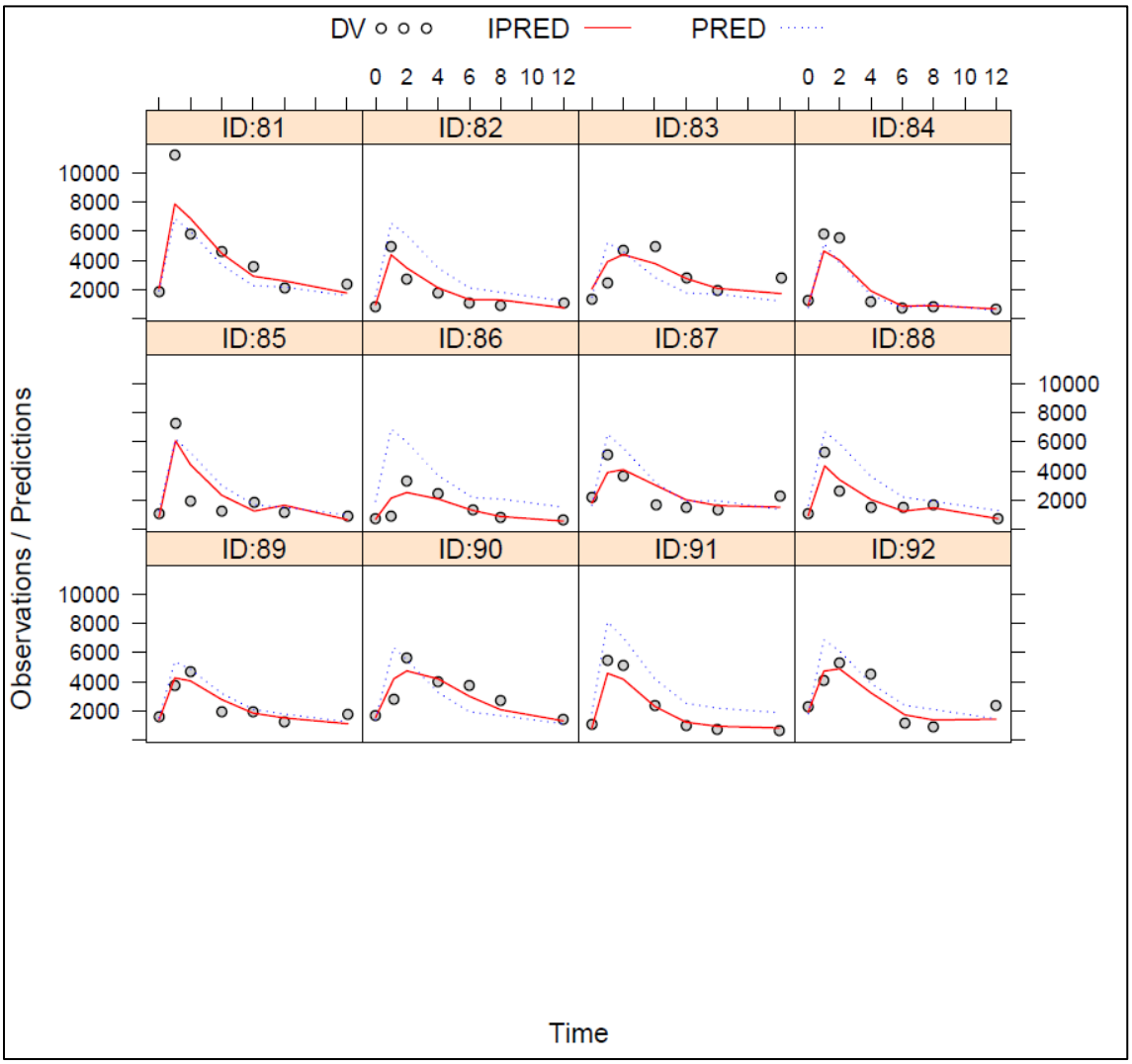

4.D: Individual Plots of MPAG

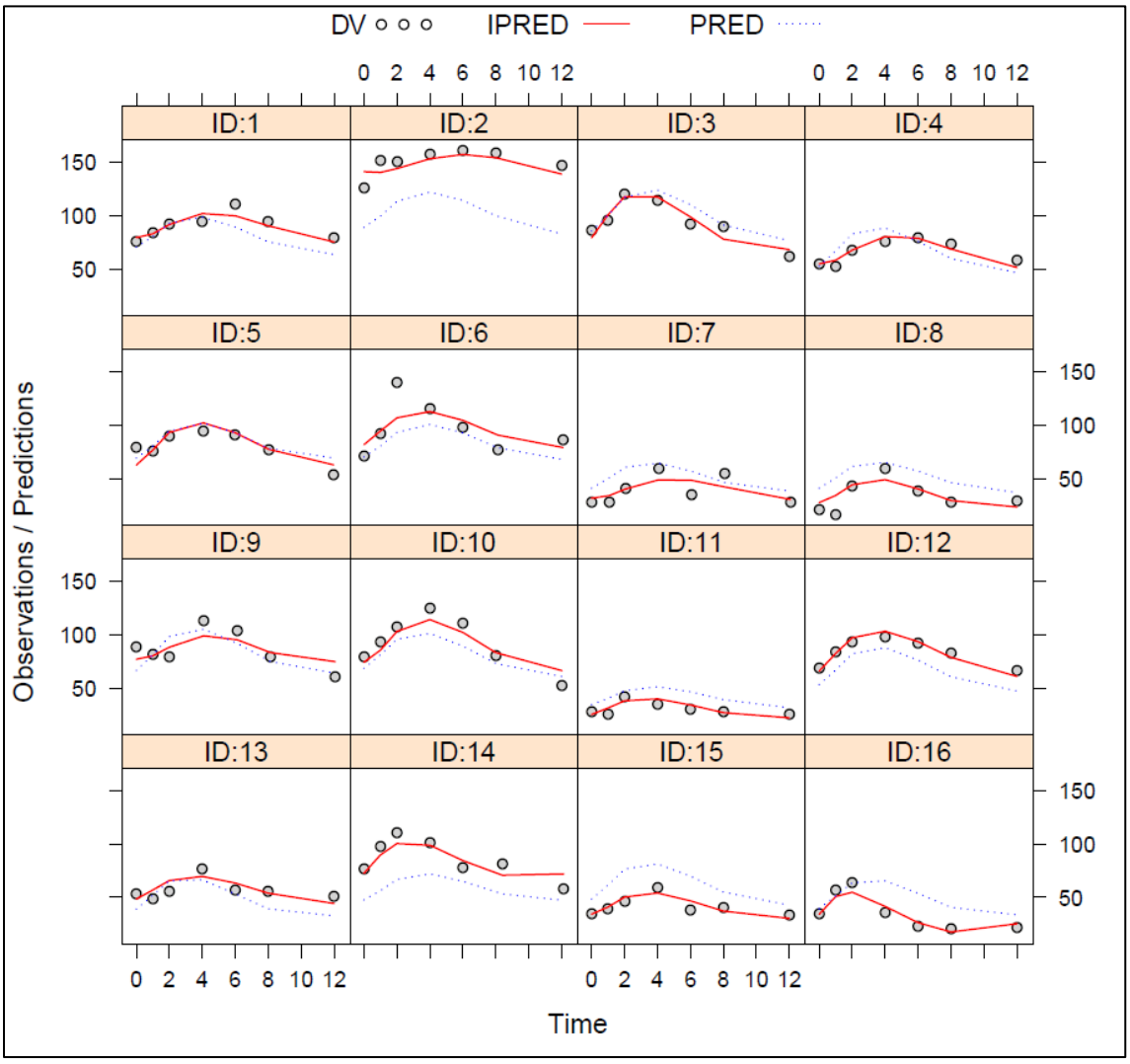

Individual Plots of MPAG

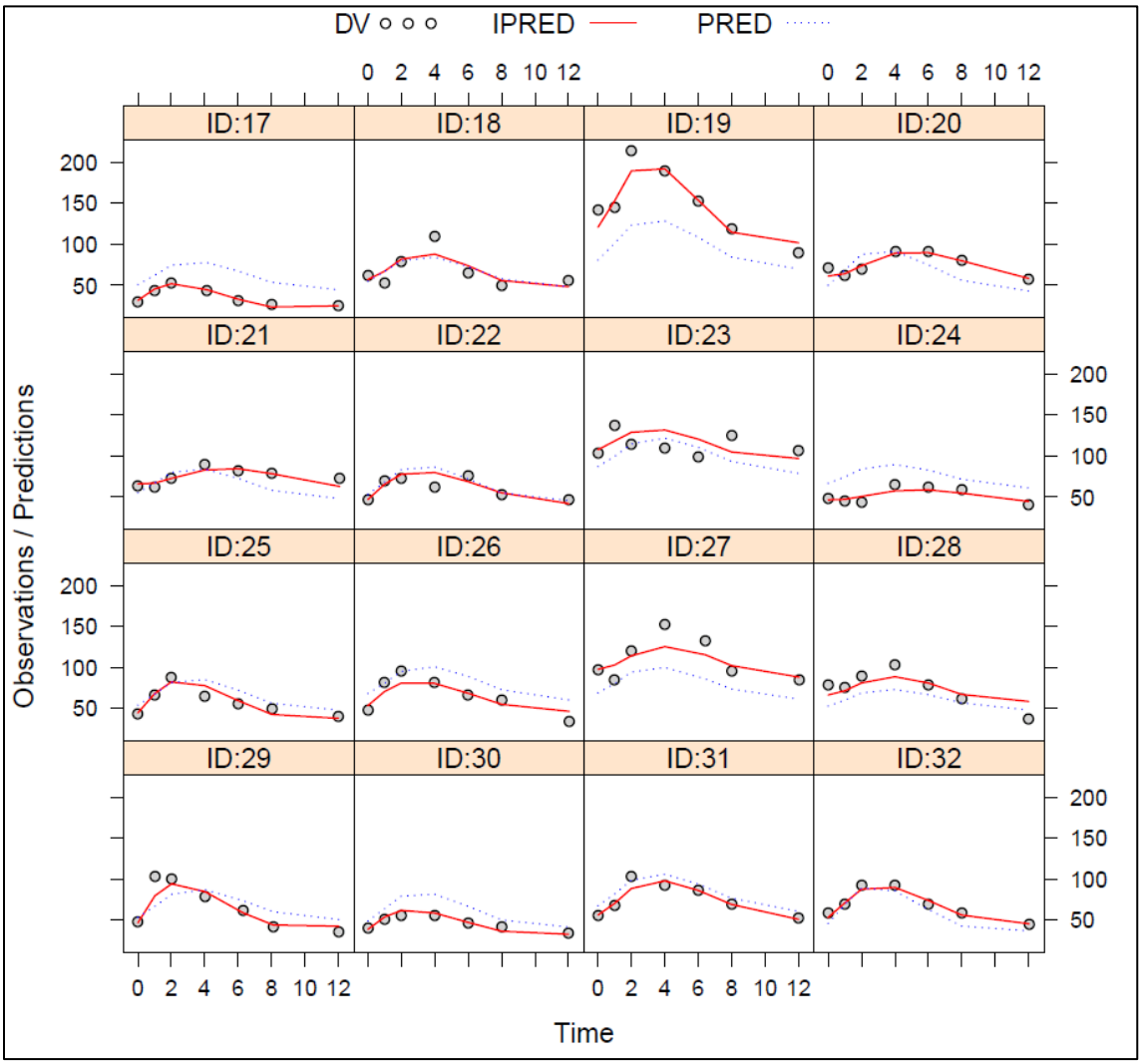

Individual Plots of MPAG

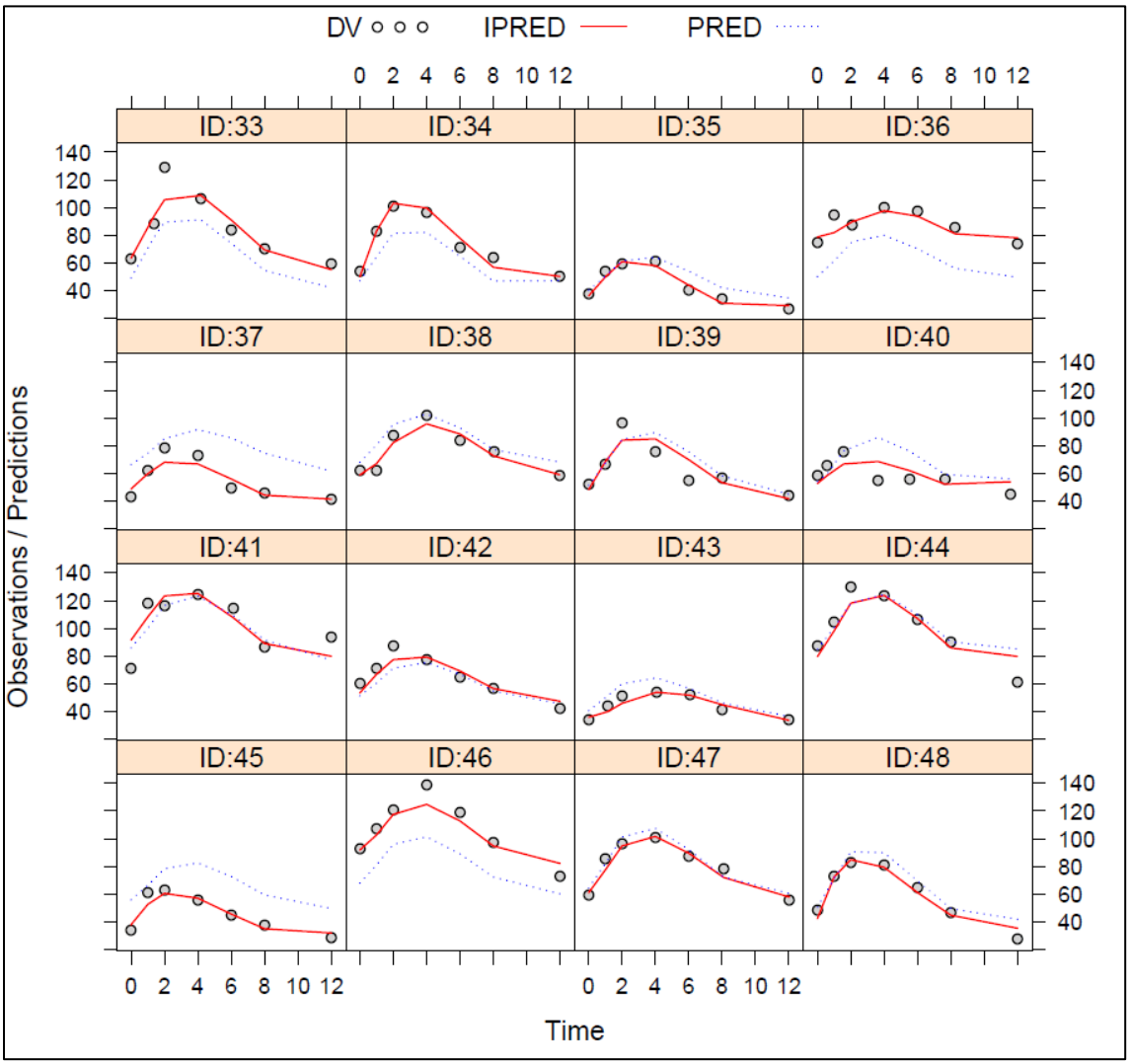

Individual Plots of MPAG

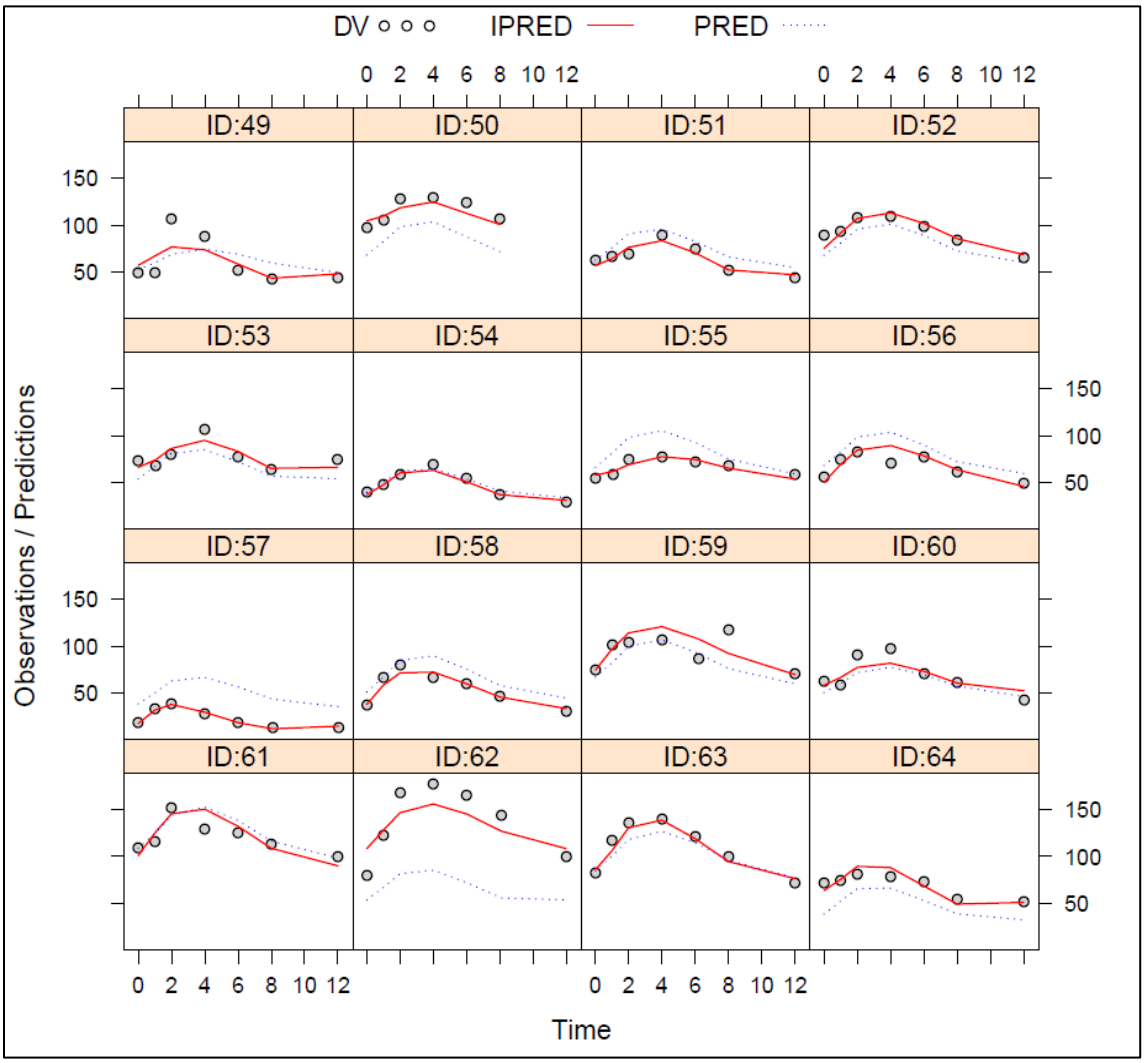

Individual Plots of MPAG

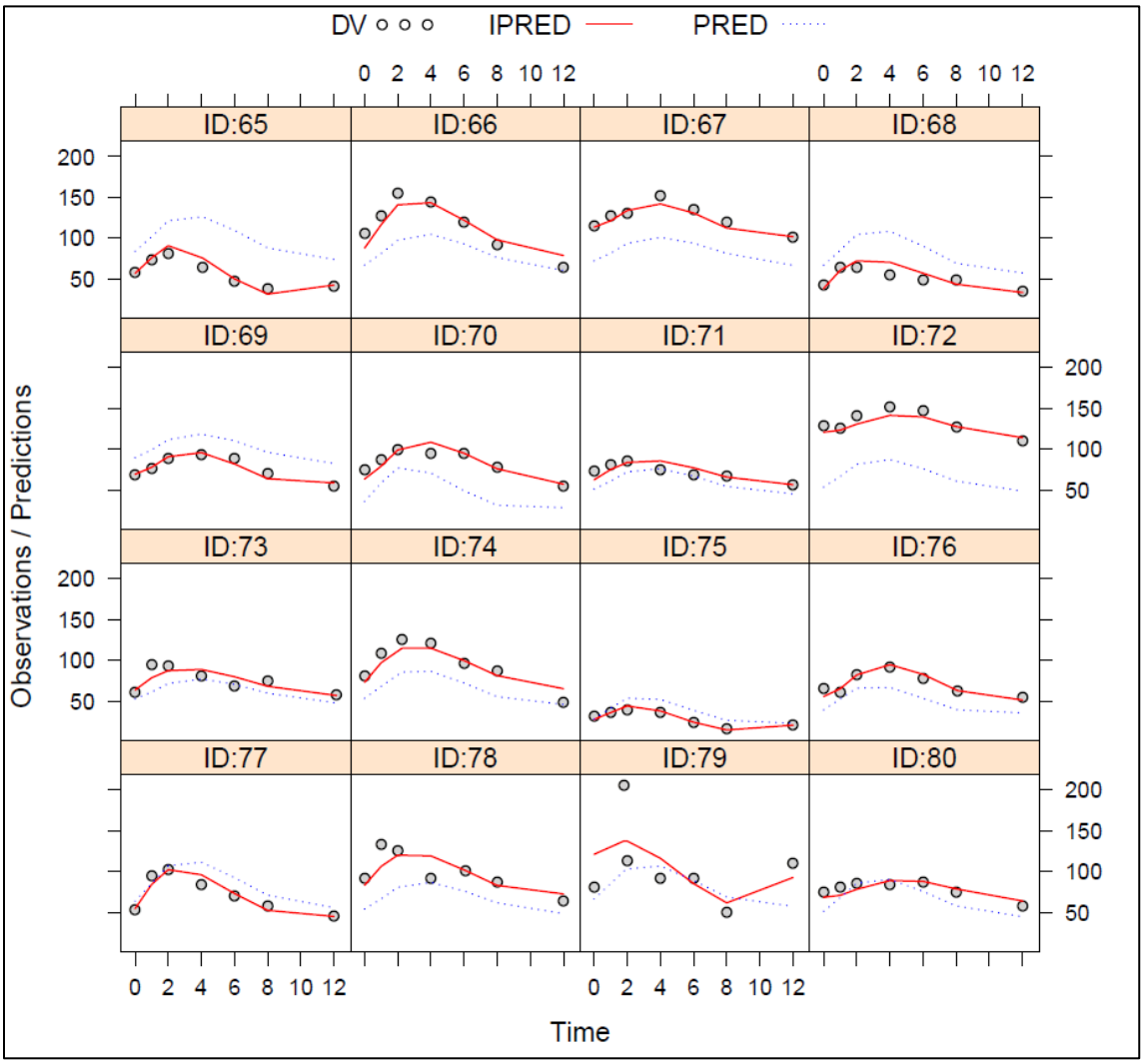

Individual Plots of MPAG

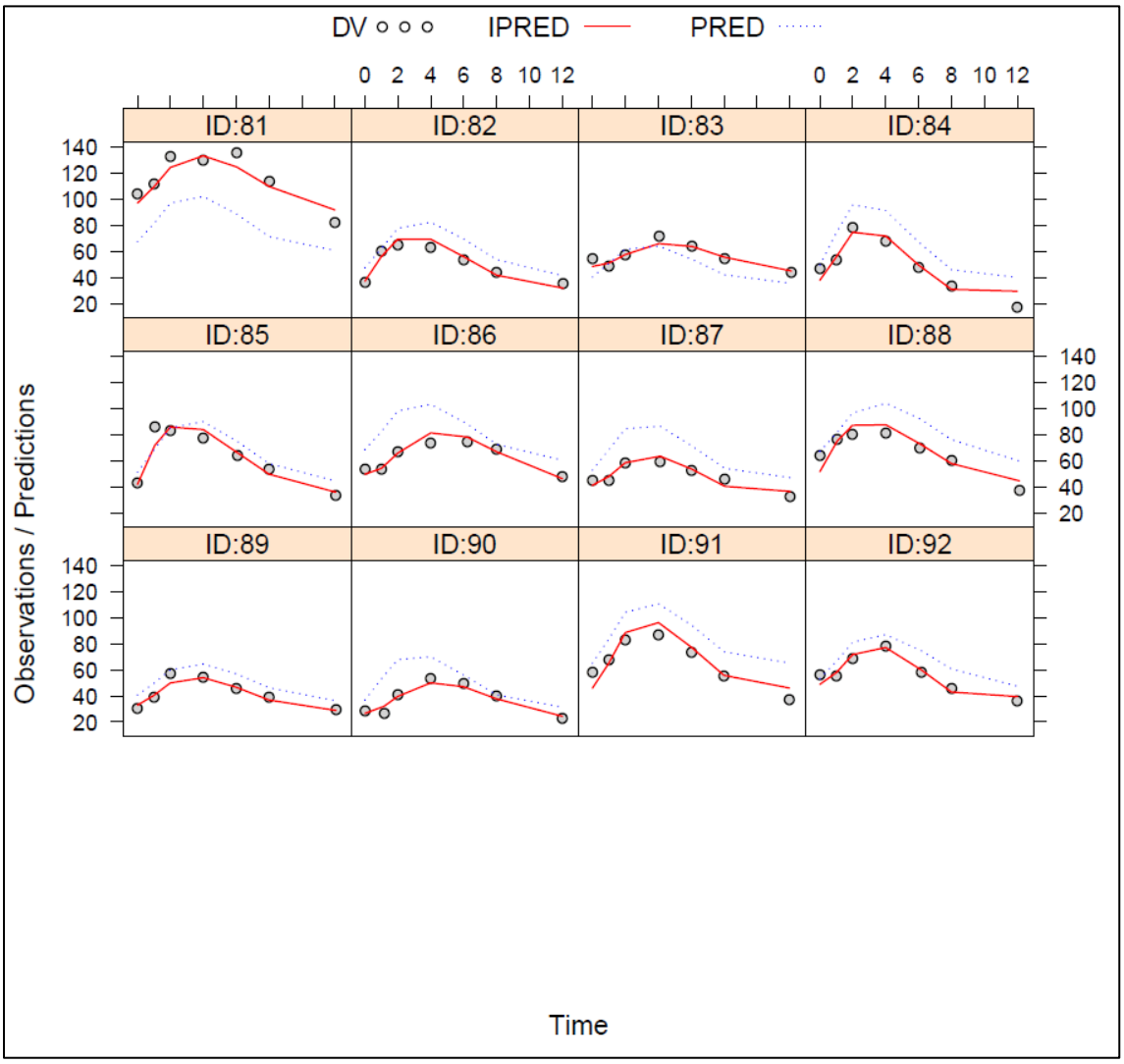

4.E: Individual Plots of Acyl- MPAG

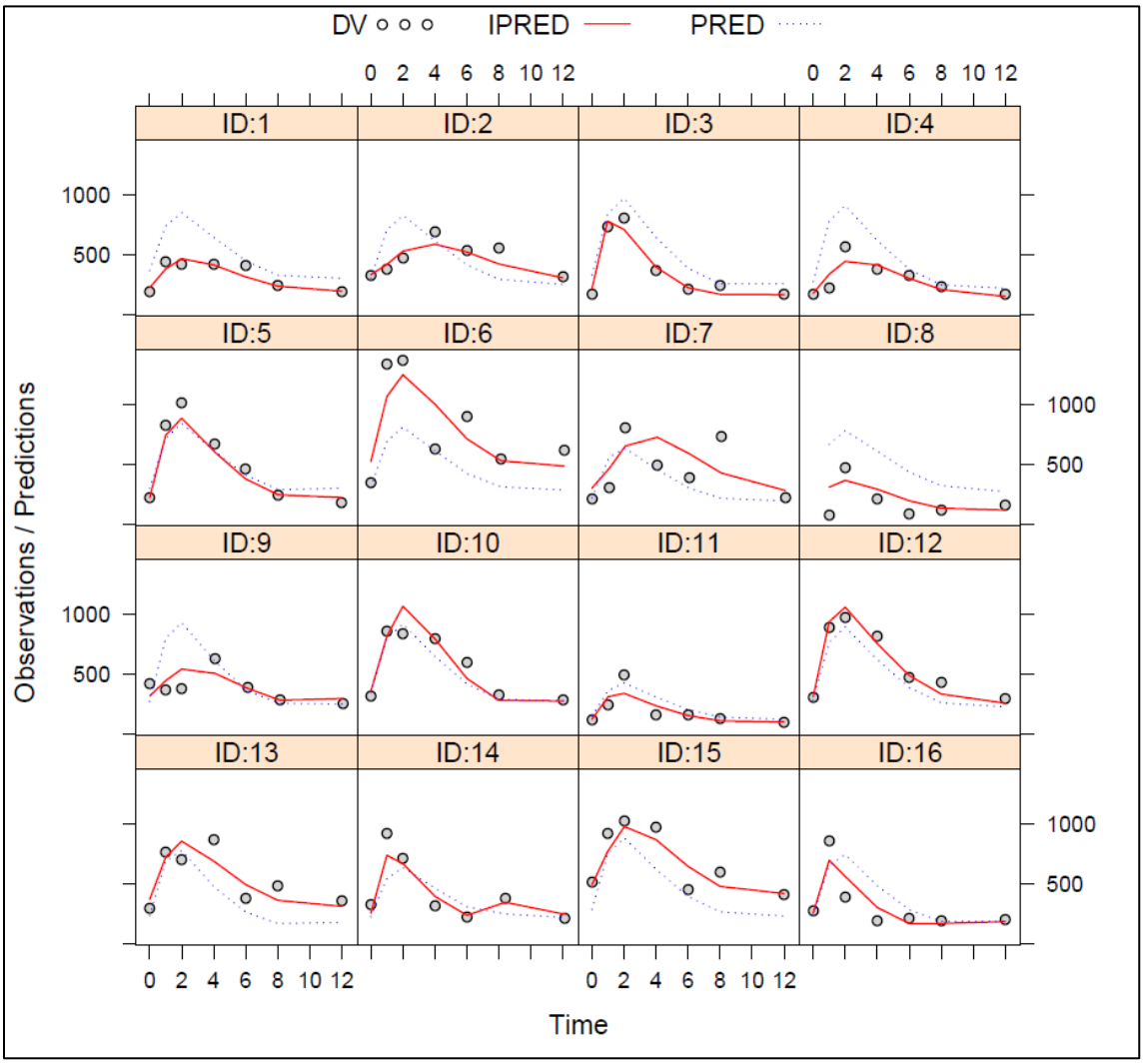

Individual Plots of Acyl- MPAG

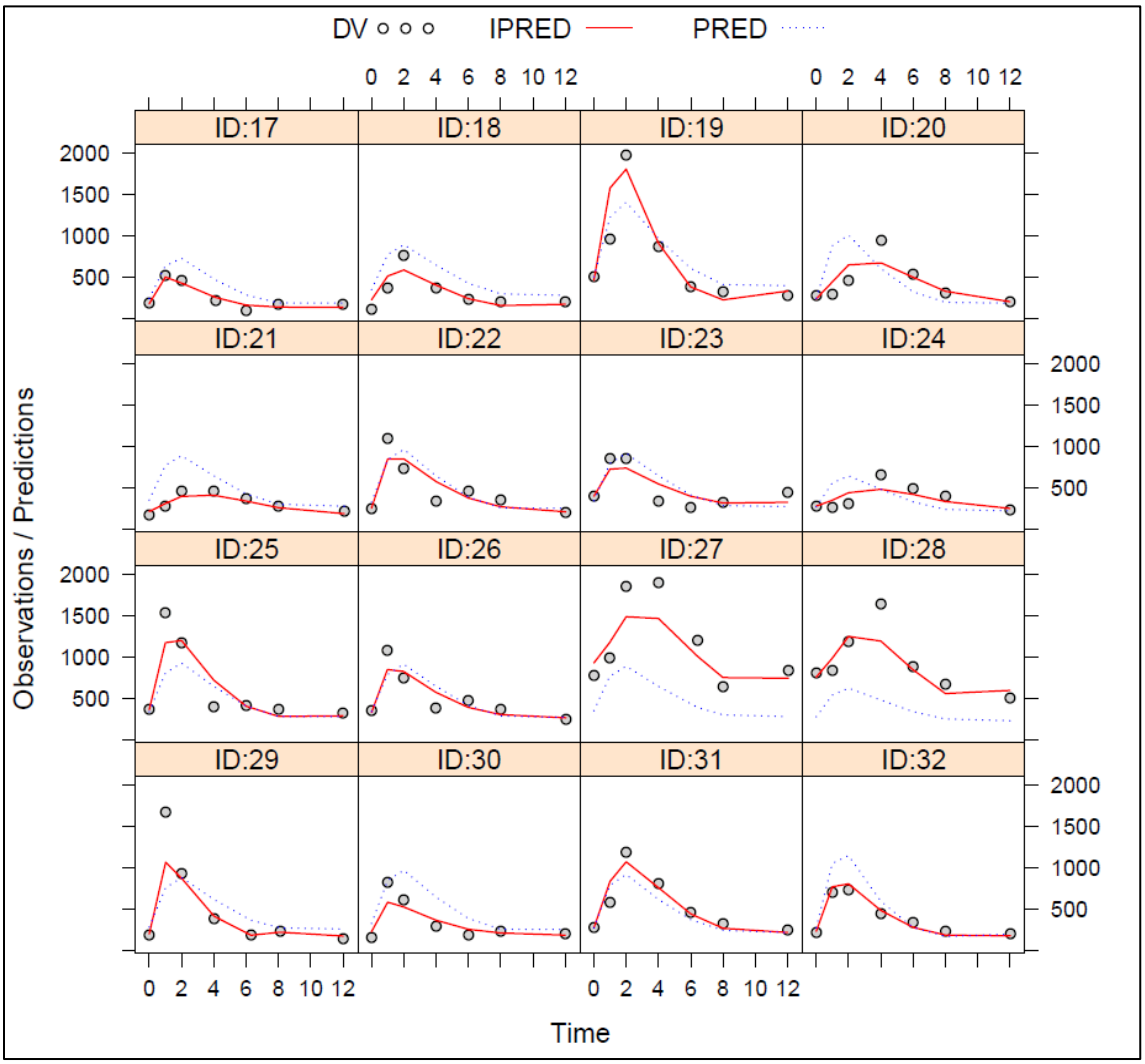

Individual Plots of Acyl- MPAG

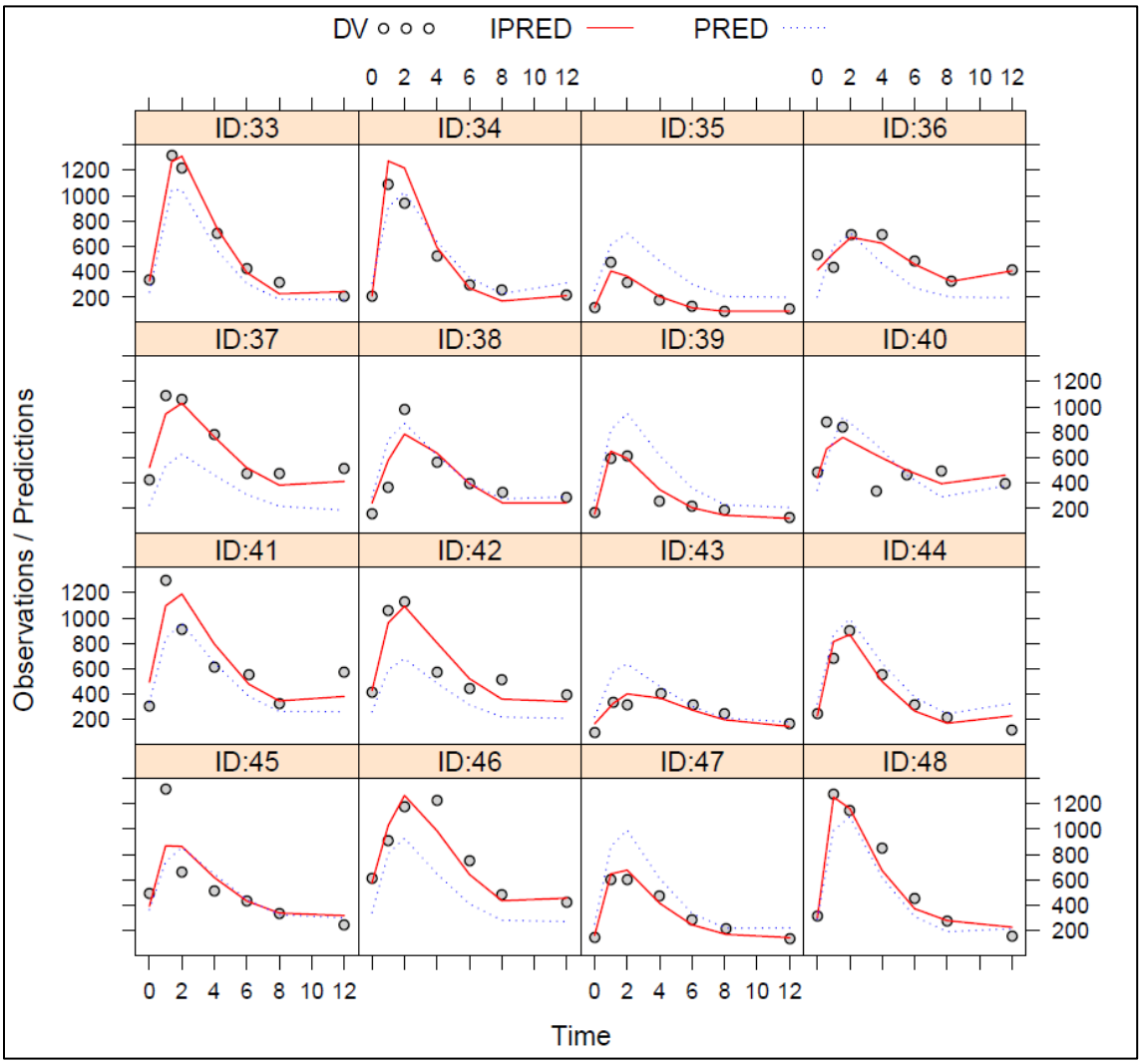

Individual Plots of Acyl- MPAG

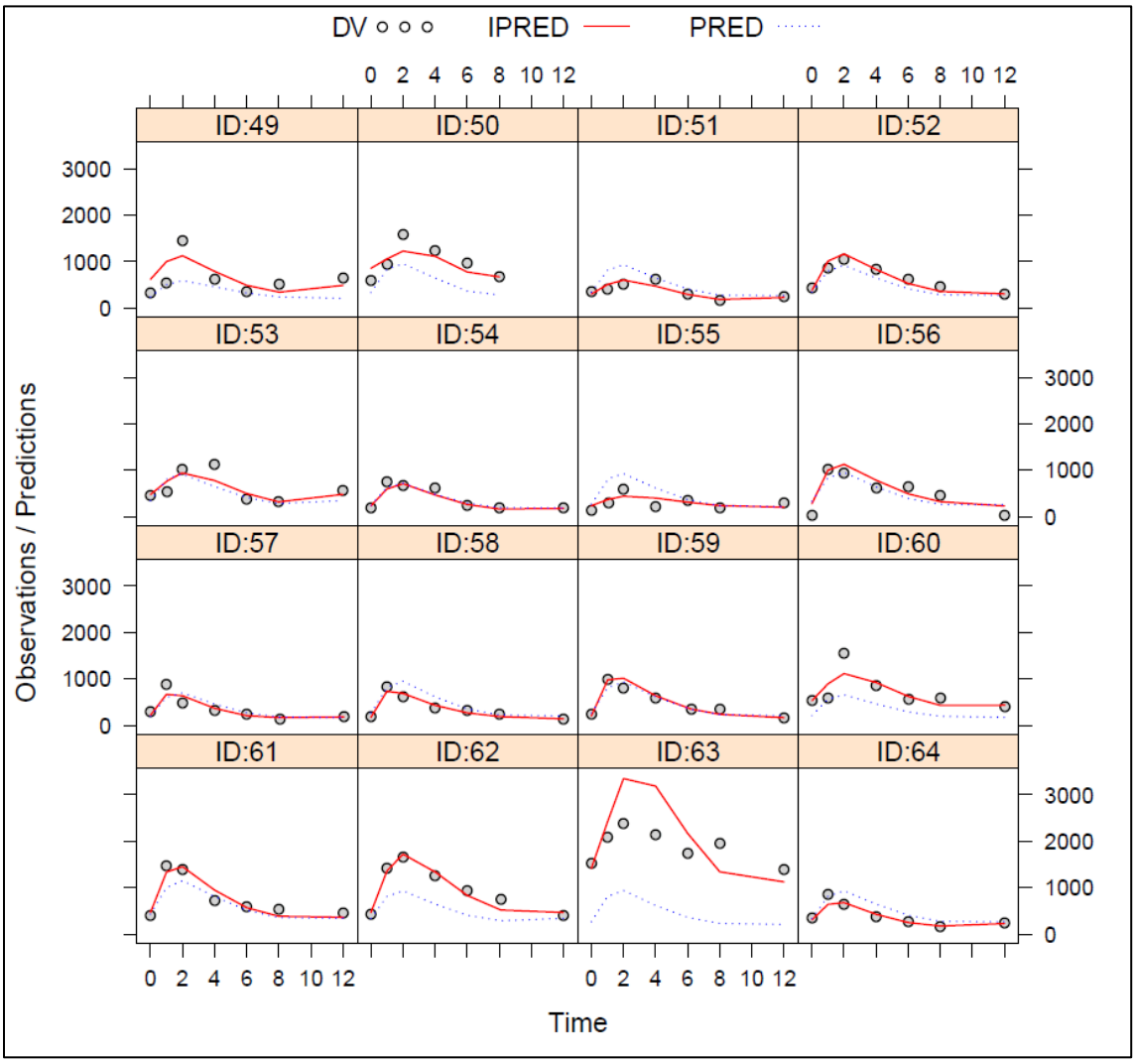

Individual Plots of Acyl- MPAG

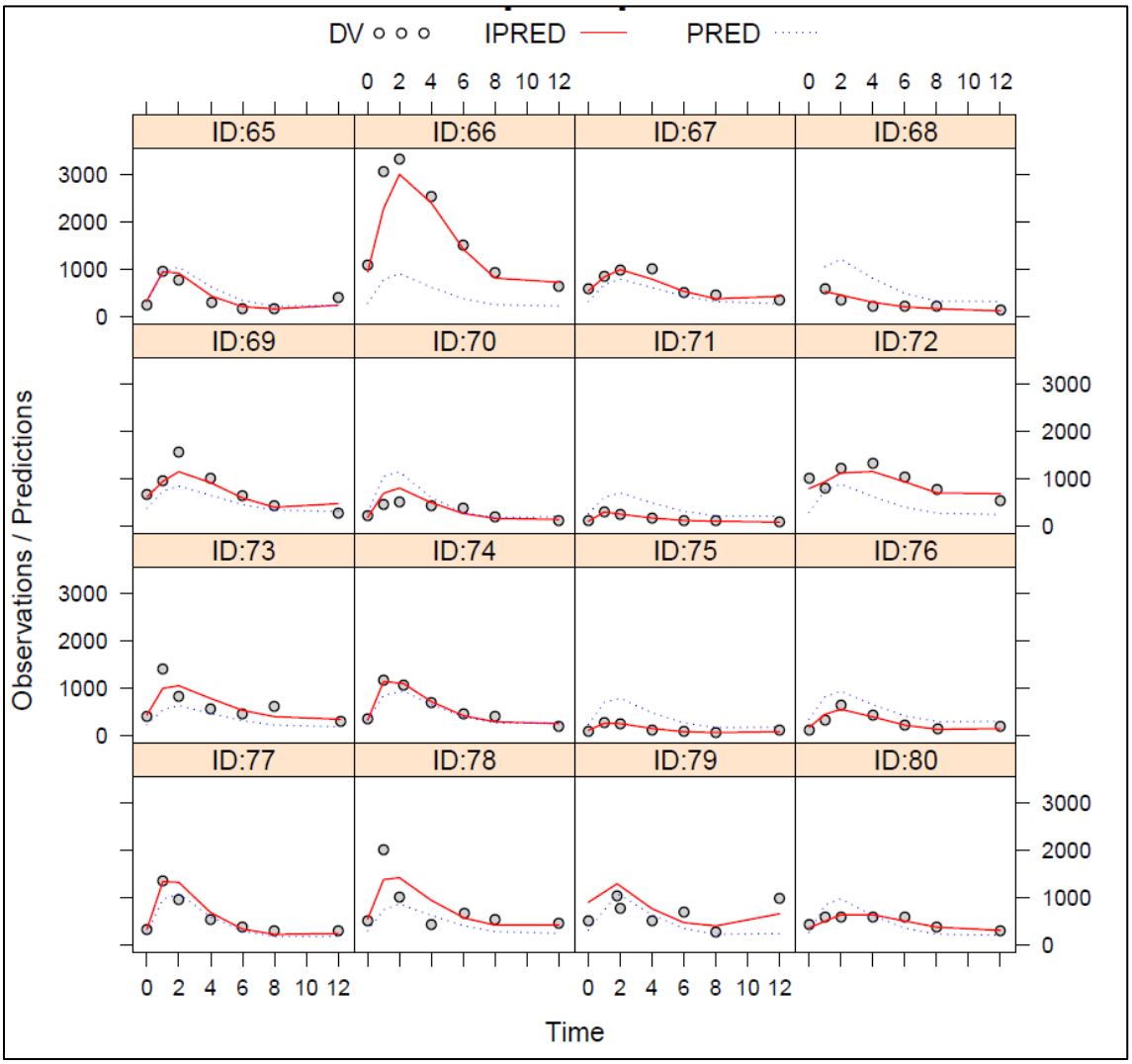

Individual Plots of Acyl- MPAG

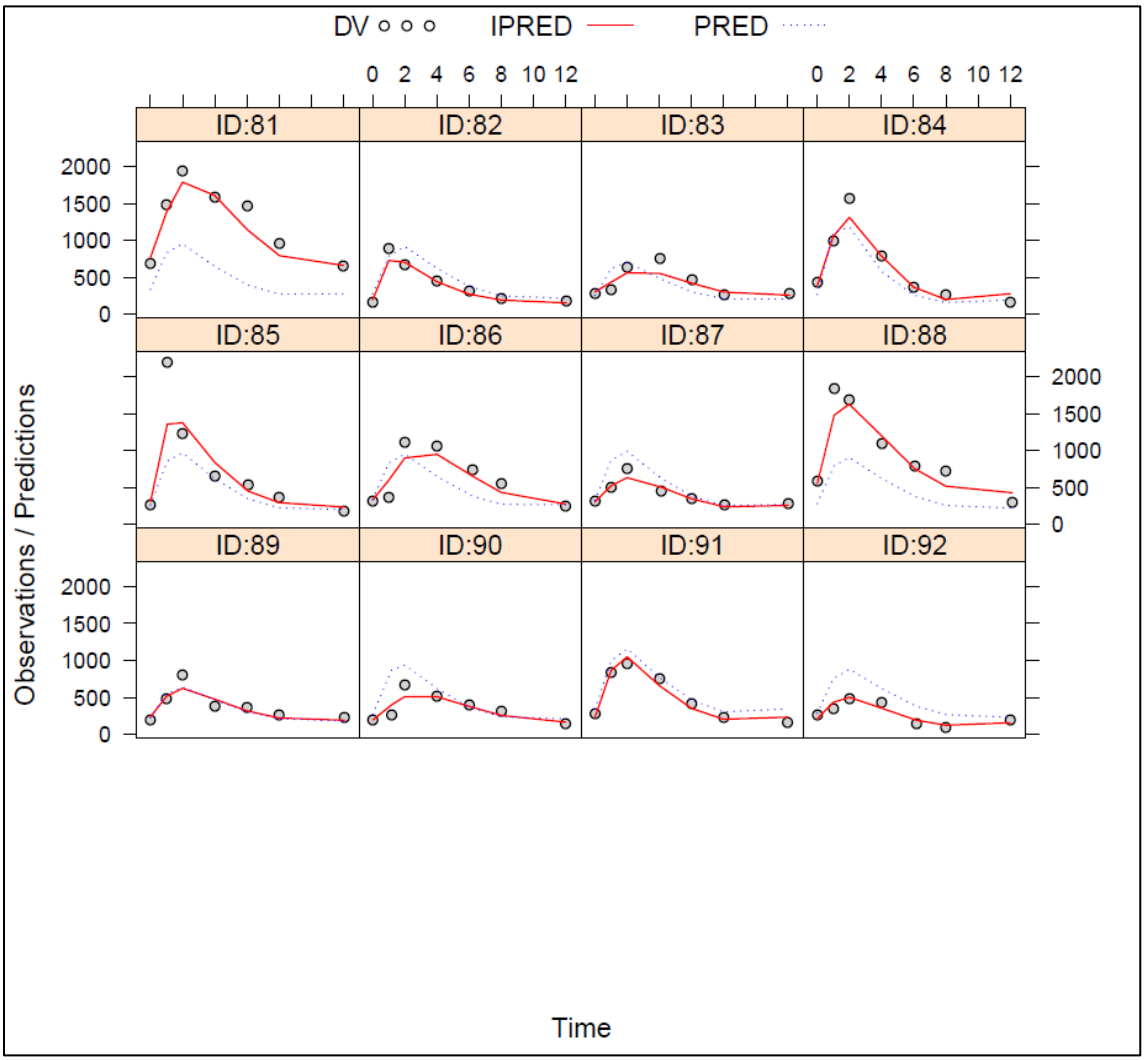

Chapter 5:

5. A: The R Code Used in Conducting the Several Univariate Logistic Regression Analyses

data_3<-data_3 ; **includes all the exposure metrics (continuous and dichotomized) and response outcomes (acute rejection and leukopenia)**

```
exposures<-names(data_3[match(c("Unbound_Cmax" , "Unbound_Clast" ,
"Unbound_AUCall" ,  "Total_Cmax"    ,   "Total_Clast"
 , "Total_AUCall"  ,   "Acyl_Cmax"   ,    "Acyl_Clast"    ,   "Acyl_AUCall"
 , "unb_AUC_d_AR"  ,   "tot_AUC_d_AR"   ,  "acyl_auc_d_AR"  ,  "unb_clast_d_AR"
 , "tot_clast_d_AR"  , "acyl_clast_d_AR" , "unb_cmax_d_AR"  ,  "tot_cmax_d_AR"
    , "acyl_cmax_d_AR"  , "unb_AUC_d_leu"  ,  "tot_AUC_d_leu"  ,  "unb_clast_d_leu"
   , "tot_clast_d_leu" , "unb_cmax_d_leu" ,  "tot_cmax_d_leu" ,  "acyl_auc_d_leu"
    , "acyl_clast_d_leu" ,"acyl_cmax_d_leu"), names(data_3))])
outcomes_names<-names(data_3)[match(c("AR" ,"Leukem"), names(data_3))]

for (i in outcomes_names) {
   assoc =lapply(exposures,
              function(x) {
              formula    <- as.formula(paste(i," ~", x))
              lm <- glm(formula, data = data_3, family = "binomial")
               summary<-(coef(summary(lm)))
             })
 df <- do.call("rbind", assoc)
 df <- as.data.frame(do.call("rbind", assoc))
 df$covariate=rownames(df)
 rownames(df)<-NULL
 df<-df[,c(5,1:4)]
 colnames(df)<-c("covariate"    ,    "Estimate" ,  "Std..Error", "t.value"  ,   "p_value")
 df$p_value<-as.numeric(as.character(df$p_value))
 df$sig<-NULL
 df$sig[df$p_value<=0.05]<-"***"
 df$sig[df$p_value>0.05]<- "  "
 df2<-df
 #df2<-df[ -which(df$covariate=="(Intercept)"),]
```

```
  df2$OddsRatio<-exp(df2$Estimate)
  df3<-df2[ which(df2$sig=="***"),]
  dir.create("results/univariate_analysis_results")
  write.csv(df2, file=paste0("results/univariate_analysis_results/",i,"_univariate.csv"))
}
```